SOME ASPECTS of the INTERACTION of HUMIC SUBSTANCES with METAL IONS

MARK MICHAEL SCANLON

Doctor of Philosophy

THE UNIVERSITY OF ASTON IN BIRMINGHAM

October 1991

THE UNIVERSITY OF ASTON IN BIRMINGHAM

SOME ASPECTS of the INTERACTION of HUMIC SUBSTANCES with METAL IONS

MARK MICHAEL SCANLON

Doctor of Philosophy

October 1991

Humic substances are the major organic constituents of soils and sediments. They are heterogeneous, polyfunctional, polydisperse, macromolecular and have no accurately known chemical structure. Their interactions with radionuclides are particularly important since they provide leaching mechanisms from disposal sites. The central theme to this research is the interaction of heavy metal actinide analogues with humic materials. Studies described focus on selected aspects of the characteristics and properties of humic substances. Some novel approaches to experiments and data analysis are pursued. Several humic substances are studied; all but one are humic acids, and those used most extensively were obtained commercially. Some routine characterisation techniques are applied to samples in the first instance.

Humic substances are coloured, but their ultra-violet and visible absorption spectra are featureless. Yet, they fluoresce over a wide range of wavelengths. Enhanced fluorescence in the presence of luminescent europium(III) ions is explained by energy transfer from irradiated humic acid to the metal ion in a photophysical model.

Nuclear magnetic resonance spectroscopy is applied to the study of humic acids and their complexes with heavy metals. Proton and carbon–13 NMR provides some structural and functionality information; Paramagnetic lanthanide ions affect these spectra. Some heavy metals are studied as NMR nuclei, but measurements are restricted by their sensitivity.

A humic acid is fractionated yielding a broad molecular weight distribution. Electrophoretic mobilities and particle radii determined by Laser Doppler Electrophoretic Light Scattering are sensitive to the conditions of the supporting media, and the concentration and particle size distribution of humic substances.

In potentiometric titrations of humate dispersions, the organic matter responds slowly and the mineral acid addition is buffered. Proton concentration data is modelled and a mechanism is proposed involving two key stages, both resulting in proton release after some conformational changes.

Keywords: Humic Substances, Fluorescence, Light Scattering, Kinetics

DEDICATION

This thesis is dedicated to my parents.

ACKNOWLEDGEMENTS

The scientific expertise and support of Dr. J.D. Miller is acknowledged. The technical assistance of Dr. M.C. Perry and other researchers at Aston University is appreciated. Provision of Light Scattering facilities and technical assistance of staff at AEA Technology, Harwell, is acknowledged.

Financial support was provided by the Science and Engineering Research Council and supplemented by AEA Technology, Harwell.

M.M. Scanlon

CONTENTS INDEX

TABLES INDEX

FIGURES INDEX

CHAPTER 1
INTRODUCTION

1.1 Humic Substances: Introduction

Humic substances are the major organic constituents of soils and sediments and are widely distributed over the Earth's surface in almost all terrestrial and aquatic environments. They are a major reserve of organic carbon for the global carbon cycle. They arise from the chemical and biological degradation of plant and animal residues and from synthetic activities of micro-organisms. [1,2,3]

For chemists, humic substances are problematic materials since they are heterogeneous, polyfunctional, polydisperse, macromolecular and have no accurately known chemical structure. Much of the research directed at humic substances has focussed on the elucidation of their structure and properties, particularly reactions with environmental co–factors.

Humic substances can interact with metal ions, minerals and organic compounds—including toxic pollutants—to form water-soluble and water-insoluble associations of widely differing chemical and biological stabilities. These interactions occur by ion-exchange, complexation, coagulation and surface adsorption. Humic substances participate in—and control—many reactions occurring in soils and waters. [4,5,6]

In this Chapter, reported properties of humic substances are presented and areas of research need are highlighted. The experimental work described in the bulk of this thesis is introduced and set in the context of current research activities in this field.

1.2 Classification of Organic Matter

Soils and sediments contain a large variety of organic materials that can be grouped into humic and non-humic substances. The latter includes those whose physical and chemical characteristics are recognisable, such as carbohydrates, proteins, fats and low molecular weight organic acids. By contrast, humic substances do not exhibit the specific physical

and chemical properties normally associated with well-defined organic compounds, such as a sharp melting point and a detailed infrared spectrum. This is because humic substances are not pure compounds, but a heterogeneous mixture of many compounds with generally similar physical and chemical properties. This places a major constraint on their characterisation. [1]

1.2.1 Classification of Humic Substances

Humic substances are operationally defined by their classical fractionation which is based on solubility in aqueous media of different acidity. The flow-chart presented in Figure 1.1 is part of the most commonly used procedure for extracting humic matter from terrestrial sources, whether they be soil or sediment. [1,5,6] The scheme may be used to define the fractions of humic substances:

Humin	Fraction insoluble in alkaline media.
Humic Acid	Fraction soluble in alkaline media but precipitated in acidic media.
Fulvic Acid	Fraction soluble in alkaline, neutral and acidic media.

It should be noted that humic and fulvic acids do not form true solutions in aqueous media, but exist as colloids that are better described as aqueous dispersions (see Section 1.3.2). Simpler fractionation schemes have been applied to samples of aquatic origin since they contain humic and fulvic acids, but no humin. Some scientists further divide the humic acid fraction into sub-fractions based on partial precipitation by electrolyte under alkaline conditions, and solubility in ethanol. [1,6]

1.3 Structure of Humic Substances

1.3.1 Chemical Structure of Humic Substances

The chemical structure of humic substances has been an intense focus of research activity, whatever the source of the organic matter. Some studies have applied characterisation techniques to specific humic substance extracts or to chemical degradation products, whereas others have applied chemical and instrumental analysis to

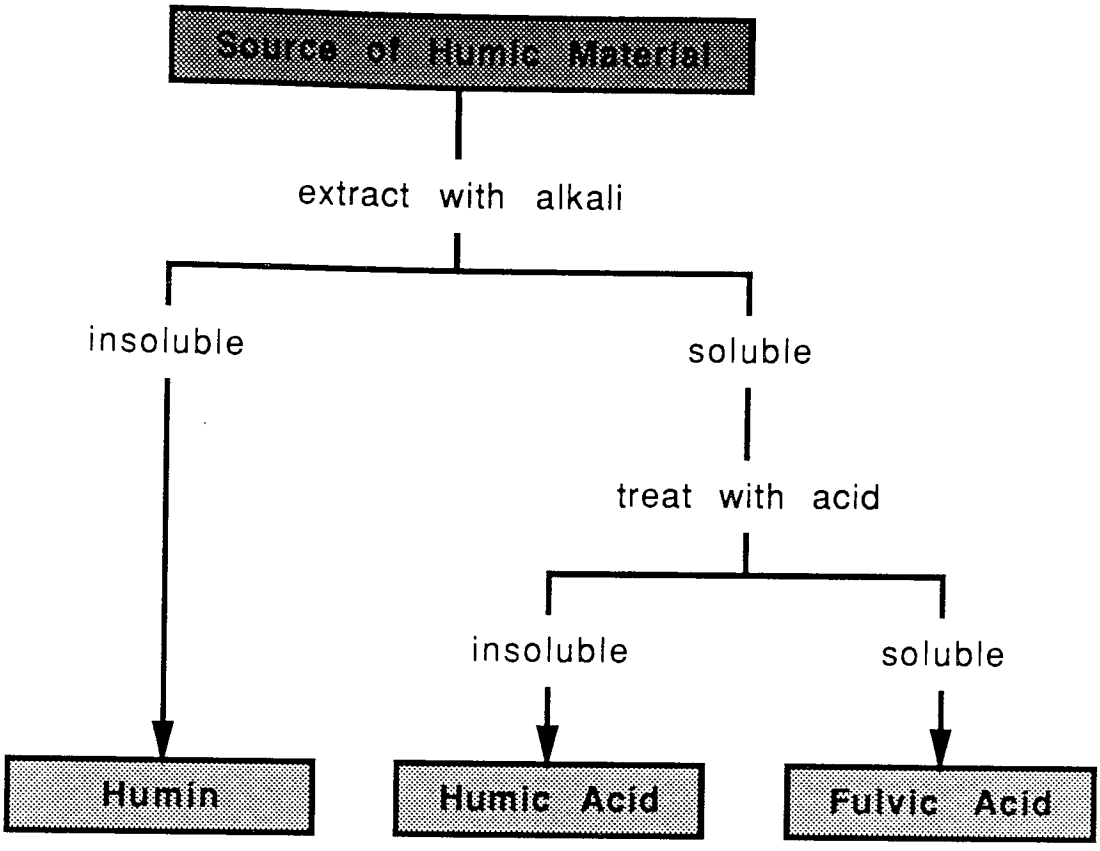

Figure 1.1
Classical Fractionation Scheme for Humic Substances

whole samples. [1,5] Despite the effort placed on these studies, the structures proposed in the literature remain somewhat speculative, [1,7,8] and the existence of a recognisable structure has been questioned. [9] After a hundred or so years of structural elucidation research, the question "What is Humic Acid?" has been posed. [10]

Schnitzer [1] proposed a partial chemical structure for fulvic acid that is in harmony with many experimental observations. Each compound making up the structure has been isolated from fulvic acid after chemical degradation. Bonding between the 'building blocks' is by hydrogen bonds which makes the structure flexible, permits the 'building blocks' to aggregate and disperse reversibly, and allows fulvic acid to react with inorganic and organic soil constituents by either the oxygen-containing functional groups on the internal or external surfaces, or by trapping them in internal voids.

From comparable analytical data published in the literature, [5] the backbone structures of the three humic fractions are similar but they differ in molecular weight, ultimate analysis and functional group content; Fulvic acid has a lower molecular weight, less

carbon and nitrogen, but more oxygen-containing functional groups (such as –COOH, –OH and >C=O) per unit weight than the other fractions. The chemical properties of humin appear to be similar to humic acid.

Some characterisation studies are carried out on the humic materials studied in this thesis. Several techniques are applied to determine their elemental proportions, and the identity of structural and functional units. Other studies are performed that concentrate on the acidic functional groups of the materials.

1.3.2 Colloidal Chemical Characteristics of Humic and Fulvic Acids

The macro-structure of aqueous dispersions of humic substances is condition-dependent: To obtain information on molecular sizes, shapes and weights of humic acids and fulvic acids, Ghosh and Schnitzer measured surface pressures and viscosities at various pHs and concentrations of humic materials and neutral salts.[11] They concluded that humic and fulvic acids are rigid, uncharged colloids at high humic concentration, low pH and high electrolyte concentration. However, at low sample concentration, high pH and low ionic strength, humic and fulvic acids are flexible, linear, negatively charged hydrophilic colloids, that is, polyelectrolytes.[4]

Chen and Schnitzer[12] observed the aggregation of fulvic acid particles with decreasing pH under a Scanning Electron Microscope (S.E.M.). Aggregation was explained by hydrogen bonding, Van der Waals forces and interactions between π-electron systems of adjacent molecules. As the pH increases, these forces become increasingly outweighed by the electrostatic repulsion due to the ionisation of –COOH and phenolic –OH groups; this results in the aggregates breaking up into smaller molecular arrangements.

Since 'dissolved' humic substances are in reality negatively charged hydrophilic colloids, one of their properties is the ability to be coagulated by electrolytes.[13] Ong and Bisque[14] explained this effect by the attachment of cations to the negatively charged groups of the humic colloid. This causes a reduction in the electrostatic repulsion within and between particles thus favouring their coalescence. Langford *et al*[15] found an increase in scattered light intensity when fulvic acid was coagulated by potassium

chloride.

Aqueous dispersions of humic substances are polydisperse with sizes ranging from colloidal to particulate. Here, the molecular weight of a humic acid is determined following fractionation. Further, the response of colloidal parameters to various sample and media conditions are studied by light scattering.

1.4 Environmental Significance of Humic Substances

Humic substances are of environmental importance for several reasons, a selection of which is described here. Considerable attention has focussed on the removal of dissolved humic substances from water supplies since pesticides can be solubilised, [16] chlorination of such waters produces toxic chloroform, [17,18] and coloured water is aesthetically objectionable. [19]

Humic substances have been implicated in the accelerated weathering of minerals since they degrade common soil minerals (e.g., biotite, muscovite, and kaolinite). [1,17,20]

The concentrations of trace elements in the soil solution are governed by a variety of reactions that include complexation, ion exchange, adsorption, acid-base equilibria, dissolution and precipitation. [21] A key role is often played by humic substances since complexation with metals can enhance the availability of nutritionally important trace elements leading to improved soil fertility and plant growth. [18] Trace metals that would ordinarily convert to insoluble carbonates or hydroxides under environmental conditions are found in concentrations far greater than normal solubilities due to the presence of humic substances. [17] Complexation to toxic trace metals in the environment can result in reduced toxicity effects associated with the 'free' metal ion. Yet, this can lead to the bioaccumulation of these metals.

1.4.1 Mechanisms of Interaction between Humic Substances and Metals or Minerals

Humic substances can interact with metal ions, metal hydroxides and minerals to form

metal-organic associations by several mechanisms.[4] The relatively large contents of oxygen-containing functional groups per unit weight, provide suitable interaction sites.[1]

Monovalent cations react with humic substances to form humate salts. With di– and tri–valent metals, chelation is also possible. Complexes are inner-sphere when the metal and ligand are directly attached, or outer-sphere if the metal is indirectly linked to the humic ligand by hydrogen-bonding through a water molecule in its primary hydration shell.

Mixed ligand complexes can be formed when a secondary ligand is present. In soil solutions phosphate, sulphate, bicarbonate, citrate, and salicylate are secondary ligands. Mixed ligand complexes are important in neutral and weakly acidic soil solutions for the transport of metal ions.

Humic substances can attack and degrade minerals through formation of complexes with their metal ions. The weathering of minerals in soils and sediments is often enhanced by their presence.[1,17,20]

The extent of adsorption of humic materials on mineral surfaces depends on the physical and chemical characteristics of the surface, the pH, and the water content of the system. A range of mineral-humic associations is probably involved, including chemical bonding and hydrogen bonding. Some cations on mineral surfaces may interact with humic and fulvic acid functional groups via water bridges.

1.5 Metal Ion Complexes

An important characteristic of a metal-organic complex is its stability or formation constant, the value of which provides a quantitative measure of the affinity of the metal for the ligand. Numerous problems are encountered in determining stability constants due to the nature of the humic ligand. Humic substances from any source are heterogeneous with respect to both size and shape, and a pH and ionic strength effect dictate the degree of ionisation of the acidic groups and consequently the number of sites available for binding.[22] Another complication is that several different classes of binding site may be

present. [17]

Several experimental approaches have been used to determine the binding capacity of humic substances for metal ions; These have been the subject of several reviews. [23,24] Van Dijk [25] noted that the capacity of humic substances to bind metal ions is approximately equal to the number of titratable hydrogen ions (that is, the total acidity) divided by the ionic charge of the interacting metal ions. Metals of the first transition series form complexes with humic substances whose stabilities are given by the Irving-Williams' series.

Humic substances can form soluble or insoluble complexes or colloids with radionuclides, including the actinide elements. These provide a mechanism by which radionuclides could leach from disposal sites resulting in the migration of the metal through the groundwater system back to the surface and the biosphere. [13,26–31]

The central theme to the research described in this thesis is the interaction of metal ions with humic materials. Most published studies with metal ions have been concerned with the s– and first row d–block elements which are experimentally accessible. Here, other metals are studied, particularly those that may be considered as analogues for actinide elements.

1.5.1 Analogues for Actinide Ions

The complexation of transuranic actinides with humic substances is of concern since it could influence the fate of these elements if leached from a radioactive waste repository. [13,26–31] Since the actinides are somewhat chemically inaccessible, and as it is difficult to predict their long term environmental behaviour, then analogues are required for such investigations. Krauskopf [32] summarised some criteria for the usefulness of analogues for actinides in the context of radioactive waste repositories: Of primary concern is the stability of its compounds in the appropriate oxidation state relative to those of its other available oxidation states, under the conditions of pH and redox potential to be expected in the groundwater that may invade a waste repository. The stability constants for their compounds and complexes, and the solubilities of their compounds should be of a similar order. This probably will require closeness of ionic

radii.

Inspection of the literature reveals that most citations concerning lanthanide metals associated with humic substances stem from their use as models for some trivalent actinides.[8,13,26,27,33–42] Mikheev *et al*[43] summarised some comparisons made between the lanthanides and the actinides. Bulman[44] believes that some trivalent lanthanides could serve as analogues for trivalent americium. This comparison was supported by Krauskopf[32] who noted that the actinides Am and Cm only exist as trivalent species in repository environments. The similarities between the two series of f–block elements are illustrated by the stability constants of their complexes, and the solubilities of their compounds. These derive from the closeness of their ionic radii, especially for the lighter rare earth elements. Krauskopf suggested that the analogy also could be extended to Pu^{III}. The most common oxidation state for actinides in the middle and end of the series—including Am and Cm—is trivalent; this is the dominant oxidation state among the whole lanthanide series.

Tetravalent is the most common oxidation state for plutonium in subsurface geological environments. The solid stable form is the dioxide and the principal dissolved species in equilibrium with it is the undissociated hydroxide. The element also exists in other oxidation states. Th^{4+} is considered as a good analogue for plutonium IV.[32] The metabolic effects of plutonium have been mimicked by substitution with hafnium,[45] and because of their similarities, hafnium and its congener zirconium should serve as good analogues for Pu^{IV}.

In the work described in this thesis, several heavy metals are studied that can be considered as analogues for some actinides; these are drawn from several transition metal series and from the lanthanides. However, this thesis does not attempt to correlate results obtained with those anticipated for comparable actinides. Europium is used as a probe of photophysical interactions with humic acids in aqueous media. Several heavy metals are used in two modes for nuclear magnetic resonance studies: First, praseodymium, europium, and ytterbium are employed as lanthanide shift reagents to other resonant nuclei; Secondly, accessible nuclei of scandium, yttrium, lanthanum and zirconium are themselves monitored by the technique.

1.6 Overview of Humic Substances Research

Research on humic substances is carried out by geochemists, biologists, chemists, and coal and soil scientists. Since many studies are directed towards a particular source of humic materials, an image of duplication of investigations exists. Most modern instrumental techniques have been applied to humic substances, but the success of such efforts—despite increased experimental sophistication—is limited by the inherent complexity of the materials. Several key research areas have been described in the discussion of the characteristics and properties of humic substances given so far.

One central issue is radioactive waste management. Areas of research need are the development of realistic models of radionuclide movement in the environment and an understanding of the chemical and physical processes important to the safe disposal of waste on land. A complication is that some studies of metal ion complexation have been too species- and site-specific.[27] UK NIREX has identified the complexation of radionuclides in the near-field as a particular concern. Natural organic materials have a key role.[46]

1.7 Background to the Humic Substances Studied

Several humic materials have been studied during this research. The samples used most extensively were obtained commercially whereas the others were donations from the sponsoring body, AEA Technology, and were used in specific investigations since limited supplies were available. In the course of the text the samples are sometimes referred to by codes, which are defined in Table 1.1. Background information concerning the samples and analytical data available from the suppliers of the commercial materials is detailed in the following Sections.

1.7.1 Fluka Humic Acid

This material has a terrestrial origin, but the location of its source and extraction method are not apparent. The ash content quoted by the supplier is 10–15 % and the molecular weight is 600–1000 daltons. Two batches were used in the research (see Appendix 1).

Table 1.1
Humic Material Sample Nomenclature

Sample Name	Sample Code
Fluka Humic Acid v1	FHA v1
Purified Fluka Humic Acid v1	PFHA v1
Fluka Humic Acid v3	FHA v3
Aldrich Humic Acid, Sodium Salt v1	AHA v1
Aldrich Humic Acid, Sodium Salt v2	AHA v2
Fanay—Augéres Fulvic Acid	FAFA
Fanay—Augéres Humic Acid	FAHA
Gorleben Gohy 573 Humic Acid	GGHA

Note
Supplier's Codes and Batch Numbers are given in Appendix 1

1.7.2 Aldrich Humic Acid

This material has a terrestrial origin, but again the location of the source and details of its extraction are not available. Analytical data for the composition of the major inorganic components in % w/w units are: [47]

Na	7·4	Fe	0·05	Mg	0·003–0·05
Ca	0·005–0·05	Si	0·004–0·008		

Not present: K, Li, Ba, B, Cu, Zn, Mn, P, Cr, Ni, Cd, Sr, lanthanides and actinides

On summation, these amount to an appreciable ash content. Use of 'sodium salt' in the name of the sample, and the high proportion of sodium in the analysis suggest that the final step in the extraction or pretreatment involved drying the organic matter at a non-acidic pH, or the sample was only partially washed. The material exhibits a melting 'point' greater than 300 °C. Two batches were used in this research.

1.7.3 Fanay-Augéres Fulvic and Humic Acids

These samples have been extracted from groundwater at Fanay-Augéres, France. This is the site of an underground research station where hydrogeological testing has been undertaken to assess the potential for disposal of long-lived radioactive wastes in the granite rock.[48] Some research efforts have been directed towards monitoring groundwater movement and radionuclide migration through deep groundwater sampling and analysis.

1.7.4 Gorleben Gohy 573 Humic Acid

This sample has been extracted from groundwater at the Gorleben salt dome, Germany. Research of suitable disposal sites for radioactive wastes in Germany has focussed on deep salt formations with most efforts directed towards the Gorleben salt dome.[48] This is currently a research centre but it is intended to be operational for the disposal of high- and intermediate-level waste by the end of the twentieth century.[30] Dissolved Organic Carbon in Gorleben groundwaters consists mainly of humic and fulvic acids present in a colloidal form closely associated with trace metal ions. The content of humic substances varies from less than 0·1 mg C dm^{-3} to ~100 mg C dm^{-3}.[28,29] Typical analyses show the presence of metal ions and inorganic anions as major components, and many trace metals. An analysis specific to the GGHA sample is not available, nor is its exact method of extraction and purification.

1.7.5 Usage of Commercial Humic Acids

Although some analytical data is available for the commercial samples, it is believed that this is not specific to the batches used in this study, but it is of a general nature. The sources of the commercial materials are not clear despite concern expressed to this end in the literature and personal efforts to locate such information.[49,50] Further, the pH values used to define the different fractions of the humic material in the extraction and purification procedures are not known, leading to some uncertainty in their composition.

The use of commercial humic acid samples has been criticised by some workers.[49,50] Their main concerns are that these materials are often naïvely assumed to be equivalent to soil or aquatic humic materials although they have little resemblance to them, and the

lack of information concerning their source and extraction means that it is not appropriate to attach geochemical or environmental significance to experimental results. Neither of these fallacies will be attempted in this work, yet the commercial samples remain useful for studies that are not directed towards a particular type of source material, and as a large mass of information from various investigations has been compiled enabling some comparisons and correlations to be made. Since these materials are to be studied extensively, it was decided to purify them so that greater certainty could be attached to their composition. Suitable approaches were located following reference to the literature.

1.8 Purification of Commercial Humic Acids

The generalised analyses of the humic acids given by Fluka and Aldrich in the previous Section show clearly that both commercial samples have a high ash content. This is probably inorganic material derived from the source where it is chemically associated with the humic material, or from the extraction and any purification procedure applied to the humic material by the supplier. Purification should reduce ash contents and provide some certainty to the composition of the materials by defining the alkaline and acidic solubility points, and by comparative analysis of the impure and purified samples. The approach and reagents used to purify the humic acids were selected following reference to reports of extraction and purification of humic substances.

Simple purification procedures are based on the steps of the classical fractionation procedure outlined in Figure 1.1. For a sample of impure humic acid, the humic and fulvic acid fractions must first be extracted from the humin and other insoluble matter. The main criterion for a useful extractant is that a large amount of unaltered organic material should be removed from the source. Alkalis have been used extensively as extractants since they extract around 80 % of soil organic matter as humic substances and their usage conveniently fit the definitions of humic substance fractions given in Section 1.2.1.[6] The solubility of humic substances in alkaline media is due to deprotonation of acidic functional groups and some uncoiling of the macromolecular structure. Salts of di– and trivalent metals associated with the humic material are insoluble in alkaline media and may then be separated. Alkaline extraction using 0·1 M $NaOH_{(aq)}$ forms part of the extensive extraction procedure recommended by the

International Humic Substances Society. Calderoni and Schnitzer [51] applied this scheme to a sediment sample. Alberts and Dickson [52] used the same concentration of extractant but Yong and Mourato [53] used 0·5 M $NaOH_{(aq)}$ to remove humic matter from sedimentary sources. Theng *et al* [54] used various reagents to extract humic acids from soil, and they analysed the products. The nature of the organic matter extracted as humic acids depended on the strength of extractant used, which was related to the pH of the reagent in aqueous solution and its ability to complex polyvalent metal ions. Gregor and Powell [55,56] used acidic pyrophosphate to extract soil fulvic acids. Other primary extractants used include organic solvents and chelating resins. [1,52]

The second treatment of the purification procedure involves precipitation of the humic acid. The International Humic Substances Society recommends precipitation to pH 1 by 6 M $HCl_{(aq)}$. [51] Midwood and Felbeck [57] separated humic acid from fulvic acid derived from aquatic organic matter at pH 1, but Yong and Mourato [53] used 8 M $HCl_{(aq)}$ to achieve pH 2 thereby defining their humic acid at a different acidity limit.

Consolidation of reported approaches and reagents prompted selection of an experimental strategy that applied the classical fractionation scheme using an alkali of concentration 0·1 M to effect dispersion at pH 13, and a monobasic acid of concentration 6 M to invoke precipitation at pH 1. These acidity conditions defined the limits for the fractions with the desired humic acid fraction between pH 1 and pH 13. The purification procedure was applied to Fluka Humic Acid v1 in the first instance, and experimental details are provided in Chapter 2.

1.9 Introduction to Experimental Work

The studies described in this thesis focus on selected aspects of the characteristics and properties of humic substances. The aim is not to provide a comprehensive coverage of the subject, but to probe some areas that have received little attention. Experimental approaches are outlined here; these are further developed following a detailed background in individual Chapters.

1.9.1 Chapter 2: Basic Measurements and Characterisation of Humic Substances

Some basic characteristics of the humic materials employed in the studies described in this thesis are considered. These aim to provide an understanding of the nature and behaviour of humic materials, and serve as a foundation to some advanced studies developed in other Chapters. The classical purification procedure discussed previously is applied to Fluka Humic Acid v1; the purified material is then analysed.

Elemental analysis, and moisture and ash contents, are determined by standard procedures to yield the elemental compositions of some humic acids. Infrared spectroscopy is used to deduce the nature of the backbone structure of humic materials and the identity of their functional groups through analysis of characteristic vibration frequencies. Thermal analyses are carried out on humic materials to gain an appreciation of their resistance to decomposition, and to determine the level and identity of the residual material following high-temperature degradation. This involves thermo-gravimetric analysis and residue analysis by infrared spectroscopy.

The dark colour of humic substances has prompted the use of light absorption for their analysis. A study of the ultra-violet and visible absorption by Fluka and Aldrich humic acids is undertaken to deduce the identity of their chromophores and provide wavelengths suitable for excitation of the humic matter in fluorescence studies. The fluorescence characteristics of humic substances are investigated to gain some understanding of the fate of absorbed radiation, and to provide background information for extended studies described in Chapter 3.

Aqueous dispersions of humic substances are polydisperse, therefore the best methods for determining their molecular weights provide a distribution that illustrates this polydispersity. The molecular weight profile and the weight average molecular weight of Aldrich Humic Acid are determined following fractionation by ultrafiltration. Ultra-violet absorbance is used to deduce the concentrations of the humic acid ultrafiltration fractions, and absorbance spectra in the visible and ultra-violet regions are recorded.

1.9.2 Chapter 3: Photophysical Studies of Energy Transfer between Europium(III) and Fluka Humic Acid

Humic substances fluoresce when excited by ultra-violet and visible light. Similarly, some lanthanide metal ions also fluoresce. When present in the same medium, these materials may form complexes or aggregates depending on the sample and media conditions. Trivalent europium is selected as a suitable luminescent ion and photophysical processes that result from irradiation of an aqueous medium also containing Fluka Humic Acid are investigated. This aims to provide information on the interaction between the ion and humic ligand through mechanistic modelling of the photophysical processes.

1.9.3 Chapter 4: Nuclear Magnetic Resonance Spectroscopy

Nuclear Magnetic Resonance (NMR) involves monitoring the magnetic properties of suitable nuclei. Several approaches using NMR of various nuclei are described thereby capitalising on the multinuclear nature of the technique; each approach is directed towards obtaining specific information. The structure and composition of humic materials are studied by the well-established techniques of proton and carbon–13 NMR spectroscopy in solution; This is extended to include use of lanthanide ions as shift reagents to derive extra information concerning their interactions with humic ligands in complexes. Carbon–13 spectra are also obtained for humic materials in the solid state, and in the presence of paramagnetic lanthanide ions. Finally, some studies are described using several metals as NMR nuclei to provide information about their environment in complexes with humic materials. NMR studies involving metals and humic materials have received little attention in the literature.

1.9.4 Chapter 5: Light Scattering

Aqueous dispersions of humic substances contain particles of colloidal dimensions. This enables the colloidal characterisation technique of Laser Doppler Electrophoretic Light Scattering to be applied to determine the effect of various sample and supporting medium conditions on the light scattered by such dispersions. Analysis and appropriate

manipulation of light scattering data provides electrophoretic mobilities, diffusion constants, particle sizes and zeta potentials for the humic materials. These parameters are correlated with the prevailing sample and media composition. A brief investigation of the refractive indices of humic materials is undertaken to deduce factors that influence the amount of light scattered by humic substances.

1.9.5 Chapter 6: Kinetics, Buffering and Mechanisms of the Potentiometric Titrations of Humic Acids

The chemical structure of humic materials is substituted by functional groups, the most abundant of which are carboxyls and phenolic hydroxyls. These are the main cause of the acidity of humic materials and their ability to bind metal ions on substitution. Many reports have been described that quantify the abundances and acidities of these functional groups by potentiometric titrations. Despite the widespread use of this approach, few researchers have justified their selection of end-points or commented upon the rate of equilibration following acid or alkali additions during such titrations. Experimental studies here examine the approach to equilibrium in potentiometric titrations of humic acids under various conditions. The potentiometric behaviour is analysed by applying kinetic considerations to experimental data, and mechanistic interpretations of protonation are derived. This aims to provide an understanding of operative processes through modelling of the experimental behaviour.

CHAPTER 2
BASIC MEASUREMENTS and CHARACTERISATION of HUMIC SUBSTANCES

2.1 Introduction

This Chapter considers some basic characteristics of the humic materials employed in the studies described in this thesis. These aim to provide some understanding of the nature and behaviour of humic materials, and serve as a foundation to some advanced studies developed in subsequent Chapters. Consideration is given to both physical and chemical characteristics of the materials.

2.1.1 Basic Characteristics

Some background to the origin of the humic materials studied was given in Section 1.7. All humic acids used were dark brown or black in colour whereas the fulvic acid sample was orange-brown. In solution-based experiments, the solubility of the humic materials was important but this varied for individual samples: The fulvic acid was quite soluble in water, as expected from the definition of this fraction; the resultant solution was acidic (pH ~3). The corresponding Fanay-Augéres Humic Acid could not be dispersed, even in 0·1 M alkali. This presumably reflects the purification procedure applied to the sample and its operational definition of the humic fraction. The commercial humic acids were soluble in alkaline media to ~2 % w/v, and once in a dispersed condition, adjustment of such a dispersion to a neutral condition did not result in destabilisation of the organic matter. The Aldrich humic acid was somewhat easier to disperse than the Fluka sample, possibly because of its pretreatment which results in it being supplied as a sodium salt.

2.1.2 Purification Procedure

The classical purification procedure discussed in Chapter 1 was applied to Fluka Humic Acid v1 using an alkali of concentration 0·1 M to effect dispersion at pH 13, and a monobasic acid of concentration 6 M to invoke precipitation at pH 1. Sodium hydroxide

was the chosen alkali, and hydrochloric acid was selected since it is a non–oxidising acid and therefore should not degrade the organic matter.

2.1.2.1 Experimental

~5 g of Fluka Humic Acid v1 was ground with a mortar and pestle in a nitrogen atmosphere (¢009)[1] until a uniform particle size was obtained. This material was dispersed in ~200 ml of ~0·1 M $NaOH_{(aq)}$ that was obtained by dissolution of sodium hydroxide pellets (¢010) in distilled water. Agitation by mechanical stirring and ultrasound over several hours resulted in a visually uniform dispersed state. Humin, which by definition is insoluble in alkali, was separated by filtration through a Whatman No. 1 qualitative filter paper. Some insoluble inorganic materials were probably removed at this stage. The filtrate, which contained humic and fulvic acids, was acidified to precipitate the humic acid with ~6 M $HCl_{(aq)}$ that was prepared by dilution of the concentrated acid (¢011). The pH 1 condition was checked with a doubly calibrated (¢012–015) pH electrode (¢016) attached to an electronic pH meter (¢017). Portions of the supernatant, which contained fulvic acid and some suspended humic acid, were centrifuged to separate any remaining humic acid. The solid humic acid portions were combined and filtered as above to separate the soluble fulvic acid from the humic acid residue. The humic acid was washed first with ~0·1 M $HCl_{(aq)}$, and then with distilled water until the washings were chloride free, as shown by a silver nitrate test (¢018). The humic acid was then transferred to an evaporating dish and dried over phosphorus pentoxide (¢019) in an evacuated desiccator until constant weight was attained.

2.1.2.2 Results

The yield of the purified Fluka Humic Acid v1 was 42 %. The solid was darker in colour than the impure material.

---

[1] Note: '¢' refers to details of a chemical or piece of apparatus (supplier, grade, manufacturer's code, product or model number, assay, etc.). See Appendix 1.

2.1.2.3 Discussion

The low yield reflects the success of the purification process. Some loss may be accounted for by the removal of organic matter as the humin and fulvic acid fractions which were evident as the first filtration residue and colouration in the second filtrate, respectively. These losses arise from differences in the definitions of the acidity limits (pH 13 and pH 1) from those presumably used by the supplier in their extraction procedure. Loss of inorganic components at this stage is also likely.

In the subsequent Sections, the purified and impure samples are compared to determine the success and effects of purification through analyses of their elemental proportions, ash content, water content, and spectroscopic absorbances of the functional groups and structural units of the humic acids. Further comments concerning the success of the purification procedure are given following these analyses in Section 2.8.

2.1.3 Basic Measurements and Characterisation

The characterisation experiments described in the subsequent Sections briefly investigate selected properties of humic materials rather than being extended studies. Some aspects are further developed in the following Chapters. The information derived from these studies is collated and summarised in the final Section of this Chapter.

2.2 Elemental Analysis

2.2.1 Introduction

Elemental analysis has been applied to batches of Fluka and Aldrich humic acids, and to a purified specimen of Fluka Humic Acid v1. The technique involves combustion of microgram quantities of the samples with subsequent gravimetric analysis of the products. These results are combined with analytical data for other components of the sample—such as moisture and ash determined by standard procedures—and computed to yield the elemental composition. This may be extended to provide the empirical formula of

the substance.

2.2.2 Experimental

Elemental analyses were carried out without pre–drying the humic acids. Microgram quantities were analysed ten times on the Carlo Erba Strumentazione Elemental Analyser (¢020) for carbon, hydrogen and nitrogen. Oxygen was not determined directly.

Standard tests used in coal science were adapted to provide analytical procedures for moisture and ash determinations.[58,59] Moisture was measured as the loss in mass by samples, rather than mass uptake by a desiccant. A crucible containing around a fifth of a gram of a humic acid was heated at 110 °C under vacuum for several hours, until constant mass was attained. Ash was determined by progressively heating the dehydrated humic acid in air to around 700 °C using an electric Bunsen (¢021), until the mass of the residue stabilised.

2.2.3 Results

Elemental analyses of carbon, hydrogen and nitrogen were averaged, and oxygen was determined by difference. The proportions of oxygen and hydrogen were then adjusted to account for their respective contributions to the moisture content, resulting in the moisture-free values quoted in Table 2.1.

2.2.4 Discussion

Analysis of the data in Table 2.1 shows that the materials studied have high proportions of carbon compared to the other elements. The compositions of the humic acids may be summarised through their empirical formulae that are referenced to one oxygen atom:

Fluka Humic Acid v1	$C_{4.3}\,H_{2.8}\,O_{1.0}\,N_{0}$
Purified Fluka Humic Acid v1	$C_{2.1}\,H_{1.2}\,O_{1.0}\,N_{<0.5}$
Aldrich Humic Acid v1	$C_{21.7}\,H_{11.7}\,O_{1.0}\,N_{0}$

Table 2.1
Elemental, Moisture and Ash Analysis of Humic Acids

Sample	Sample Content /% w/w						Atomic Ratio	
	C	H	N	O	H_2O	Ash	C:H	C:O
Fluka Humic Acid v1	49.6	2.7	0	15.3	11.3	21.2	1.5:1	4.3:1
Purified Fluka Humic Acid v1	55.9	2.8	<0.5	35.5	3.9	1.3	1.7:1	2.1:1
Aldrich Humic Acid v1	38.1	1.7	0	2.3	16.4	41.4	1.9:1	21.7:1

Notes:

(i) *C, H and N determined ten times and averaged. Ash and moisture determined once.*

(ii) *Oxygen calculated initially by difference.*

(iii) *H and O percentages are presented on a moisture-free basis.*

(iv) *Nitrogen content of PFHA v1 determined as <0.5 % but assumed to be equal to 0.5 % for the calculation of the oxygen proportion.*

Schnitzer [4] proposed an elemental analysis for a "model" humic acid that is an average of analyses reported for humic acids derived from a wide range of sources. When normalised to one oxygen atom, its empirical formula is: $C_{2.1}\ H_{2.1}\ O_{1.0}\ N_{0.1}\ S_{0.01}$

The samples studied here have much greater carbon-to-hydrogen and carbon-to-oxygen ratios than Schnitzer quoted. These values suggest that the commercial humic acids have fused aromatic backbones with little substitution. Balkas *et al* [60] similarly observed somewhat high C:H and C:O ratios for their batch of Fluka humic acid when compared to other samples. Elemental analysis of the Aldrich humic acid batch studied here shows an extremely low oxygen content compared to the value determined by Malcolm and MacCarthy [49,50] for their batch. Analytical data for Fluka humic acid (Table 2.1) gives higher C:H and C:O ratios than determined by both Malcolm and MacCarthy [49,50] and Balkas *et al.* [60]

Nitrogen analyses were recorded as zero for both unpurified humic acids. Other analyses of nitrogen for these samples report non–zero percentages. [49,50] The nitrogen content of purified Fluka humic acid was measured as <0·5 % for each of the ten analyses performed.

Analysis of Fluka humic acid purified by Weber and Wilson [61] using a similar procedure to that employed here reduced the ash content to 2·5 % w/w. Their C:O ratio is identical with that given in Table 2.1 for the Fluka humic acid purified in this study. It is notable that the batches of the humic acids are unlikely to be the same since their work was performed over ten years earlier.

Table 2.1 shows that the atomic ratios of the unpurified and purified Fluka humic acid samples are not identical. The carbon-to-oxygen ratio of the latter is half that of the former implying that the purified sample is twice as oxygenated. Reconsideration of the purification process may account for this since the alkaline extractant used provides some opportunity for oxidation of the humic matter. Further, it is likely that the humic matter filtered from the alkaline dispersion was humin. This fraction would have a lower level of functionality than the base-soluble humic acid, therefore resulting in an apparent increase in the oxygen content of the remaining humic acid fraction. Partly because of this further fractionation process, the purified Fluka humic acid sample was not extensively used in studies described in this thesis.

The application of elemental analysis to humic substances is limited by their heterogeneous nature and so only provides general compositional information. [62] As discussed, the results given in Table 2.1 are quite different from others reported. This suggests some level of uncertainty between batches of the commercial samples. Further examples of inconsistencies in elemental analyses are provided by Kumada [63] who observed discrepancies in the determination of elemental proportions by standard methods when analyses were carried out by the same workers. Greater differences resulted when different workers analysed the same samples. In a detailed study of elemental analysis, the proportions of carbon, hydrogen and nitrogen were correlated with the classification of the soil source. Further correlations were noted between visible absorbance and elemental composition.

Some error in the oxygen levels may be attributed to the derivation of its proportion by difference, rather than by direct measurement. It is notable that if Malcolm and MacCarthy's [49,50] carbon-to-oxygen ratios were derived by calculating oxygen by difference, the C:O value for Fluka and Aldrich humic acids would show a closer agreement with those of Table 2.1.

Infrared analysis of residues from the pyrolysis of humic acids (Section 2.4) suggests that oxygen forms part of the ash since vibrations characteristic of silicon-to-oxygen bonds are observed in their spectra. It is likely that the silicon-to-oxygen bonds derive from siliceous structures that existed in the undegraded humic acid, and not from bonds formed during pyrolysis. Therefore, the oxygen content calculated is that of the organic part of the sample since inorganic oxygen will not affect the measured value.

The value of the oxygen and hydrogen contents reported are reliant on the measured moisture level, which itself relies on measuring mass losses due solely to dehydration. However, it is unlikely that other components of the humic acids vaporise or degrade at 110 °C, thus the mass loss at this temperature is only accounted for by the loss of water.

The moisture contents of the unpurified acids show that water forms a significant proportion of their composition. Water is probably associated with polar functional groups and inorganic components of the samples. Its effect on the infrared spectra of humic acids is described in the following Section. It is notable that the purified humic acid has a low equilibrium water content, reflecting the low precipitation pH used during its purification procedure.

It would be difficult to use the thermogravimetric analysis data of Section 2.4 to calculate the water contents of the samples since they were continually heated in the pyrolysis programme, and therefore are unlikely to have reached an equilibrium mass at the chosen temperature, 110 °C. Inspection of the thermograms of Section 2.4 suggest that the mass losses at 110 °C were consequently much smaller than those measured here.

The method described for the measurement of ash provides lower results than from the thermogravimetric analysis data of Section 2.4. In the latter method, ash was determined at a higher temperature and therefore would be expected to result in smaller values. However, the comments concerning the non–attainment of equilibrium in moisture determinations are probably applicable here, therefore the values measured by heating to a constant mass are more reliable.

Purification of Fluka humic acid produced a large decrease in its ash content. Aldrich humic acid, which was supplied as the "sodium salt," has a very large ash that is mainly due to a high sodium content. The ash content determined for Fluka humic acid is greater

than the 10–15 % range quoted by the suppliers. Further comments concerning ash contents, and their chemical identities, are given in Section 2.4.4.7.

Malcolm and MacCarthy [49,50] analysed a different batch of Aldrich humic acid to that used here, and calculated the sum of the elemental proportions to be 123 %, when oxygen was determined directly. They suggested that the poor result was caused by overestimation of the oxygen content and the high level of ash in the sample. They stated that ash contents of greater than 10 % tend to result in total elemental percentages with greater than 5 % error. They concluded their study of the elemental analyses of several commercial humic acids by suggesting that the samples originate from a common type of source material that is different from soil or stream humic acids. This was supported by results from infrared and nuclear magnetic resonance spectroscopy (see Section 2.3 and Chapter 4).

2.2.5 Conclusions

Elemental analysis has been applied to representative batches of commercially obtained Fluka and Aldrich humic acids. These samples have high proportions of carbon relative to other elements implying that they are predominantly aromatic. Other studies in this Chapter also investigate the nature of the carbon skeleton of the humic material and probe the functional form of the constituent elements.

Moisture and ash form a large proportion of the composition of the samples. Purification of Fluka humic acid succeeded in reducing the ash content of the sample, but the atomic proportions also changed because of the solubility-based fractionation procedure.

Some attention was paid to sources of procedural error in the determination of elemental analyses. Inconsistencies between representative batches of commercial samples was highlighted as a particular problem.

2.3 Infrared Spectroscopy

2.3.1 Introduction

Humic materials have been analysed by infrared spectroscopy to determine the nature of their backbone structures and the identity of their functional groups. The technique involves the selective absorption of radiation from the infrared region of the electromagnetic spectrum (2·5–25 μm, 4000–400 cm^{-1}) by substances. Absorbance produces changes in the vibrational (and rotational) movements of certain functional groups and structural features. Infrared frequencies not absorbed by a substance are transmitted. This information is usually presented as a spectrum of transmitted relative to incident light intensity against frequency, in wavenumber units. [64]

Use of the technique stems from the ability to deduce the existence of bonds within a sample from the presence of their characteristic vibrational frequencies as absorption bands in the infrared spectrum. The frequencies of each vibrational mode for a given bond are determined by the masses of the atoms, the strength of the bond and the specific nature of the vibration. It should be noted that vibrational frequencies for a given bond occur across a range of frequencies due to variation in the nature of neighbouring functional groups or the backbone structure of the sample. This often leads to multiple interpretations of spectral features.

The infrared spectra of several humic acids, a purified humic acid, a fulvic acid and a complex between a trivalent metal ion and a humic acid, have been run on a Fourier transform spectrophotometer. In this equipment, infrared light from a suitable source passes through a scanning Michelson interferometer and is detected. Fourier transformation of the detected radiation converts the resultant interferogram from the time domain to give a plot of intensity against frequency. When a sample is placed in the beam it absorbs its resonant vibrational frequencies, so that their intensities are reduced in the interferogram, and the ensuing Fourier Transform is the infrared spectrum of the sample. [64,65]

2.3.2 Experimental

Samples of humic materials were desiccated by phosphorus pentoxide (¢019) under vacuum before infrared analysis. A small amount of the sample was mixed with some oven-dried spectroscopic or infrared grade potassium bromide (¢022,023) that was ground to a powder of apparent uniform particle size using an agate pestle and mortar. The homogenised mixture was pressed in a suitable die under a ten ton load to produce a circular disc containing the humic material distributed within the KBr matrix.

Infrared spectra were run on a Perkin-Elmer 1710 Fourier transform spectrophotometer (¢024,025). The collection of data and subsequent transformation to a spectrum for each sample was followed by acquisition of a spectrum for the prevailing atmospheric gases, which were then subtracted from the sample spectra. This was achieved by automatic movement of the sample shuttle in and out of the beam for successive sampling periods. An averaging routine on the resultant subtracted spectra was performed to provide greater improvement in signal-to-noise ratios through the reduction of random noise. Spectra were generally adjusted by routines available on the spectrometer Data Station (¢026) that permitted flattening and expansion of the spectrum to fill the abscissa scale. A further option is storage of the spectrum and subsequent investigation of its peaks through databases of correlation charts.

2.3.3 Results

Table 2.2 provides an analysis of the location, vibrational modes and corresponding assignments of the infrared spectral peaks relevant to humic substances.[1,6,60,64,66,67] Spectra of the humic materials are given in Figures 2.1–2.8 as transmittance against frequency (wavenumber).

2.3.4 Discussion

The infrared spectra presented in Figures 2.1–2.8 have been interpreted using the table of relevant peak identities given in Table 2.2. Interpretations will be provided for each

Table 2.2
Infrared Spectral Peaks, Vibration Modes and Assignments

Frequency Range (Wavenumber) / cm^{-1}	Vibration Mode	Assignment
3500–3100	N–H *str*	Primary and secondary amines and amides
3400–3300	O–H *str*	Alcohol, phenol, water
3100–3000	C–H *str*	Alkene and aromatic
3000–2850	C–H *str*	Alkane and alkyl
3000–2500	O–H *str*	Hydrogen bonded carboxylic acid
2900–2700	C–H *str*	Aldehyde
1800–1650	C=O *str*	Carboxylic acid, amide, aldehyde, ketone
1700–1630	C=O *str* & N–H *def*	Primary, secondary and tertiary amide
1650–1560	C≈O *str anti*	Carboxylate
1650–1560	C=O *str*	Quinone or ketone with conjugated C=C or COO⁻
1650–1550	N–H *def*	Primary amine
1650–1450	C≈C *str*	Aryl
1650–1630	O–H *def*	Hydroxyl (water)
1500–1350	C–H *def*	Alkane, alkyl, alkene
1450–1400	C=O *str* & N–H *def*	Primary amide
1400–1300	C≈O *str symm*	Carboxylate
1400–1100	C–O *str* or O–H *def* (coupled)	Phenol
1400–1000	C–O *str* or O–H *def* (coupled)	Alcohol
1350–1250	N–H *def*	Primary, secondary and tertiary aryl amine
1300–1200	C–O *str* or O–H *def*	Carboxylic acid
1170–950	Si–O	Silicate impurity
1000–800	C–H *def* (out of plane)	Alkene
850–700	C–H *def* (out of plane)	Aryl

Key to Vibration Modes

str = stretch; def = deformation;
symm = symmetrical; anti = antisymmetrical

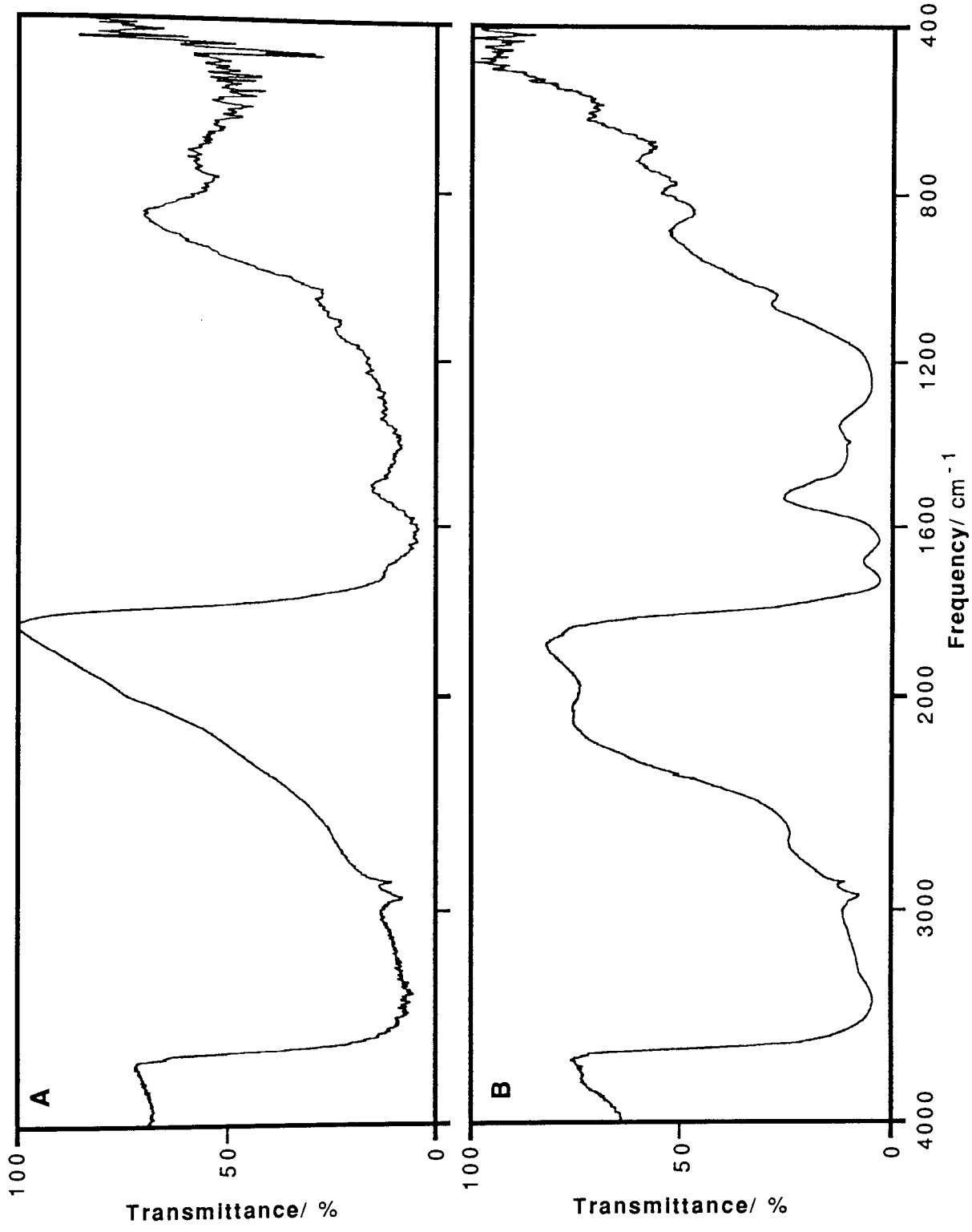

Figures 2.1 & 2.2

Fluka Humic Acid v1 and Purified Fluka Humic Acid v1 Infrared Spectra

A Figure 2.1 Fluka Humic Acid v1 (FHAv1) Infrared Spectrum

B Figure 2.2 Purified Fluka Humic Acid v1 (PFHAv1) Infrared Spectrum

Spectral Acquisition Conditions: Resolution = 4 cm $^{-1}$; Number of scans = 10
Sample Format: KBr pressed disc

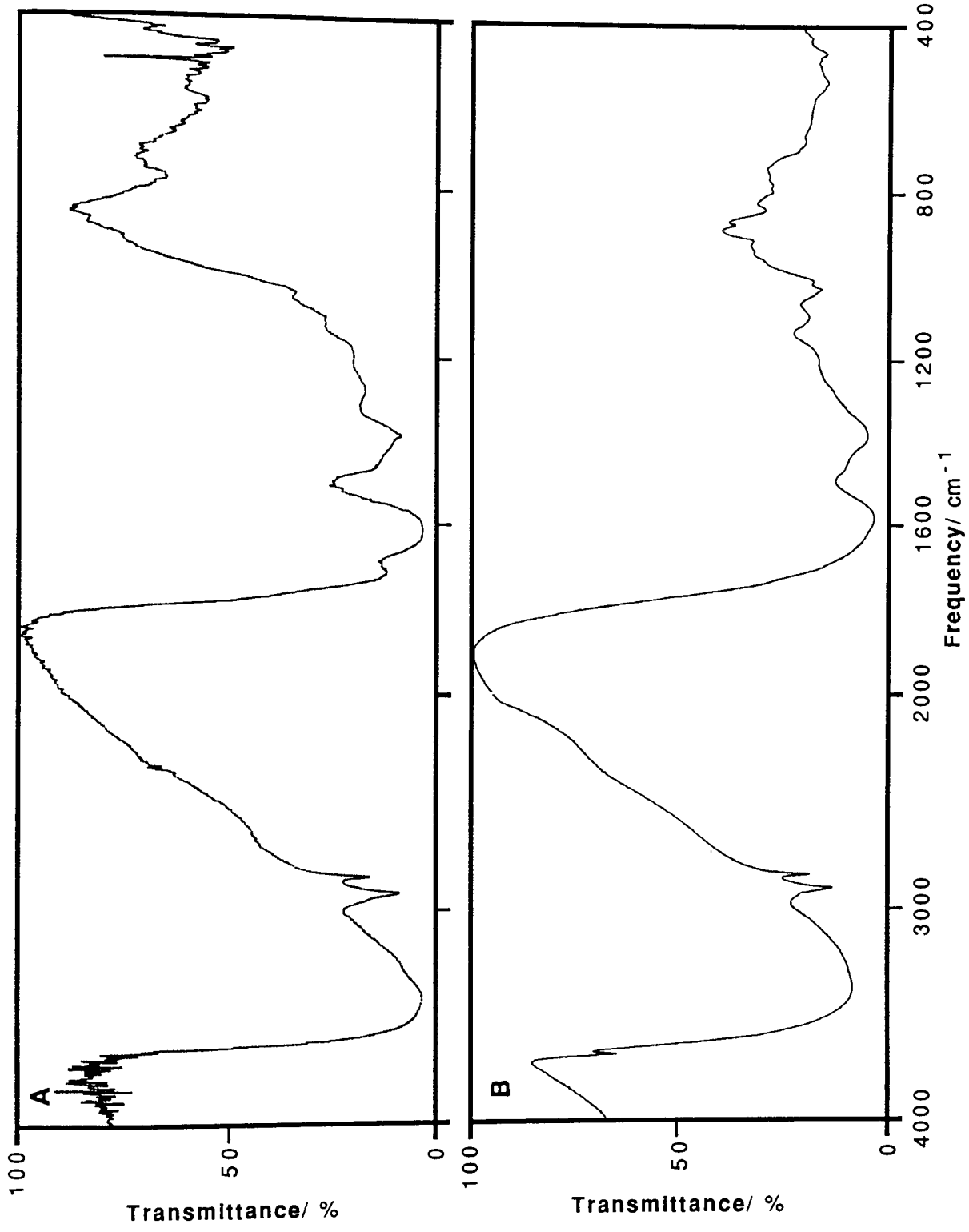

Figures 2.3 & 2.4

Fluka Humic Acid v3 and Aldrich Humic Acid v1 Infrared Spectra

A Figure 2.3 Fluka Humic Acid v3 (FHAv3) Infrared Spectrum

B Figure 2.4 Aldrich Humic Acid v1 (AHAv1) Infrared Spectrum

Spectral Acquisition Conditions: Resolution = 4 cm $^{-1}$; Number of scans = 10
Sample Format: KBr pressed disc

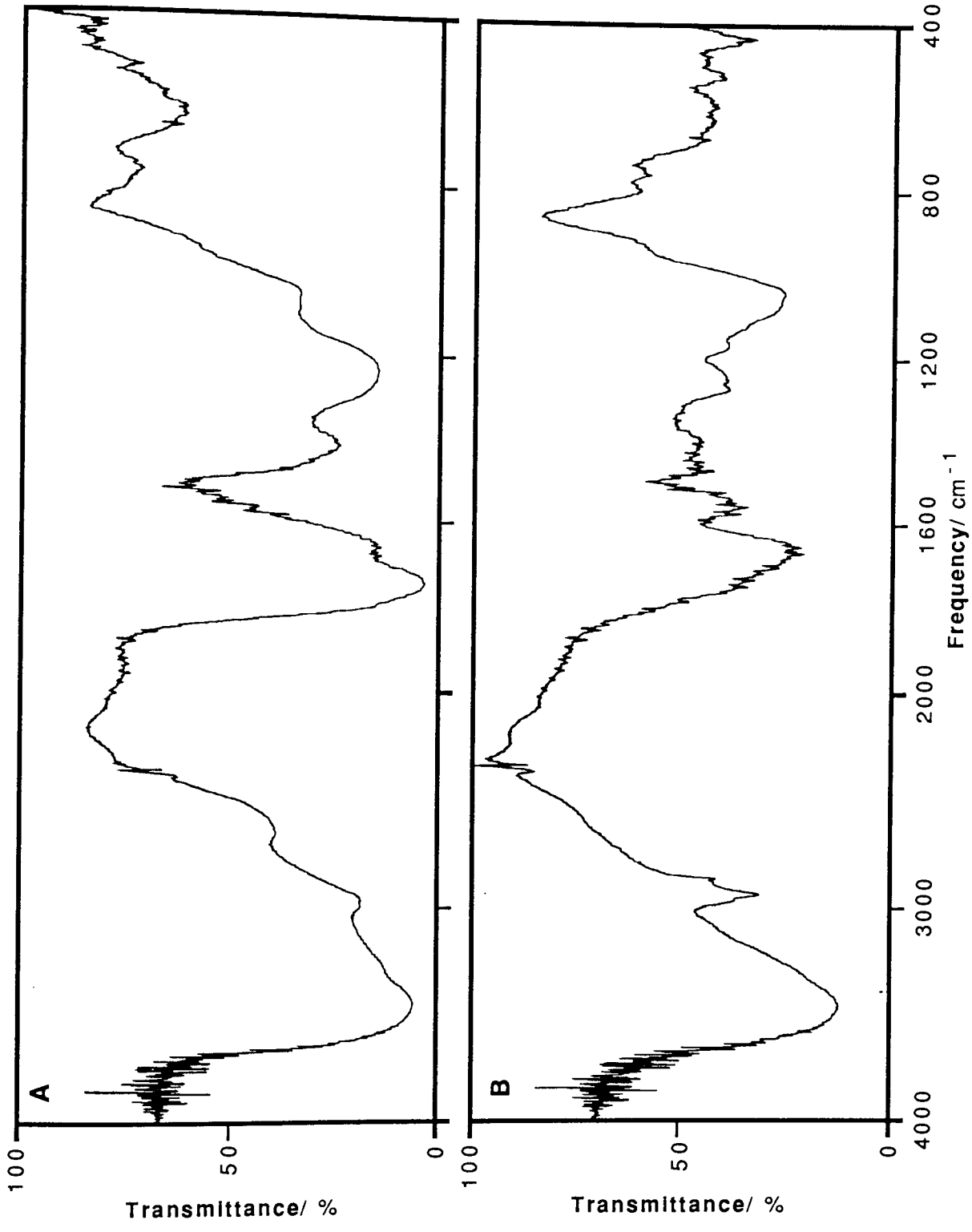

Figures 2.5 & 2.6

Fanay Augéres Fulvic Acid and Fanay Augéres Humic Acid Infrared Spectra

A Figure 2.5 Fanay Augéres Fulvic Acid (FAFA) Infrared Spectrum

B Figure 2.6 Fanay Augéres Humic Acid (FAHA) Infrared Spectrum

Spectral Acquisition Conditions: Resolution = 4 cm $^{-1}$; Number of scans = 10
Sample Format: KBr pressed disc

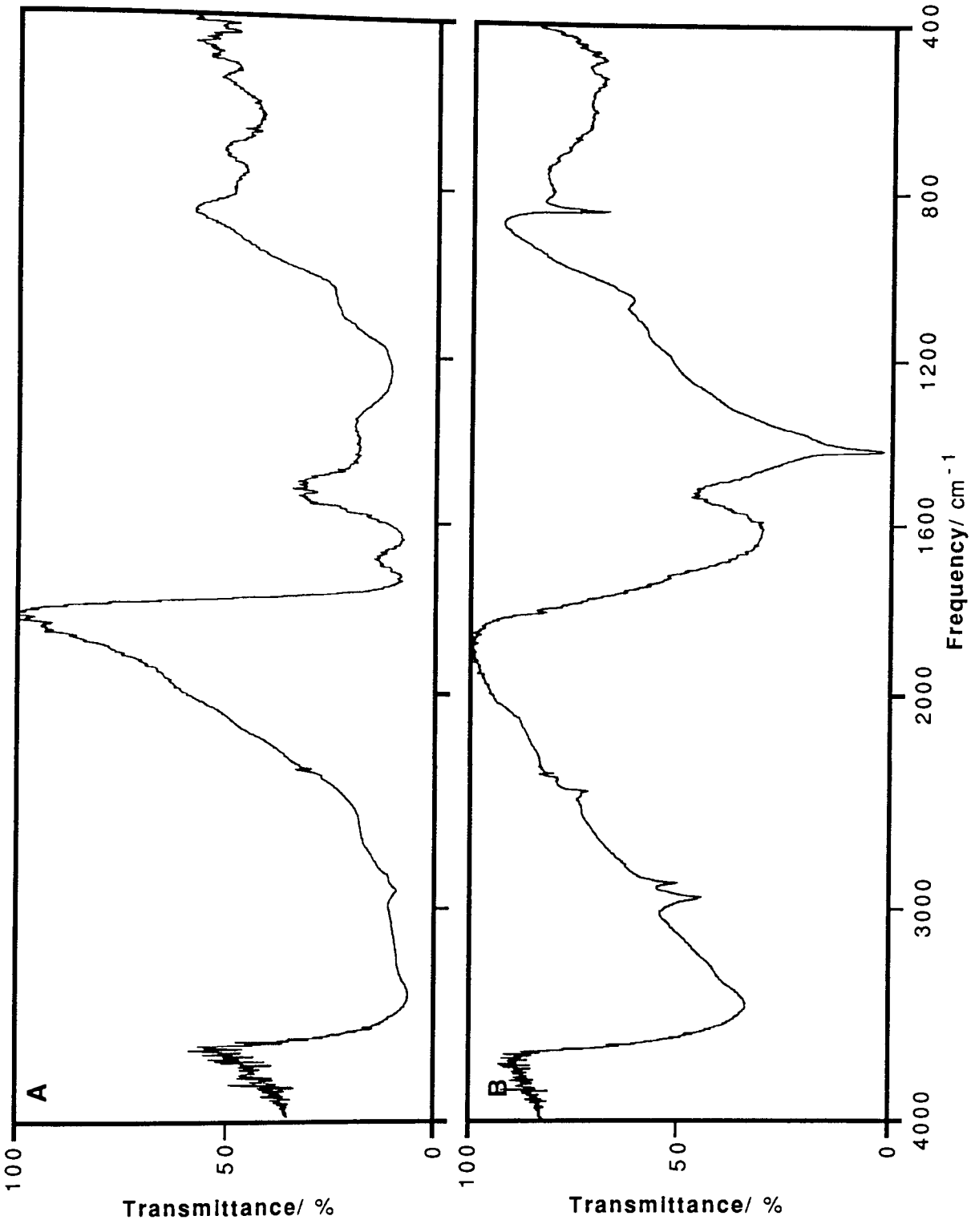

Figures 2.7 & 2.8

Gorleben Gohy Humic Acid and Europium(III)-Fluka Humic Acid v3 Complex Infrared Spectra

A Figure 2.7 Gorleben Gohy Humic Acid (GGHA) Infrared Spectrum

B Figure 2.8 Europium(III)-Fluka Humic Acid v3 Complex (Eu-FHAv3) Infrared Spectrum

Spectral Acquisition Conditions: Resolution = 4 cm $^{-1}$; Number of scans = 10
Sample Format: KBr pressed disc

sample following some general comments. The most striking feature of the infrared spectra of humic substances compared to pure organic compounds is their simplicity. The spectra consist of few bands, most of which are broad. Humic substances are complex mixtures of closely related compounds so that a particular functional group or structural feature can exist in a variety of chemical environments, each characterised by slightly different force constants. These individual bands overlap considerably producing the broadness and apparent simplicity of the spectra.[66] Acquisition of the spectra on a Fourier Transform Infrared Spectrometer has succeeded in producing higher spectral definition than dispersive infrared, due to both the higher energy throughput and an improved signal-to-noise ratio. The superior resolution of the instrument has not been of importance since the peaks are broad.[66]

The infrared spectrum of Fluka Humic Acid v1 (Figure 2.1) suggests that the material is predominantly aliphatic. Evidence for alkyl carbon-to-hydrogen bond stretching is observed at high wavenumber, and deformations of the same bonds occur at 1397 cm^{-1}. The latter may be caused to some extent by alkene carbon-to-hydrogen bonds. The spectral feature centred at 769 cm^{-1} suggests that some of the carbons are aromatic. Further information concerning the nature of the carbon skeleton is not apparent from these studies, however, this has been obtained by others from second derivative infrared spectra.[68,69] The infrared spectrum reflects the preponderance of oxygen-containing functional groups. The broad band at 3400 cm^{-1} represents the region where hydrogen bonded O–H stretching occurs. Hydrogen bonding results in broader bands due to the statistical distribution in the extent of hydrogen bonding in a system of molecules.[66] Hydrogen bonding is associated with hydroxyl stretching in alcohols, phenols or imbibed water. Primary and secondary amines and amides also absorb infrared radiation in this region, however, their contribution is probably small since the elemental proportion of nitrogen in the sample is low (see Section 2.2). The carbon-to-hydrogen bond stretch at 2850 cm^{-1} may also be accounted for by aldehyde functionality. Carboxylate groups are present since both the antisymmetric (1588 cm^{-1}) and symmetric (1397 cm^{-1}) stretching modes appear in the spectrum. The carboxylate groups are probably associated with residual metal ions in the sample. Note that there is little evidence for the protonated carboxylic acid form. The occurrence of quinone or conjugated ketonic structures are possible since their carbonyl stretching frequencies coincide with the 1588 cm^{-1} carboxylate band. Functional groups involving nitrogen are suggested by a shoulder at 1700 cm^{-1} that may be caused by an amide group, and the region between

1550 and 1650 cm^{-1} that may be explained by primary amine functionality. Primary amides, alcohols and phenols also absorb around 1397 cm^{-1}, the wavenumber region for the second carboxylate band.

The purified Fluka Humic Acid v1 has a similar backbone structure to the raw material. Inspection of Figure 2.2 suggests that this is unaffected by the purification process, however infrared spectroscopy is not sufficiently sensitive to provide specific structural information. The functionality of the purified sample bears a significant difference since bands corresponding to carboxyl groups are now observed at 2630 cm^{-1}, 1714 cm^{-1} and 1245 cm^{-1}. This correlates with the data suggesting a reduction in the metal ion content of the sample (see Section 2.2). However, the presence of bands at 1588 cm^{-1} and 1397 cm^{-1} implies that some of the carboxyl groups remain in their dissociated carboxylate form. Theng *et al*[54] found that the absorbance of the carbonyl band at 1720 cm^{-1} in humic acid spectra, and of the carboxylate band at 1380 cm^{-1} in the spectrum of the corresponding potassium salt, could be correlated with the exchange capacity of the humic acid. MacCarthy and Malcolm[50] similarly noted an increased absorbance of the carboxyl group when the ash content of a humic acid was reduced.

Bands in the infrared spectrum of Fluka Humic Acid v3 suggest similar structure and functionality to the first batch, FHA v1. The bands are not as broad in the second batch possibly reflecting less hydrogen bonding due to a reduced water content.

Infrared analysis of Aldrich Humic Acid v1 suggests that this material is predominantly aliphatic, although evidence for alkene and aryl out-of-plane carbon-to-hydrogen deformations are observed at low wavenumber. Functionality is similar to both Fluka humic acid samples (FHA v1 and FHA v3) with broad features corresponding to carboxylate group stretching modes at 1380 cm^{-1} and 1550 cm^{-1}, and hydroxyl group vibrations at 3400 cm^{-1}, 1200 cm^{-1}, 1095 cm^{-1} and 1000–1050 cm^{-1}. The presence of functionality involving other carbonyl groups, nitrogen atoms and silicon to oxygen bonds also may occur.

MacCarthy and Malcolm[50] stated that infrared spectra of Fluka and Aldrich humic acids are similar to each other, and to Wyoming dopplerite. Their batch of Fluka humic acid was in the salt form, like the batch studied here. Similarities between other commercially available humic acids were observed using infrared spectroscopy suggesting that the technique is not sufficiently sensitive to discriminate commercial humic acids. However,

differences between them were observed using other techniques.

The infrared spectrum of Fanay-Augéres Fulvic Acid (Figure 2.5) has broader bands than the corresponding Humic Acid (Figure 2.6), possibly due to more extensive hydrogen bonding. The broadness of the bands in the fulvic acid sample makes it uncertain whether features equivalent to those in the humic acid are present. The infrared spectra of the samples suggest that the materials are predominantly aliphatic since alkyl carbon-to-hydrogen bond stretching occurs at 2930 cm^{-1} in the humic sample. Both samples absorb at 1400 cm^{-1}, a frequency that may be correlated with aliphatic carbons. The spectral features between 700 cm^{-1} and 800 cm^{-1} suggest the presence of aromatic carbons, but there is no evidence for alkene carbon atoms. Several functional groups are present but their compositions in the humic and fulvic samples are not identical. The very broad absorption at high wavenumber correlates with hydrogen bonded hydroxyl stretching in alcohols, phenols or imbibed water. Primary and secondary amines and amides also absorb infrared radiation in this region. The band at 2860 cm^{-1} in the humic acid also may be accounted for by carbon-to-hydrogen bond stretching in the aldehyde functional group. This feature is not observed in the poorly resolved fulvic sample. The fulvic acid shows the presence of both carboxyl and carboxylate groups whereas the humic sample only contains the latter. Carboxyls absorb at 2630 cm^{-1}, 1719 cm^{-1} and 1250 cm^{-1}, whereas carboxylates absorb at 1650 cm^{-1} and around 1400 cm^{-1}. Note that the strength of both bands in the spectrum of the fulvic sample is greater than in the humic acid spectrum, thus suggesting a greater abundance of these functional groups in the fulvic acid. The carboxylate groups are probably associated with residual metal ions in both samples. The presence of quinone, conjugated ketonic structures, hydroxyl groups, amines and amides are possible since they coincide with some of these bands. The humic acid shows an absorbance at 1540 cm^{-1} that is not observed in the fulvic sample. This may be accounted for by a stretching vibration between aromatic carbon atoms or the deformation of a nitrogen-to-hydrogen bond in a primary amine. Low wavenumber features at 1050 cm^{-1} in the humic acid and 1080 cm^{-1} in the fulvic acid are probably due to hydroxyl groups or the presence of siliceous impurities.

The infrared spectrum of the Gorleben Gohy Humic Acid sample is simplistic since the bands are very broad (Figure 2.7). Evidence for alkyl carbons in the backbone structure of the sample derives from the presence of a carbon-to-hydrogen stretch at 2926 cm^{-1}

and the carbon-to-hydrogen deformation around 1400 cm^{-1}. Note that there are no bands corresponding to aromatic or alkene carbon-to-hydrogen stretches in the 3000–3100 cm^{-1} region of the spectrum. Deformations of hydrogen atoms attached to aromatic carbons are apparent at 780 cm^{-1}, but no evidence for the corresponding alkene vibrational mode is apparent. The main functional groups in the sample are the oxygen-containing carboxyl and carboxylate. The presence of both suggests that the material is in a partially dissociated form. Hydroxyl functionality is apparent from the spectrum. Other likely functional groups are quinones, conjugated ketones, amides, and hydroxyls since some of their resonant vibrational frequencies coincide with the characteristic absorptions of carboxyl and carboxylate groups. The presence of silicate impurities is also likely.

Complexation of trivalent europium to Fluka Humic Acid v3 changed the infrared spectrum such that carboxylate bands at 1385 cm^{-1} and 1579 cm^{-1} dominate the spectrum. There is no evidence for bands associated with the corresponding protonated carboxyl forms. These spectral changes are characteristic of complexation of metal ions to humic substances [5,68,70]. A new band at 836 cm^{-1} not observed in the spectrum of the free ligand is probably due to bonding involving the metal ion. Byler *et al* [68] noted differences in the frequencies of carboxylate vibrational modes on binding of ferric ions to a fulvic acid in second derivative infrared spectra of a very large number of scans. Uncertainty in the location and width of carboxylate bands here prevents an investigation of these effects. Boyd *et al* [71] made similar observations on complexation of cupric and ferric ions to a humic acid. Their studies were extended to suggest that the mode of binding was through a unidentate complex rather than bidentate or bridging complexes for the conditions studied.

2.3.5 Conclusions

Infrared spectroscopy of humic materials contradicts the elemental analyses reported in the previous Section since results here imply that the humic and fulvic acid samples studied are predominantly aliphatic, although some evidence for aromatic and alkene carbons was observed. However, the spectra provide little information concerning the precise chemical structure of the humic and fulvic nuclei. The samples are functionalised mainly with oxygen-containing groups such as carboxyl, carboxylate, hydroxyl and other

carbonyls. The main effects of purification and complexation of Fluka humic acids are manifested in the conversion between carboxyl and carboxylate groups in their spectra. The infrared spectra of a fulvic and humic acid from the same source have been compared. The nature of both structures appears to be the same, but the fulvic acid is more functionalised than the humic sample. The similarities presumably derive from their difference being of a procedural, not chemical, designation.

Studies described in the following Section apply infrared spectroscopy to determine the nature of pyrolysis products of humic materials.

2.4 Thermal Properties

2.4.1 Introduction

Thermal analyses have been carried out on humic materials to gain an appreciation of their resistance to decomposition, and to determine the level and identity of the residual material, or ash, following high-temperature degradation. Analysis of thermal properties has involved thermogravimetric analysis (T.G.A.) for a detailed assessment of the thermal stability and ash content of the materials.

2.4.2 Experimental

Thermal Analyses of commercial humic acids, a purified humic acid, and a metal ion complex with a humic acid have been carried out on a Stanton Automatic Thermo-Recording Balance (¢027).

A Vitreosil silica crucible was used as the sample container for thermogravimetric measurements. A full heating cycle to 1000 °C was applied to the empty crucible to determine its mass loss over this temperature range. The values derived from this measurement are required for the correction of sample weight loss data. The humic solids were ground to a uniform particle size and a representative fraction was distributed evenly in the base of the crucible. Generally less than one micro-spatula of the material was employed. The amount selected was limited by the maximum weight loss range of the

thermobalance (100 mg) and the anticipated weight loss of the crucible itself over the temperature span of interest. It was appreciated that large sample masses would impede the diffusion of released gases. The chosen initial sample mass was measured on an analytical laboratory balance.

Samples were heated in air under the prevailing atmospheric pressure and humidity, without a crucible lid. The thermobalance was used in the "Auto-Operate" mode which added weights automatically to the balance to compensate for the weight loss of the sample. This weight loss, and the corresponding temperature, were recorded in parallel against a time base. The visual appearance of the sample during heating cycles was monitored at intervals. Note that cooling curves for the samples were not recorded.

The heating rate and the maximum attainable temperature were not independently controllable. Generally several heating ranges were employed in a complete cycle thus avoiding excessive heating rates through lower temperatures. Heating to 1000 °C typically took in excess of three hours. The temperature measured by the thermocouple was that of the furnace wall, which was some distance from the crucible. Some attention was paid to the possibility of discrepancies between the thermocouple temperature and that of the sample. This was investigated using a wide range mercury-in-glass thermometer located above the sample zone, and through the vaporisation of sulphur as a temperature marker (¢028).

Following heating to the required temperature of study, the furnace was switched off and allowed to cool. After sometime, the crucible was removed, placed on an aluminium heat sink and stored in a desiccator over phosphorus pentoxide (¢019) for several hours. Once cool, the crucible and heated residue were reweighed on an analytical balance to confirm the total mass loss of the sample. The degraded sample was retained for infrared spectroscopic analysis. A second pyrolysis run on the thermobalance would not be attempted until several hours had elapsed to allow a sufficient cooling period for the furnace.

Infrared spectra of the degraded humic residues were recorded on the Perkin-Elmer 1710 F.T.I.R. Spectrometer (¢024) in the manner described in the previous Section. Potassium bromide (¢022,023) was used as a support. KBr blanks were routinely run to assess spectral purity.

2.4.3 Results

Data was read from the T.G.A. charts of weight loss and the corresponding temperature against time to permit the calculation of true weight losses (which make an allowance for the crucible weight loss), and then to present the data in selected formats. No further attention was paid to the time axis since several heating cycles were generally employed in a complete pyrolysis programme.

Based on personal communications and confirmatory measurements, the temperatures recorded on the T.G.A. charts were believed to be accurate above around 150 °C. Therefore, for weight loss data corresponding to temperatures above this value, data was recorded directly from the charts. For temperatures below 150 °C, the chart coverage appeared to be too large compared to the true temperature. Temperatures in this range were recalculated based on the fixed points of 150 °C and the initial room temperature, which was measured with a mercury-in-glass thermometer. A combination of the speed of the chart paper, and the rate of change of sample weight and temperature, signified that the maximum resolution of the temperature data over a typical heating cycle was 10 °C. Weight losses were tabulated against the corresponding temperatures using this interval.

A sample set of data has been tabulated in Appendix 2 to illustrate the procedures employed in the derivation of appropriately formatted data sets. Sample weight losses recorded from the charts are given in the second data column. The third column provides the weight losses of the crucible used in these studies when heated to 1000 °C. This data set has been fitted by a least squares procedure to eliminate inconsistencies. True sample weight losses were calculated by subtraction of the crucible weight loss at a given temperature from the corresponding sample weight loss. Positive weight losses derived from this calculation have been truncated to zero. This generally affects just the first few points of the data series and arises from the fitting procedure applied to the crucible weight loss data. Smoothed true weight loss data is presented in the next column. Smoothing is performed by averaging the weight loss data around a temperature, T. For example, considering a smoothing range of seven points, true weight loss data at (T–30), (T–20), (T–10), T, (T+10), (T+20), (T+30), are averaged and presented as the smoothed true weight loss data point at T. Note from the data set that smoothing removes points corresponding to the upper and lower temperature values for which there is

insufficient data to perform this operation. Smoothed true weight loss data has also been truncated where positive points arise, as necessary.

Percentage weight losses have been calculated by division of true weight losses at each temperature by the initial mass of the sample. The data in Table A2.1 has been smoothed and truncated to the limits of 0 to −100 % w/w.

The final data format is a first derivative of the true weight loss with respect to temperature. This data set shows the rate of weight loss from the sample with respect to a constant temperature interval. Data has been calculated by the formula:

$$\text{Derivative Weight Loss}_{(T)} = \frac{\text{Weight Loss}_{(T+10)} - \text{Weight Loss}_{(T-10)}}{20}$$

The calculated derivative data point is quoted at temperature T, in units of mg/°C. As before, smoothing of data points is used, but the data has not been truncated since the derivative could feasibly assume positive values corresponding to some gain in sample mass. An alternative derivative format of weight loss with respect to the current weight has been calculated, but is not included here.

The formats employed in graphs presented here use a combination of percentage weight loss and derivative weight loss abscissa scales to help the revelation of features in the pyrolysis curves, such as rapid weight changes. The smoothing interval has been selected to remove scattered data without removing genuine features of the curves. In the combination graphs, a compulsory curve-fitting exercise in invoked resulting in a point-to-point interpolated fit.

Total mass losses for the heating sequence applied to samples measured on an analytical balance have been correlated with those determined from the T.G.A. data sets. These, and calculated ash contents for both methods, are reported in Table 2.3.

2.4.4 Discussion

Thermograms for two test samples are included as it was necessary to confirm the

Figure 2.9
Sulphur Thermogram

(% Weight Loss Data: 3—Point smoothing and truncation outside 0 % ≥ Losses ≥ -100%)
(Derivative Data: 3—Point smoothing but untruncated)

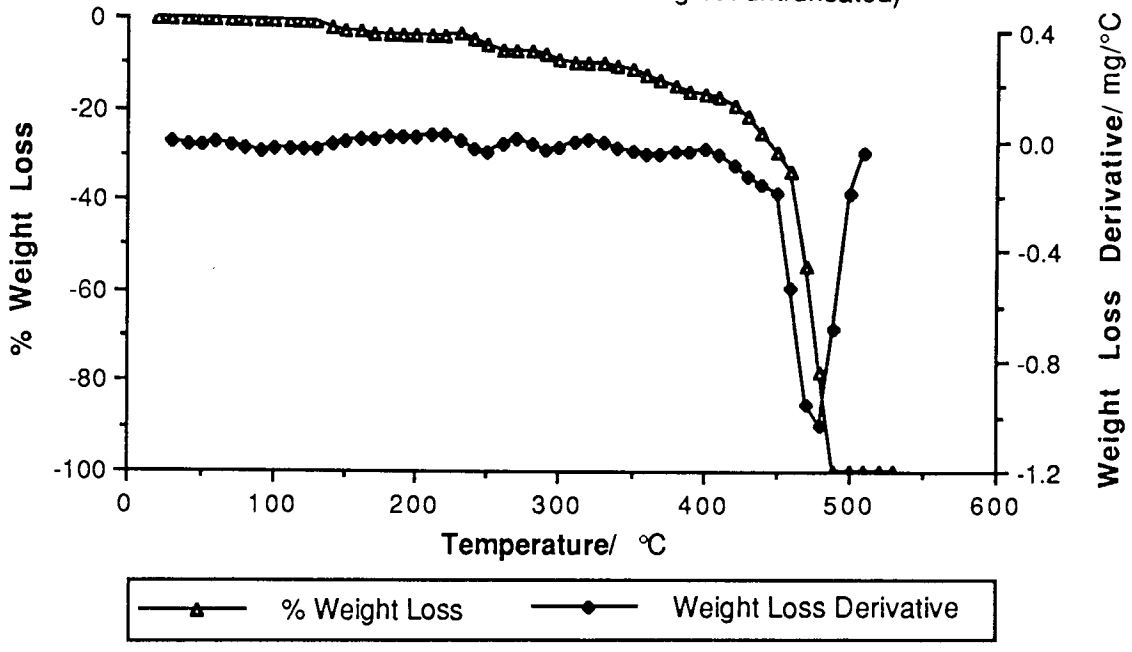

Figure 2.10
Calcium Oxalate Hydrate Thermogram

(% Weight Loss Data: 7—Point smoothing and truncation for Losses > 0 %)
(Derivative Data: 7—Point smoothing but untruncated)

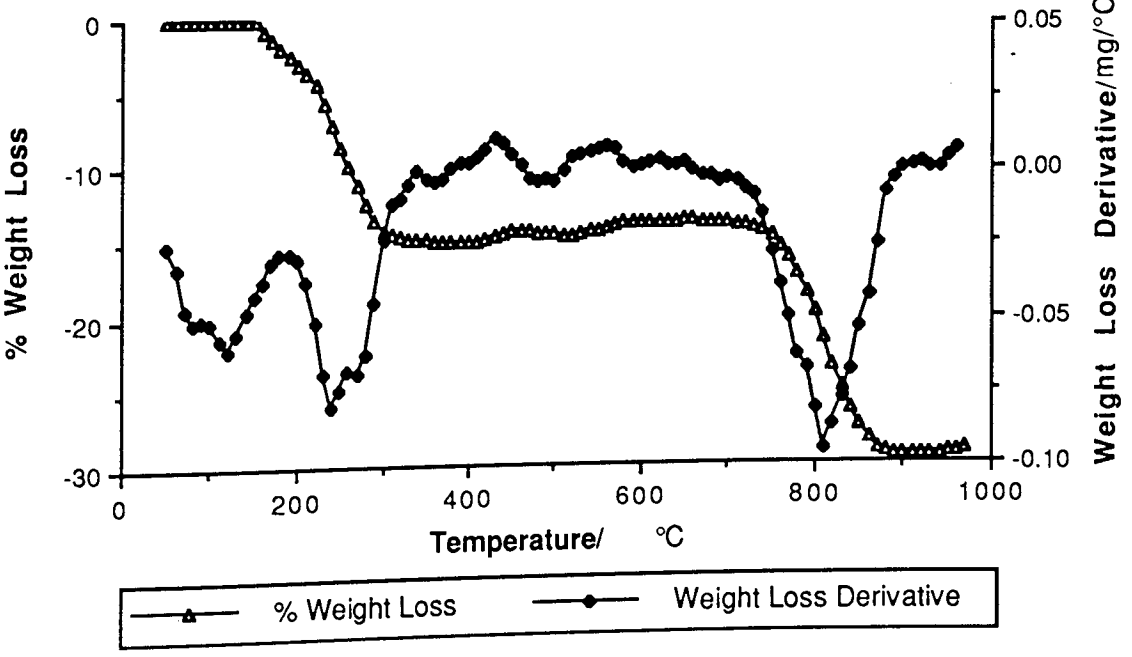

Figure 2.11
Fluka Humic Acid v1 Thermogram

(% Weight Loss Data: 7—Point smoothing and truncation for Losses > 0 %)
(Derivative Data: 7—Point smoothing but untruncated)

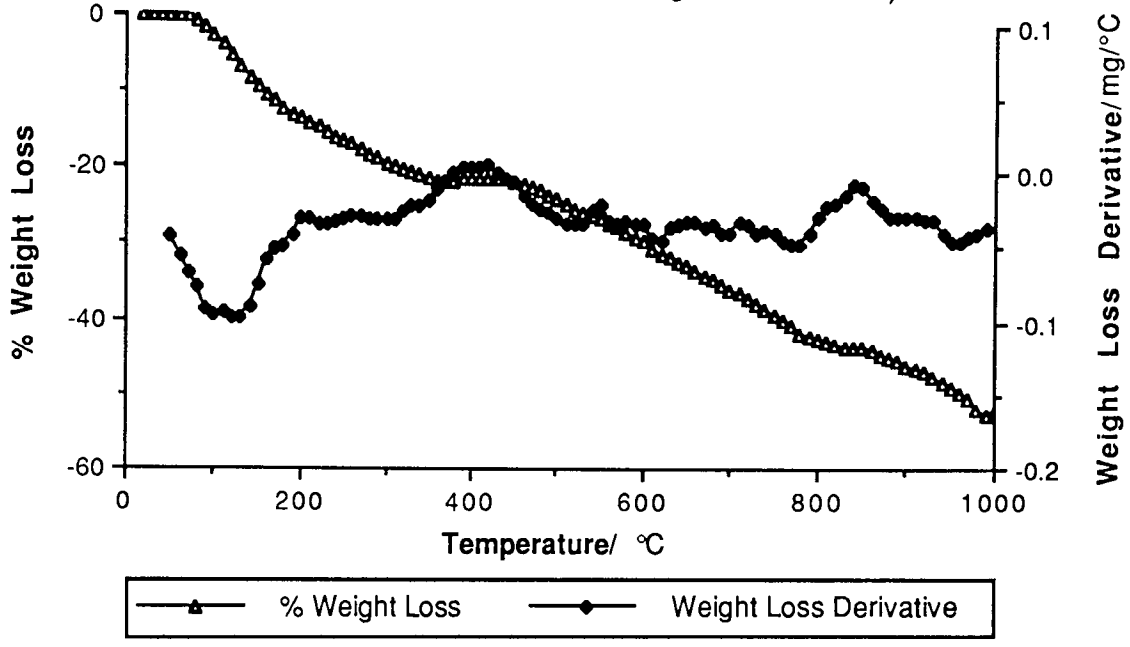

Figure 2.12
Purified Fluka Humic Acid v1 Thermogram

(% Weight Loss Data: 7—Point smoothing and truncation outside 0 % ≥ Losses ≥ -100 %)
(Derivative Data: 7—Point smoothing but untruncated)

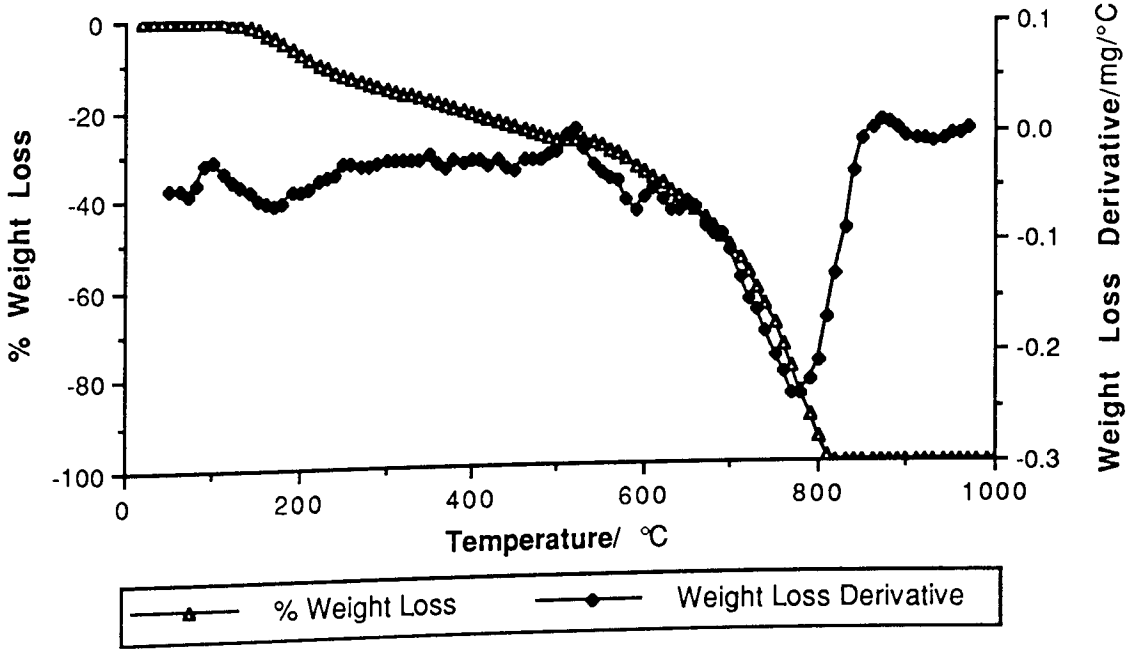

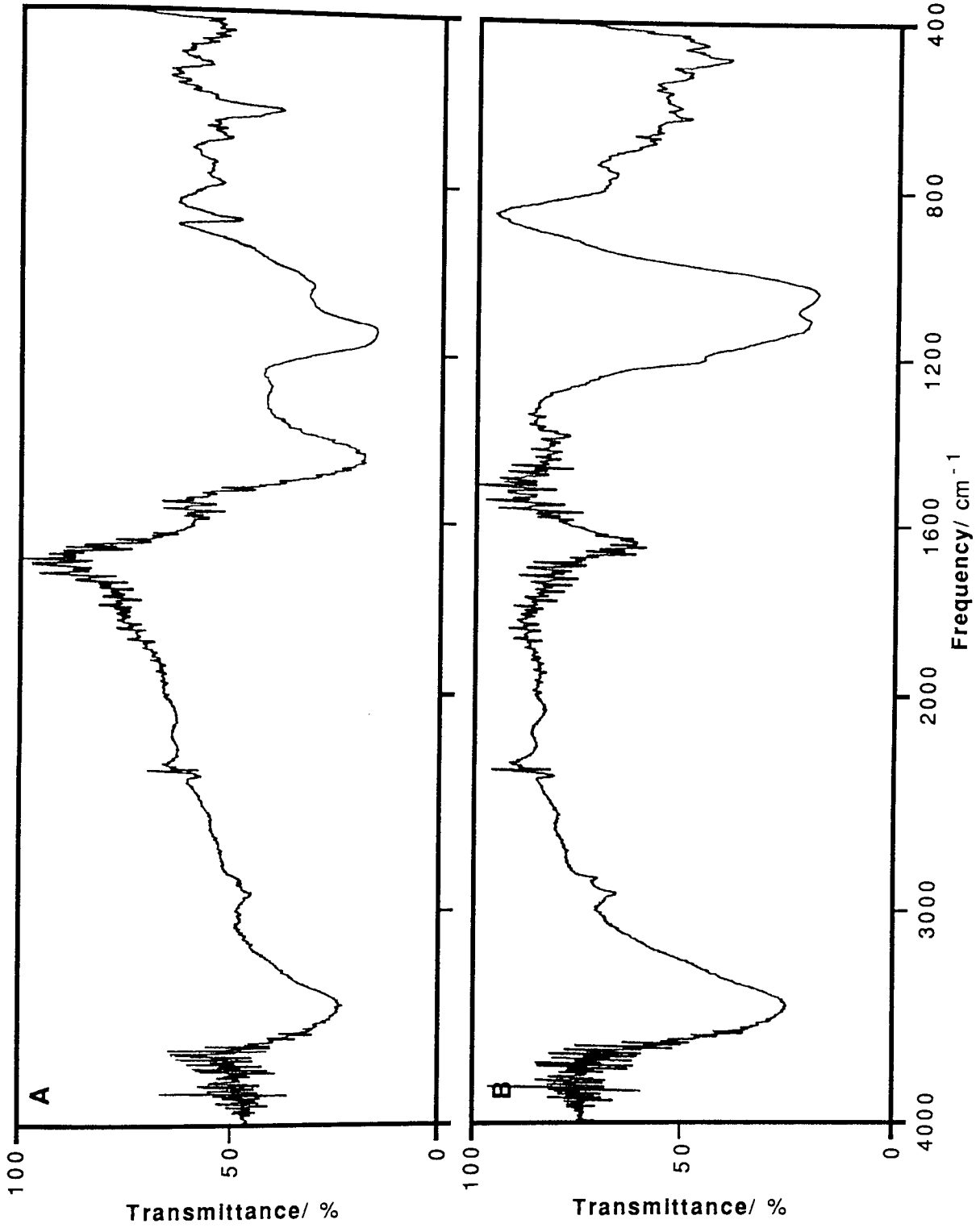

A Figure 2.13 Fluka Humic Acid v1 Residue Infrared Spectrum (After Pyrolysis to 1000 °C)

B Figure 2.14 Purified Fluka Humic Acid v1 Residue Infrared Spectrum (After Pyrolysis to 1000 °C)

Spectral Acquisition Conditions: Resolution = 4 cm $^{-1}$; Number of scans = 10
Sample Format: KBr pressed disc

Figure 2.15
Fluka Humic Acid v3 Thermogram

(% Weight Loss Data: 7—Point smoothing and truncation for Losses > 0 %)
(Derivative Data: 7—Point smoothing but untruncated)

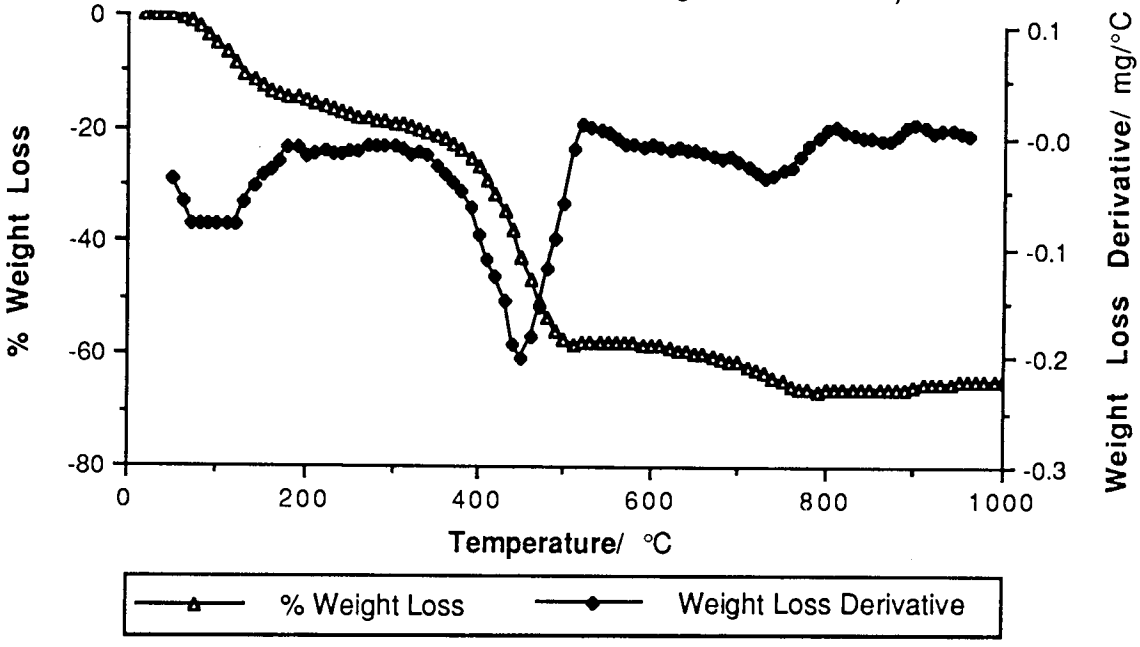

Figure 2.16
Aldrich Humic Acid v1 Thermogram

(% Weight Loss Data: 7—Point smoothing and truncation for Losses > 0 %)
(Derivative Data: 7—Point smoothing but untruncated)

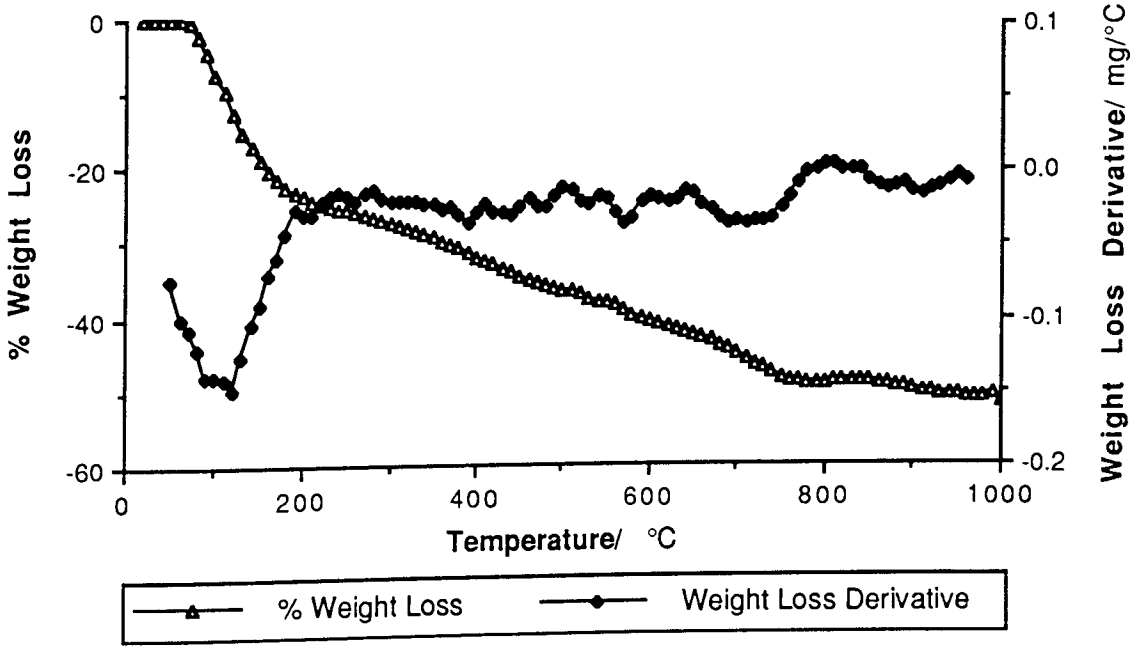

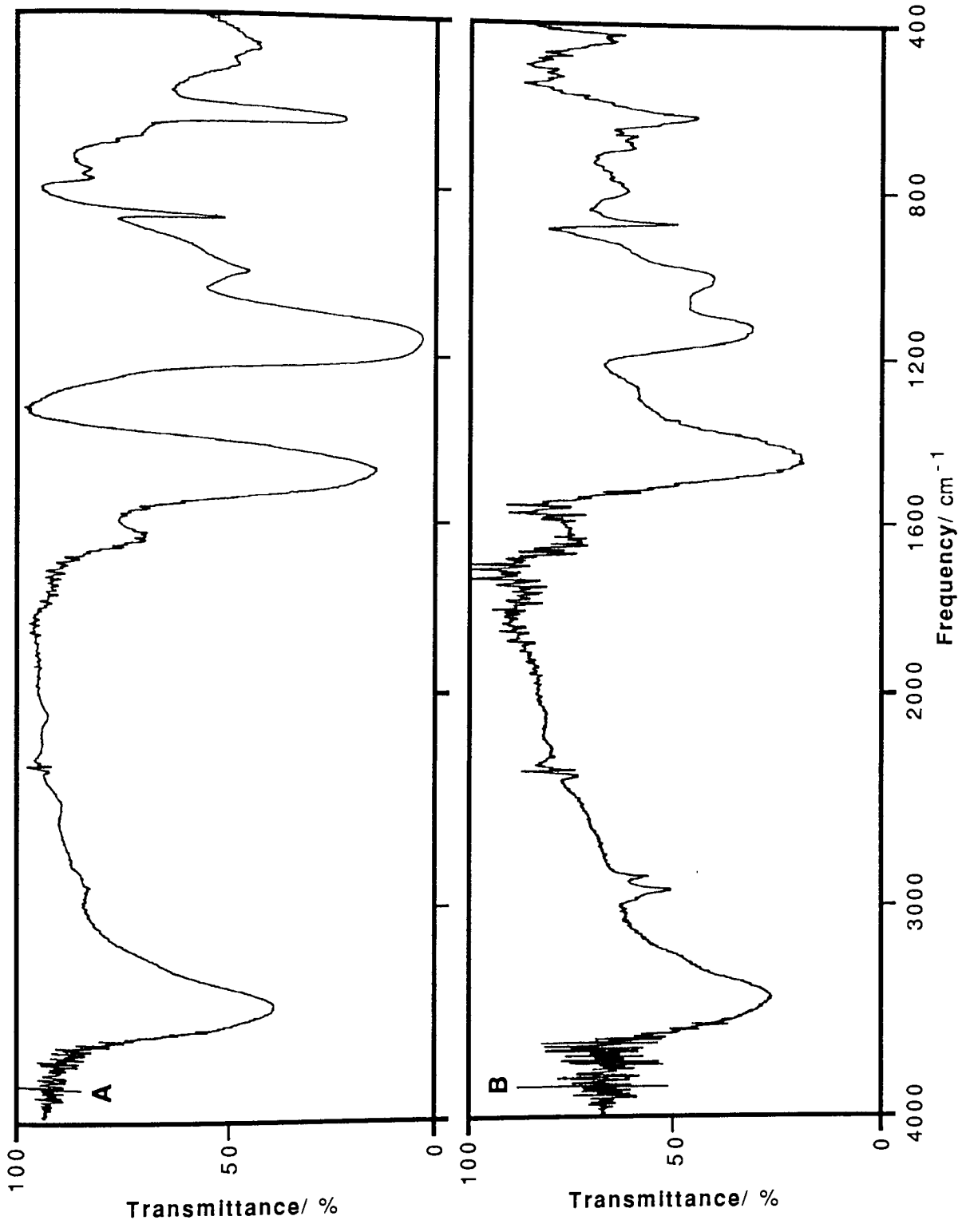

A Figure 2.17 Fluka Humic Acid v3 Residue Infrared Spectrum (After Pyrolysis to 1000 °C)

B Figure 2.18 Aldrich Humic Acid v1 Residue Infrared Spectrum (After Pyrolysis to 1000 °C)

Spectral Acquisition Conditions: Resolution = 4 cm $^{-1}$; Number of scans = 10
Sample Format: KBr pressed disc

Figure 2.19

Europium(III)-Fluka Humic Acid v3 Complex Thermogram

(% Weight Loss Data: 7—Point smoothing and truncation for Losses > 0 %)
(Derivative Data: 7—Point smoothing but untruncated)

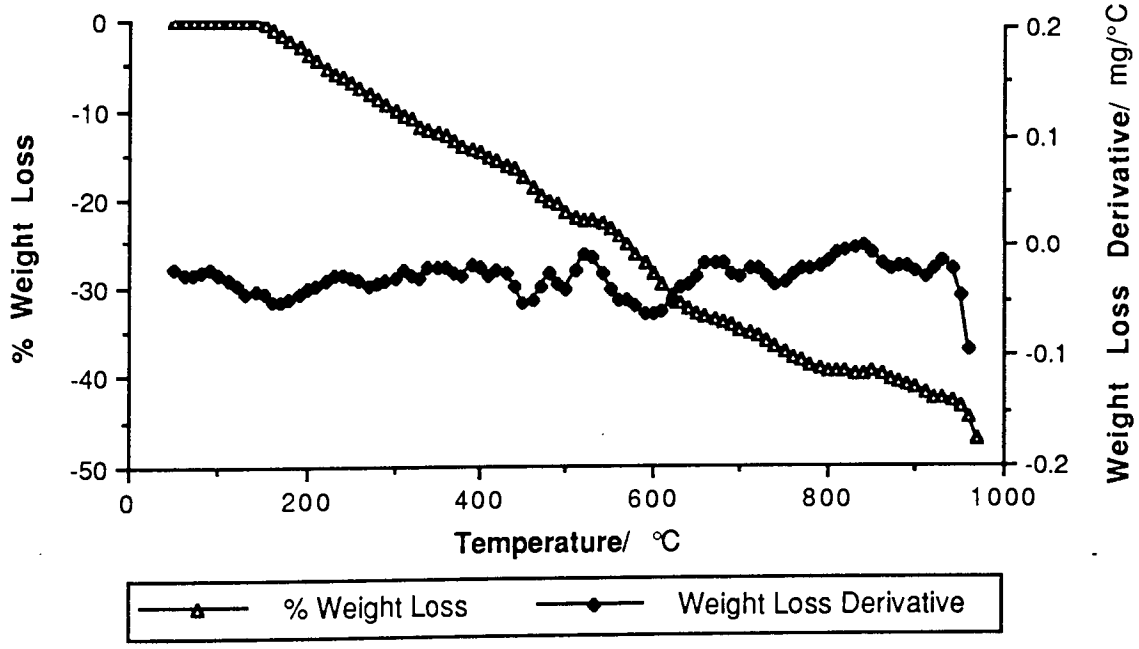

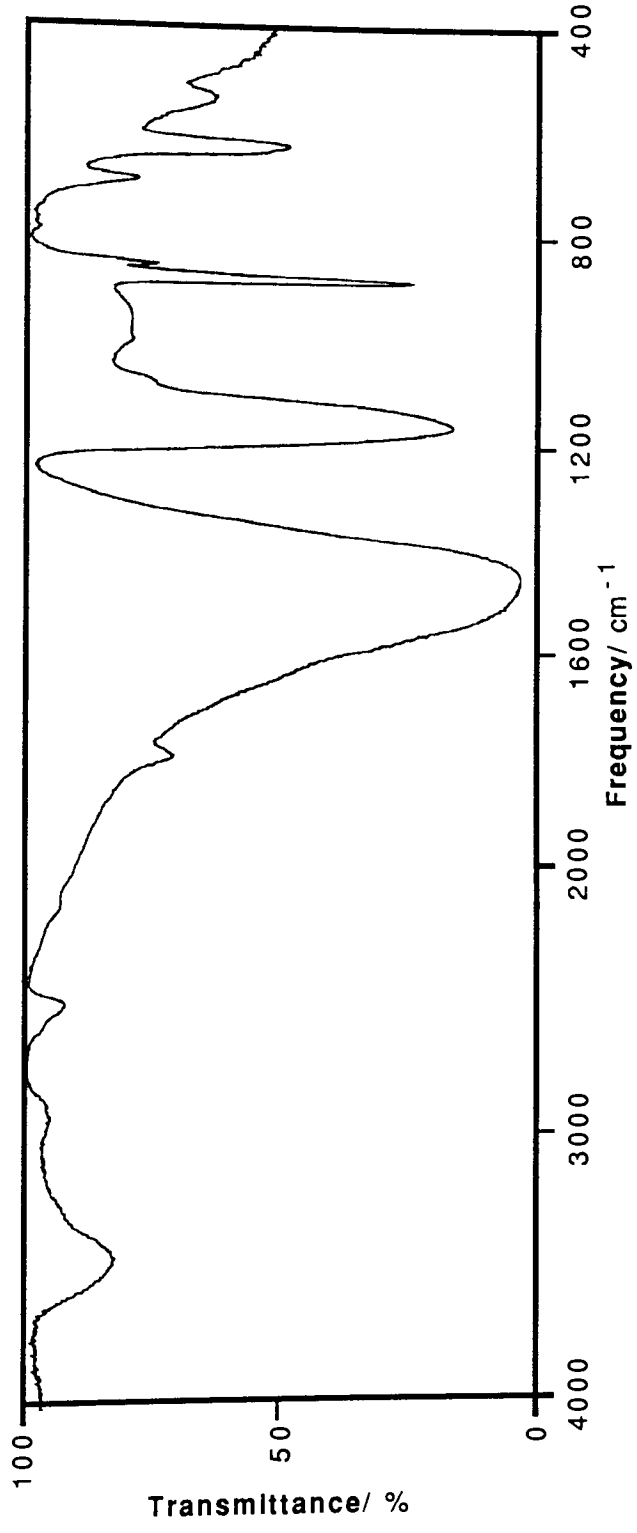

Figure 2.20 Europium(III)-Fluka Humic Acid v3 Complex Residue Infrared Spectrum (After Pyrolysis to 1000 °C)

Spectral Acquisition Conditions: Resolution = 4 cm $^{-1}$; Number of scans = 10
Sample Format: KBr pressed disc

Table 2.3
Total Percentage Weight Loss and Ash Content of Humic Acids and Europium(III)—Fluka Humic Acid v3 Complex

Sample	Analytical Balance Measurements		Thermobalance Measurements	
	Total % Weight Loss / %w/w	Ash Content / %w/w	Total % Weight Loss / %w/w	Ash Content / %w/w
Fluka Humic Acid v1	-41.5	58.5	-52.3	47.7
Purified Fluka Humic Acid v1	-99.6	0.5	-100.0	0.0
Fluka Humic Acid v3	-56.8	43.2	-65.1	34.9
Aldrich Humic Acid v1	-39.9	60.2	-50.7	49.3
Europium(III)—Fluka Humic Acid v3 Complex	-51.0	49.0	-48.2	51.8

accuracy and reliability of both the thermocouple and the balance mechanism of the instrument. Sulphur was chosen as a temperature marker since it should give a single, sharp weight loss corresponding to its boiling point, 445 °C.[72] The thermogram presented in Figure 2.9 of percentage and derivative weight loss against temperature reveals that large mass losses commence in this region. The loss occurs over a wide range since the furnace was continually heated during vaporisation at a rate that is probably too large to permit isothermal evaporation of the element. Inspection of the derivative curve reveals that the maximum rate of weight loss, which corresponds to the point of inflection in the percentage weight loss curve, occurs at 480 °C. Pyrolysis of sulphur using a lower heating rate near to the boiling point probably would approach the condition of isothermal evaporation at the quoted fixed point. However, it is suspected that there is a temperature lag between the furnace wall, where the thermocouple is located, and the sample.

The pyrolysis of calcium oxalate was briefly examined to check the accuracy of the balance weighing mechanism. Two major decompositions are evident from Figure 2.10 at 240 °C and 810 °C separated by a stability plateau. The percentage weight losses correlate well with the dehydration of the monohydrate and the subsequent decomposition of the oxalate to a white powder, calcium carbonate. Infrared spectral analysis of the residue confirmed this identity. The final percentage weight loss also correlates with that

measured by an analytical balance thus confirming the accuracy of the thermobalance weighing mechanism. However, calcium carbonate should decompose to oxide below the maximum temperature employed in the heating programme. [73]

2.4.4.1 Pyrolysis of Fluka Humic Acid v1

The pyrolysis curve of this humic acid (Figure 2.11) shows a continual decline in weight during the heating programme suggesting that several physical or chemical processes occur whose characteristic temperatures overlap. This is interrupted by a plateau between 350 °C and 450 °C indicating stability to further decomposition over this range. The derivative curve confirms this since it returns to the baseline in this region. The initial weight loss is rapid and so produces a pronounced minimum in the derivative weight loss curve. The colour of the sample lightened from the original dark brown as a consequence of the heating programme. The sample had not attained constant weight at 1000 °C since the percentage weight loss curve is still decreasing. Decomposition or vaporisation reactions are still occurring at a finite rate in this region.

Infrared spectral analysis of the humic acid before subjection to pyrolysis (Figure 2.1) and the resultant char (Figure 2.13) reveal the loss of most of the bands characteristic of the organic content, and the broadness attributed to the hydrogen bonding in the sample (see Section 2.3.4). The transmittance of the degraded sample could not be further amplified to fill the abscissa chart scale since the abundance of the absorbing functionality is low. Many features of this spectrum resemble those of a blank potassium bromide disc run under identical conditions and presented similarly with maximised abscissa expansion.

The band centred at 3436 cm^{-1} arises from residual hydroxyl functionality or moisture absorbed by the hygroscopic KBr since preparation of the disc. Much of the intense absorption at this wavenumber has been lost since the residue is dehydrated. Dehydration probably correlates with the initial mass loss in the thermogram and the moisture determined in Section 2.2. Some structural features associated with organic components of the sample remain in the spectrum. Alkyl carbon-to-hydrogen stretching occurs at high wavenumber and the corresponding deformations are observed at 1439 cm^{-1}. A shoulder at 1580 cm^{-1} is probably due to residual carboxylate groups, however, there

is no evidence for the symmetrical carboxylate stretch, or the presence of carboxyl groups. Other low wavenumber features are probably caused by silicates that withstand high temperature decomposition. These are relatively important in the spectrum of the residue since the chart is presented with maximum amplification. A new sharp peak at 879 cm^{-1} may be due to a vibration from a decomposition product. Many spectral features below 800 cm^{-1} can be correlated with those in an expanded KBr spectrum. Some may arise from the decomposition products.

The total percentage weight loss from heating to 1000 °C based on both the thermogram results and analytical balance measurements of the original material and the resultant residue, are given in Table 2.3. The corresponding ash contents reveal that this sample is relatively impure thus prompting the purification procedure to reduce this (see Section 2.1.2). It is notable that the ash contents given in Table 2.3, and those derived from equilibration at a fixed temperature in Table 2.1, are much greater than the 10–15 % range quoted by the supplier.

2.4.4.2 Pyrolysis of Purified Fluka Humic Acid v1

The percentage weight loss pyrolysis curve for this sample (Figure 2.12) displays a slow weight loss, and a region of accelerated weight loss in which most of the sample rapidly decomposes. The derivative weight loss curve shows a maximum rate of weight loss equal to 0·24 mg/°C (or 0·54 %/°C) at 780 °C, corresponding to the point of inflection in the percentage weight loss curve. A small tan-coloured char resulted. The total weight loss data of Table 2.3 reveals that the purification process was successful. However, it is notable that only the analytical balance measurements confirm the presence of the observed ash. Inspection of Table A2.1 shows that the source of the problem for the thermobalance measurements rests with the observation of total weight losses greater than 100 %. This suggests some element of disparity between the analytical balance measurements and those of the thermobalance. It is notable that the ash content determined for the purified sample is similar to that reported by Weber and Wilson [61] who applied a similar purification procedure to their batch of Fluka humic acid.

The infrared spectrum of the pyrolysis product (Figure 2.14) has greatly reduced

absorbance compared to the unheated sample (Figure 2.2) reflecting degradation of much of the organic matter and dehydration. Several low wavenumber bands that appear as minor features in the spectrum of the unheated sample are of relatively greater importance in the spectrum of the char. Other high wavenumber spectral features are retained in the ash. These are the alkyl carbon-to-hydrogen stretches between 2850 cm^{-1} and 2925 cm^{-1}, and some hydroxyl functionality at 3436 cm^{-1}, possibly due to water absorbed by the hygroscopic disc matrix. Spectral features between 2400 cm^{-1} and 1300 cm^{-1} are identical with an expanded KBr spectrum. Spectral bands previously assigned to carbonyl groups, and alkene and aryl out-of-plane carbon-to-hydrogen deformations are absent. The band centred at 1100 cm^{-1} results from pyrolysis of the sample. The faint colour of the char may be caused by degraded organic matter or inorganic components of the ash.

The reduction in ash results from the removal of the less-functionalised humin fraction, and use of a low pH in the purification procedure that released metal ions previously associated with anionic functional groups. The residual ash still contains evidence for siliceous matter.

2.4.4.3 Pyrolysis of Fluka Humic Acid v3

The thermogram of this material (Figure 2.15) shows that distinct decomposition stages occur when it is strongly heated. An initial weight loss commencing at room temperature produces a trough in the derivative curve. A deeper trough occurs between 360 °C and 510 °C with the maximum weight loss rate at 450 °C. Note that the area above the minimum in the derivative curve corresponds to the fractional weight loss for this process, which has been estimated to be 36·5 % w/w. Above 770 °C the weight of the sample is nearly constant and the derivative curve tends to the baseline. The colour of the sample changed from dark brown to grey because of intense heating programme used.

Infrared spectra of the unheated sample and the pyrolysis residue are given in Figures 2.3 & 2.17. The spectrum of the latter contains several bands that are not present, or that are obscured by the broad bands characteristic of the hydrogen-bonded organic matter in the spectrum of the unheated sample. The ash spectrum has been strongly amplified to fit the chart scale and several bands are found to coincide with those of a blank potassium bromide disc run under identical conditions.

Although pyrolysis has degraded the organic matter, several features in the infrared spectrum of the unheated sample described in Section 2.3.4 are still evident in the corresponding spectrum of the char. Some hydroxyl absorption is observed at high wavenumber and carbon-to-hydrogen stretching occurs between 2850 cm^{-1} and 2950 cm^{-1}. The band remaining at 1640 cm^{-1} is probably caused by water rather than residual carboxylate groups. The 1441 cm^{-1} carbon-to-hydrogen deformation assumes a relatively greater importance in the residue since it has withstood the high pyrolysis temperature. The low wavenumber bands observed are due to thermally stable components of the ash or products of decomposition reactions.

The total percentage weight loss and the corresponding ash contents using the two methods of weighing are given in Table 2.3. It should be noted that the pyrolysis curve and ash content of this humic acid are different from those of the other batch of Fluka Humic Acid reported previously. This implies that the two materials are not identical in their compositions and thermal stabilities. It is notable that the ash contents given in Table 2.3, and those derived from equilibration at a fixed temperature in Table 2.1, are much greater than the general 10–15 % range quoted by the supplier.

2.4.4.4 Pyrolysis of Aldrich Humic Acid v1

The pyrolysis curve of Aldrich Humic Acid v1 from room temperature to 1000 °C (Figure 2.16) shows an initial rapid decrease in sample mass (evident from the trough in the first derivative of the weight loss curve) followed by slower weight loss processes that occur over a wide temperature range. Heating did not affect the dark colour of the sample.

The infrared spectrum of the ash is of low absorbance so that it was not possible to fill the chart scale using the maximum data amplification available. Several spectral features match those of the disc matrix run under the same conditions and presented with large amplification. The bands observed are different from those of the unheated humic acid in both location and shape. The broadness that typified the spectrum of the latter has disappeared suggesting that hydrogen bonding and heterogeneity are decreased in the residue. Evidence for carbonaceous components of the ash are apparent from the presence

of alkyl C–H stretches at high wavenumber and deformations at 1439 cm^{-1}. Some bands between 700 cm^{-1} and 1000 cm^{-1} may be caused by alkene or aryl carbon-to-hydrogen bonds. Bands in the low wavenumber region have a greater importance than in the corresponding spectrum before pyrolysis. These may be present in the spectrum of the original material but would be masked by the broad, intense organic-type bands. Absorption at 624 cm^{-1} is probably caused by a decomposition product. These infrared changes suggest that Aldrich Humic Acid is extensively degraded by the high temperatures used.

The total percentage weight loss from heating to 1000 °C based on both the thermogram results and analytical balance measurements of the original material and the resultant residue are given in Table 2.3. The corresponding ash contents are also quoted. The Aldrich Chemical Company [47] has provided typical analysis data for batches of their humic acid; these were given in Chapter 1. Assuming the final pyrolysis residues suggested by Duval [73] for each of these elements, and taking the maximum percentages where a range is quoted, these components would lead to a total inorganic residue of ~10·2 % w/w. Therefore most of the ash is not accounted for by this composition. Malcolm and MacCarthy [49] also noted this discrepancy. Further comments concerning the composition of the ash are given in Section 2.4.4.7.

2.4.4.5 Pyrolysis of Europium(III)-Fluka Humic Acid v3 Complex

The thermogram for the complex of Fluka Humic Acid v3 with europium(III) ions (Figure 2.19) displays a continual decline in weight during the heating programme suggesting the occurrence of several decompositions of overlapping temperature range. A more pronounced—but incomplete—decomposition occurs beyond 950 °C. During the whole heating cycle, the sample colour lightened from brown to sandy-grey.

The total weight losses presented in Table 2.3 from the two methods of measurement do not equate. Note that the thermogram-derived loss reflects a temperature of 980 °C, whereas the weight loss measured by the analytical balance corresponds to heating to 1000 °C. Further, for the latter temperature, the weight loss was accelerating therefore accentuating the discrepancy. The thermogram does not display weight losses corresponding to 990 °C and 1000 °C since they are lost in the data smoothing process.

The total weight losses are less than those observed for uncomplexed Fluka Humic Acid v3 described in Section 2.4.4.3, reflecting the presence of europium in the complex. Assuming that pyrolysis converts the metal into its oxide which becomes part of the ash, [73] then the complex contained 14·6 % w/w or 5·0 % w/w of elemental europium, depending on whether the value is determined from the thermobalance data, or the analytical balance measurements, respectively. The latter is more likely to be accurate since some doubts have already been expressed concerning the reliability of thermobalance measurements. This calculation also assumes that complexation of the humic acid by europium does not affect the proportions of other thermally stable components of the sample.

Comparison of Figures 2.19 & 2.15 suggests that the complex is somewhat more thermally stable than the humic acid itself. Work by Schnitzer and Kodama [74] employing Differential Thermal Analysis showed that complexation of their fulvic acid with polyvalent metals reduced definitive degradation temperatures. This was explained by complexation of the metals with several functional groups introducing strain into the fulvic structure that increased susceptibility to thermal degradation. Using the same technique, Tan [70] observed less correlation between cationic charge and the thermal stability of his humic acid complexes.

Heating reduces infrared spectral features associated with imbibed water and produces a spectrum with bands of greater distinction, some of which are similar to those observed for the Fluka Humic Acid v3 treated similarly. Evidence for the retention of carboxyl groups in the sample is provided by the absorptions at 2500 cm^{-1} and 1775 cm^{-1}. Carboxylate groups have been degraded by pyrolysis and are not observed in the resulting infrared spectrum. A carbonaceous component of the residue is suggested by the aliphatic deformations at 1435 cm^{-1} and below 1000 cm^{-1}. Bands in the low wavenumber region also may be accounted for by decomposition products, or thermally stable components of the sample.

2.4.4.6 Correlation Between Total Percentage Weight Losses

The data presented in Table 2.3 shows a poor correlation between total percentage weight

losses calculated by the two methods. Losses calculated from thermobalance data are generally greater than those derived from the analytical balance for each sample. One possible source of error is that thermobalance measurements were taken in a hot atmosphere compared to the room temperature measurement of the analytical balance. A further error source is the possibility of a gain in weight by the residue during the initial stages of cooling, though the sample was subsequently desiccated to prevent moisture uptake.

A further comparison of Table 2.3 with Table 2.1 shows that heating to a fixed temperature of 750 °C produced smaller ash contents than derived from the higher temperature used in the T.G.A. analysis (1000 °C). As discussed in Section 2.2.4, this possibly arises from non–equilibration of the samples at 1000 °C, therefore the measurements at the lower temperature are probably more reliable.

2.4.4.7 Ash Contents

Pyrolysis of humic acid samples, except where purified, has revealed large ash contents. Their nature has been investigated by infrared spectroscopy but little insight was gained to their chemical identity. Clearly the residues are of a predominantly inorganic nature since few organic infrared absorbances were apparent in their spectra. It is likely that their organic components would have been further reduced if the samples were completely equilibrated at the maximum temperature used. A large component of the ash is believed to comprise of sodium monoxide derived from decomposition of sodium peroxide, which is the initial oxidation product of the sodium associated with the humic samples. [73] Quantification of sodium contents by Flame Photometry and Atomic Absorption Spectroscopy (not reported here) suggest that high sodium levels exist in the unpurified humic acids, but they are not large enough to account for the ash contents of the samples. Similarly, although the ash content of the purified Fluka humic acid is reduced, the elemental proportion of sodium is proportionately reduced. Infrared spectra suggest that part of the ash may be accounted for by silicious matter derived from minerals at the humic acid source.

A large reduction in ash content occurs because of the purification process applied to Fluka Humic Acid v1. This correlates with the protonation of carboxylate functional groups to carboxyls. The high ash content of the unpurified Fluka Humic Acid batches

support the infrared results given in Section 2.3 that suggest their existence mainly in the humate salt form, balanced by cations.

2.4.4.8 Significance of Pyrolysis Results

The calculated ash contents imply that the humic materials supplied are impure, therefore when concentrations of the samples are quoted in these studies, the concentration reflects that of the sample as a whole rather than just the organic material. For the purified Fluka Humic Acid v1, quoted concentrations closely approximate those of their constituent organic matter.

The pyrolysis curves and the total percentage weight loss data reveal that most of the sample mass decomposes, but some components are thermally stable. Infrared analysis of the degraded humic materials shows that many spectral characteristics associated with imbibed water, organic structures and functional groups are reduced or disappear resulting in high transmittance to infrared radiation. Thermograms tend not to exhibit sharply defined features separated by plateaus of stability. Schnitzer and Hoffman [75] noted that pyrolysis of their humic materials under a nitrogen atmosphere similarly produced monotonous thermograms. However, when pyrolysis was carried out in air, definitive decomposition reactions were identified. Several reaction types were postulated by these workers, namely dehydration, decarboxylation, deoxygenation and dehydrogenation based on the application of infrared spectroscopy and elemental and functional group analyses at regular intervals during heating programmes. No attempt has been made in the studies reported here to correlate thermogram features with chemical and physical processes occurring with the samples since most pyrolysis curve features overlap and a more detailed analysis of chars and evolved gases would be necessary.

2.4.5 Conclusions

Pyrolysis-induced decomposition of humic acids occurred over a wide temperature span with few uniquely defined processes apparent from thermograms. Some components of the samples are quite thermally stable resulting in significant ash contents. Purification was

confirmed to be effective in reducing ash to a low level.

2.5 Ultra-violet/Visible Spectroscopy

2.5.1 Introduction

Many surface waters have a characteristic yellow or brown colouration that is imparted by fulvic and humic acids. These natural organic materials are mainly derived from soil humus, and in some areas, peat. Most of the research on the yellow colouration in water has focussed on the development of methods for its removal (e.g., coagulation by iron and aluminium salts [76]) since the level of colouration is controlled by drinking water standards and is aesthetically objectionable to domestic consumers and bulk users in manufacturing industries. [57,77]

The dark colour of humic substances has prompted chemists to use light absorption for the analysis of these materials. [5] Kumada [63] described an early classification system for humic materials that was based on their intrinsic colour and used ultra-violet and visible absorbances as the classification criteria. This was later extended to elucidate their nature and properties.

The ultra-violet region of the electromagnetic spectrum is considered to be 190–400 nm and the visible range is 400–800 nm. Typical chromophores that absorb in these regions are conjugated electron systems and multiply bonded substituents. A molecule can absorb a particular frequency ν, if there exists within the molecule an energy transition of magnitude $\Delta E = h\nu$, where h equals the Planck constant. [64] When absorption of ultra-violet or visible light occurs, the most probable transition involves promotion of one electron from the highest occupied molecular orbital of the chromophore to the lowest unfilled orbital. However, several transitions often occur causing multiple absorptions in the spectrum. Not all transitions from filled to unfilled orbitals are allowed since some are restricted by symmetry relationships. After sometime the molecule relaxes by dissipating the absorbed energy. Note that ultra-violet and visible absorption spectroscopy provides no information concerning the deactivation mechanisms of electronically excited states. [64] This is provided by fluorescence spectroscopy (see Section 2.6).

A study of the ultra-violet and visible absorption by Fluka and Aldrich humic acids has been undertaken to deduce structural information regarding the identity of their chromophores. Location of specific absorptions may provide wavelengths suitable for excitation of the humic matter in fluorescence studies since it is possible that chromaphoric absorption results in fluorescent emission (see Section 2.6).

2.5.2 Experimental

The technique of ultra-violet and visible absorption spectroscopy has the advantages of being nondestructive and small sample masses are required. Dilutions were made to humic acid dispersions of concentration 0.1 g l^{-1} in ~10^{-4} M $NaOH_{(aq)}$ (¢010) with further alkali so that full spectra could be recorded within the normal absorbance range of the spectrophotometer. This procedure was performed for Aldrich humic acid v1, Fluka humic acid v3, Fluka humic acid v1 and the corresponding purified sample. Absorbance spectra were recorded on the Pye-Unicam SP8–100 spectrophotometer (¢029). The instrument has a dual beam optical arrangement providing cuvette slots in both sample and reference beams. A combination of lamps provides illumination across the full spectral range. Quartz cuvettes of path length 4 cm were used to maximise sensitivity. Water, which was made slightly alkaline, was used as the solvent for the humic acids to ensure adequate dispersion. Once the instrument stabilised it was zeroed across the appropriate wavelength range by placing cuvettes containing solvent in both beam slots. Solvent was kept in the reference beam and the sample replaced the solvent in the second cuvette which was then returned to the sample beam slot. Absorbance spectra were recorded for samples referenced to the solvent, against wavelength λ in the range 200–800 nm. Measurements were not made below 200 nm since molecular oxygen absorbs in this region. Spectral acquisition conditions were selected to provide maximised resolution.

2.5.3 Results

The ultra-violet/visible absorption spectra of the humic acid samples are presented as absorbance against wavelength in Figure 2.21.

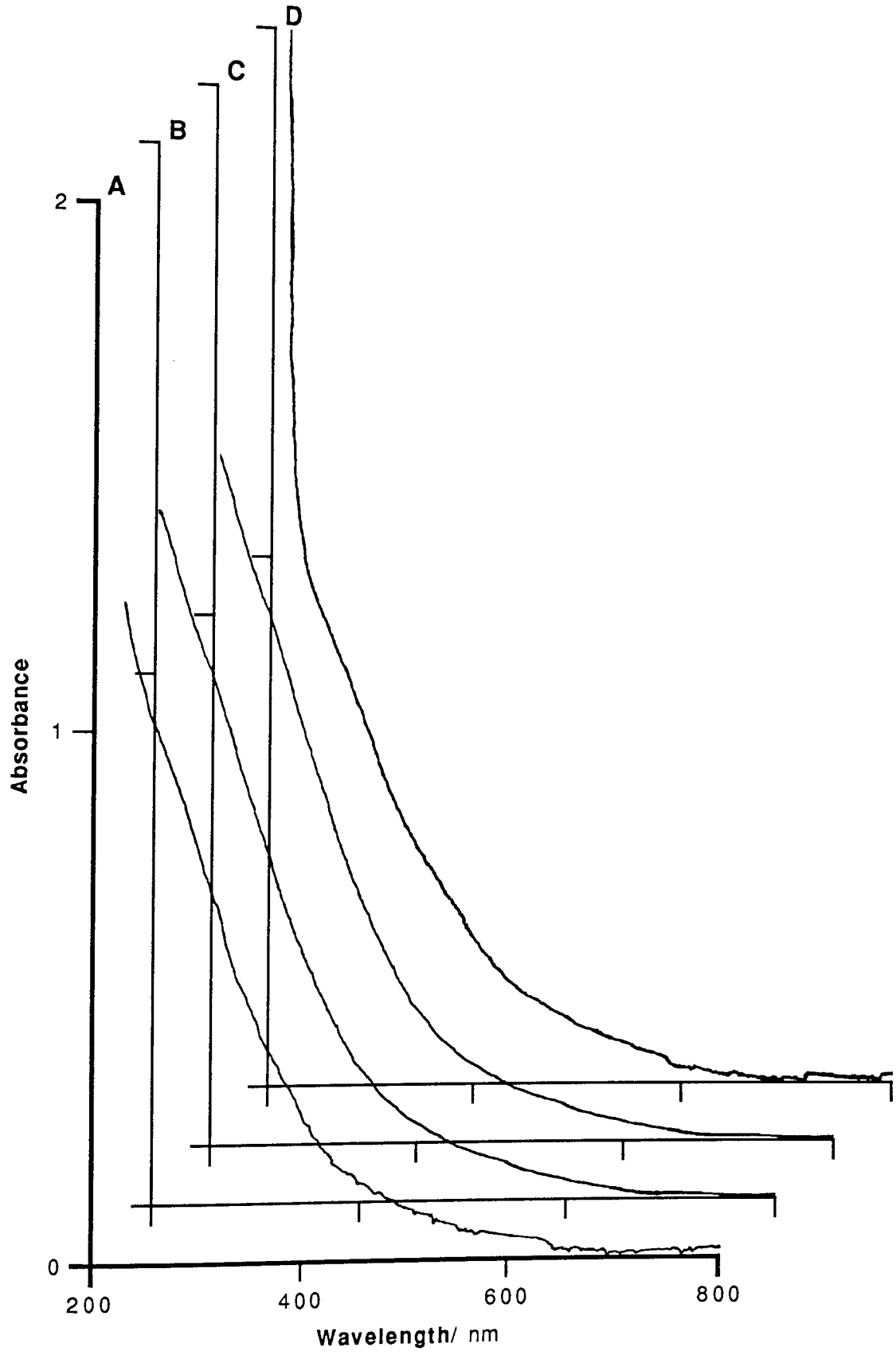

Figure 2.21

Ultra-Violet/Visible Absorbance Spectra of Humic Acids

A Aldrich Humic Acid v1
B Fluka Humic Acid v3
C Fluka Humic Acid v1
D Purified Fluka Humic Acid v1

Sample Conditions: Humic Acid Concentration = 10 mg/l; Solvent = 0.0001 M NaOH(aq)
Spectral Acquisiton Conditions: Scan Speed = 2 nm/s; Chart Speed = 20 s/cm;
Bandwidth = 2 nm; 4 cm Quartz Cuvette; Reference = 0.0001 M NaOH(aq)

Absorbances are related to the concentration of the humic matter by the Beer-Lambert law:

$$A = \log_{10}\frac{I_0}{I} = \varepsilon c l$$

Where:

A	=	Absorbance
I_0	=	Incident light intensity (reference beam light intensity)
I	=	Transmitted light intensity
ε	=	Molar absorptivity (molecular extinction coefficient) /m^2 mol^{-1}
c	=	Concentration of the solution /mol dm^{-3}
l	=	Path length of sample cell /cm

The molar absorptivity is a constant for a particular compound at a given wavelength.

2.5.4 Discussion

The humic acid absorption spectra given in Figure 2.21 are featureless showing a progressive decrease in absorbance with increased wavelength and no distinct maxima or minima. They are very similar to each other, however the absorbance of the purified sample is greatest at low wavelength possibly reflecting its greater concentration of organic matter per gram compared to the unpurified samples (see Sections 2.2.4 & 2.4.4.8). The spectra do not permit deduction of the identity of constituent chromophores from their characteristic wavelengths. Absorption lines would not be expected in the spectra because vibrational and rotational effects are superimposed on the electronic transitions.[64] Featureless spectra have been observed by many workers,[1,54,60,78–81] yet a few have noted shoulders in their spectra. Some studies are described.

Dkhar *et al*[80] noted a progressive decrease in absorption with increased wavelength but absorption bands were apparent with maxima observed between 238 nm and 250 nm. These were correlated with the presence of $NHCOCH_3$, $COCH_3$, CHO-substituted benzene rings. The intensity of ultra-violet absorption differed considerably between

fulvic acids of different soils, except at very high and very low wavelength where the spectra tend to coincide. Frimmel and Bauer [78] noted that the spectra of fulvic acids were generally monotonous but some shoulders were observed between 250 and 300 nm. Absorbances normalised to dissolved organic carbon showed increases with increased age of the samples. Kumada [63] described a type of soil humic acid that had discrete absorption bands. Ghosh and Schnitzer [79] observed a shoulder for most samples in the region 250–270 nm that they attributed to a quinoid moiety. Theng *et al* [54] noted that humic acids obtained from the same source using different extractants resulted in monotonous spectra that coincided at high and low wavelength, but some differences were observed at intermediate wavelengths. These were correlated with infrared evidence that showed different carbonyl contents.

The similarity of absorbance spectra for many reported samples, regardless of origin, method of extraction and purification, has lead to the suggestion that humic substances have similar basic structures. [66,79] There are several chromophores, such as aromatic nuclei and carbonyl groups, and a complete spectrum represents the summation of responses from many different, but closely similar, humic molecules. [5,66,82] Variations between samples probably arise from different proportions of constituent chromophores.

The ultra-violet and visible absorption spectra of Fluka and Aldrich humic acids are not useful in suggesting wavelengths suitable for excitation of humic matter in fluorescence studies since spectra cannot be related to specific photophysical processes because of the ill-defined polychromaphoric structures present. [81] Further, it is not possible to calculate the energies of the molecular orbitals involved in electronic transitions and hence in the absorption of ultra-violet and visible light since this is difficult even for simple organic molecules with well-defined absorptions. [64] Therefore excitation wavelengths can only be determined from an excitation scan on a fluorescence spectrophotometer (see Section 2.6).

Schnitzer [1] and Stevenson [6] both summarised the factors responsible for absorption of light by humic substances. Absorption increases with increased: degree of condensation of the aromatic rings; ratio of carbon in aromatic nuclei to carbon in aliphatic side chains; total carbon content and molecular weight. Stevenson [6], Schnitzer and Ghosh [79], and Kumada [63] noted that at any wavelength, the absorbance decreased stepwise with

decreased pH. This result was attributed to changes in physical properties, such as the degree of dissociation of carboxyl and phenolic-hydroxyl groups. Kumada [63] applied this dependence to calculate difference spectra for samples by subtraction of spectra acquired under different pH conditions. These were used for discrimination of individual humic acids. Other attempts to provide extra spectral information, such as the enhancement of shoulders, have been made through determination of derivative spectra of humic acids. [83]

One reported application of absorbance spectroscopy involved monitoring the visible absorbance of humic substances and the americium(III) ion thus permitting quantification of their interaction. [84] Application of the Beer-Lambert law to the estimation of concentrations of humic substances is considered in Section 2.7.

Rayleigh light scattering may contribute to the apparent absorption behaviour of the humic acids. Rayleigh scattering intensity depends on the inverse fourth power of the wavelength [85] (see Section 5.6.1) therefore the proportion of light scattered is greatly increased at lower wavelengths. However, comparison of the experimental variations in absorbance (Figure 2.21) with data generated using the Rayleigh scattering model suggests that scattering is unable to fully account for the increased absorbance. The actual contribution of scattering to the measured absorption is not known and has not been further explored since the spectra obtained in these studies are of limited applicability. Further attention is given to light scattering by humic substances in Chapter 5.

2.5.5 Conclusions

Humic acid absorption spectra are typically featureless showing a progressive decrease in absorbance with increased wavelength thus it has not possible to deduce the identity of constituent chromophores. The ultra-violet and visible absorption spectra of Fluka and Aldrich humic acids have not been useful in suggesting wavelengths suitable for excitation of the humic matter in fluorescence studies. However, these studies have been useful since the intense absorbances at low and medium wavelengths may be used to provide estimations of humic concentrations.

2.6 Fluorescence Spectroscopy

2.6.1 Introduction

The absorption of ultra-violet or visible radiation by a molecule usually raises it from the ground electronic and vibrational state to an excited state. Most molecules relax by dissipating most of this energy as heat. In some molecules, however, a significant amount of the absorbed energy is lost by emission at a longer wavelength than the incident radiation. This process is termed fluorescence. In order for a molecule to fluoresce it must possess certain functional or structural features, termed fluorophores, which can undergo excitation by the incident radiation and subsequent emission following some degree of energy degradation. Humic substances are known to fluoresce under both ultra-violet and visible light.[5,86]

The fluorescence characteristics of humic substances have been investigated to gain some insight into the fate of the excitation energy, and to provide background information for the work described in Chapter 3. The determination of fluorescence characteristics of humic materials has involved the recording of excitation and emission spectra. An excitation spectrum is obtained by scanning the incident radiation over a range of wavelengths whilst monitoring the fluorescent emission at a fixed wavelength. An emission spectrum results from irradiation of the sample with light of a fixed wavelength (usually the wavelength of maximum excitation) whilst scanning the emission (fluorescence) spectrum. Three-dimensional excitation-emission matrices have been generated for Fluka Humic Acid v3 and Aldrich Humic Acid v1 by appropriate combination of many such spectra. The matrices provide a complete representation of the fluorescence characteristics of the humic materials studied. Note that ultra-violet/visible absorption spectra of these humic acids (see Section 2.5) have not been useful in suggesting excitation wavelengths.

2.6.2 Experimental

Fluorescence studies were carried out on a Perkin Elmer 3000 Fluorescence Spectrometer (¢030) with an attached servo-operated Flat-Bed Chart

Recorder (¢031). The spectrometer employs a xenon discharge lamp and a ratioing system that compensates for variations in source intensity from one flash to the next. The dark current is reduced to an insignificant level by measuring the photomultiplier output for very brief periods of the duty cycle. A quantum correction reference system and automatic gain control results in the presentation of fully corrected spectra for the spectral range 230–600 nm. Wavelengths are selected by grating monochromators with an accuracy of ±2 nm when the variable monochromator slits are set to 10 nm. Several instrumental scanning rates and chart recording rates are available. The spectrometer permits amplification of spectral features by fixed multiples. The chart recorder provides a similar feature. Other spectrometer features include a fluorescence averaging routine for fixed wavelength studies and a variable integration step (time constant) for recording spectra scanned at different rates. Note that the equipment does not permit the study of phosphorescence or the lifetime of excited states.

Periodically, the accuracy of the instrument, especially the monochromators, was checked by scanning the spectra of fluorescent standards sealed in cuvettes, and comparing these to spectra supplied.

Humic acid samples were studied in the liquid state as dispersions in dilute alkali. Solid samples could be studied in powder or pressed disc form by fitting the appropriate spectrometer attachment. The liquid sample turret can hold four 1 cm path length cuvettes. This physical arrangement provides illumination perpendicular to a face of a cuvette and detection at 90° to avoid complications from transmitted light. Both glass and quartz cuvettes were employed, the latter specifically for low wavelength studies. All are optically polished on all four sides.

Initially it was necessary to determine the best working concentration of Fluka Humic Acid v3 and Aldrich Humic Acid v1 for subsequent fluorescence measurements. Dispersions of concentration 0·1 gl^{-1} in ~10^{-4} M $NaOH_{(aq)}$ (¢010) were found to provide a good compromise between intensity and resolution over a wide spectral range.

Fluorescence spectra were obtained by irradiation of samples at a fixed wavelength whilst the emission was scanned. Forty four spectra were run for each sample in 10 nm excitation wavelength (λ_{ex}) steps in the range 230–660 nm whilst scanning the emission from λ_{ex} + 20 nm up to 800 nm. The 20 nm differential was intended to avoid complications derived from light scattering. Three-dimensional excitation-

emission matrices were generated by combination of these spectra for each humic acid sample.

2.6.3 Results

A sample fluorescence spectrum from the forty four acquired for Fluka Humic Acid v3 is given in Figure 2.22. The excitation wavelength, 440 nm, corresponds to an excitation maximum.

Excitation-emission matrices have been generated for Fluka Humic Acid v3 and Aldrich Humic Acid v1 from such fluorescence spectra by reading fluorescence intensities at 10 nm intervals of emission wavelength. Intensities were read with an accuracy of under 1 %, however, subsequent multiplication to take account of chart and instrumental amplification factors effectively reduced this for some data. Note that if instrumental artefacts were suspected in the spectra, data was approximated by a manual curve fitting routine. This is justified since spectral features tend not to be sharp and much information would otherwise be lost. Data has not been smoothed since the spectra are not excessively noisy. Data sets for the samples have not been included due to their excessive size.

Graphs have been presented in two formats. The wireframe three-dimensional plots have been generated from over 1400 excitation-emission data pairs each. They provide a complete assessment of the fluorescence characteristics of the samples over accessible wavelengths. The contour plots are more useful in locating the precise excitation-emission maxima since they focus on the region of greatest fluorescence. Note that extra intensity data has been plotted in some regions of the 3D and contour plots where measurements have not been made, such as for excitations below 230 nm and above 660 nm, or emissions below λ_{ex} + 20 nm. This is an unavoidable artefact of the computational methodology employed to produce the graphs. Also note that for the wireframe plots, and to a lesser extent the contour graphs, the sharp demarcation observed with emission wavelengths is an artefact of the theoretical requirement for excitation wavelengths to be less than the corresponding emission wavelength. This is realised in a 10 nm increase in the first data point available for each 10 nm increase in excitation wavelength.

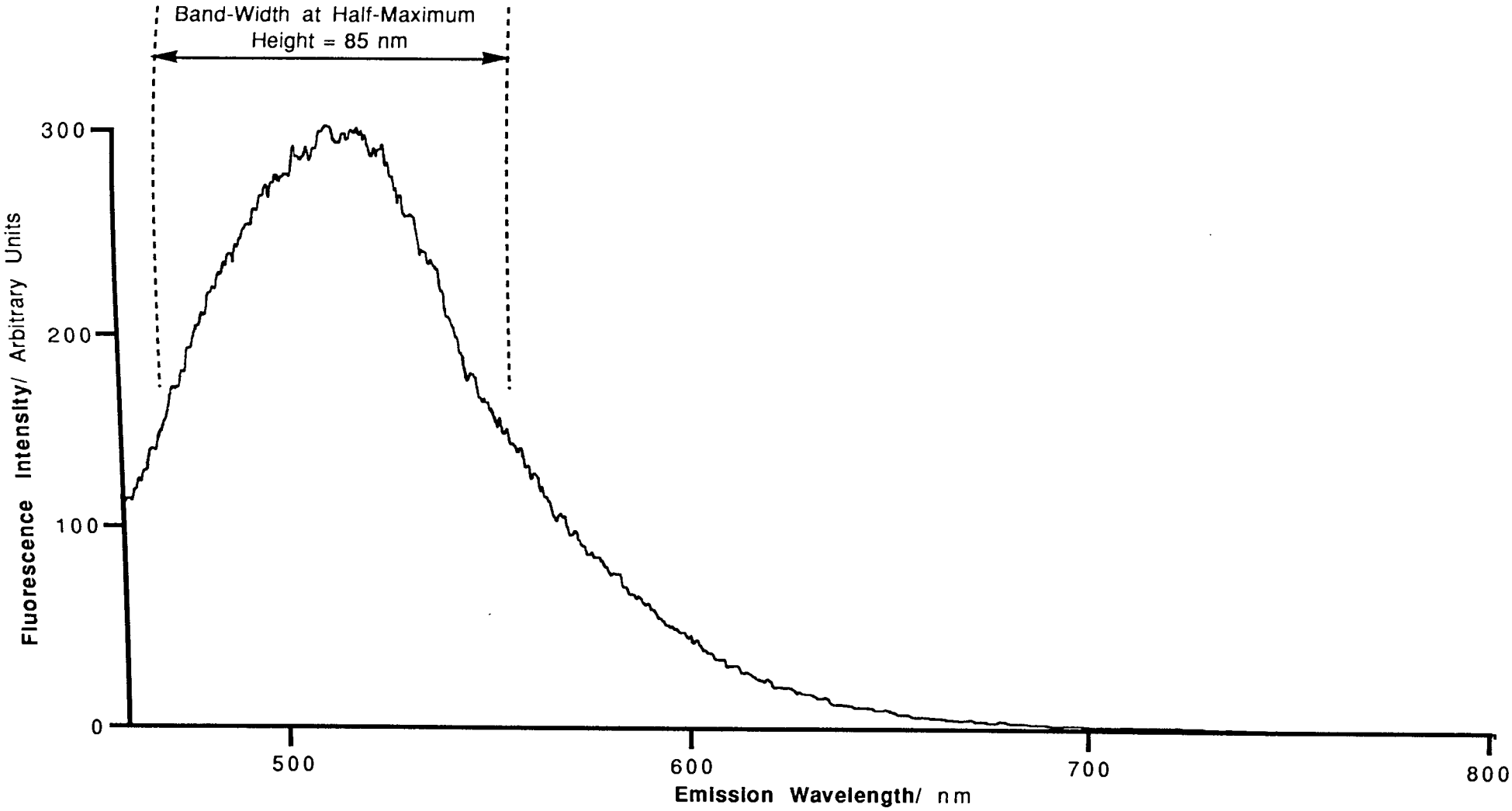

Figure 2.22

Fluka Humic Acid v3 Emission Spectrum (λ_{ex} = 440 nm)

Sample and Spectral Paramaters: Sample Concentration 0.1 gl $^{-1}$ in 10 $^{-4}$M NaOH; 1 cm Quartz Cuvette; Excitation Slit = 5 nm; Emission Slit = 5 nm; Scan Speed = 60 nm/min; Chart Speed = 60 mm/min; Time Constant = 2 s

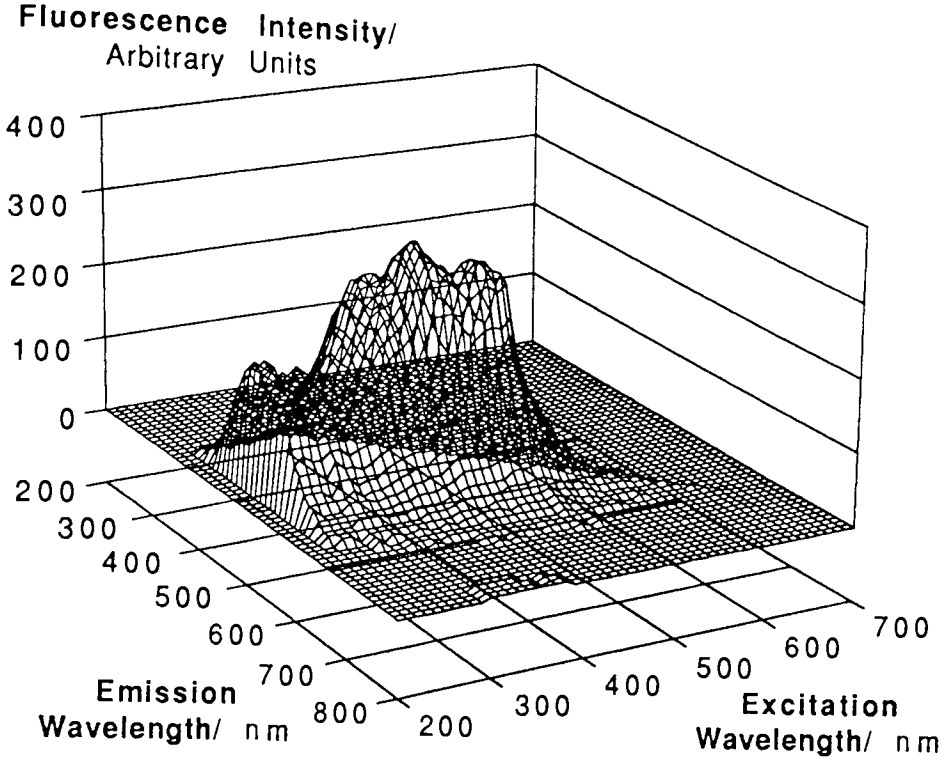

Figure 2.23

Fluka Humic Acid v3

Fluorescence Excitation—Emission 3D Matrix

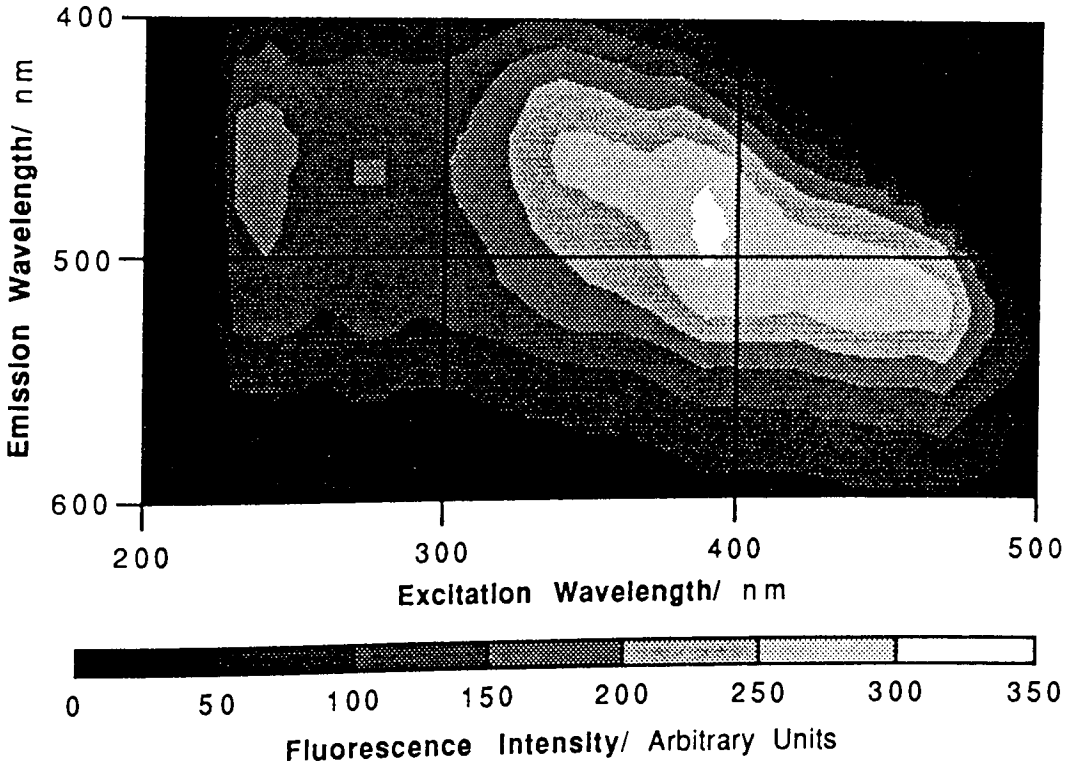

Figure 2.24

Fluka Humic Acid v3

Fluorescence Excitation—Emission Contour Plot

Sample and Spectral Paramaters for Fluka Humic Acid v3:

Sample Concentration 0.1 gl $^{-1}$ in 10 $^{-4}$ M NaOH; 1 cm Quartz Cuvettes

Excitation Slit = 5 nm; Emission Slit = 5 nm

Scan Speed = 60 nm/min; Chart Speed = 60 mm/min; Time Constant = 2 s

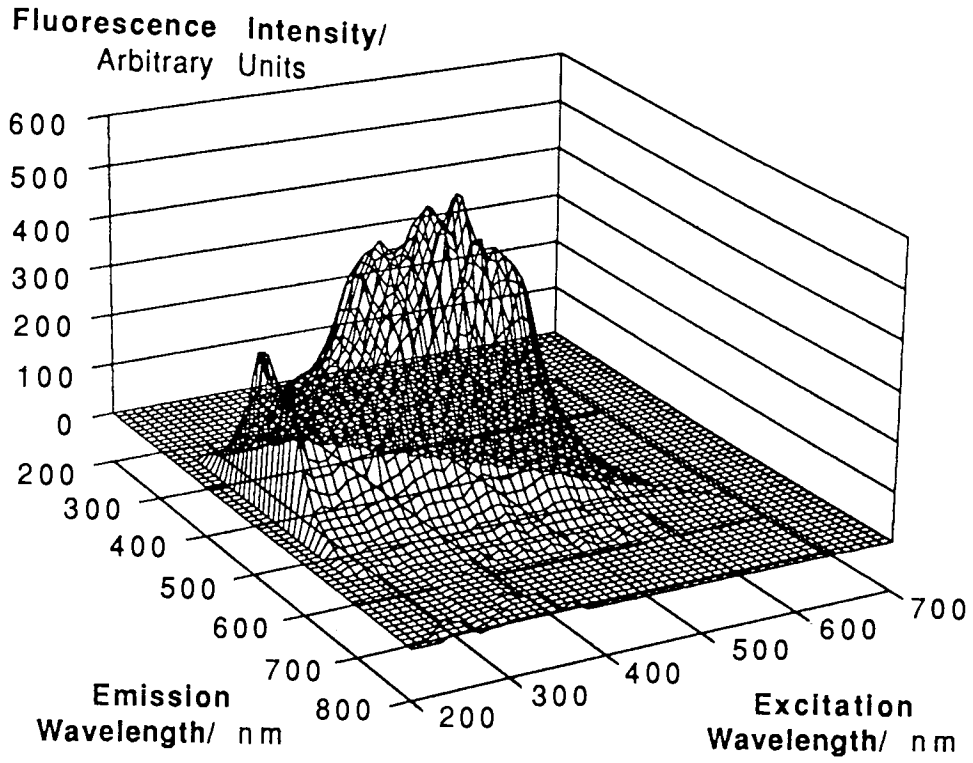

Figure 2.25
Aldrich Humic Acid v1
Fluorescence Excitation—Emission 3D Matrix

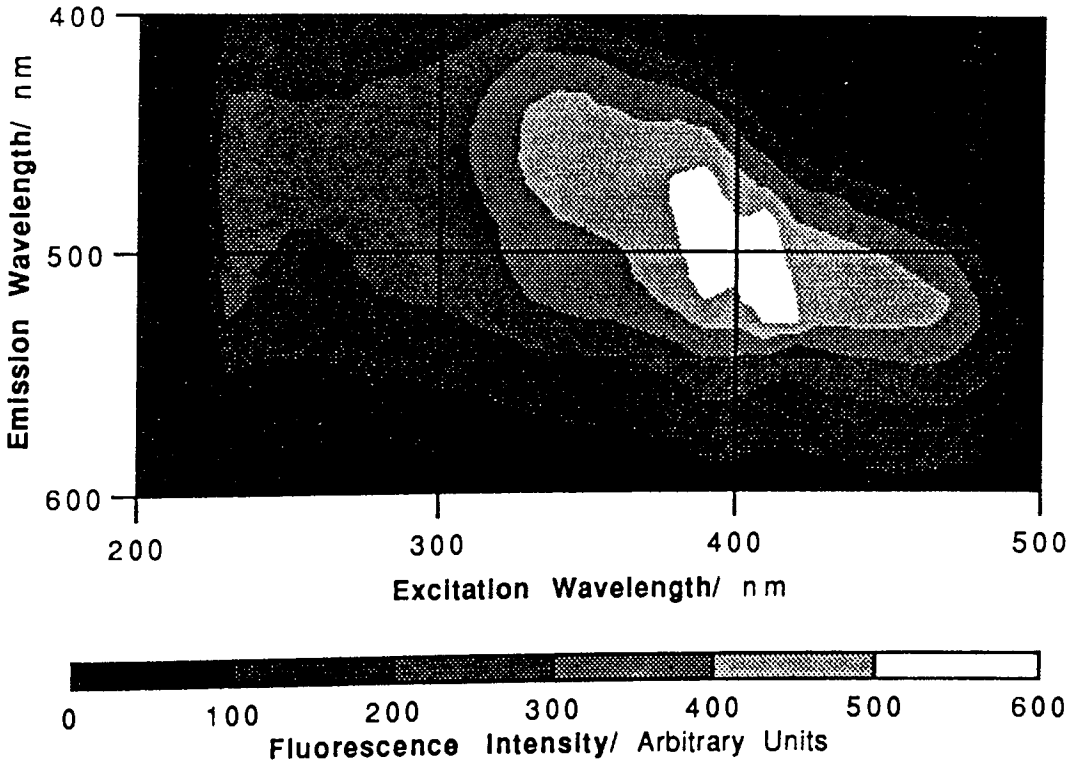

Figure 2.26
Aldrich Humic Acid v1
Fluorescence Excitation—Emission Contour Plot

Spectral and Aldrich Humic Acid v1 Sample Paramaters:
Sample Concentration 0.1 gl $^{-1}$ in 10 $^{-4}$ M NaOH; 1 cm Quartz Cuvettes
Excitation Slit = 5 nm; Emission Slit = 5 nm
Scan Speed = 60 nm/min; Chart Speed = 60 mm/min; Time Constant = 2 s

Table 2.4
Fluorescence Characteristics of
Fluka Humic Acid v3 & Aldrich Humic Acid v1

Sample	Excitation Maximum / nm	Emission Maximum / nm	Fluorescence / Arbitrary Units
Fluka Humic Acid v3 (FHAv3)	390 440	490 520	315 290
Aldrich Humic Acid v1 (AHAv1)	350 390 410	460 485 505	480 550 580

Note:
The Emission Maxima result from irradiation at the Excitation Maxima quoted

The fluorescence characteristics of the two samples are given in Table 2.4. These have been determined from the matrices and contour graphs with subsequent detailed analyses of feature locations from the fluorescence data sets.

2.6.4 Discussion

The emission spectrum given in Figure 2.22 is typical of those recorded for both humic acid samples. All display a single broad emission but are otherwise featureless with no sub–spectral features apparent. Excitation at 440 nm for the Fluka sample was noted in Table 2.4 to correspond to fluorescence maxima conditions, thus the spectrum is relatively intense.

The three-dimensional excitation-emission matrices presented for Fluka Humic Acid v3 and Aldrich Humic Acid v1 show clearly that both fluoresce over a wide range of wavelengths, but particularly when excited by ultra-violet or blue light. The matrices indicate the fluorescence maxima and give a complete description of the fluorescence characteristics of the samples. This information will be used to assist the selection of wavelengths in further studies described in Chapter 3.

The broad features of these matrices represent the summation of fluorescence from an

ensemble of functional and structural types within the heterogeneous samples, therefore it is not possible to deduce information concerning functionality or structure.

The fluorescence characteristics of the two samples have been presented in Table 2.4. These have been approximated from the graphs and determined with greater precision from the data sets. For both samples, exact location of the excitation and emission wavelengths have not been possible due to the spectral acquisition parameters selected. A more accurate determination of the maxima would involve the use of a smaller excitation scan interval (e.g., 1 nm), a slower scan speed, and a more advantageous combination of excitation and emission slits. However, it is likely that the broadness of the emission peaks would limit such efforts.

The Fluka Humic Acid sample apparently exhibits three regions of intense fluorescence; but one of these has not been quoted in Table 2.4 since it is believed to be an instrumental artefact. The Aldrich sample gives rise to four maxima pairs, one of which is not quoted for the same reason. The graphs show that these maxima are not strongly pronounced from the surrounding regions.

Consideration of Table 2.4 permits some appreciation for the fate of the excitation energy. The maxima pairs quoted are the most favourable combinations for excitation and emission of radiation. Thus for Aldrich Humic Acid v1, the most probable fluorescence process involves excitation at 410 nm with subsequent emission at 500–510 nm. This process may be favoured for a variety of reasons including the availability of fluorophores and the lack of alternative energy degradation pathways.

Inspection of the table and graphs reveal that Fluka Humic Acid exhibits much weaker fluorescence than the Aldrich sample. It was noted in Sections 2.2.4 & 2.4.4.8 that the former contained more organic material per gram than the latter, therefore if the fluorescence emanates solely from the humic matter and not components of the ash, then fluorescence from the organic material of the Aldrich sample must be much stronger than that from the Fluka. This could be interpreted in terms of a greater concentration of fluorophores, or fluorophores that are more efficient in emitting radiation instead of degrading it by other processes.

In theory, the absorption spectrum of a substance should resemble the mirror image of its emission spectrum when averaged over all excitation wavelengths. For humic acids,

absorption spectra were found to show a continuous decline in absorbance with increasing wavelength (see Section 2.5.3) whereas fluorescence spectra provided broad maxima (Figure 2.23 & 2.25). A violation of this "mirror image" relationship is generally attributed to an appreciable configurational change as a consequence of excitation of the molecule. However, for humic substances it is believed that the fluorophores are present in a low concentration that produces a small but measurable amount of fluorescence, but that their contribution to absorption is negligible.[87]

The fluorescence of the humic acids studied is rather weak. This can be attributed to several factors such as the low concentration of fluorophores, the presence of fluorescence-inhibiting functional groups, structural flexibility, chromaphoric absorption of emitted radiation, static quenching by metal ions present in the ash, and other photochemical processes that do not result in fluorescence.[88–90]

Seal *et al*[88] suspect the fluorophore of humic and fulvic acid to be an aromatic nucleus substituted by at least one electron donating group, or a conjugated unsaturated system capable of a high degree of resonance. The former view is supported by the isolation of several aromatic compounds from the oxidative degradation of humic acid that fluoresce under ultra-violet light. Recent work by Goldberg and Negomir[91] using Fluorescence Depolarisation Spectroscopy suggest the presence of two fluorophores. Visser[86] stated that the probability of the emissive transition between singlet and ground state is increased by electron-donating groups, such as hydroxyl, whereas electron withdrawing groups, such as carboxyl, diminish it. The dependence of fluorescence lifetimes on pH has prompted Milne *et al*[92] to speculate on the role of ionisable functional groups in the fluorophore.

Buffle *et al*[93] have noted that few compounds, including "model" phenol carboxylates, have excitation wavelengths as high as those observed for humic substances. It was also noted that the fluorescence of humic substances is concentration—and so aggregation—dependent. These observations have been explained by analogy with synthetic polymers. A photophysical process that is characteristic of these materials is the formation of excimers or exciplexes by the face-to-face alignment of aromatic ring structures with a typical spacing of 4 Ångstroms. The fluorescence of excimers and exciplexes are typically broadband, featureless and significantly red-shifted from the unassociated (monomeric) fluorescence. Humic substances, because they are aggregated to some

extent, provide many possibilities for achieving the conformations required for excimer formation. Exciplexes, for which the aromatic fluorophores are dissimilar, may have increased red-shifts in their excitation spectra due to a greater charge transfer character in the transitions. [94] The involvement of excimers in the fluorescence of Fluka Humic Acid has also been postulated by Balkas *et al.* [60]

2.6.5 Conclusions

The fluorescence characteristics of Fluka Humic Acid v3 and Aldrich Humic Acid v1 have been determined. Both samples were found to fluoresce over a wide range of wavelengths with several maxima superimposed on a broad feature. Fluorescence is strongest for irradiation in the ultra-violet or the blue end of the electromagnetic spectrum. Fluorescence spectra show little resemblance to ultra-violet/visible absorption spectra, suggesting that fluorescence is not the most likely mechanism for degrading the absorbed radiation possibly since the fluorophores are present in a small concentration.

2.7 Fractionation and Molecular Weight Distribution

2.7.1 Introduction

The molecular weight profile and the weight average molecular weight of Aldrich Humic Acid have been determined following fractionation by ultrafiltration. Electronic absorption spectroscopy has been used to determine the proportions of the humic acid ultrafiltration fractions from their characteristic absorbances, and absorbance spectra in the visible and ultra-violet regions have been recorded.

The macro-structure of humic substances is believed to be of coiled, long-chained molecules, or two- or three-dimensional cross-linked macromolecular structures (see Chapter 5). [6] Aqueous dispersions of humic substances are polydisperse with sizes ranging from colloidal to particulate. The best methods for determining their molecular weights provide a molecular weight distribution that illustrates this polydispersity. Molecular weight is an important attribute of humic substances since the extent of some physical and chemical processes such as adsorption, coagulation and metal ion

complexation, depend on the specific molecular weight of fractions. [95,96]

A variety of methods have been used for measuring the molecular weights of humic substances. These are normally grouped into three classes depending on the type of average molecular weight measured: Number average molecular weights, $\overline{M}_n$, are determined by colligative methods; weight averages, $\overline{M}_w$, by measuring the weights of fractions; and z–averages, $\overline{M}_z$, by ultracentrifugation. Wide ranges in values for various humic substances have been reported. [1,50] In this study, the weight average molecular weight distribution of Aldrich Humic Acid is deduced from the proportions and molecular weights of individual fractions produced by ultrafiltration. Ideally, such fractions should be monodisperse. $\overline{M}_w$ is the mean of the weight fraction distribution curve and is defined by:

$$\overline{M}_w = \frac{\sum \left(w_i \times \overline{M}_i \right)}{\sum w_i}$$

Where:

w_i = Weight of fraction i

$\overline{M}_i$ = Mean molecular weight of fraction i

The Σw_i term may be regarded as a normalisation factor. The masses of each fraction determined through a calibration procedure may be equated with w_i, and the mean molecular weight of the fraction with $\overline{M}_i$, since the ultrafiltration fractions have a range of sizes rather than a unique value.

Fractionation of humic substances has been reported using several methods. [95–100] Some, such as gel filtration, are subject to problems resulting from the interaction of the organic matter with the fractionation medium. [95] Gjessing [101,102] concluded that Amicon ultrafilters give a better estimate of molecular dimensions than Sephadex® gel filtration since ultrafiltration membranes are less likely to give charged interactions than Sephadex® materials.

Ultrafiltration is the selective rejection of solutes by convective solvent flow through an anisotropic membrane. Particles of dimensions larger than the specified membrane cut-off are quantitatively retained whilst solutes smaller than the pore size of the skin pass through the membrane sub–structure. Ultrafiltration is more refined than simple

filtration which removes all particles. The sizes of the particles sieved are in the macromolecular range rather than the particulate range, namely 1 nm–0·02 μm. Each membrane is characterised by its nominal molecular weight cut–off which is operationally defined with model solutes. The cut–off level refers to the approximate molecular weight of a globular solute that is 90 % rejected by the membrane. The broad range of selectivities available through various Amicon membranes permits fractionation into size-graded classes.[103]

Amicon ultrafilters membranes are cast from a variety of polymer solutions. They consist of a dense skin of controlled pore structure that opens to a more open-celled spongy layer of the same polymer. Retained substances are rejected at the membrane surface.[103] To minimise any differences in filter-to-humic material interactions, just two types of filter were used in the fractionation scheme here. The relationship between the pore size and the molecular weight is illustrated by the XM 300 filter which has a nominal molecular weight cut–off of 300000 daltons and an average pore size of 0·018 μm, which lies within the colloidal range.

Migration of molecules through membranes is generally accompanied by a combination of advective flow and molecular diffusion. The flux of solute is directly related to the area of the membrane, the concentration gradient and molecular diffusion while being inversely related to the temperature. Donnan potentials may be generated through non–transport of some solutes leading to an unequal distribution across the membrane. Maintenance of a constant pH and ionic strength help to minimise this effect.[104] The problem of concentration polarisation, which is the accumulation of retained macrosolute above the membrane, is overcome by continually breaking up the layer as it forms by magnetic stirring above the membrane. If left undisturbed, concentration polarisation restricts solvent and solute flow and creates a secondary membrane.

Ultrafiltration of Aldrich Humic Acid was performed using the concentration method that was also used by Alberts and Dickson.[52] In this method, while the concentration of the non–permeating species is increased and the volume of the retained fluid is reduced, the concentration of the membrane-permeating species (salts and micro–ions) remains unchanged in the retained fluid.[105] This procedure is preferable since adjustments to the compositions of the filtrates are not required. In this scheme the first membrane used has a large pore size resulting in a retained fraction of high molecular weight. The

filtrate is refiltered using a filter of the next smallest pore size following dilution to its original volume. Fractions obtained in this way have sizes within a range rather than just a collection of all sizes below a certain limit, as obtained by Collins *et al.* [106]

The dark colour of humic substances permits use of light absorption for the analysis of these materials (see Section 2.5). A study was undertaken to establish the relationship between the concentration of humic matter and absorbances at selected wavelengths. Proportionality in a calibration curve would permit determination of the concentration of humic acid fractions following ultrafiltration. Some studies have used the absorbance at 254 nm to monitor the total organic carbon content of humic substances [107] and the concentration of humic substances. [95] Buffle *et al* [108] used the absorbance at 285 nm to estimate the concentration of humic substances of fulvic and humic acids following fractionation in unpolluted fresh waters. The applicability of these wavelengths is assessed.

The ratio of the absorbances of dilute, aqueous solutions of humic materials at 465 nm and 665 nm, E_4:E_6, is widely used by soil scientists in the characterisation of these materials. [1] Chen *et al* [109] have shown that the ratio is primarily governed by the particle size (or molecular weight); a low ratio implying a high molecular weight, and vice versa. Therefore, the ratio can be used to demonstrate fractionation. The ratio is related to the concentrations of free radicals, contents of O, C and COOH, and the total acidity. The ratio is affected to some extent by the pH of the dispersion and the ash content of the organic matter. [110] It does not appear to be affected by the concentration of the condensed aromatic rings or by the concentration of the humic dispersion. [109]

2.7.2 Experimental

The dispersion medium for the humic material was 0·001 M $NaOH_{(aq)}$ that was obtained by serial dilution of a B.D.H. A.R. concentrated volumetric solution of sodium hydroxide (¢032). Aldrich humic acid v2 was prepared for fractionation by dispersing 10·0 g in the dilute alkali yielding a dispersed concentration of 2·0 % w/v. This was towards the upper end of the 0·05–10 % w/v concentration range suggested by the ultrafiltration membrane manufacturer. The alkali concentration was within the limits suggested by the manufacturer for the membranes and the ultrafiltration cell

components. [103] The pH of the dispersion medium was controlled since it was realised that the molecular weight distribution may be affected by the composition of the dispersion medium.

The ultrafiltration apparatus was prepared by soaking each membrane (¢033) in distilled water that was repeatedly exchanged. This procedure removed traces of glycerin which was added to prevent dehydration, and sodium azide present as a preservative. [111] The first cleaned membrane (XM 300) was inserted into the Standard Cell of maximum volume 400 ml (¢034). This cell is useful for concentration down to around 10 ml. 250 ml of the dispersion (equivalent to 5 g of Aldrich Humic Acid) was poured into the cell chamber and sealed. The cell was placed on a magnetic stirrer and gas pressure (¢009) between 10–70 p.s.i. was applied, according to the manufacturer's recommendations for the best separation. Following concentration of the retentate to around 20 ml, the pressure was released and ultrafiltration was stopped. The retained material was quantitatively transferred to a volumetric flask and diluted to 250·0 ml with distilled water. The membrane was discarded and replaced by one with the next smallest pore size (XM 100A). The ultrafiltrate was also diluted to 250·0 ml and then refractionated through the XM 100A membrane. This procedure was repeated for the other membranes given in Figure 2.27. Following ultrafiltration with the final membrane (YM 2), both filtrate and retentate were quantitatively diluted.

The 2·0 % w/v Aldrich humic acid stock was serially diluted with distilled water to yield concentrations between 0·0005 % w/v and 0·004 % w/v. Absorbance spectra of the dilutions were recorded against wavelength λ in the range 200–700 nm, on the Pye-Unicam SP8–100 spectrophotometer (¢029) in the manner described in Section 2.5.2. Absorbances of the calibrants were recorded with the monochromator fixed at 254 nm to produce a calibration graph relating measured absorbances to humic acid concentrations.

Absorbance spectra and absorbances at 254 nm were similarly recorded for the fractions at suitable dilutions such that their absorbances were within the calibration range. Absorbances were also recorded with the monochromator located at 465 nm and 665 nm on less diluted samples of each fraction since absorption in the visible region of the spectrum is lower than in the ultra-violet. This permitted calculation of the E_4:E_6 ratio for each fraction.

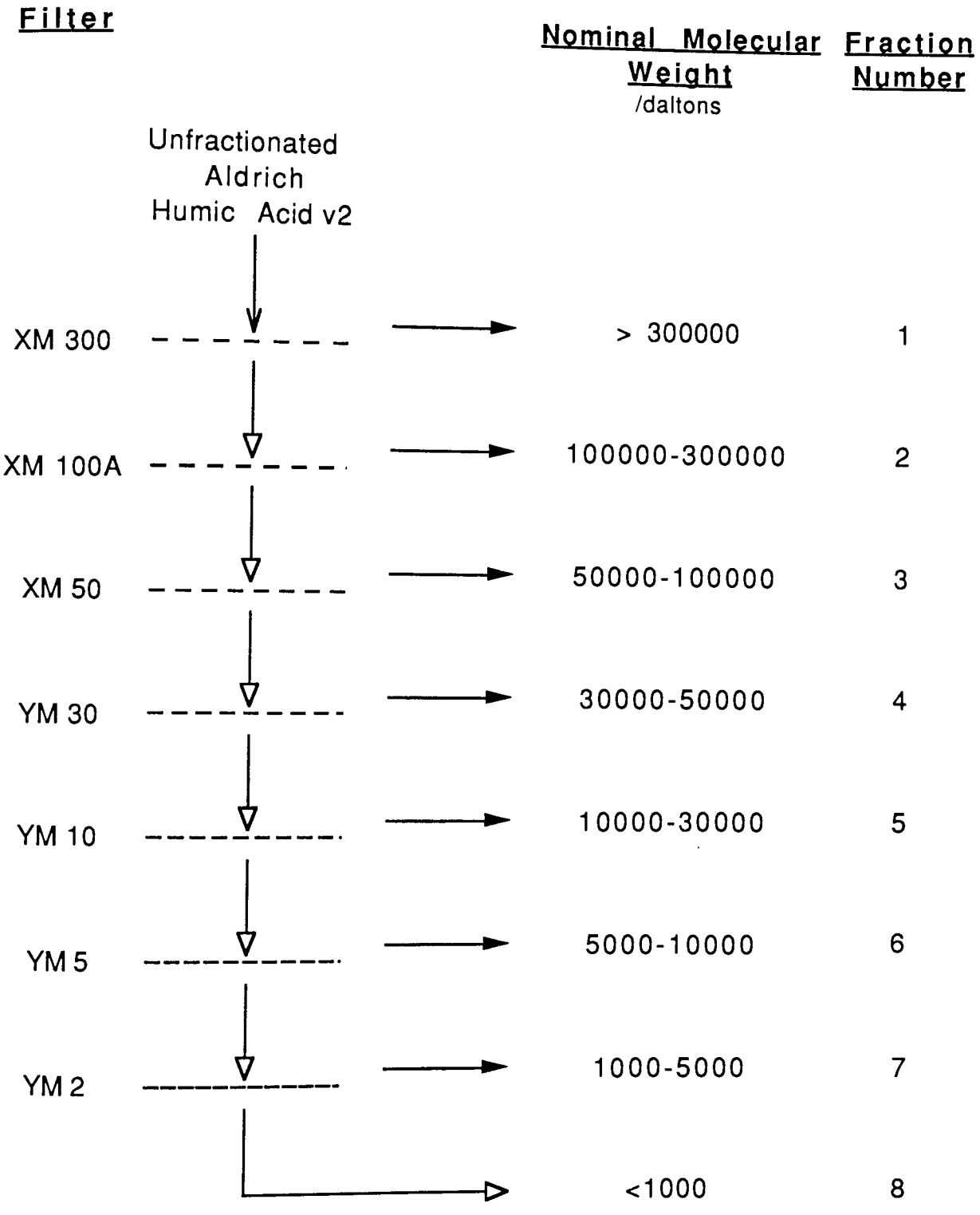

Figure 2.27

Fractionation of Aldrich Humic Acid v2 by Ultrafiltration

Notes:
Filled arrows represent retentate collection and unfilled arrows represent filtrates that are refractionated
Nominal Molecular Weight Values are based on 90 % retention of the solute

2.7.3 Results

The electronic absorption spectra for serial dilutions of Aldrich Humic Acid v2 are given as absorbance against wavelength in Figure 2.28. Absorbances at 254 nm are plotted against the concentration of the humic acid in Figure 2.29 yielding a calibration curve. The best fit is a straight line hence absorbances at 254 nm, $A_{(254\ nm)}$, are proportional to the concentration of the humic matter, c. The Beer-Lambert law (discussed in Section 2.5.3) applies and the proportionality constant is the molar absorptivity (molecular extinction coefficient) of the absorbing species. The molar absorptivity was not calculated since it requires concentrations to be in mol dm^{-3} units, however the equation for the best fit line can be used to give the concentrations of the humic acid fractions:

$$\text{Concentration, c (\% w/v)} = \frac{A_{(254\ nm)} + 4.975 \times 10^{-3}}{242.65}$$

Electronic absorption spectra at various dilutions for several fractions are given in Figure 2.30. The absorbances at 254 nm for all fractions obtained at suitable dilutions are given in Table 2.5. The corresponding concentrations of each fraction, calculated from the above equation and accounting for the dilution used are also given.

Table 2.5 includes the nominal molecular weight range for each fraction and the corresponding mean value. These were used to calculate the molecular weight profile and the weight average molecular weight of the humic acid. The weights of each fraction, w_i were equated with the calculated concentrations. The sum of these, Σw_i has a value of 2·1 % w/v. This gives a deviation of around 6 % from the 2·0 % w/v actually used in the preparation of the stock. Weight fractions, $w_i \times \overline{M}_i$ were calculated by multiplication of the weight of the fraction, w_i by its mean molecular weight, $\overline{M}_i$. These were then used to calculate the weight average molecular weight by insertion into the equation:

$$\overline{M}_w = \frac{\sum \left(w_i \times \overline{M}_i \right)}{\sum w_i}$$

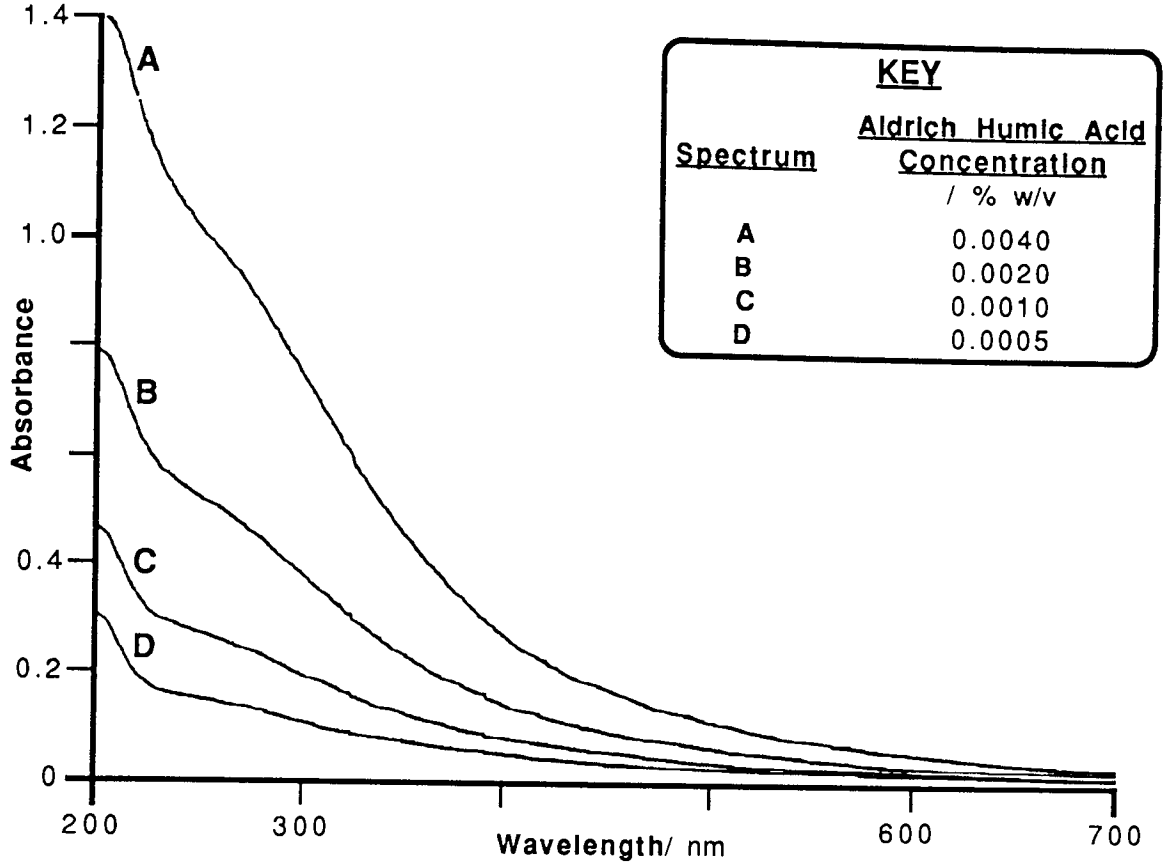

Figure 2.28

Ultra-Violet/Visible Absorbance Spectra for Serial Dilutions of Aldrich Humic Acid v2 (Beer-Lambert Law Proportionality Determination)

Sample Conditions: Dispersion Medium: ~0.00001 M NaOH(aq)
Spectral Acquisiton Conditions: Scan Speed = 2 nm/s; Chart Speed = 10 s/cm; Bandwidth = 2 nm; 1cm Quartz Cuvette; Reference = Distilled Water

Figure 2.29

Aldrich Humic Acid Calibration Graph for 254 nm Absorbance

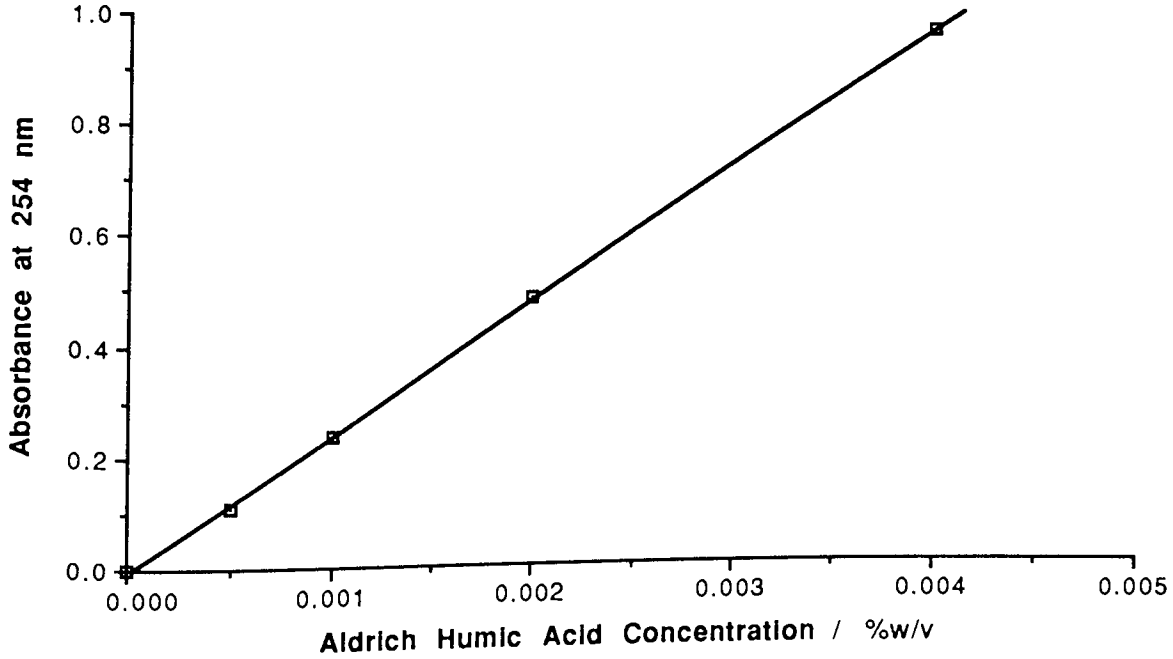

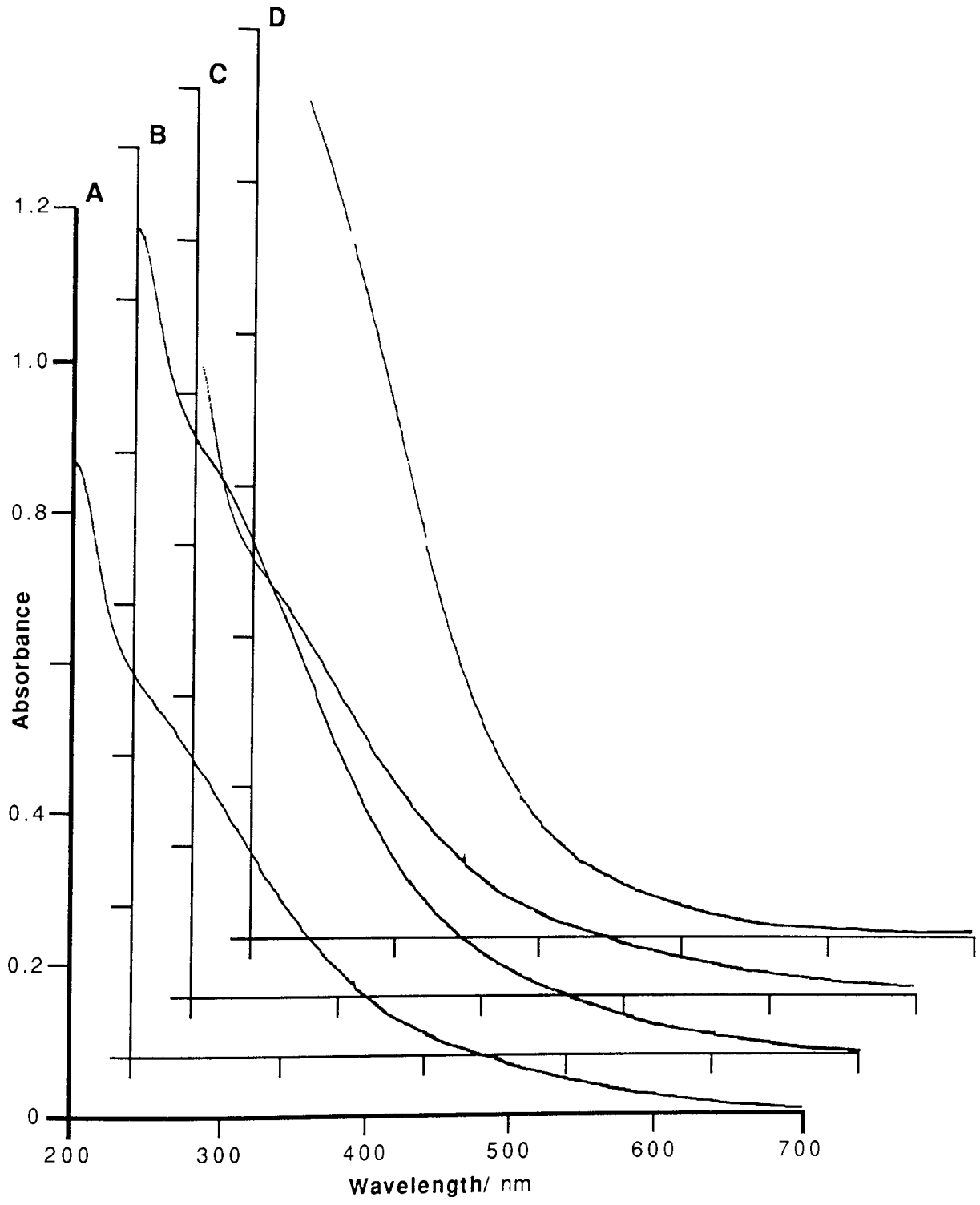

Figure 2.30

Ultra-Violet/Visible Absorbance Spectra for Aldrich Humic Acid v2 Fractions Obtained by Ultrafiltration

Spectrum	Fraction Number	Nominal Molecular Weight Range/ daltons	Dilution
A	1	<1000	200
B	3	5000-10000	200
C	5	30000-50000	50
D	7	100000-300000	100

Sample Conditions: Dispersion Medium: ~0.00001 M NaOH(aq)
Spectral Acquisiton Conditions: Scan Speed = 2 nm/s; Chart Speed = 20 s/cm; Bandwidth = 2 nm; 1cm Quartz Cuvette; Reference = Distilled Water

Table 2.5
Analytical Information for the Fractionation of Aldrich Humic Acid v2 by Ultrafiltration

Fraction Number	Nominal Molecular Weight Range / daltons	Mean Molecular Weight of Fraction (M_i) / daltons	Absorbance at 254 nm (A_{254})	Dilution of Fraction	Aldrich Humic Acid Concentration † (w_i) / % w/v	Weight Fraction ($w_i \times M_i$)	Absorbance at 465 nm (A_{465})	Absorbance at 665 nm (A_{665})	Dilution of Fraction	Absorbance Ratio ($E_4:E_6$) ($A_{465}:A_{665}$)
8	<1000	500	1.32	20	0.11	55	0.63	0.03	1	22.6
7	1000-5000	3000	1.03	100	0.43	1280	1.29	0.04	5	32.3
6	5000-10000	7500	0.97	50	0.20	1500	0.98	0.07	5	14.6
5	10000-30000	20000	0.53	50	0.11	2220	0.76	0.09	5	8.1
4	30000-50000	40000	0.45	50	0.09	3740	0.65	0.09	5	7.6
3	50000-100000	75000	0.80	200	0.67	50000	0.25	0.04	100	6.6
2	100000-300000	200000	0.48	25	0.05	10000	0.38	0.06	5	5.9
1	>300000*	650000	1.12	100	0.46	300000	0.45	0.15	50	3.0

Notes

** Upper value not defined*

† Determined from calibration graph of unfractionated Aldrich Humic Acid v2

1 cm path length quartz cuvettes used for absorbance determinations

Figure 2.31
Aldrich Humic Acid Molecular Weight Profile
Showing Weight Fractions

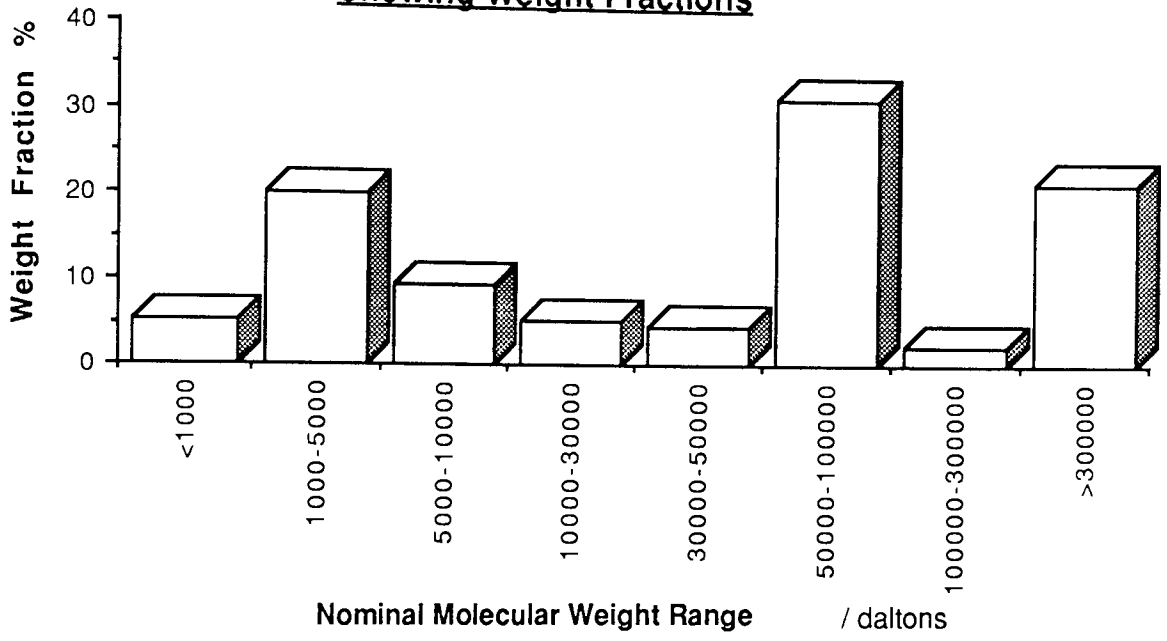

Note: Weight Fraction data determined from normalised absorbances of fractions at 254 nm

Figure 2.32
Aldrich Humic Acid Molecular Weight Profile
Showing Weights of Fractions per Molecular Weight Unit

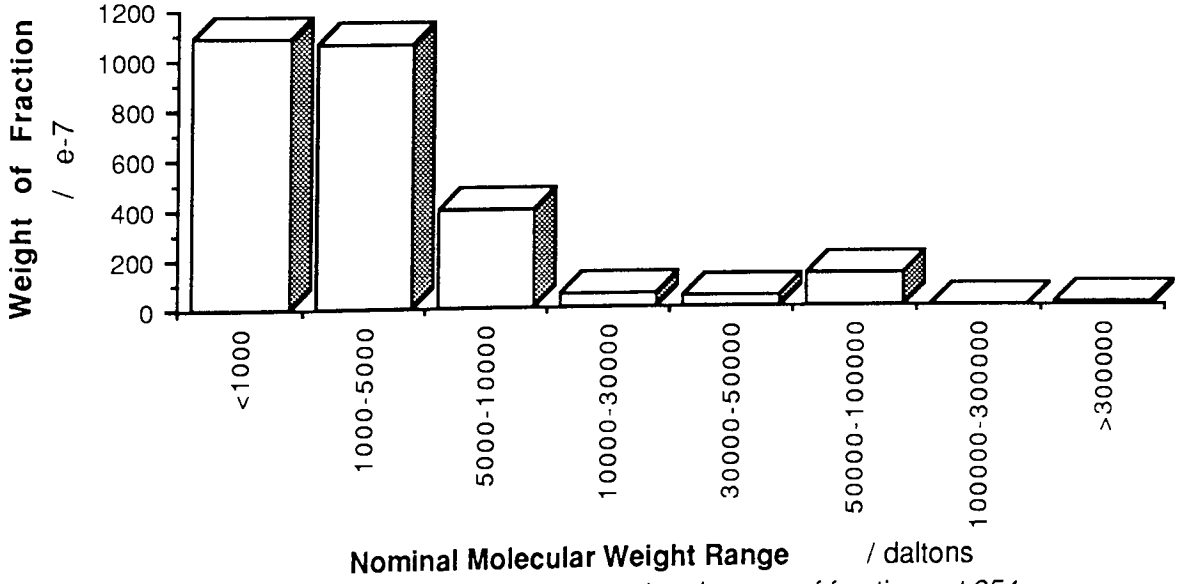

Note: Weight Fraction data determined from absorbances of fractions at 254 nm and modified for the molecular weight ranges of the fractions

Figure 2.33

Ratio of Absorbances at 465 nm and 665 nm (E4:E6) against Molecular Weight of Aldrich Humic Acid Fractions

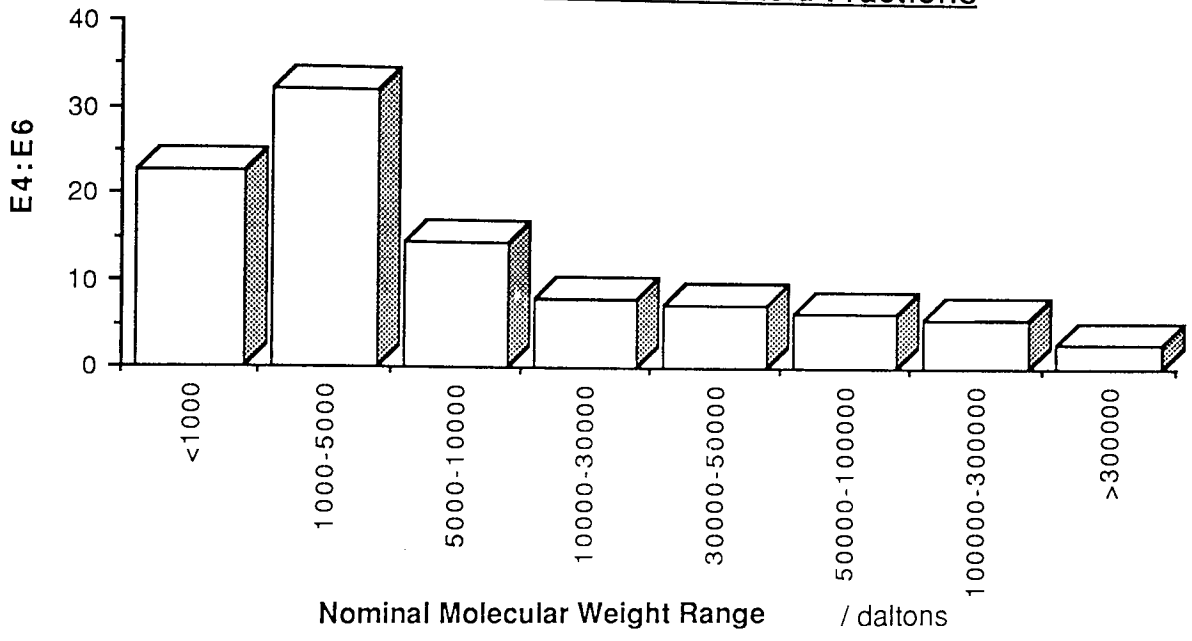

Note: Pairs of absorbances determined for the same dilution and a constant path length

Where:

$$\sum \left(w_i \times \overline{M}_i \right) = 370000$$

$$\sum w_i = 2{\cdot}1$$

Therefore,

$$\overline{M}_w = 170000 \text{ daltons}$$

Figure 2.31 shows the weights of fractions, w_i expressed as percentages of $\sum w_i$. This provides a molecular weight distribution of the humic acid that does not account for the molecular weight ranges of individual fractions. Figure 2.32 gives the molecular weight distribution with an ordinate of weight of each fraction modified for its molecular weight range.

Table 2.5 also gives the absorbances of the fractions at 465 nm and 665 nm. The dilutions used were such that the absorbances were within sensible measurement limits. The calculated E_4:E_6 ratios are given and these are plotted in Figure 2.33 against the molecular weights of the fractions.

2.7.4 Discussion

The electronic absorption spectra of the unfractionated calibrants (Figure 2.28) show a simple variation with humic acid concentration across the spectral range implying that no significant concentration-dependent interactions occur at these dilutions, when studied using this technique. Their 254 nm absorbances have a linear variation with humic acid concentration thus permitting the concentrations of the fractionated organic matter to be determined from absorbances at this wavelength. This is consistent with the work of Dobbs *et al*[107] and Amy *et al.*[95]

It is somewhat unexpected that the sum of the concentrations of the fractions is greater than that of the unfractionated material. This implies that there were minimal losses during ultrafiltration. However, the 6 % discrepancy prompted closer examination of the calibration procedure since the sum is important in the derivation of the weight average molecular weight. The calibration relies on the assumption that the unfractionated Aldrich Humic Acid and its ultrafiltration fractions have the same content of chromaphoric groups per unit mass and equal molar absorptivities, thus enabling direct comparisons between them. The discrepancy implies that the assumption doesn't hold when applied to different fractions since these probably contain different proportions of absorbing species. Over the whole sample, it would simplistically be anticipated that this would be removed by the summation routine. During fractionation, the composition of the sample was not monitored but Buffle *et al*[108] concluded that the effect of electrolyte concentration, pressure and pH on the ultrafiltration of organic matter from fresh waters was minimal if extreme conditions were avoided. Therefore this can be discounted as a potential source of problems.

The humic acid absorption spectra shown in Figure 2.30 are typically featureless showing no maxima or minima. However, some variation occurs in the shape of the spectra which implies that fractionation has occurred. However, there is little evidence for the emergence of peaks in the spectrum therefore suggesting that the fractions are still heterogeneous and the spectra represent the summation of the absorbances from structural and functional units in many similar macromolecules. The differences are clearer from the ratio of absorbances at 465 nm and 665 nm, E_4:E_6, given in

Table 2.5 which changes with the molecular weight of the fraction. The lower molecular weight fractions have high ratios, and vice versa thereby confirming that fractionation was successful. It is notable that the intensity of (Rayleigh) scattered light at 465 nm and 665 nm based solely on these wavelengths should differ by a factor of four (see Section 5.6.1) since this depends on the inverse fourth power of the wavelength. Since humic substances *are* known to scatter light (see Chapter 5), this may have a significant contribution to the E_4:E_6 ratio since this assumes that the amount of light transmitted is solely dependent on absorption.

The molecular weight profiles of Figures 2.31 and 2.32 show clearly that Aldrich Humic Acid has a broad molecular weight distribution which explains its polydispersity in aqueous dispersions. The presentation formats employed emphasise high or low molecular weight fractions: Figure 2.32 emphasises low molecular weights since these fractions have a relatively high concentration but over a narrow molecular weight span. The graph of the E_4:E_6 ratio against the molecular weight of the fraction in Figure 2.33 displays a smooth decline towards high molecular weights and shows clearly that fractionation was successful.

The weight average molecular weight was reconstructed from the measured weights and mean molecular weights of the humic acid fractions. Note that use of concentrations as the weights of fractions is justified since the appropriate factors required to convert these into true weights cancel from the expression for $\overline{M}_w$. Ideally, each fraction should be monodisperse, however the nature of the fractionation procedure is crude since just exclusion of one broad type of molecules from another occurs. The results provide an index of apparent molecular weight than can be used for relative comparisons. This should be considered with scrutiny for several reasons, mainly associated with the techniques used. Ultrafiltration is not a real measure of molecular weight but rather of molecular size. Nominal molecular weight cut–off levels are operationally defined as the approximate molecular weight of a model solute that is 90 % rejected by the membrane.[103] Humic substances do not necessarily have the same macromolecular configurations as the calibrants, which tend to be of tightly coiled, globular molecular configurations, whereas the shapes and sizes of humic substances are a complex function of solution variables, such as pH and ionic strength (see Chapter 5). Further, in practice, the molecular weight cut–offs quoted by the manufacturer tend not to be precise.[104] Jeffrey[112] noted that in practice, many biological molecules are in a concentration-dependent self-association equilibrium, so that the effective molecular

size at the membrane surface may be much larger than the unassociated molecule and increased rejection may occur. A similar situation may occur with humic materials since they too can exist in condition-dependent macromolecular configurations.

The weight average molecular mass has a strong bias towards high molecular mass fractions in the calculation of $\overline{M}_w$. Measurement of the number average molecular weight by colligative methods tends to emphasise the low molecular weight components. [85]

2.7.5 Conclusions

An aqueous dispersion of Aldrich humic acid has been fractionated by ultrafiltration into eight fractions. The E_4:E_6 ratio was sensitive to the fractionation procedure and some differences were apparent in the absorption spectra of the fractions. The concentrations of the fractions were determined by electronic absorption spectroscopy and thence the molecular weight distribution and the weight average molecular weight were calculated. The molecular weight distribution was broad with organic matter collected for all the ultrafilters employed. A weight average molecular weight of 170000 daltons was derived for Aldrich Humic Acid v2.

2.8 Conclusions

Although purification of the Fluka Humic Acid v1 sample was successful so that it can be reliably defined by the acidity limits of pH 1 and pH 13, it was decided not to apply this procedure to the other commercial humic acid sample, or to use the purified Fluka sample as a focus for the experimental studies described in the main Chapters. This arose following reconsideration of the experimental methodology. One aim of the purification procedure is to make the composition of the sample more certain, however removal of various components of the sample in the fractionation procedure creates a different material that other workers cannot necessarily refer to, unless the same purification procedure is applied. Preferential extraction of some material probably occurred thereby changing the nature of the sample. This is confirmed by elemental analysis of the purified humic acid which showed different atomic proportions because of the solubility-based fractionation procedure. However, it is appreciated that whatever the extractant used,

some selectivity will occur since impure humic substances contain a variety of materials, not just organic matter. Malcolm and MacCarthy [49,50] purified a sample of Aldrich Humic Acid. They observed changes in its elemental analysis that were difficult to evaluate since they may have resulted from preferential extraction of selected components or from a more precise analysis following ash removal. Further concern derives from subsequent evaluation of the literature which suggests some uncertainty in the usage of the alkaline extractant since it may have caused some chemical alteration of the sample through autoxidation of the organic matter on standing. [6] Condensation reactions between amino acids and carbonyls of aromatic aldehydes and quinones may have occurred. It is possible that phenolics may oxidise under alkaline conditions and under acidic conditions in the presence of ferric ions available from inorganic impurities. [55,56] Yong and Mourato noted that their alkaline extraction procedure altered the chemical characteristics of the extract. [53] Other chemical extractants tend to have less associated problems than sodium hydroxide but much less organic matter is extracted so that the fraction removed is preferentially extracted.

The humic acids and fulvic acid used in this thesis were characterised by the application of several techniques. Elemental analysis of commercially obtained Fluka and Aldrich humic acids revealed high proportions of carbon implying that they are predominantly aromatic. Infrared spectroscopy of humic materials contradicts this since spectra imply that the humic and fulvic acid samples studied are predominantly aliphatic, although some evidence for aromatic and alkene carbons was observed. However, the spectra provided little information concerning the precise chemical structure of the humic and fulvic nuclei. The samples are functionalised mainly with oxygen-containing groups such as hydroxyl, carboxyl, carboxylate, and other carbonyls.

Compositional analysis also showed that moisture and ash form a large proportion of the samples. Purification of Fluka humic acid succeeded in reducing the ash content of the sample and resulted in the conversion of carboxylate to carboxyl groups. Complexation of Fluka humic acid produced an opposite infrared spectral effect. The infrared spectra of a fulvic and humic acid from the same source were compared; these had similar structures, but the fulvic acid is more functionalised than the humic sample. Further attention is paid to the structural form and functionality of the humic materials in Chapter 4 where proton and carbon–13 nuclear magnetic resonance spectroscopy is applied to humic acids.

Infrared spectroscopy was used to supplement studies of the thermal stability of humic materials through analysis of their pyrolysis residues; these were mainly siliceous but some evidence for carbonaceous matter was apparent. Thermogravimetric analysis of humic acids revealed that some components of the samples are quite thermally stable resulting in significant ash contents. Pyrolysis-induced decomposition of humic acids occurred over a wide temperature span but uniquely defined processes were not identified.

Although humic substances are coloured their ultra-violet and visible absorption spectra are typically featureless showing a progressive decrease in absorbance with increased wavelength. It was not possible to deduce the identity of constituent chromophores as characteristic bands were not observed. Further, spectra were of no use in suggesting wavelengths suitable for excitation of the humic matter in fluorescence studies.

Both Fluka Humic Acid v3 and Aldrich Humic Acid v1 fluoresce over a wide range of wavelengths with maxima superimposed on a broad feature. Fluorescence is strongest for irradiation in the ultra-violet or the blue region of the electromagnetic spectrum. Fluorescence spectra show little resemblance to ultra-violet/visible absorption spectra, suggesting that fluorescence is not the most likely mechanism for degrading the absorbed radiation, possibly since the fluorophores are present in a small concentration. The fluorescence characteristics of Fluka Humic Acid v3 and Aldrich Humic Acid v1 are reconsidered in Chapter 3 where photophysical processes are studied in the presence of a fluorescent metal ion.

An aqueous dispersion of Aldrich humic acid has been fractionated by ultrafiltration to yield a weight average molecular weight of 170000 daltons from a broad molecular weight distribution. The E_4:E_6 ratio was sensitive to the fractionation procedure. The particle sizes of aqueous dispersions of humic materials are considered in Chapter 5 since these macromolecules have colloidal dimensions.

CHAPTER 3
PHOTOPHYSICAL STUDIES of ENERGY TRANSFER between EUROPIUM(III) and FLUKA HUMIC ACID

3.1 Introduction

Humic substances exhibit fluorescence following irradiation by both ultra-violet and visible light (see Section 2.6). Similarly, lanthanide metal ions may absorb light and emit fluorescent light following some degree of energy degradation. [113–115] When present in the same medium, these materials may form complexes [6,13,26,27,33–38,41] or aggregates [26] under certain conditions. Literature citations of these materials stem from the significance of humic substances in environmental transport of trivalent actinides for which the europium(III) ion serves as a good analogue. [8,13,26,27,33–42]

The studies described in this Chapter investigate photophysical processes that result from irradiation of an aqueous medium containing europium(III) and Fluka Humic Acid. The photophysical characteristics are exploited and the transfer of energy between the components is probed. A mechanism is proposed that models these processes.

3.1.1 Electronic Structure and Luminescence of Lanthanides

The electronic structures of trivalent lanthanide ions are of the type $[Xe]4f^n$, yet the 4f electrons are not the outermost ones: They are shielded from external fields by the $5s^2$ and $5p^6$ sub–shells which have a larger radial extension. [116] Because of this shielding, the various states arising from f^n configurations are split by external fields only to the extent of ~100 cm^{-1} and are little affected by ligand field effects. Thus when f–f transitions occur, the absorption bands are very sharp: They are similar to those of free atoms and quite unlike the broad bands observed for spectra of the d–block metals. The weakness of the lanthanide absorption bands arises since the f–f transitions are formally electric dipole or Laporte forbidden. [117] Small transition probabilities result in long luminescence lifetimes.

Rare earth ions in which the 4f electronic orbitals are incompletely filled absorb

electromagnetic radiation in the near ultra-violet, the visible and the near infrared. [118] Charge transfer transitions may also occur in this region of the electromagnetic spectrum when an easily oxidised ligand is bound to a reducible trivalent ion, such as europium(III). The position of these bands in the spectrum depends markedly on the ligand. [118]

Lanthanide ions in the middle of the series, like europium(III), form complexes that may emit visible radiation when excited in the ultra-violet. The strength of this fluorescent emission depends on the environment of the cation. [118] Experiments described in this Chapter monitor fluorescent emissions from "complexes" of europium(III) with Fluka Humic Acid to probe the transfer of energy between them.

3.1.2 Boltzmann Population of Europium(III) Energy Levels

The electronic energy levels and term scheme for the Eu^{3+} ion are given in Figure 3.1. The population of ground state energy levels in the Eu^{3+} ion at room temperature can be calculated from the Boltzmann distribution: [119]

$$\frac{N_i}{N_j} = \exp\left[-\frac{(E_i - E_j)}{kT}\right]$$

Where:

E_i = Energy of level$_i$
E_j = Energy of level$_j$
N_i = Population of level$_i$
N_j = Population of level$_j$
k = Boltzmann constant
T = Absolute temperature

When applied to the Eu^{3+} ion, this treatment predicts a 19 % occupancy for the first excited state, $^7F_1$, 0·9 % for the second, $^7F_2$, and 0·01 % for the third, $^7F_3$. Thus Eu^{3+} excitations may well stem from energy levels above the ground state but with rapidly diminishing probability.

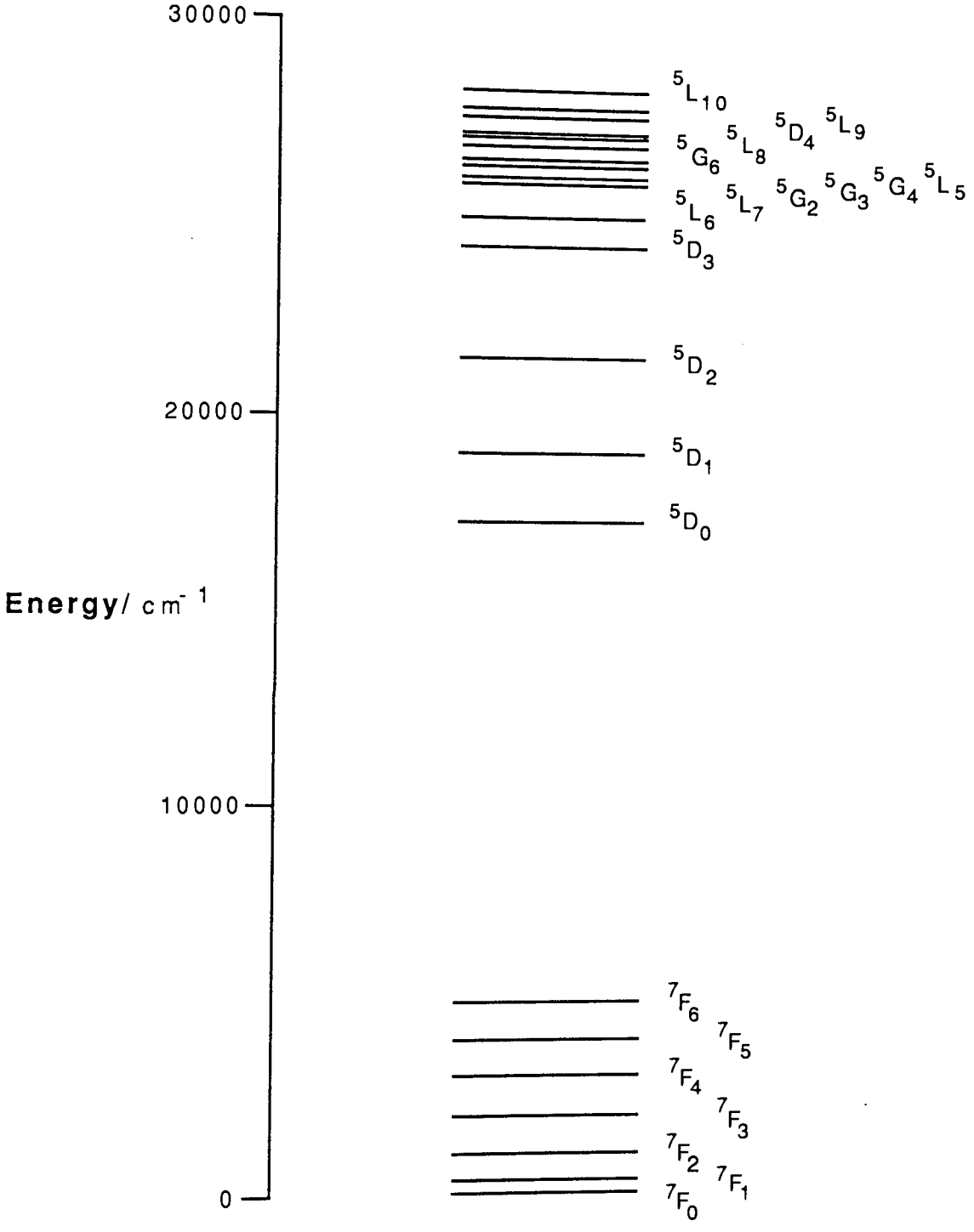

Figure 3.1

Free Ion Energy Levels and Term Scheme of Eu^{3+}

The first and second electronically excited states of Eu^{3+} occur at lower energies than the lowest excited state for any of the other lanthanide elements. Therefore, for Eu^{3+} these levels have appreciable occupancies at room temperature whereas for other elements in the series, occupancies are negligible. This results in excitations originating from three energy levels (see Figure 3.1). Higher electronically excited states of Eu^{3+} are accessible using ultra-violet and visible radiation.

3.1.3 Europium(III) Solution and Co-ordination Chemistry

Trivalent europium(III), $[Xe]4f^6$, is the stable oxidation state of the metal in aqueous solution. The divalent state, $[Xe]4f^7$, which can be produced by zinc amalgam reduction, is more stable than the other divalent lanthanides, yet aeration still results in re-oxidation. [113,117]

For europium(III) in aqueous solution, water is a better ligand than other complexing agents (and is present in a much larger quantity) thus aqua complexes dominate. A strong preference is expressed towards negatively charged donor groups that are also "hard" bases. For neutral ligands, the preferred donors are: O > N > S. Complexes with polydentate chelating ligands in which oxygen is the donor atom are the most stable formed. Europium complexes have predominantly ionic interactions between the metal and the ligands. They lack directionality and so stereochemical preferences within the inner co-ordination sphere are determined almost entirely by solvation effects and ligand characteristics (conformational properties, and the number, sizes, and charged nature of the donor groups).

3.1.4 Donor-Acceptor Energy Transfer Processes

Förster [120] described several mechanisms for energy transfer between a donor and an acceptor. McCapra [121] recently reported the exploitation of such processes in homogeneous assays resulting in the transfer of excitation energy to an acceptor molecule and the appearance of a different emission wavelength. Separate literatures exist concerning energy transfer processes that involve trivalent europium ions or humic substances.

3.1.4.1 Energy Transfer Processes Involving Europium(III)

The fluorescence of rare earth complexes is of particular interest due to the occurrence of electronic energy transfer from some organic ligands to the rare earth ion and hence their applicability in laser systems.[122,123]

Europium is known to partake in energy transfer reactions in aqueous solution. For example, Alpha and co-workers[124] noted that the inclusion of europium into the intramolecular cavity of a macropolycyclic cryptate ligand provided an efficient shielding of the bound species from interaction with the solvent and other solute molecules and thus modified physical properties. An emission in aqueous solution at room temperature was observed whereas simple aqua europium complexes do not luminesce under the same conditions. Europium emission from $^5D_0$ was observed following intramolecular energy transfer from the π,π^* excited state of the ligand. A contribution from charge-transfer was not excluded, although no such band was observed.

3.1.4.2 Energy Transfer Processes Involving Humic Substances

The central role of humic substances in photosensitised transformations involving electronic energy transfer in natural waters has been discussed by several workers.[78,125,126] For example, Frimmel and Bauer[78] stated that humic substances are the main sunlight absorbing components in surface waters. Photochemical processes that may result include absorption, intersystem crossing, and deactivation. Photochemical reactions can occur to the humic substances themselves or involve other molecules after energy transfer.

3.1.5 Selection of Energy Transfer Monitoring Wavelengths

In order to study photophysical processes in aqueous "complexes" of europium(III) with humic acid so that an unambiguous image of such processes is provided, appropriate monitoring wavelengths have to be selected.

In Section 2.6, the fluorescence characteristics of two humic acids were determined by analysis of three-dimensional and contour excitation-emission matrices. It was shown that Fluka Humic Acid v3 fluoresces over a wide range of wavelengths, but particularly when excited by ultra-violet or blue light. A broad excitation maximum was observed with the most favourable irradiation wavelength of 390 nm resulting in emission at 490 nm and a second favourable excitation at 440 nm providing emission at 520 nm. However, it was found that these maxima are not strongly pronounced from the surrounding regions. The continuous nature of the humic acid fluorescence makes the selection of wavelengths for monitoring energy transfer rather difficult. This arises since it is not easy to avoid excitation of, or emission by, the humic component. It is notable that the fluorescence of humic acid becomes weaker at high wavelengths suggesting a possible spectral region for investigation.

In order to decide appropriate monitoring wavelengths, the fluorescence characteristics of the second component, namely europium(III), need to be determined. Both electronic absorption spectra and fluorescence spectra will be run. Reference will be made to the Eu^{3+} ion term scheme of Figure 3.1 as this may assist the interpretation of spectral peaks. Many Eu^{3+} terms depicted are accessible using ultra-violet and visible wavelengths.

Richardson [113] provided useful comments on suitable investigation wavelengths and experimental approaches in his review of the use of europium(III) ions as luminescent probes and stains for biomolecular systems. He stated that essentially all emission emanates from the $^5D_0$ level when excitation is below 580 nm ($\upsilon > 17300\ cm^{-1}$). The strongest emissions are invariably observed in the $^5D_0 \rightarrow {}^7F_1, {}^7F_2$ transition regions. The $^7F_4$ emission at 694 nm is frequently observed to have a moderately strong intensity. Emissions in the remaining ^7F_J transition regions are generally too weak to be observed.

Studies which monitor the emission of Eu^{3+} at 694 nm (corresponding to the transition $^5D_0 \rightarrow {}^7F_4$) have been reported by Chapman *et al*: [127] They showed that ultra-violet excitation of the metal ion in the complex tris(2,2',2"–terpyridyl)europium(III) lead to 694 nm emission both in the solid state and in acetonitrile solution. Hilmes and Riehl [128] used the same emissive transition to study the total luminescence and

circularly polarised luminescence of a europium(III) complex with 2,6–pyridine-dicarboxylic acid in basic media. The 694 nm emission lies in a spectral region where humic acid fluorescence is somewhat inefficient and thus may provide a useful wavelength for investigation.

3.2 Experimental

3.2.1 Electronic Absorption and Fluorescence Characteristics of Europium(III)

The electronic absorption spectrum of $Eu^{3+}_{(aq)}$ was scanned on a Pye-Unicam SP8–100 Ultra-violet Spectrometer (¢029) using 4 cm path length quartz cuvettes for maximised optical advantage. A rather concentrated europium nitrate solution (0·15 M), obtained by simple dissolution of the pentahydrate salt (¢035) in distilled water, was studied since some spectral peaks were believed to have low molar absorptivities. Peaks were located at reduced band-width for increased accuracy.

Fluorescence studies were carried out on a Perkin Elmer 3000 Fluorescence Spectrometer (¢030) with an attached servo-operated Flat-Bed Chart Recorder (¢031) in the manner described in Section 2.6.2. An investigation of the 694 nm europium(III) emission was made using 0·15 M $Eu(NO_3)_{3\,(aq)}$: The emission monochromator of the fluorometer was set to 694 nm and an excitation spectrum was scanned to locate irradiation wavelengths that cause 694 nm emission. Fluorescence spectra of the same sample following irradiation at 450 and 461 nm were then determined under identical optimised instrumental conditions to permit a simple comparison between their efficiencies at producing 694 nm $^5D_0 \rightarrow {}^7F_4$ emission.

3.2.2 Sample and Supporting Medium Composition Considerations

Consideration of the requirements for useful investigations of energy transfer effects suggested that close control of sample composition needed to be maintained since several factors that could complicate the interpretation of measurements were identified. Therefore, the preparation of samples was subject to several requirements and

constraints:

1 Measurable fluorescence over a wide range of concentrations without the need for excessive data amplification that would generate instrumental noise.

2 Sensible metal:humic acid ratios covering a wide range and including the range in which all the humic acid functional groups are saturated with metal ions.

3 A sensible addition of $Eu^{3+}_{(aq)}$ such that an effect, if apparent, could be observed.

4 Ability to control sample composition within a narrow range of specified media conditions. This arises since the degree of dissociation, and therefore the complexing ability, of humic acid is strongly dependent on both pH and ionic strength,[6] therefore these variables must be maintained.

5 Stability of the "complexes" to coagulation over a wide range of europium(III):humic acid concentration ratios and over a reasonable time scale.

6 Minimised total concentration of inert electrolytes since this may tend to coagulate the samples.

7 A compromise in the pH of the medium since the humic acid would precipitate under acidic conditions and the metal under alkaline conditions.

8 Avoidance of excessive volumes: The stocks employed must be sufficiently concentrated whilst remaining stable so that aliquots can be dispensed using the volumetric apparatus available and a single total volume can be specified for all samples.

The experimental strategy selected for preparing samples was to employ a constant $Eu^{3+}_{(aq)}$ concentration and a variable humic acid concentration within a supporting medium of closely controlled composition. To assist the interpretation of fluorescence measurements it was deemed necessary to prepare a parallel series of samples in which the humic acid concentration was varied in the absence of metal ions. This procedure should permit the isolation of any effects observed for the "complexes" from those due to an increasing concentration of the humic acid itself. The preparation of both sample sets will be outlined.

3.2.3 Stoichiometry of Samples

The ratios of metal to ligand employed in the samples are intended to cover a wide range of binding ratios up to a condition in which all the trivalent metal ion added is saturated with

humic acid. The ratios have been calculated as ionic equivalents although the nature of the binding is not necessarily a simple ionic interaction. However, this method ensures that sensible proportions are used.

The experimental approach was to consider a constant addition of the trivalent metal ion and a variable addition of the humic acid. The chosen europium(III) ion addition was $2{\cdot}0\times10^{-6}$ mol of trivalent metal which (in theory) could bind up to $6{\cdot}0\times10^{-6}$ mol of monovalent humic acid functional groups if simple ionic interactions are considered. The binding capacity of humic acids is generally quoted to lie in the range 1–5 meq g^{-1} of replaceable functional groups.[1,5,6,101] Fluka Humic Acid v3 additions ranged up to 1·2 ml of a 0·20 % w/v dispersion. This would be equivalent to between 2·4 and 12×10^{-6} moles of functional groups. These calculations show that the maximum humic acid addition should saturate the binding capacity of the added metal.

The calculations assume that all the added Fluka Humic Acid v3 is of an organic nature capable of binding to the lanthanide metal. In Section 2.4.4.3, it was shown that Fluka Humic Acid v3 contains between 34·9 and 43·2 % w/w ash, thus the binding capacity should be reduced by such a proportion. Other assumptions are that three independent functional groups are simultaneously accessible to the metal, and that the metal ion exists as a simple unhydrolysed $Eu^{3+}_{(aq)}$ species with the capacity to accommodate three such functional groups in its co–ordination sphere.

3.2.4 Preparation of Samples for Energy Transfer Studies

The subject materials of the samples were first prepared. These were then combined in the appropriate proportions to produce the samples for fluorescence analysis.

A europium(III) stock solution was prepared by dissolving 0·17 g of Aldrich $Eu(NO_3)\cdot5H_2O$ (¢035) in distilled water and quantitatively making up to 100·0 ml giving a solution of concentration $4{\cdot}03\times10^{-3}$ M. A sodium hydroxide stock solution for pH adjustment and dispersion of the humic acid was prepared by dissolution of B.D.H. pellets (¢010) in distilled water. This was standardised with potassium hydrogen phthalate (¢036) using phenolphthalein (¢037) as an indicator. The concentration was calculated as 0·01 M. A nitric acid stock for pH adjustment was prepared by dilution of

concentrated F.S.A. $HNO_{3\,(aq)}$ (¢038): Standardisation with dilute $NaOH_{(aq)}$ revealed a concentration of 0·01 M. Two humic acid stocks were prepared at concentrations of ~0·05 and ~0·20 % w/v by dispersion of Fluka Humic Acid v3 (¢002) in distilled water to which the minimum amount of 0·01 M $NaOH_{(aq)}$ was added to ensure adequate dispersion and a final medium condition of near-neutrality. This procedure was carried out under a nitrogen (¢009) tent whilst the dispersion was continually agitated and its pH monitored using a two-point calibrated pH meter (¢012–017). The additions of alkali were recorded. A 0·10 M sodium nitrate (¢039) solution for ionic strength adjustment was prepared by quantitative dissolution of the salt in distilled water. All sample media were carefully controlled such that they had a pH of 7·0±0·1, an ionic strength of 0·005±0·0001 M and a total volume of 10·0±0·1 ml. Samples showing discrepancies from these limits were discarded.

The procedure adopted in making the samples was first to select a desired humic acid concentration and to decide whether a europium ion addition was to be made. These volumes were dispensed using Finnpipette (¢040) or Agla (¢041) micropipettes into a glass sample vial (volume ~20 cm^3) containing a small magnetic stir-bar. Aliquots of distilled water were added until a total volume of 10·0 ml was approached. A pH electrode attached to a pH meter and doubly-calibrated was carefully inserted into the vial such that the membrane was covered by the mixture. The pH of the medium was monitored whilst the mixture was agitated. Additions of acid or alkali as indicated by the prevailing pH were made to the system so that neutrality was approached. At this stage the BASIC computer program "IONSTG" (see Appendix 3) for the Apple IIe or BBC micro-computers was employed to determine the additions of sodium nitrate required to produce the desired ionic strength of 0·005 M. Note that this electrolyte was selected since its constituent ions are the same as those provided by other species present in the samples. The suggested electrolyte volume was dispensed and the sample equilibrated. This interactive cycle was repeated until the prescribed media conditions were attained. Failure to meet any one of the criteria resulted in the disposal of that particular sample. On completion, the pH electrode was withdrawn from the sample without transferring washings to it thus avoiding disturbance of the sample specifications.

Samples were prepared in this way covering large ranges of humic acid concentration both in the presence and absence of europium(III). Two further samples prepared to the same media conditions of ionic strength and acidity were termed "buffered blanks". One contained europium(III), and the other, humic acid at the same concentrations as in a

"complex" with $[Eu^{3+}_{(aq)}] = 2{\cdot}0 \times 10^{-4}$ M and 0·02 % w/v humic acid. These samples were employed in comparative measurements.

3.2.5 Determination of Optimum Fluka Humic Acid Fluorescence Monitoring Conditions

An excitation spectrum for a buffered blank of 0·02 % w/v Fluka Humic Acid v3 was run with the emission monochromator set at 694 nm to determine its excitation efficiency in the range 350–650 nm.

3.2.6 Europium(III)-Fluka Humic Acid Fluorescence Measurements

The europium(III)-Fluka Humic Acid v3 "complexes" were agitated before making fluorescence measurements to ensure a representative distribution within the sampling zone. This was achieved by ultrasonic vibration (¢042) at 48 W for 30 minutes followed by equilibration at 25 °C for a similar period.

Fluorescence measurements were made on the two series of samples in glass cuvettes using equal monochromator band-widths of 10 nm. The emitted light intensity following excitation at 450 nm was measured by locating the emission monochromator at 694 nm and recording the instrumental "read" average fluorescence from five displays.

The contribution of aggregation-derived light scattering to the observed spectra was estimated by fixing the excitation monochromator to 450 nm and scanning "emissions" in the range 430–470 nm. This procedure was performed for buffered blanks of $2{\cdot}0 \times 10^{-4}$ M $Eu^{3+}_{(aq)}$, 0·02 % w/v Fluka Humic Acid v3, a "complex" containing the metal and ligand at the same constituent concentrations, Ludox TM colloidal silica (~1 % w/v SiO_2) and distilled water.

3.3 Results

Table 3.1
Electronic Absorption Characteristics of Europium (III)

Wavelength λ / nm	Energy Level Transition	Absorbance	Molar Absorptivity A / l mol^{-1} cm^{-1}
659.0	$^7F_3 \rightarrow {}^5D_0$	0.007	0.012
592.0	$^7F_0 \rightarrow {}^5D_0$	0.010	0.017
536.0	$^7F_1 \rightarrow {}^5D_1$	0.008	0.014
525.6	$^7F_0 \rightarrow {}^5D_1$	0.020	0.034
465.2	$^7F_0 \rightarrow {}^5D_2$	0.029	0.049
416.6	$^7F_0$, $^7F_1 \rightarrow {}^5D_2$	0.018	0.030
393.8	$^7F_0 \rightarrow {}^5L_6$	0. 765	1.295
385.0	$^7F_0 \rightarrow {}^5L_7$	0.168	0.284
380.2	$^7F_0 \rightarrow {}^5G_2$, $^5G_3$	0.156	0.264
375.6	$^7F_0 \rightarrow {}^5G_4$	0.178	0.301
366.6	$^7F_0$, $^5D_4 \rightarrow {}^5L_8$	0.030	0.051
361.6	$^7F_0 \rightarrow {}^5D_4$	0.119	0.201

The absorption spectrum of 0·15 M $Eu^{3+}{}_{(aq)}$ in the ultra-violet and visible regions of the electromagnetic spectrum is given in Figure 3.2. The spectrum is presented with an expanded ordinate to reveal high wavelength peaks. The locations, absorbances, molar absorptivities and energy level identities of the absorptions are given in Table 3.1. Figure 3.3 provides an excitation spectrum for 0·15 M $Eu^{3+}{}_{(aq)}$ under conditions where the emission monochromator was fixed at 694 nm. This was intended to locate europium(III) excitation transitions that cause $^5D_0 \rightarrow {}^7F_4$ emission. The fluorescence spectra presented in Figure 3.4 display the relative efficiency of the excitation wavelengths 450 nm and 461 nm at producing 694 nm emission from 0·15 M $Eu(NO_3)_{3\ (aq)}$. The spectra were scanned under identical instrumental conditions.

The excitation spectrum for a "buffered blank" of 0.02 % w/v Fluka Humic Acid v3 causing emission at 694 nm is presented in Figure 3.5. Figure 3.6 provides a simple comparison of the light scattering ability of a "complex" of europium(III) with Fluka Humic Acid v3, europium(III), Fluka Humic Acid v3, Ludox TM colloidal silica and distilled water. The diagram shows an "emission" spectrum across the spectral range 430–470 nm resulting from 450 nm excitation.

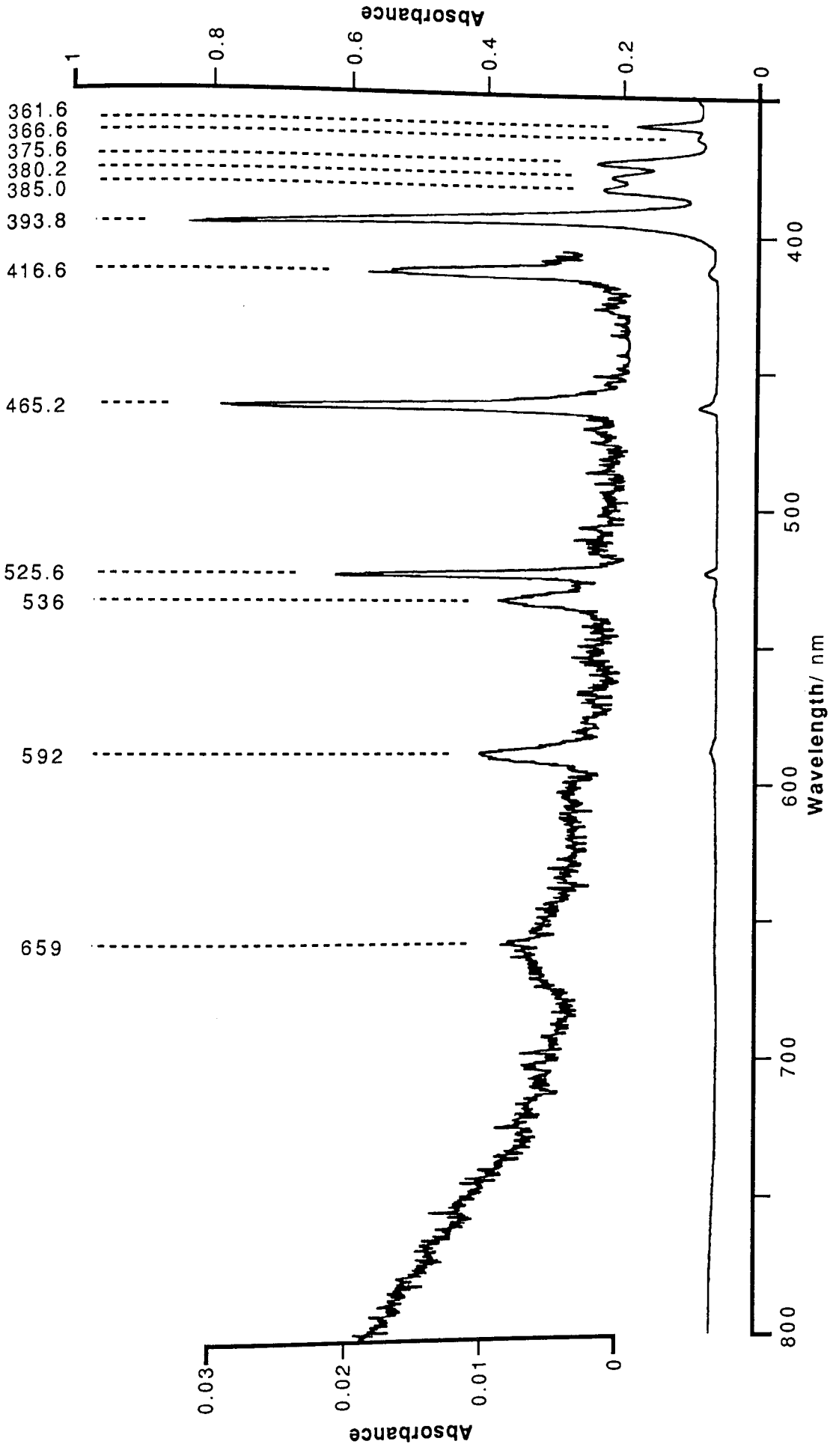

Figure 3.2 Electronic Absorption Spectrum of 0.15 M $Eu(NO_3)_3$ (aq)

Scan Conditions: 4 cm Path Length Quartz Cuvette; Scan Speed = 1 nm/s; Chart Speed = 20 s/cm; Scanning Bandwidth = 2 nm; Peak Determination Bandwidth = 0.2 nm; Distilled Water Reference

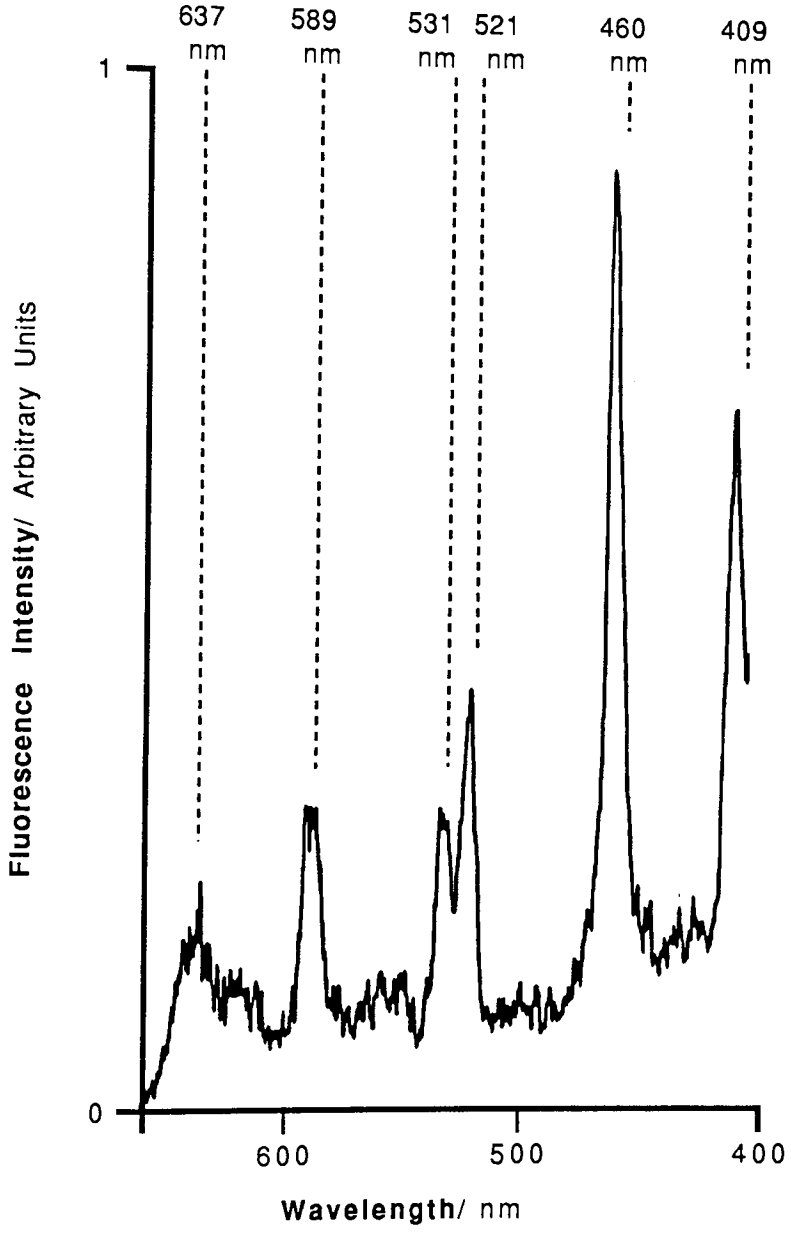

Figure 3.3

Excitation Spectrum for 0.15 M $Eu(NO_3)_{3(aq)}$ (λ_{em} = 694 nm)

Scan Conditions: Scan Speed = 30 nm/min; Chart Speed = 10 mm/min;
Excitation Bandwidth = 5 nm; Emission Bandwidth = 20 nm;
Time Constant = 4.8 s; 1 cm Quartz Cuvette

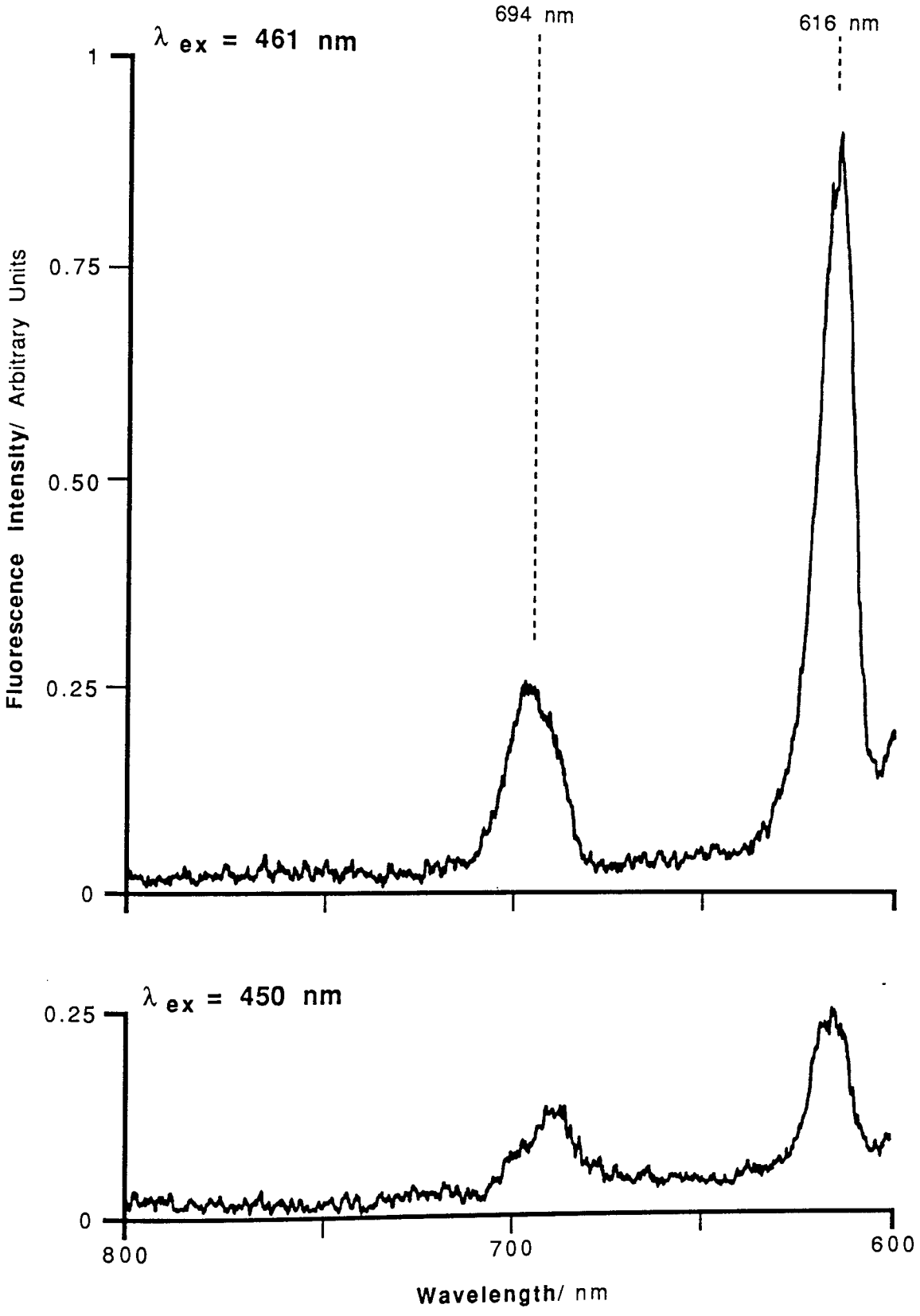

Figure 3.4

Emission Spectra for 0.15 M $Eu(NO_3)_{3\,(aq)}$

(Excitation at 450 and 461 nm)

Scan Conditions: Scan Speed = 30 nm/min; Chart Speed = 20 mm/min; Excitation Bandwidth = 15 nm; Emission Bandwidth = 5 nm; Time Constant = 4.8 s; 1 cm Quartz Cuvette

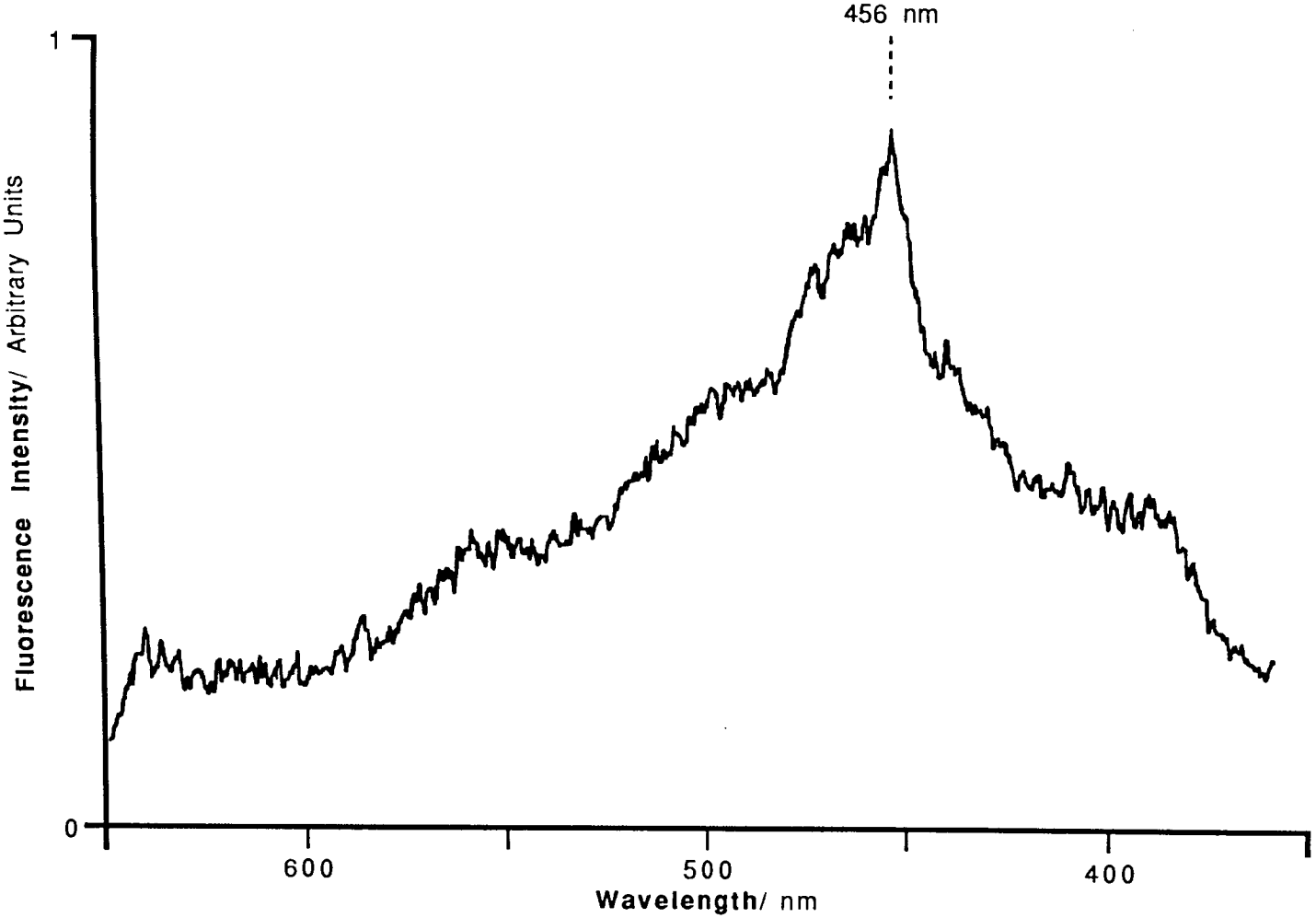

Figure 3.5 Fluka Humic Acid v3 Excitation Spectrum (λ_{em} = 694 nm)

Scan Conditions: 1 cm Path Length Glass Cuvette; Scan Speed = 30 nm/min; Chart Speed = 20 mm/min; Excitation Bandwidth = 5 nm; Emission Bandwidth = 20 nm; Time Constant = 4.8 s

Sample Details: Buffered Blank of 0.02 % w/v Fluka Humic Acid v3; [Eu(III)] = 0; pH = 7.06; Ionic Strength = 5.0E-03

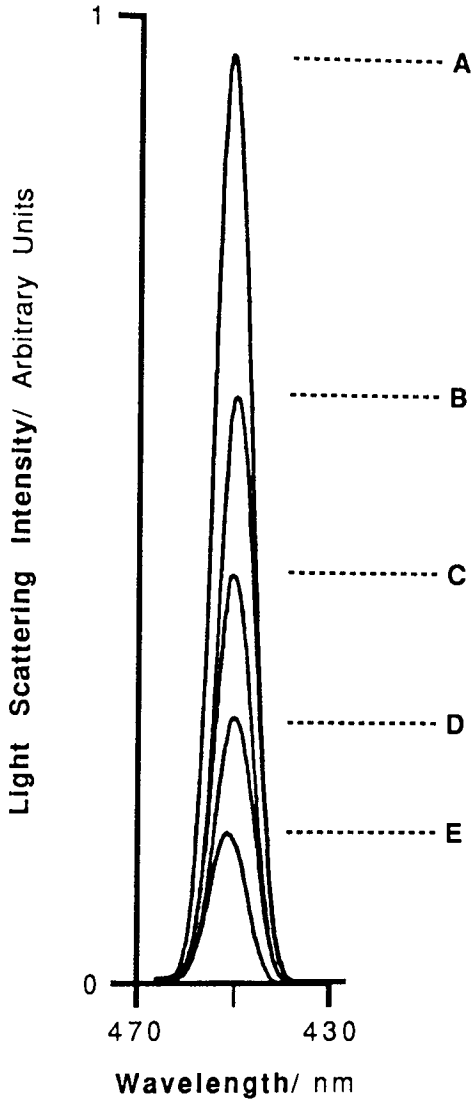

Emission Spectrum (λ_{ex} = 450 nm)

Figure 3.6

Assessment of Aggregation in Europium(III)—Fluka Humic Acid v3 'Complexes' by Light Scattering at 450 nm

Spectral Acquisition Conditions:

1 cm Glass Cuvette; Scan Speed = 30 nm/min; Chart Speed = 20 mm/min; Excitation Bandwidth = 5 nm; Emission Bandwidth = 5 nm; Time Constant = 4.8 s

*Sample Details: (Note **A-D** are 101x dilutions of the aqueous dispersions/solutions listed)*

A *Ludox TM Colloidal Silica (~1 % w/v; pH = 8.07)*

B *Europium(III)—Fluka Humic Acid v3 'Complex' ([Eu(III)] = 2.01E-04 M; FHAv3 = 0.02 % w/v; pH = 7.02; Ionic Strength = 5.0E-03 M)*

C *Fluka Humic Acid v3 Buffered Blank ([Eu(III)] = 0 M; FHAv3 = 0.02 % w/v; pH = 7.06; Ionic Strength = 5.0E-03 M)*

D *Europium(III) Buffered Blank ([Eu(III)] = 2.02E-04 M; FHAv3 = 0 % w/v; pH = 6.97; Ionic Strength = 5.0E-03 M)*

E *Distilled Water*

Table 3.2
Statistical Variation of Media Conditions for Fluorescence Samples

Media Condition	Mean	Standard Deviation	Variance
Total Volume/ ml	10.02	0.024	0.001
Ionic Strength/ M	5.00E-03	2.021E-05	4.086E-10
pH	7.00	0.041	0.002

The composition of the sample media was monitored by analysis of their total volume, pH and ionic strength at the instant of preparation. Table 3.2 provides statistical analyses of these quantities. Note that the humic acid concentrations of the samples have been adjusted for deviations from a total volume of 10·0 ml. However, since the total volume deviation range was very small, the adjustments required were proportionately small. The ionic strengths quoted correspond to the total volume of an individual sample, therefore a similar correction is not required.

The "read" average fluorescence intensities over five instrumental outputs for samples both in the presence and absence of europium ions are provided in parallel with their humic acid concentrations in Table 3.3. The data has not been modified by subtraction of a background or application of a mathematical smoothing procedure. The final column for each set of samples gives fluorescence values which have been calculated from equations modelling the raw data. These are derived in Section 3.4.3.

Graphs depicting the variation in fluorescence with humic acid concentration in the presence and absence of europium ions are displayed in Figure 3.7 and 3.8. Superimposed on each graph are the corresponding calculated fluorescence values. An overlay graph of the calculated fluorescence of both samples sets (Figure 3.9) permits a simple comparison of the effect of added europium(III) on humic acid fluorescence.

Table 3.3
Fluorescence Data for Fluka Humic Acid v3 and Europium(III)-Fluka Humic Acid v3 "Complexes"

Fluka Humic Acid v3 Samples			Europium(III)-Fluka Humic Acid v3 Samples		
Humic Acid Concentation 10^4/ % w/v	Measured Fluorescence / Arbitrary Units	Calculated Fluorescence / Arbitrary Units	Humic Acid Concentation 10^4/ % w/v	Measured Fluorescence / Arbitrary Units	Calculated Fluorescence / Arbitrary Units
0	29	0	0	112	0
1.5	23	8.3	1.0	152	8.6
3.5	27	17.0	2.0	110	16.9
4.0	40	18.9	3.0	88	24.7
5.0	58	22.3	4.0	94	32.1
8.0	31	30.6	5.0	86	39.2
15.0	47.5	42.9	7.0	43	51.6
17.5	57	45.9	8.0	59	57.1
20.1	42	48.6	10.1	80	66.9
22.5	51	50.7	12.0	92	75.0
25.1	50	52.7	15.1	132	84.8
30.3	53	56.0	18.0	64	92.0
35.3	55	58.5	22.6	103	99.6
40.4	62	60.5	27.5	99	104.2
45.4	60	62.2	30.2	168	105.8
50.5	62	63.6	35.0	93	107.4
60.6	61	65.9	37.6	96	107.8
80.7	71	68.9	40.1	119	108.0
101.1	74	70.9	45.2	93	107.9
121.1	85	72.2	47.7	97	107.6
140.3	77	73.2	49.9	88	107.3
161.6	77	74.0	60.6	106	105.5
181.8	75	74.7	80.5	109	101.3
202.1	72	75.2	100.9	108	97.5
222.1	72	75.6	120.7	101	94.4
242.4	61	75.9	161.4	84	89.7
			181.5	75	87.9
			202.0	51	86.4
			220.6	60	85.2
			242.3	64	84.1

Figure 3.7
Variation in Fluorescence of Fluka Humic Acid with Humic Acid Concentration

(Full unsmoothed data set)

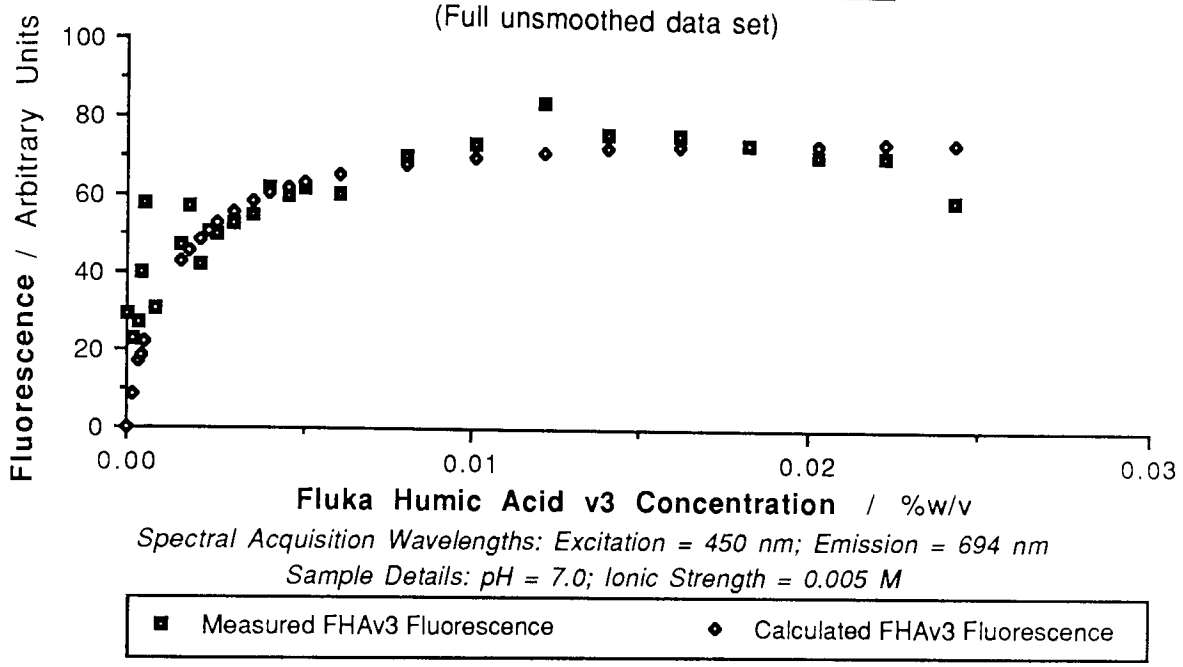

Figure 3.8
Variation in Fluorescence of Europium(III)-Fluka Humic Acid with Humic Acid Concentration

(Full unsmoothed data set)

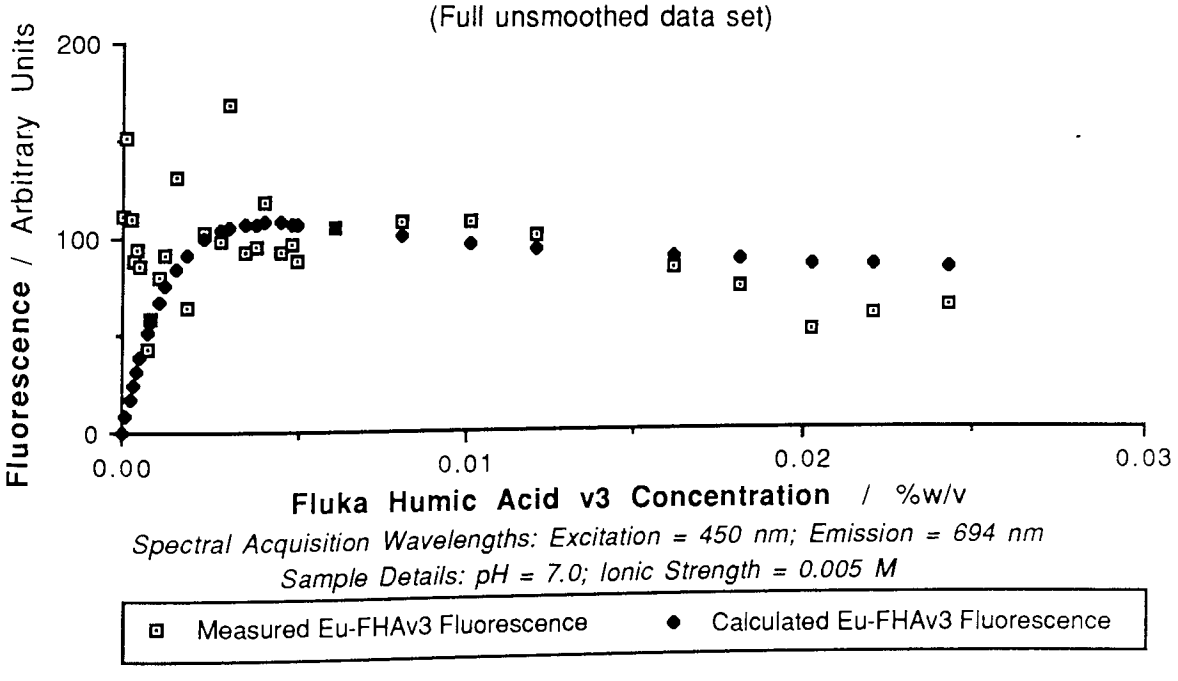

Figure 3.9
Variation in Fluorescence of Europium(III)-Fluka Humic Acid and Fluka Humic Acid with Humic Acid Concentration
(Full unsmoothed data set)

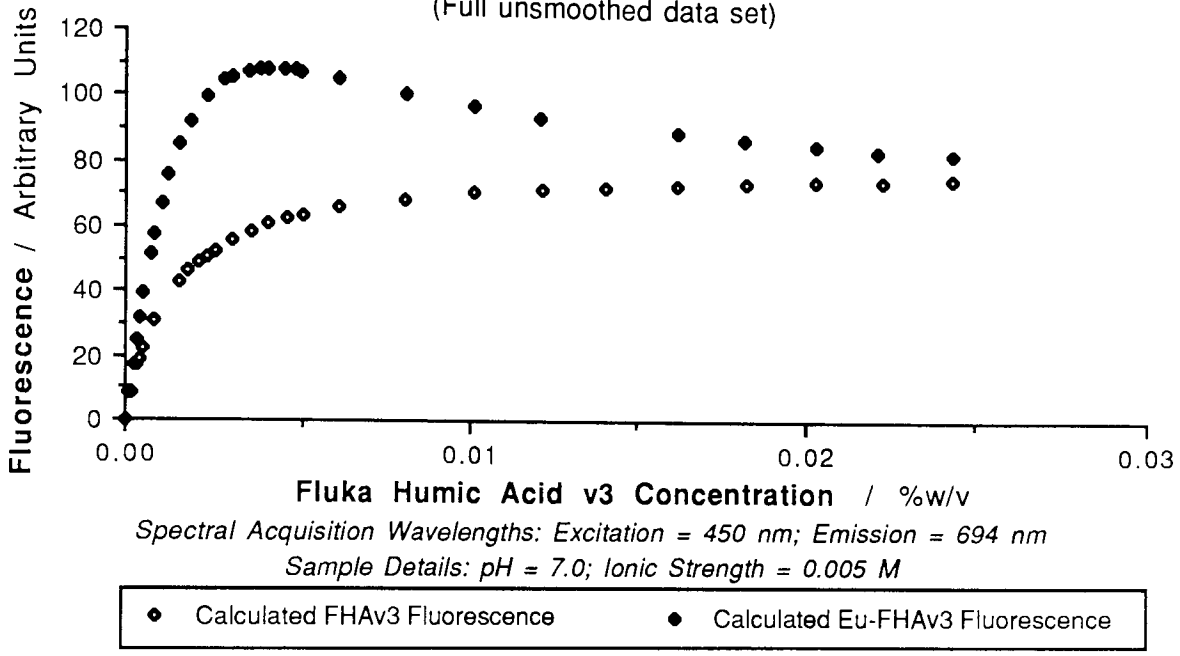

3.4 Discussion

3.4.1 Spectral Analysis

The electronic absorption spectrum of aqueous europium(III) displays regions where absorption is inefficient and sharp peaks corresponding to absorbed radiation. Peaks are quite weak in the visible region of the electromagnetic spectrum but stronger in the ultra-violet. Note that the absorption spectrum of the europium(III) buffered blank is similar to that of Figure 3.2 but of reduced intensity and apparent resolution reflecting the lower metal ion concentration. Analysis of Figure 3.2 shows that absorption by $Eu^{3+}_{(aq)}$ is weak at 450 nm but stronger at 461 nm.

Table 3.1 gives absorbances, molar absorptivities and term assignments for the peaks observed in the electronic absorption spectrum of aqueous europium(III). Most of the transitions emanate from the ground state but a few peaks of low molar absorptivity originate from the first excited state, $^7F_1$. Their weakness reflects the reduced

Boltzmann population of this state at room temperature, as discussed in Section 3.1.2. The 659 nm absorption does not correlate with excitation from either the ground or first excited states but excitation from the third excited state, $^7F_3$, to $^5D_0$, appears to match this wavelength.

Figure 3.3 depicts $Eu^{3+}{}_{(aq)}$ excitation wavelengths that result in relaxation from $^5D_0$ to $^7F_4$ at 694 nm. Five peaks are apparent in the region presented but none occur at 450 nm. Note that the wavelengths of the peaks observed do not correlate exactly with those given in the table of spectral transition identities (Table 3.1). This may be accounted for by the higher spectral resolution of the ultra-violet spectrophotometer compared to the fluorometer: The spectral locations of absorption peaks were determined at a reduced band-width of 0·2 nm whereas the excitation spectrum was run using a 5 nm slit width. The accuracy of the fluorometer monochromators quoted by the manufacturer is ±2 nm with a wavelength repeatability of 1 nm. [129] It is also notable that the spectral peaks in the excitation spectrum have larger half-widths and poorer shape definition.

The comparative efficiency of 450 nm and 461 nm excitation of $Eu^{3+}{}_{(aq)}$ resulting in emission at 694 nm was determined by acquiring spectra under identical conditions. Figure 3.4 shows that excitation of $Eu^{3+}{}_{(aq)}$ at 450 nm is much less efficient than at 461 nm when the selected emission wavelength is 694 nm. The spectrum also shows an efficient emission at 616 nm corresponding to the transition $^5D_0 \rightarrow {}^7F_2$ that results from excitation at these wavelengths. Note that selection of a wide excitation band-width that could significantly excite the 461 nm transition was avoided when making fluorescence measurements on the luminescence samples: A band-width of 10 nm (i.e., 450±5 nm) was chosen thus excitation of the 461 nm $Eu^{3+}{}_{(aq)}$ transition should be further diminished compared to that of Figure 3.4 where a 15 nm band-width was used.

The excitation scan for the buffered blank of Fluka Humic Acid v3 corresponding to emission at 694 nm (Figure 3.5) reveals that excitation is strongly favoured in the spectral region 440–480 nm with maximum efficiency at 464 nm. Therefore fluorescence of the humic acid is efficient at 694 nm when irradiated at 450 nm.

Selection of an excitation wavelength of 450 nm and an emission wavelength of 694 nm thus provides efficient excitation of the humic acid but not the europium(III) ion whereas

emission from both components is favourable. This experimental investigation strategy of energy transfer effects has been implemented in the fluorescence studies.

An attempt was made to determine the nature of the light detected in fluorescence measurements since it is possible that the samples may scatter light. Both of their components can scatter and their interaction could produce large aggregated structures with greater scattering ability.

The contribution of light scattering was estimated in a rather simplistic manner by fixing the excitation monochromator of the fluorometer to 450 nm and scanning the "emission" across the same wavelength. Under such conditions, light of a scattering nature should be detected and fluorescence, by definition, should not be apparent. Figure 3.6 shows that scattering from Ludox TM was greater than that from the buffered "complex" which itself was greater than that from the europium(III) and humic acid buffered blanks at the same concentrations. Interestingly, scattering from the "complex" was less than the scattering sum from its components. This implies that the "complex" is not extensively aggregated and that light detected for the luminescence samples under conditions where unequal wavelengths are selected is of a fluorescent rather than a scattering nature. This is supported by comparison of the magnitude of scattered light to that of Ludox TM colloidal silica, a well known scatterer.

The light detected is probably not of a phosphorescent nature since water is quite effective at preventing phosphorescence by relaxing excited systems over a reasonable time-scale. Detection of phosphorescence, if apparent, would require modified apparatus that would enhance the likelihood of collecting delayed emissions.

The spectrum shows that an appreciable scattering intensity was observed for distilled water under the same instrumental conditions. Similar observations were made in the absence of a cuvette and sample. These effects are due to the primitive nature of the experiment and because the light intensity was large and therefore liable to emphasise surface reflections.

3.4.2 Fluorescence Measurements

Table 3.2 provides statistical analyses of the sample media specifications at the time of

preparation. Small deviations from the three desired criteria are apparent implying that sample composition is not a source of error in the fluorescence measurements.

Inspection of the raw fluorescence data in Table 3.3 provides justification for the derivation of calculated values since the data is quite scattered, especially at low humic acid concentrations. Figures 3.7&3.8 depict the variation in the fluorescence of both sample sets with humic acid concentration. For samples without metal, although the fluorescence data is scattered, it rises with humic acid concentration and tends towards a constant value at high concentration. The calculated data clarifies this variation. When a europium(III) ion addition is made, the fluorescence variation curve tends towards the same limiting value at high humic acid concentration after passing through a maximum at medium concentration. The effect of the europium(III) addition is clearly revealed by inspection of Figure 3.9 which shows an increased fluorescence in the presence of europium(III) ions. This enhancement in fluorescence is believed to be caused by a photophysical mechanism involving ligand-to-metal energy transfer. The trends in the fluorescence of the systems studied have been analysed by consideration of likely photophysical processes that involve these components with subsequent development into a model.

3.4.3 Photophysical Mechanistic Considerations

A photophysical mechanism has been devised to describe the enhanced 694 nm fluorescence observed in experimental measurements when europium(III) ions are added to Fluka Humic Acid v3. It is proposed that this is caused by energy transfer from humic acid to europium(III). The scheme is depicted in Figure 3.10.

The main species of the scheme are the ground states of Fluka Humic Acid v3 and europium(III) ions, represented by H and M, and their corresponding excited states, H^* and M^*. Note that [H] is a variable using the experimental approach selected and [M] is constant. Likely photophysical processes involving these species are:

1 Fluorescence at 694 nm by H^* or M^*.

2 Deactivation by bimolecular collisions involving the metal ion or the ligand resulting in no emission. Collisions between excited species are considered unlikely due to their transient nature and low concentration.

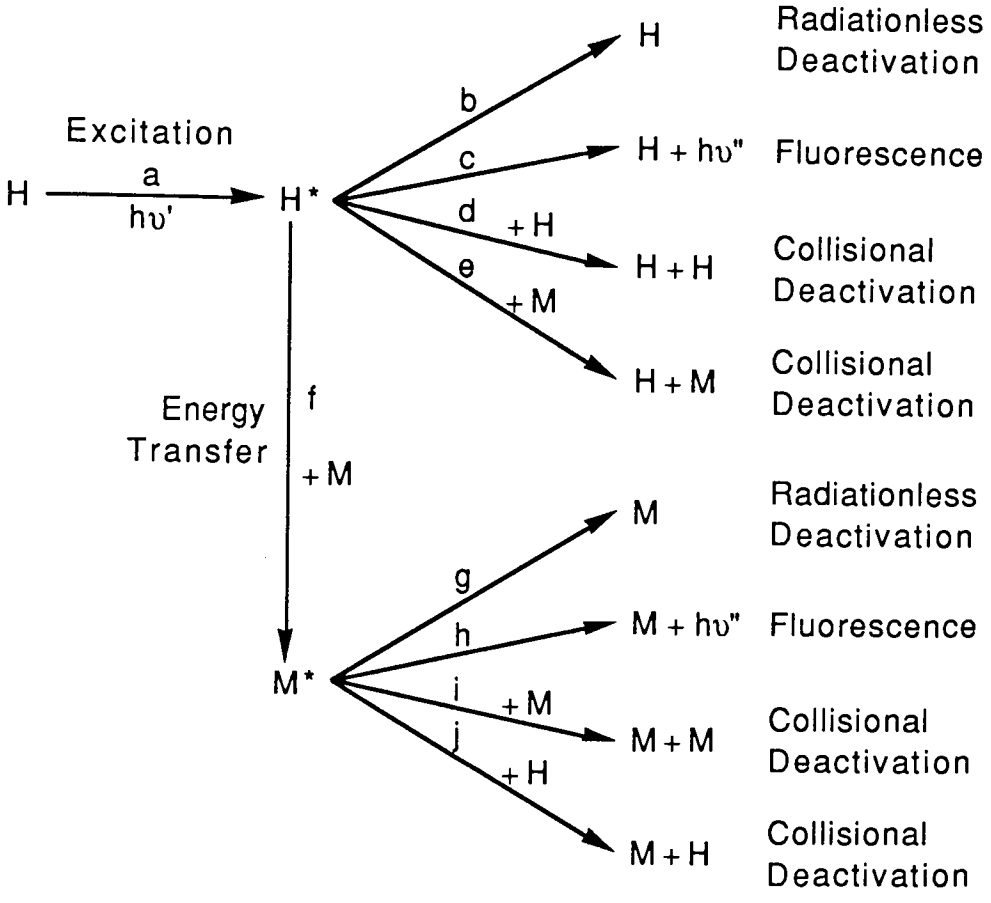

Key

H = Unexcited Fluka Humic Acid v3
M = Unexcited europium(III)
H* = Excited Fluka Humic Acid v3
M* = Excited europium(III)
a - j = Transition probabilities or efficiencies
υ' = 450 nm
υ" = 694 nm

Figure 3.10
Photophysical Scheme for Energy Transfer between Europium(III) and Fluka Humic Acid

3 Radiationless deactivation of H* and M* involving energy dissipation by other mechanisms.

4 Energy transfer from H*, the sensitiser, to M, the acceptor resulting in formation of M*. This process only occurs when M is present.

The photophysical processes of Figure 3.10 are characterised by probabilities or efficiencies that denote the likelihood of occurrence for each process, a–j. The scheme has been analysed mathematically by applying the steady state approximation to the excited states: This assumes that after a short initiation period, the concentrations [H*] and [M*] remain constant providing the system is not perturbed by changing the conditions. Thus the rates of formation and decay for each respective excited state are equal.

In step a, humic acid is excited by 450 nm light and forms its excited state, H*. The rate of formation of H* at any instant is given by the equation:

$$\frac{d[H^*]}{dt} = a[H] - b[H^*] - c[H^*] - d[H][H^*] - e[M][H^*] - f[M][H^*]$$

Under the steady state condition, formation of H* is balanced by processes that destroy it. Therefore, the rate of formation of H* may be equated to zero:

$$\frac{d[H^*]}{dt} = 0$$

The steady state concentration of the humic acid excited state, [H*], may now be written as:

$$[H^*] = \frac{a[H]}{(b + c + d[H] + e[M] + f[M])} \qquad (1)$$

Europium(III) ions are excited by energy transfer from H* in process f. Steps g–j result in destruction of M*. The rate of formation of M* at any instant may be represented by the equation:

$$\frac{d[M^*]}{dt} = f[M][H^*] - g[M^*] - h[M^*] - i[M][M^*] - j[H][M^*]$$

Application of the steady state condition to [M*] permits its rate of formation to be equated to zero since step f is balanced by processes that destroy M*:

$$\frac{d[M^*]}{dt} = 0$$

The steady state concentration of M* may therefore be written as:

$$[M^*] = \frac{f[M][H^*]}{(g + h + i[M] + j[H])}$$

The concentration of M* may be expressed as a function of the variable [H] by substitution of [H*] from equation (1):

$$[M^*] = \frac{af[M][H]}{(g + h + i[M] + j[H])(b + c + d[H] + e[M] + f[M])} \quad (2)$$

The intensity of the 694 nm fluorescence caused by excitation of the humic acid at 450 nm is given by:

$$I_c = c[H^*]$$

Substitution for the concentration of the excited humic acid, [H*], from equation (1) gives:

$$I_c = \frac{ac[H]}{(b + c + d[H] + e[M] + f[M])} \quad (3)$$

Consider the samples that had no added metal. Here, [M] = 0 and equation (3) may be reduced to:

$$I_0 = \frac{ac[H]}{(b + c + d[H])} \quad (4)$$

This equation may be simplified by insertion of new constants, α and β, which will be defined as:

$$\alpha = \frac{ac}{d} \quad (5)$$

$$\beta = \frac{b + c}{d} \quad (6)$$

Equation (4) may be re-written in terms of α and β:

$$\therefore I_0 = \frac{\alpha[H]}{\beta + [H]} \quad (7)$$

Equation (7) describes the variation in the 694 nm fluorescence of Fluka Humic Acid v3 given in Figure 3.7. Application of appropriate limiting conditions to

equation (7) permits approximation of the shape of the fluorescence curve:

(a) When $[H] \rightarrow 0$, $I_0 \rightarrow 0$ and approaches it with a slope of α/β

(b) When $[H] \rightarrow \infty$, $I_0 \rightarrow \alpha$

Inspection of Figure 3.7 shows that these limits do agree with the shape of the curve: The fluorescence declines to zero almost linearly as the humic acid concentration falls. At high humic concentrations the fluorescence tends asymptotically towards a limiting value equivalent to α.

The calculated fluorescence data was derived by insertion of values for α and β into equation (7). I_0 data was plotted alongside the measured fluorescence data until a satisfactory correlation was obtained. The calculated fluorescence data (in the absence of europium(III) ions) of Table 3.3 was derived using the values of $\alpha = 80$ and $\beta = 13$. A plot of this data shows a good fit with the raw data (Figure 3.7) implying that equation (7) provides a good description of the fluorescence of Fluka humic acid over a wide concentration range.

When a metal ion addition is made to Fluka Humic Acid v3, the fluorescence at 694 nm can be caused by humic or europium emission. The observed emission, I, may be expressed as:

$$I = I_c + I_h$$

$$\therefore I = c[H^*] + h[M^*]$$

Substitution for $[H^*]$ and $[M^*]$ from equations (1) and (2) gives:

$$I = \frac{ac[H]}{(b + c + d[H] + e[M] + f[M])} + \frac{afh[M][H]}{(g + h + i[M] + j[H])(b + c + d[H] + e[M] + f[M])}$$

$$\therefore I = \frac{ac[H](g + h + i[M] + j[H]) + afh[M][H]}{(g + h + i[M] + j[H])(b + c + d[H] + e[M] + f[M])} \qquad (8)$$

Casual inspection of equation (8) does not provide a simple description of the variation in the fluorescence of the "complexes" with humic acid concentration. However, consideration of limiting conditions provides insight to the shape of the curve:

(a) When $[H] \rightarrow 0$, $I \rightarrow 0$ since all denominator terms include the humic acid concentration. The shape of the approach to zero is not readily apparent.

(b) When $[H] \rightarrow \infty$, $I \rightarrow \alpha$. Equation (8) contains two terms that involve the square of the humic acid concentration. When substituted by infinity, the other terms are insignificant and the total fluorescence, I, reduces to:

$$I \rightarrow \frac{ac}{d}$$

Recalling equation (5), this may be simplified to:

$$I \rightarrow \alpha$$

Inspection of Figure 3.8 shows that I has a complex dependence on [H]. Although the infinity limit of $I \rightarrow \alpha$ is observed, the fluorescence data at low concentration is too scattered to unambiguously decipher its trend. The low concentration scatter may be due to the occurrence of processes that are not accounted for by the photophysical scheme of Figure 3.10. For example, under these conditions, the relatively large metal:humic acid ratio may affect the nature of the sample, or extra processes that result in 694 nm emission may operate.

Further consideration of equation (8) permits regions other than the limits to be modelled providing that some of the processes are grouped together. Several new constants will be defined as:

$$\gamma = (g + h + i[M])$$

$$\delta = \left(\frac{afh[M]}{d}\right)$$

$$\varepsilon = \frac{[M](e + f)}{d}$$

Insertion of these constants permits equation (8) to be rewritten as:

$$I = \frac{(\alpha\gamma + \delta)[H] + \alpha j[H]^2}{\gamma(\beta + \varepsilon) + (\gamma + j\beta)[H] + j[H]^2} \qquad (9)$$

Fluorescence data has been generated using equation (9) by inserting values for the terms following further grouping. The data given in the final column of Table 3.3 have been calculated using the equation:

$$I = \frac{5300[H] + 70[H]^2}{600 + 20[H] + [H]^2} \qquad (10)$$

The derived fluorescence values are plotted in Figure 3.8 against humic acid concentration. Although the raw data is scattered, the form of the curve derived from equation (10) does model it. The curve accounts for the maximum in the data and the infinity limit of α. It should be noted that a range of values could be inserted into equation (9) to generate curves of similar fits to that given in Figure 3.9. Therefore, the relevance of the grouped constants in equation (10) is not clear, although it is notable that a value for j *could* be derived. Other individual processes cannot be quantified.

The curves describing the fluorescence in the absence and presence of the metal ion tend to the same constant value at high humic acid concentration. Under such conditions, addition of the metal ion makes no difference to the magnitude of the fluorescence. Figures 3.7 and 3.8 show that this was realised experimentally, and Figure 3.9 shows that both theoretical descriptions given by equations (7) and (9) account for this. Therefore, at high humic acid concentration, deactivation processes balance emissive processes, and in the presence of the metal, process f does not affect the photophysical behaviour.

The photophysical scheme closely approximates the observed trends in fluorescence, therefore it is very likely that energy transfer is responsible for the enhanced 694 nm emission. Comments concerning the mechanism of the energy transfer reaction will be addressed in Sections 3.4.5 and 3.4.6.

3.4.4 Donor-Acceptor Energy Transfer Processes Involving Europium(III) and Humic Substances

Separate literatures exist concerning energy transfer processes that involve trivalent europium ions or humic substances. Some useful mechanistic insights can be gained from such studies. One group of workers have studied the luminescence of systems containing europium(III) and humic substances but energy transfer was not described.

3.4.4.1 Energy Transfer Processes Involving Europium(III)

Energy transfer involving europium(III) has been reported in various systems including simple complexes,[130] complexes dispersed in polymer matrices[122,123] and biomolecular complexes.[113,131] Most involve energy transfer to the metal but transfer emanating from the metal has also been observed.

Ismail and El–Bayoumi[130] observed an intense fluorescence from the europium(III) ion at room temperature in DMF or DMSO solutions of the europium chelate with salicylidene-valinate Schiff base as a result of intramolecular energy transfer from a ligand triplet state to the metal. Crosby *et al*[132] also discussed the involvement of a ligand triplet state in the energy transfer mechanism from ligand to metal in rare earth chelates.

Li *et al*[122] studied the fluorescence of transparent poly(methylmethacrylate) films containing Eu^{3+} ß–diketonate chelate complexes. The experiments involved excitation of the ligands with ultra-violet light followed by intramolecular energy transfer to the metal. The intensity of the rare earth emission was dependent on the nature of the ß–diketonate used. Okamoto *et al*[123] also observed energy transfer in polymers containing rare earth metal complexes.

Richardson[113] observed sensitisation and enhancement of Eu^{3+} emission by ligand to metal transfer when europium was bound to *E. coli* tRNA. Fluorescence ranged from 460–570 nm and had a maximum at 510 nm. This fluorescence completely overlaps the Eu^{3+} $^7F_0 \rightarrow {}^5D_1, {}^5D_2$ absorptions allowing resonant energy transfer to these excited states with subsequent relaxation to the $^5D_0$ emitting level.

Hwang *et al*[131] substituted Eu^{3+} for Ca^{2+} as an allosteric factor in hemocyanin and studied its laser-induced f–f fluorescence to probe the allosteric effects on the Ca^{2+} binding site induced by deoxygenation of the binuclear copper active site. Internal energy transfer from the Eu^{3+} allosteric site to the coupled binuclear copper active site was monitored and used to estimate their separation by the application of Förster-type considerations.[120]

3.4.4.2 Energy Transfer Processes Involving Humic Substances

Support for the occurrence of energy transfer between humic substances and europium is provided by reference to other studies that focus on different aspects from those investigated here. Some workers have postulated detailed mechanistic involvement of humic acids.

The role of humic substances in photosensitised transformations involving energy transfer in natural waters has been discussed and useful analogies can be drawn between their work and that described herein. Zepp *et al* [125] studied photosensitised reactions of pentadiene and dimethylfuran with humic substances including Fluka Humic Acid. Kinetic measurements indicated that the key steps in both photochemical reactions involved the transfer of electronic energy from triplet states of the humic substances. The mechanism proceeded by excitation of the humic acid to a singlet state by sunlight followed by intersystem crossing to give a long-lived humic triplet that acted as the sensitiser. Various reactions involving the latter were postulated, including its deactivation. The lifetime of the singlet humic state was too short to interact significantly with the organic substances or oxygen present. Fischer *et al* [126] noted the importance of the triplet state of humic acid in photochemical processes. Power *et al* [94,133] also suggested that triplets were one component of the transients observed.

3.4.4.3 Luminescence Studies on Systems Containing Europium(III) and Humic Substances

Luminescence studies on systems containing fulvic acid and trivalent europium ions have been reported by Dobbs *et al.* [134,135] In their work the luminescent properties of the lanthanide ion were used to probe the metal ion binding sites in fulvic acid. Their experimental strategy exploited the larger lifetime of the metal which permitted the isolation of the europium luminescence from the large background levels of the fulvic acid. The hypersensitive $^5D_0 \rightarrow {}^7F_2$ transition at 616 nm was monitored and the fractions of metal bound and free were determined from the intensity of the peak relative to that of a non–hypersensitive transition. A continuous multiple-site ligand binding model was developed from such measurements. It was stated that *complexes* were quickly

formed between the components. The studies were later extended to consider competitive binding of protons and metal ions with humic substances: [135] This permitted prediction of thermodynamic binding constants of a single metal species when complexed to humic substances. Their work did not consider photophysical interactions between components of the systems studied possibly since the apparatus design permitted filtration of the large fulvic fluorescence so that monitoring of the europium transitions was facilitated.

3.4.5 Theoretical Considerations of Energy Transfer Processes

Figure 3.9 shows that addition of an aliquot of Eu^{3+} to a dispersion of Fluka Humic Acid v3 leads to an increased fluorescence at 694 nm. By the application of an appropriate model, this observation has been accounted for by an energy transfer process from humic acid to the europium ion.

The theoretical basis of energy transfer reactions was first advanced by Förster [120] with the proposal of several mechanisms involving transfer:

1 Through an intermediate molecule
2 During a collisional encounter
3 By emission and subsequent re–absorption
4 Between distant atoms without emission and re–absorption.

Hercules [136] and Richardson [113] have examined these mechanisms in detail. Collisional quenching is a bimolecular process that depends on contact between the excited molecule and the quencher. It is diffusion controlled and leads to no emission. In the re–absorption mechanism, transfer occurs through an emissive transition of the donor with subsequent excitation by the acceptor. The latter may then relax by emission.

The non–radiative transfer mechanism arises because of vibronic coupling between excited states of the donor and acceptor and therefore depends on the extent of overlap between the fluorescence or phosphorescence spectrum of the donor and the absorption spectrum of the acceptor. This mechanism is most efficient when the acceptor state of the Eu^{3+} ion is identical with, or strongly coupled to, the emitting state, $^5D_0$, so that transferred energy leads to population of the emissive levels.

A theoretical equation describing this form of energy transfer derived by Förster [120]

shows that transfer efficiency is inversely proportional to the inverse sixth power of the distance of separation of the donor from the acceptor and inversely proportional to the lifetime of the excited sensitiser. The mechanism has been observed to operate over separations much larger than the contact distances of molecular collisions: Typical values lie in the range 50–100 Å. [136]

Förster [120] presented a Table of characteristic properties of the different transfer mechanisms. Measurement of the suggested bulk solution properties and luminescence characteristics permit identification of the appropriate mechanism. For luminescence measurements, this requires the isolation of spectral characteristics for each component within samples.

For the system considered in these studies, the humic acid acts as a sensitiser by absorbing low energy light and the europium(III) ions act as an acceptor resulting in emission at higher wavelengths. The exact nature of the transfer mechanism cannot be determined from the experiments described herein since it has not been possible to apply Förster's [120] considerations of mechanistic properties due to the difficulty in isolating spectral characteristics for the samples. However, analysis of some properties of the mechanisms suggest that several alternatives could operate.

Richardson [113] analysed the energy levels of the trivalent europium ion and found suitable energy acceptor levels below 580 nm ($\upsilon > 17300\ cm^{-1}$). Energy transfer to the $^5D_2$, $^5D_1$, or $^5D_0$ levels will generally lead to sensitisation and enhancement of the $^5D_0 \rightarrow {}^7F_J$ emission.

Inspection of the Fluka Humic Acid v3 emission spectrum (Figure 2.23), the europium(III) electronic absorption spectrum (Figure 3.2), the excitation spectrum for 694 nm Eu^{3+} emission (Figure 3.3) and reference to the Table of europium(III) transitions (Table 3.1) suggest that appropriate energy levels exist so that the re–absorption and non–radiative transfer mechanisms are plausible for the system studied: The emission spectrum caused by excitation of Fluka Humic Acid v3 with 440 nm light reveals a broad maximum centered around 510 nm. Excitation of europium(III) at 521 and 531 nm provides efficient emission at 694 nm. Thus a pathway for energy transfer to the $^5D_1$ Eu^{3+} electronic excited state from the $^7F_0$ and $^7F_1$ ground states are available. These conditions are similar to those described by

Richardson who observed sensitisation and enhancement of Eu^{3+} emission on binding to *E. coli* tRNA. [113]

It should be appreciated that exact co–incidence of the humic acid emission levels and the europium(III) electronic excitation levels is not a requirement for resonant transfer since it is likely that vibrational levels are available that can provide the necessary overlap with subsequent rapid thermal dissipation of energy. Further, the broad-band humic acid emission suggests that there are opportunities for co–incidence of electronic energy levels due to the heterogeneous nature of the material.

Formation of complexes between europium(III) ions and humic acid is quite likely in the aqueous medium employed since the (conditional) stability constants reported by many workers are of a large magnitude. [13,27,33–40] Detailed comments concerning the ratios of metal to humic acid employed in these studies were given in Section 3.2.3, but it should be stressed that the samples covered sensible complexation ratios ranging up to complete saturation of the metal ion by humic acid, based on ionic equivalents. However, it is not necessary to invoke complexation of the components to explain energy transfer between them since transfer can occur over distances of 50–100 Å by the non–radiative transfer mechanism. Similarly, Zepp *et al* [125] showed that photosensitised reactions of pentadiene and dimethylfuran did not involve bonding of the chemicals by the sensitising humic substances studied, including Fluka Humic Acid.

Studies described earlier in this Chapter [94,125,126,133] suggested the importance of humic triplet states in energy transfer from humic materials. Ohnesorge [137] stated that in general, the extent of intersystem crossing increased in the presence of paramagnetic transition or lanthanide metal atoms due to greater opportunities for spin-orbit coupling. Population of europium(III) terms above the ground state (see Section 3.1.2) has important consequences here since the $^7F_0$ ground state is diamagnetic, but the significant room temperature occupancy of the $^7F_1$ and $^7F_2$ levels provides paramagnetic states that may interact significantly with the humic acid.

If the humic sensitising state is a triplet that is facilitated by the presence of a metal ion, then the transfer mechanism is likely to be of a non–radiative nature since phosphorescent emission from the sensitiser in the re–absorption mechanism would probably be prevented through quenching by the solvent.

The enhanced fluorescence at 694 nm *could* be explained by the effect of europium(III) upon the humic acid without the need to invoke energy transfer if the presence of the ion made processes emitting at this wavelength more favourable compared to other deactivation mechanisms. This *could* be true if the sensitiser emission involved relaxation from the triplet state by phosphorescence since heavy paramagnetic metal ions tend to enhance intersystem crossing to triplet states. However, this process can be discounted since it is unlikely that phosphorescent emission occurs due to efficient quenching of the triplet state by the solvent. Further, detection of phosphorescence is not favoured using an unmodified fluorometer.

It is possible that energy transfer occurs between other electronic levels of the europium ion and the humic acid. These have not been investigated here since their resolution from the intense humic acid emission spectrum is not as clear as the transition studied. More sophisticated experimental methods such as those used by Dobbs *et al* [134,135] may facilitate such investigations.

The increased emission observed at 694 nm is due to the availability of a more favoured pathway for the dissipation of electronic excitation energy that was presumably degraded by an alternative method in the absence of the metal ion. It is not apparent from spectra of the "complexes" if reduced emission intensities appeared at other wavelengths due to the diversion of the radiative degradation pathway to 694 nm.

Note that charge-transfer bands were not observed in spectra of the "complexes." These may not occur for several reasons:

1 The nature of the interactions does not include charge-transfer
2 Inappropriate selection of wavelengths
3 Charge-transfer bands may be obscured by the broad-band humic acid fluorescence at higher frequencies.

Richardson [113] pointed out that energy transfer to a charge-transfer state generally does not sensitise $^5D_0 \rightarrow {}^7F_J$ emission, being lost instead by thermal relaxation to the ground state. Appearance of enhanced ^7F_J emission at 694 nm suggests that charge-transfer plays a minor contribution in the energy relaxation processes.

Several workers [138–151] have studied the fluorescence of systems containing humic substances and metal ions to determine (conditional) stability constants for complexation

of the metal ions. This method hinges on the quenching of humic substance fluorescence by the added metal ions. Quenching occurs readily with paramagnetic ions if strong complexes are formed involving close approach of the metal to the fluorescing species. [139] Quenching mechanisms have been summarised by Gauthier *et al.* [140]

In the experiments described within, quenching of humic acid 694 nm emission was not observed on addition of europium(III) ions despite the metal ions having some paramagnetic character. Other humic acid fluorescent emission wavelengths were not monitored closely for this effect. The lack of quenching may be because the metal has energy levels that permit emission rather than resulting in its loss. Alternatively, interactions between the metal and the ligand may not be strong since the requirement for close approach may not be achieved. The ligand may be located outside the inner co–ordination sphere of the metal in an outer co–ordination sphere. This suggestion of non–close approach of the metal to the ligand can be extended to the energy transfer mechanism by proposing that transfer occurs by a mechanism that is able to operate over large distances, namely the non–radiative mechanism. Ryan [138] made similar observations with the paramagnetic Mn^{2+} ion: It was suggested that the ion was insulated from the humic substance binding site by its hydration sphere making its influence on quenching poor.

3.4.6 Energy Transfer Mechanisms and the Photophysical Scheme

The photophysical scheme of Figure 3.10 applies whether the mechanism involves transfer by re–absorption or by the non–radiative mechanism.

For the re–absorption mechanism, the transfer efficiency is primarily dependent on the ability of the sensitiser to achieve a state that can emit a photon, $h\upsilon'''$, of wavelength between 450 nm and 694 nm. The likelihood of this process is dependant on the concentration of the excited state, [H*]. The second component of the re–absorption efficiency is the probability of excitation of the metal by $h\upsilon'''$ which depends on its concentration, [M], and the availability of this radiation. These processes are summarised in the scheme as f[M][H*] where f[M][H*] takes account of both the humic acid emission of $h\upsilon'''$ and excitation of the metal by $h\upsilon'''$.

If the non–radiative mechanism operates, transfer requires the presence of H* and M

(although they may be some distance away from each other) and the transfer probability can be denoted as f. Similarly, this mechanism may be summarised as f[M][H*].

Therefore, the transfer mechanism can simply be represented by f[M][H*] whichever of these mechanisms operate. It is notable that the same energy levels of the humic acid and the europium(III) ion are probably used in both mechanisms.

3.4.7 Derivation of Transition Probabilities from the Photophysical Scheme

It has not been possible to assign values to individual transition probabilities as there are simply too many unknown quantities. Modelling of the shape of non–limiting regions of the fluorescence curve only provides relative values of transfer efficiencies.

Although it is experimentally possible to determine the efficiency (quantum yield) of the humic excitation process compared to a chemical actinometer, quantitative determination of "a" is hampered by the requirement for the concentration of the humic acid to be expressed in molar terms. Further experiments, such as an experiment similar to that described here but using a constant humic acid concentration and a variable metal ion addition, do not result in the isolation of transition probabilities: The derivation of a photophysical model for this approach is similar to that presented here and results in equation (8) but with [H] as a constant and [M] as a variable. The variation of the fluorescence with [M] is therefore represented by a complex equation involving quadratic terms whose form is not revealed by the application of zero and infinite concentration limits.

Knowledge of the exact transfer mechanism would permit the application of Förster-type considerations which would be desirable since this leads to an estimate of (some average of) the distance between the metal and the humic acid.

3.5 Conclusions

Consideration of the absorption and fluorescence characteristics of Fluka Humic Acid v3 and europium(III) led to an experimental investigation strategy that permitted monitoring of photophysical processes in an aqueous medium. This was achieved by excitation of the ligand at 450 nm and detection of emission at 694 nm. Addition of an aliquot of $Eu^{3+}_{(aq)}$ to a dispersion of Fluka Humic Acid v3 resulted in an enhanced fluorescence at 694 nm. Derivation of an appropriate model accounted for this observation by incorporation of an energy transfer process from the humic acid to the metal ion. Other photophysical processes that could lead to the same result have been discounted. Several energy transfer mechanisms have been forwarded but the identity of the mechanism is not apparent. However, it is probable that it is of a non–radiative nature that does not involve complexation of the metal ion and humic acid. The nature of the system has prevented determination of quantum efficiencies for the photophysical processes and an estimate for the distance of separation of the metal from the ligand.

CHAPTER 4
NUCLEAR MAGNETIC RESONANCE SPECTROSCOPY

4.1 Introduction

Studying materials by Nuclear Magnetic Resonance (NMR) involves monitoring the magnetic properties of suitable nuclei. Several approaches using NMR of various nuclei are described in this Chapter. The structure and composition of humic materials are studied by the well-established techniques of proton and carbon–13 NMR spectroscopy in solution; this is extended to include use of lanthanide ions as shift reagents to derive extra information concerning their interactions with humic ligands in complexes. Carbon–13 spectra are also obtained for humic materials in the solid state, and in the presence of paramagnetic lanthanide ions. Finally, some studies are described using several metals as NMR nuclei to provide information about their environment in complexes with humic materials.

Theoretical aspects of NMR spectroscopy underlying the experimental work, and the origin of information accessible from the technique, are detailed in the following Sections.[64,152,153]

4.1.1 Development of NMR Spectroscopy

Early studies of NMR were limited to ^{1}H, and to a lesser extent ^{19}F, ^{31}P and ^{11}B. At this stage it was possible to count nuclei by looking at coupling patterns, and use chemical shifts and coupling constants to give information about the chemical environments of atoms. The introduction of Fourier Transform pulse methods enabled many more nuclei to be observed, and double resonance methods—particularly noise decoupling—greatly simplified the spectra of complex systems. Studies of the relaxation of nuclei were enabled. Vast improvements in computation technology, electronics, probe design, and magnet technology, have resulted in the easier acquisition of data and large gains in signal-to-noise ratios.

4.1.2 The Nuclear Magnetic Resonance Phenomenon

The spin of a nucleus is the basis of nuclear magnetic resonance. For every isotope of an element there is a ground state nuclear spin quantum number I which has the value of n/2, where n is an integer. Isotopes having atomic and mass numbers that are both even (e.g., $^{12}_{6}C$, $^{28}_{14}Si$) have I = 0 and give no NMR spectra. Isotopes with odd atomic number but even mass number (e.g., $^{2}_{1}H$, $^{14}_{7}N$) have n even, and those with odd mass numbers (e.g., $^{1}_{1}H$, $^{13}_{6}C$) have n odd. When I is non–zero, the nucleus has a magnetic moment μ, given by:

$$\mu = \frac{\gamma h}{2\pi} (I(I+1))^{1/2} \qquad (1)$$

Where:

γ = The gyromagnetic ratio, a constant for a given nucleus

h = Planck's constant

In the presence of a strong magnetic field B_0, the spin axis orientation is quantised, with magnetic quantum numbers taking values of I, I–1, I–2, ..., –I. Irradiation at an appropriate (radio) frequency induces transitions with a selection rule of $\Delta m = -1$, and it is these transitions that are observed in NMR. The resonance frequency characteristic of a given nucleus A, called the Larmor frequency υ_A, is defined by:

$$\upsilon_A = \frac{\gamma}{2\pi} B_0 \qquad (2)$$

Therefore υ_A is directly proportional to the gyromagnetic ratio of the nucleus and the magnetic field.

4.1.3 Parameters Available from NMR Spectroscopy

General analysis of NMR spectra yields chemical shifts, coupling constants, the numbers of each nucleus, and relaxation times. These parameters are related to the chemical

structure of the system.

4.1.3.1 Chemical Shifts

Compared to isolated nuclei, those in atoms are screened to some extent from the magnetic field by their electrons so that the effective magnetic field at a nucleus B_{eff} is:

$$B_{eff} = B_0 \ (1-\sigma_A) \qquad (3)$$

Where:

σ_A = The nuclear shielding (screening) constant

Differences between shielding constants of a nucleus in a sample and in a reference σ_{ref}, are called chemical shifts δ_A :

$$\delta_A = \sigma_{ref} - \sigma_A \qquad (4)$$

Chemical shifts are quoted in parts per million (ppm) of the observation frequency υ_0 :

$$\delta_A = \frac{\upsilon_A - \upsilon_{ref}}{\upsilon_0} \qquad (5)$$

The most common convention is that a shift to a high frequency is positive so that an increase in deshielding increases the chemical shift. These are a major source of information from NMR since they primarily depend on the local electronic charge and therefore the neighbouring atoms or structural units.

4.1.3.2 Signal Intensities

The intensity of a NMR signal is proportional to the population difference between the energy levels of the transition, and the number of nuclei causing it. Using Fourier Transform NMR methods, it is only possible to obtain accurate integrals providing that allowances are made for the different relaxation times of nuclei in various environments.

4.1.3.3 Coupling Constants

The frequencies of the transitions between energy levels observed in NMR experiments provide information primarily concerning the nuclei directly involved, but also about neighbouring spinning nuclei since their spins interact with each other. For the simplest cases, stationery state energies E, are given by:

$$E = -h \sum_{A} \upsilon_A m_A + h \sum_{A<B} J_{AB} m_A m_B \qquad (6)$$

Where:

J_{AB} = The spin-spin coupling constant for nuclei A and B

m_A = Magnetic quantum number of nucleus A

m_B = Magnetic quantum number of nucleus B

Coupling constants are several orders of magnitude smaller than the Larmor frequencies. In fluids, the direct dipole-dipole coupling is averaged to zero by molecular tumbling. It is the indirect coupling—which is transmitted by the valence electrons of the structure—that is observed. Equation 6 is only valid when the coupling constant J_{AB}, is much less than the chemical shift, $\sigma_A - \sigma_B$.

4.1.3.4 Relaxation Times

Relaxation mechanisms are radiationless processes by which nuclei return to equilibrium after absorbance of their resonance frequency. For a nucleus having two possible spin states, there is a Boltzmann distribution between the two levels, which for nuclei under typical conditions results in a population difference of a few parts per million. The absorption signal—which is proportional to the population difference—would soon disappear because of saturation but for relaxation processes. There are two broad relaxation mechanisms, the first involves exchange of energy between the spin system and the surroundings (e.g., through molecular vibrations and rotations of local solvent molecules) and is characterised by a Spin-Lattice Relaxation Time T_1. The second relates to the redistribution of energy between spins of different nuclei (dipole-dipole

interactions) and is described by a Spin-Spin Relaxation Time T_2. The former effectively controls the overall rate of relaxation of nuclei since the latter results in no change in the total spin populations. The Heisenberg Uncertainty Principle suggests that short relaxation times lead to broad NMR resonances and uncertainties in the accurate determination of resonance frequencies.

4.1.4 Introduction to Experimental Work

Several distinct approaches are pursued in the experimental investigations described in this Chapter, each is directed towards obtaining specific information. NMR studies are made on several nuclei thereby capitalising on the multinuclear nature of the technique, and spectra are acquired for both solutions and solids. These two issues will be addressed first. Subsequently, selected theoretical aspects of NMR are further developed to provide a foundation to each area of experimental investigation. The potential sources of NMR information are described, and the design of experiments to access the various parameters are considered.

4.1.4.1 NMR Parameters of Selected Nuclei

Although all nuclei with $I > 0$ undergo magnetic resonance, the most useful for NMR spectroscopy are those with $I = ½$, hence proton NMR—and carbon–13 NMR to a lesser degree—have been performed routinely for many years. Many pulses have been developed that enhance their sensitivity or ease of access to information. For nuclei with $I > ½$, nuclear electric quadrupole moments, Q are important since large moments will shorten the T_1 relaxation times as they can interact with both magnetic and electric fields. New pulse techniques have been of limited use to quadrupolar nuclei since the increased sensitivity and signal selection available primarily derives from stronger magnetic fields that cause a more favourable Boltzmann distribution of spins. [154]

Table 4.1 lists the NMR parameters of some nuclei of interest: The relative frequency is referenced to a field in which protons of tetramethylsilane (TMS) resonate at 100 MHz. The relative receptivity is a guide to the signal strength obtainable from equal concentrations of nuclei; it is proportional to $\gamma^3 NI(I + 1)$, where N is the natural

Table 4.1
NMR Parameters of Selected Nuclei

Isotope	Nuclear Spin Quantum Number I	Natural Abundance N %	Gyro-magnetic Ratio γ e^3 rad / G s	Relative Frequency Ξ MHz	Relative Recep-tivity	Nuclear Electric Quadrupole Moment Q e^{-28} m^2
^{1}H	1/2	99.985	26.75	100.0	1.0	0
^{13}C	1/2	1.11	6.73	25.1	0.00018	0
^{45}Sc	7/2	100.0	6.51	24.3	0.3	-0.22
^{89}Y	1/2	100.0	–1.32	4.9	0.00012	0
^{139}La	7/2	99.9	3.80	14.2	0.060	0.22
^{175}Lu	7/2	97.41	3.05	11.4	0.028	5.58
^{91}Zr	5/2	11.2	–2.50	9.3	0.0011	-0.21
^{177}Hf	7/2	18.5	1.08	4.0	0.00026	4.5

Data source: Brevard and Granger [191]

abundance of the isotope. Comments concerning these nuclear parameters are developed in subsequent Sections.

4.1.4.2 Solution and Solid State NMR

Routine NMR involves analysis of non–viscous liquids or solutions; for commonly studied nuclei resonances are usually sharp because molecular orientations of fluids are random, consequently their spin-lattice relaxation is inefficient. The development of the NMR of solids has been slow as several difficulties had to be overcome before high resolution spectra were obtainable: [64] One such problem is that dipolar couplings are not averaged to zero by molecular tumbling thereby giving broad resonances; Secondly, the chemical shift of a nucleus depends on its orientation with respect to the magnetic field, and in solids the effect of this chemical shift anisotropy is not averaged by molecular tumbling hence further line broadening; Finally, because of the immobility of the nuclei in solids, spin-lattice relaxation times are very long making multi-pulse methods inefficient.

The very large line-widths associated with solids can be markedly reduced: The chemical

shift anisotropy can be averaged out by Magic Angle (Sample) Spinning (MAS or MASS): If a sample is rotated rapidly about an axis inclined at an angle θ to the magnetic field, the expression describing the line broadening due to chemical shift anisotropy includes a term $(3\cos^2\theta - 1)$ that vanishes when $\theta = 54{\cdot}7\,°$, providing the sample is rotated at a sufficiently high rate. Dipolar couplings are reduced to zero providing the rotation rate is greater than the line-width. Decoupling in heteronuclear systems also helps to give high resolution spectra. The problem of long T_1s can be overcome for dilute spin ½ nuclei in the presence of abundant spins by the technique of Cross-Polarisation (CP). This involves polarisation transfer from an abundant spin (commonly ^1H) to a dilute spin (e.g., ^{13}C) thus enabling the dilute spin to relax at the rate of the abundant spin, and therefore permitting faster accumulation of data and increased sensitivity.[155]

Solid state NMR is not usually applied to highly abundant nuclei like protons because of difficulties in reducing the line broadening. The dominant line broadening mechanism for protons is normally the ^1H–^1H dipolar interaction that cannot be removed by simple decoupling since protons are to be observed. Further, it is not possible to rotate samples at high enough speeds to reduce these couplings.[156] Line-width reduction can only be achieved by combining very complicated pulse sequences with MAS. Quadrupolar nuclei also present difficulties when analysed in the solid state due to the broadness of their lines. This may be overcome for nuclei with half-integral spins by looking only at transitions between the $m = +½$ and the $m = -½$ states.

4.1.5 NMR Studies of Protons and Carbon–13

NMR of carbon has several advantages over that of protons: First, the carbon skeleton is observed rather than the adjacent protons; Secondly, carbon has a larger chemical shift range hence separate signals often occur, even for quite similar environments.[155] However, the data of Table 4.1 shows that ^{13}C–NMR is less sensitive than proton–NMR because both the natural abundance and gyromagnetic ratio of the nucleus are lower.

These complementary techniques have been applied to humic substances from various origins to reveal information about their composition of structural units and functional groups, and to gain information about the genesis of humic matter.[157–173] Here, two commercial humic acids are examined as solutions by proton and carbon–13 NMR, and as solids by carbon–13 CPMAS NMR. The solution studies use sodium deutroxide as solvent

since it disperses a high concentration of the organic matter without selectivity. Polar aprotic solvents tend to dissolve selectively some fractions of underivatised humic substances, but they are more useful for derivitised samples. [1] Solid state carbon–13 NMR has the advantage of enabling analysis of whole samples of humic substances without pretreatment or subjection to solvents. Chemical shifts and signal intensities are the main NMR parameters of interest for humic substances; relaxation rates studied by line-width analysis are a lesser source of information.

4.1.6 NMR Studies of Metals

The complexation of transuranic actinides with humic substances is of concern, but as these metals are somewhat chemically inaccessible then analogues are required to model their properties. The main criteria for useful analogues are similarities in the ionic radii and stability of their oxidation states since these determine much of the chemical properties of the metals. Availability of alternative techniques to study them is desirable.

Use of some lanthanides as analogues for trivalent actinides—such as americium and curium—has been suggested. [32,43,44] Their ionic radii are very similar—especially for the lighter rare earth elements (see Table 4.2)—and the main oxidation state is trivalent for actinides in the middle and latter regions of the series, whereas for lanthanides it is the main state for the whole series. Although scandium and yttrium are transition metals, they are commonly grouped with lanthanum and lutecium since the series presents a gradation in ionic radii of their diamagnetic trivalent ions. The decrease in ionic radii from lanthanum to lutecium is caused by the lanthanide contraction. [117]

The most common oxidation state for plutonium is Pu^{IV} although it can exist in other states. Thorium(IV) is considered a good analogue for plutonium(IV) [32] however, the metabolic effects of plutonium have been mimicked by substitution with hafnium, [45] therefore hafnium—and zirconium—may have the potential to function as analogues. As a consequence of the lanthanide contraction, the ionic radii of tetravalent zirconium and hafnium are virtually identical, although somewhat different from that of Pu^{IV} (see Table 4.2). This closeness in size usually results in very similar chemical properties for Hf and Zr. [174] Like Pu^{IV}, discrete M^{4+} ions do not exist and complexes with oxygen and nitrogen donor ligands are preferred.

Table 4.2
Ionic Radii of Some Metal Ions

Ionic Radius of Trivalent Metal Ions, $r_{/M^{III}}$ / Å		Ionic Radius of Tetravalent Metal Ions, $r_{/M^{IV}}$ / Å	
Sc	0.73		
Y	0.89		
La	1.06	Zr	0.72
Pr	1.01	Hf	0.71
Eu	0.95		
Yb	0.86	Pu	0.90
Lu	0.85		
Am	0.99		

Note:
The data assumes that the metals exist as "real" ions.
Co–ordination numbers are not clearly defined by the source. [117]

Two independent approaches to NMR using metals are described in this Chapter: In the first, magnetic and electronic effects of paramagnetic lanthanide ions on the NMR of resonant nuclei in humic substances are studied since these ions are known to function as shift reagents; Secondly, NMR accessible nuclei of several metals are studied directly to deduce information about the interaction of their ions with humic substances in complexes. The background to both areas are outlined in the following subsections.

4.1.6.1 NMR Studies Using Lanthanides as Probes of the Co–ordination and Structure of Humic Materials

Hetero-nuclei in compounds containing paramagnetic metal ions have expanded chemical shift ranges, but when paramagnetic nuclei are studied themselves by NMR, their resonances are too broad to be of use. The signals from diamagnetic materials in the presence of paramagnetic substances also show some spectral expansion and broadening. Paramagnetic lanthanide ions can function in this manner causing both induced chemical shifts and enhanced relaxation rates, hence they are termed lanthanide shift reagents (LSRs). [175] Their use is advantageous for protons since ^{1}H chemical shifts normally exhibit a low sensitivity to changes in chemical and stereochemical

environments, therefore in spectra of complex organic molecules, signals are often bunched together in featureless clusters from which little definitive structural information can be obtained. LSRs have been used extensively to obtain information concerning the binding of biological macromolecules to lanthanide ions, therefore they may be of similar use to humic substances. [176–178]

Lanthanide induced chemical shifts (LIS) have diamagnetic and paramagnetic components: [177] These are the diamagnetic complex formation shift, and the paramagnetic contact and pseudo-contact terms. Paramagnetic shifts are the most fruitful source of information hence the components of LIS need to be separated. Trivalent lanthanum and lutecium ions are diamagnetic and can be used to assess changes in chemical shifts caused only by the charge of the ion; The diamagnetic complex formation shift is determined since LIS of these ions are independent of paramagnetic interactions. [175] Such values are applicable to the other lanthanide complexes since their chemical properties and ionic sizes are similar to each other therefore their complexes are isomorphous. [177]

The contact shift arises from coupling between the nucleus and the electrons of the paramagnetic ion through the intervening bonds. Their magnitude gives a measure of the unpaired spin density at the nucleus and the covalency of the bonding. There is usually a considerable contact shift on nuclei of atoms or groups in the first co–ordination sphere of lanthanide ions. Contact shifts therefore indicate which atoms are directly bonded to the ion, but structural information is not available from them. [176]

The pseudo-contact shift is a through-space dipolar interaction between the magnetic moments of electrons in the paramagnetic ion and the resonant nucleus. Its magnitude is determined by the geometrical orientation of the ligands around the metal ion and by metal ion-to-solvent interactions. The pseudo-contact component is generally greater than the contact shift and since these have different chemical origins they too are usually separated from each other.

The paramagnetic effects of the lanthanide ions should result in broadened or shifted NMR spectra of resonant nuclei in humic substances, possibly providing improved spectral appearance and structural information concerning the co–ordination of the humic materials to the metal ions. Such effects probably will be greatest on the humic acid binding groups.

LSRs are used in two forms: The first are often complexes of europium or praseodymium with 2,2,6,6-tetramethylheptane-3,5-dionato (thd) or 1,1,1,2,2,3,3,-heptafluoro-7,7-dimethyloctane-4,6-dionato (fod) ligands. These ligands are selected for several reasons: they confer solubility in most media; they restrict the mobility of the substrate in complexes; and they prevent strong bonding between the lanthanide ion and the substrate which would tend to slow down exchange processes and consequently increase the line-width. [175,176] The second form are ionic salts of the lanthanides which were used before the ß–diketonate complexes. They have long T_1s and therefore a minimal line broadening effect. However, the salts give smaller LIS since the metal ions are solvated by water molecules in the inner co–ordination sphere thus reducing the ability of the metal ions to interact with substrates. The shifts produced tend to be opposite to those induced by the ß–diketonates with europium giving high field shifts and praseodymium, low field. For lanthanide salts it can be difficult to assess the relative contributions of the contact and pseudo-contact shifts as they tend to be equal and opposite.

The lanthanides offer fewer advantages to carbon–13 NMR regarding spectral clarification since this nucleus has a larger range of chemical shifts than protons. Pseudo-contact information tends to be obtained as the carbon atoms are not directly bonded to the ions. Fewer studies are apparent for ^{13}C than protons; some other nuclei have been studied. [175]

The experimental approach adopted in these studies is to use a selection of lanthanides that cause high and low field shifts, and lanthanum as a diamagnetic ion since it causes only a complex formation shift. Europium, praseodymium, and ytterbium are the preferred LSRs since they give useful shifts without inducing appreciable line broadening; LSRs causing the largest shifts also tend to cause the largest line broadening effect. A series of soluble complexes between these lanthanide metal ions and Fluka and Aldrich humic acids are prepared and analysed by ^{1}H– and ^{13}C–NMR. Since close association of the metal and the humic ligands are required, the complexes will be made using quantitative amounts of the metal ions. Also, some complexes are prepared for analysis by solid state ^{13}C–NMR.

4.1.6.2 NMR Studies of Metal Nuclei

Most lanthanides and all actinides are excluded from direct observation by NMR since their nuclei possess undesirable characteristics, such as low receptivities and transition frequencies, and large quadrupole moments. Paramagnetism in many of their cations further broadens spectral resonances of their nuclei. Most of the work published for lanthanide nuclei has been concerned with solid state studies. For the actinides the only observations have been indirect ones involving uranium.[179]

The only reported work involving the NMR of metals associated with humic materials is a brief ^{113}Cd study with Fluka Humic Acid:[180] Three resonances were observed for the metal; those at ∂ –22·7 ppm and ∂ +2·48 ppm were assigned to complexed metal; the third at ∂ +0·9 ppm was the free cation. The primary resonances were further correlated with possible co–ordinating groups.

The elements scandium, yttrium, lanthanum and lutecium have few techniques suitable for their investigation as they are diamagnetic. Their closed shell electron configurations mean that they do not absorb light of accessible wavelengths so NMR provides a useful means of studying them directly. To date, the only report concerning the complexation of these metals with humic substances by any technique is a brief study of the association of yttrium with peat.[181] This provides added weight for a NMR investigation.

Both ^{45}Sc and ^{139}La are high sensitivity nuclei, however as Table 4.1 shows, they have appreciable quadrupole moments resulting in broad resonances, except in symmetric environments. For example, in aqueous solution line-widths may be several hundred hertz.[182] The first report of lanthanum–139 chemical shifts was made by Rinaldi *et al*;[183] shifts were found to be sensitive to inner- and outer-sphere complexation of the metal ion. ^{89}Y is a relatively sensitive spin-half nucleus, yet its long relaxation times of several minutes—due to its low gyromagnetic ratio—makes its study by NMR difficult. Cations of Sc, Y and La give transitory interactions with ligands in solution since exchange processes are fast, thus their resonances are usually time-averages for all species present. The first solid state NMR investigation of these three elements was reported in 1987.[184] The size of lutecium–175's quadrupole moment prevents its use in high resolution NMR and it will be given no further consideration here.

The few studies of zirconium NMR have concentrated on its organometallic

compounds.[154] The first study of ^{91}Zr was reported in 1981 by McGlinchey and co-workers.[185] The quadrupole moment of the nucleus suggests that symmetric environments may be required to obtain spectra with acceptable line-widths. ^{177}Hf is the preferred nucleus for hafnium but it is poor for NMR investigations because of its low resonance frequency, moderate receptivity and very large quadrupole moment.[182] No further consideration is given to it in these studies. The only reports concerning the complexation of these metals with humic substances using any technique is a brief study of zirconium associated with peat.[181]

The NMR of the ^{45}Sc, ^{89}Y, ^{139}La and ^{91}Zr nuclei are studied here in complexes with humic acids and appropriate model systems since NMR studies of biomolecules associated with metals have provided some useful information for those macromolecular systems that is potentially available for analogous studies with humic materials.[186–188] Direct observation of metallic nuclei enables information to be obtained about their local environment including chemical structure, oxidation state, electronic configuration, and the number and dynamics of co-ordinating ligands.[154] For metallic nuclei, the main sources of information are chemical shifts and relaxation parameters; the origin of useful parameters will be detailed.

Chemical shifts of metallic nuclei are due to the paramagnetic and diamagnetic contributions to the shielding constant.[153,186,154] The paramagnetic term σ_{para} dominates, whereas the diamagnetic term is practically constant. σ_{para} arises from the local paramagnetic motion of electrons surrounding the metal nucleus, which in turn depends on the average radius of the valence orbital from the nucleus r, and the average electronic excitation energy ΔE (which is the LUMO-HOMO gap). This may be expressed as:

$$\partial \approx \sigma_{para} \approx \frac{c^3}{r^3 \Delta E} \qquad (7)$$

Where:

c = A coefficient of the molecular orbitals taking part in the transitions

Nuclei of $I = ½$ usually give sharp resonances with half-widths of several hertz due to slow relaxation.[154] For quadrupolar nuclei, symmetrical environments cause small

electric field gradients and hence low line broadening as quadrupolar relaxation is inefficient. [179] On complexation, the asymmetric environment of the metal ion gives rise to an electric field gradient and consequently, an increase in the quadrupole coupling constant. As a result, the relaxation rate of the quadrupolar nucleus increases and the resonance lines broaden to widths of up to several thousand hertz. [188] Line-widths $W_{1/2}$, of quadrupolar nuclei are proportional to: the square of the quadrupole moment Q; the square of the electric field gradient q_{zz}; the motion of the molecule (characterised by a correlation time, τ_c); and dependent on the nuclear spin quantum number I, in a more complex manner. [154,189] For a given nucleus, Q and I are constant, therefore:

$$W_{1/2} \propto q_{zz}^2 \tau_c \qquad (8)$$

Since the relaxation rate depends on the local electric field gradient, studies of the local environment—such as the molecular dynamics of the complexes—are enabled. [190]

4.2 Experimental

4.2.1 Instrumentation

The basic features of the Bruker ACE 300 spectrometer (¢043) are a superconducting 7·1 tesla magnet (which provides proton resonance at 300 MHz), a radio-frequency source, a detection system, and a computer to control the spectrometer and perform data manipulation, including Fourier Transformation. The spectrometer provides pulsed NMR in which all transitions of a given nucleus are stimulated simultaneously by a strong radio-frequency pulse that contains all likely resonance energies. Nuclei absorb their resonance frequencies from the pulse and the detected free induction decay is converted to the frequency domain by Fourier Transformation. [64]

4.2.2 Sample Preparation

4.2.2.1 Proton and Carbon–13 Liquid State NMR Samples

Sodium deutroxide was selected as the solvent for liquid state ^1H– and ^{13}C–NMR analyses

of humic acids. It was prepared by dissolution of sodium hydroxide pellets (¢010) in heavy water (¢044) under a nitrogen atmosphere (¢009). Assuming that the pellets were dry, then the 0·1 M solution prepared should contain approximately one proton per thousand duetrons, and it can therefore be reliably formulated as $NaOD_{(D_2O)}$. This alkali concentration enabled dispersion of Fluka Humic Acid v3 and Aldrich Humic Acid v1 at 0·1 % w/v and 1·0 % w/v.

4.2.2.2 Carbon–13 Solid State NMR Samples

Underivatised humic acids were analysed by solid state ^{13}C NMR.

4.2.2.3 Lanthanide Shift Reagents for Proton and Carbon–13 Liquid State NMR and for Carbon–13 Solid State NMR Samples

Consideration of the requirements for useful investigations of the effects of lanthanide ions as shift reagents for humic acids suggested that close control of sample composition was needed, therefore sample preparation was subject to several requirements and constraints similar to those described in Section 3.2.2:

1 The humic acids needed to be at concentrations that produced measurable spectra, such as those used in the absence of the lanthanide ions.

2 Stable, soluble complexes are required with sensible metal ion-to-humic acid ratios at near-neutral pH conditions.

3 Ability to control sample media composition since the degree of dissociation—and therefore the complexing ability—of humic acids are condition dependent. [6]

The experimental strategy selected for preparing samples was to employ a constant humic acid concentration and use several lanthanide ions within supporting media of defined composition. The ratio of metal-to-ligand employed in the samples was calculated as ionic equivalents, although the nature of the binding is not necessarily a simple cation-anion interaction. The chosen trivalent cation additions were $4{\cdot}0\times10^{-6}$ mol which (in theory) could bind up to $1{\cdot}2\times10^{-5}$ mol of monovalent humic acid functional groups. The binding capacity of humic acids typically lies in the range 1–5 meq g^{-1} of replaceable functional groups. [1,5,6,101] The Fluka Humic Acid v3 and Aldrich Humic Acid v1 additions were

5·0 ml of 0·20 % w/v dispersions; these would be equivalent to between $1x10^{-5}$ mol and $5x10^{-5}$ mol of functional groups. Therefore the minimum binding capacity of the humic acid addition is satisfied by the added metal.

A 0·10 M sodium hydroxide stock solution for pH adjustment and dispersion of the humic acids was prepared by dissolution of B.D.H. pellets (¢010) in distilled water. This was standardised with potassium hydrogen phthalate (¢036) using phenolphthalein (¢037) as indicator. Nitric and hydrochloric acids for pH adjustment were prepared by dilution of their concentrates (¢038,011): Both were standardised against the dilute $NaOH_{(aq)}$.

The ~0·20 % w/v Fluka Humic Acid v3 and Aldrich Humic Acid v1 stocks were prepared by dispersion of their solids in distilled water to which the minimum amount of the 0·10 M $NaOH_{(aq)}$ was added to ensure adequate dispersion and a final medium condition of near-neutrality. This procedure was carried out under a nitrogen (¢009) tent while the dispersion was continually agitated and its pH monitored using a two-point calibrated pH meter (¢012–017).

The four metals to be assessed for their ability to serve as shift reagents were prepared by dissolution of their salts—lanthanum chloride (¢045), europium nitrate (¢035), and praseodymium perchlorate (¢046)—in distilled water, or for ytterbium, slices of the metal (¢047) were cut under a nitrogen tent and dissolved in the dilute nitric acid.

Samples for NMR analysis were prepared by dispensing solutions with Finnpipettes (¢040) or Agla micropipettes (¢041): The humic acid aliquot was first measured into a glass sample vial (volume ~20 cm^3) containing a small magnetic stir—bar. The metal salt solution aliquot was added, followed by distilled water until a volume of 9·9 ml was approached. The mixture was agitated and its pH was monitored with a doubly—calibrated pH electrode connected to a digital pH meter. Additions of acid or alkali indicated by the prevailing pH were made to the system so that neutrality was approached. The final pH was recorded and a 0·1 ml $D_2O_{(l)}$ aliquot was added. All sample media were carefully controlled so they had a pH of 7·0±0·1, and a total volume of 10·0±0·1 ml; samples that deviated from these limits were discarded.

Two solid complexes of europium(III) were prepared for solid state carbon–13 NMR analysis. Similar considerations to those previously described regarding the ratios of

metal ions to humic acid ligands were applied. 2·0 % w/v Fluka Humic Acid v3 and Aldrich Humic Acid v1 were prepared by dispersion of their solids in 0·10 M $NaOH_{(aq)}$ (¢010,048). Appropriate additions of 0·02 M $Eu(NO_3)_{3\ (aq)}$ were made to the humic acids such that they were near the range of the humic acid binding capacities. These were acidified to ~pH 2 with standardised 0·13 M $HNO_{3\ (aq)}$ (¢049) and centrifuged to precipitate the complexes. The solids were dried in a vacuum desiccator over phosphorus pentoxide (¢019).

4.2.2.4 Metallic Nuclei Liquid State NMR Samples

The magnetic resonance of scandium–45, yttrium–89, lanthanum–139 and zirconium–91 had not been previously studied on the Bruker spectrometer therefore concentrated solutions for each nucleus were required for the location and subsequent optimisation of their signals. The materials prepared were those suggested in Brevard and Granger's NMR handbook. [191] For scandium, a 1·0 M solution of the chloride (¢050) was dissolved in deuterium oxide (¢044). Yttrium nitrate (¢051) was made at the same concentration, but for lanthanum chloride (¢045), 0·05 M was suggested. For zirconium, a saturated solution of zirconocene dichloride (¢052) was dissolved in dry tetrahydrofuran.

Following location of the signals, the sensitivities of the resonances to the concentrations of their nuclei were assessed by serially diluting some concentrated metal salt solutions. This procedure is necessary since a compromise must be reached between low metal ion concentrations required to prevent coagulation of the humic substances in complexes, and high metal ion concentrations that favourably increase sensitivity and therefore decrease instrument time.

Since these elements have not been studied extensively some simple complexes were made to indicate the likely chemical shift ranges of their nuclei. For example, a lanthanum phthalate complex was made since the equilibrium constants for its formation are favourable ($\log_{10} K_1 = 4{\cdot}1$ & $\log_{10} K_2 = 3{\cdot}2$). [192] Phthalic acid (¢053) has a low solubility in water but dissolves in alkali with consequent neutralisation of both of its carboxyl groups ($pKa_1 = 2{\cdot}89$, $pKa_2 = 5{\cdot}51$) [193] on reaching of a neutral pH condition. 1·98 g of the acid was dissolved in 250 ml of 0·1 M $NaOH_{(aq)}$ to yield ~0·05 M sodium phthalate at pH 7·3. To a portion of this, lanthanum chloride solution was added such that the metal ion was just saturated with the ligand, based on ionic

equivalents.

Complexes of the metals with humic acids were prepared bearing in mind the binding considerations discussed in Section 4.2.2.3. Metal ion-to-humic acid concentrations were such that they ranged from above, to within and below the range in the number of functional groups in a selected mass of Fluka Humic Acid v3 or Aldrich Humic Acid v1. The samples were made from concentrated solutions of the metal salts and 2·0 % w/v dispersions of these humic acids using the same procedures described for the lanthanide shift reagents (see Section 4.2.2.3). For zirconium, a solution of the nitrate (¢054) was used as the source of the metal ion; this was assumed to contain Zr^{4+} for the purpose of calculations.

4.2.3 Spectral Acquisition

4.2.3.1 Proton and Carbon–13 Liquid State NMR

Liquid state proton and carbon–13 spectra were acquired for the humic acids in sodium deutroxide; this functioned both as the solvent and internal deuterium lock. For proton spectra, residual protons in hydroxides were irradiated using gated presaturation at approximately 4·7 ppm. This pulse is used since ionic solutions would otherwise become hot. Various irradiation power levels were assessed until the complicating peaks were reduced without distorting other resonances.

4.2.3.2 Carbon–13 Solid State NMR

Solid state CPMAS carbon–13 spectra were run using the solid state probe with rapid sample rotation (~4·5 kHz) at the magic angle (54·7 °), and high power proton decoupling. Solids were uniformly distributed by grinding, and then packed into a rotor made of boron nitride with a delrin (poly(oxymethylene)) tip. The spectra were obtained using a relaxation delay of 2·0 s and a cross-polarisation contact time of 3·0 ms. These values were a compromise between those used by others for similar samples as it was not possible to deduce the best relaxation conditions on the spectrometer. [161,163–167,194] Composite Pulse Decoupling—which is a form of broadband decoupling—was used to

remove the complicating effects of coupling of the carbon–13 nuclei to protons. At least 20000 scans were taken for each spectrum.

4.2.3.3 Lanthanide Shift Reagents for Proton and Carbon–13 Liquid State NMR and Carbon–13 Solid State NMR

Liquid state proton and carbon–13 spectra of complexes of the lanthanide ions associated with the humic acids were acquired under similar conditions to those described previously (Section 4.2.3.1). The spectra of the europium(III)-Fluka Humic Acid v1 and europium(III)-Aldrich Humic Acid v1 complexes were also run using comparable conditions to those used for the underivatised humic acids described in Section 4.2.3.2.

4.2.3.4 Metallic Nuclei Liquid State NMR

NMR spectra of the metallic nuclei were run in the liquid state using the broadband probe. Initially it was necessary to locate their signals since they had not been previously detected on the Bruker spectrometer. For this procedure, the spectrometer and probe were adjusted to the specifications given by Brevard and Granger [191] and concentrated solutions were used to enable optimisation of the resonances. Some concentration sensitivity tests were then performed and then the complexes of the metal ions were scanned. Further samples were prepared and their magnetic resonances were determined immediately.

4.3 Results

NMR spectra acquired for various samples are given in Figures 4.1–4.7. Most are presented with some line broadening which is achieved through exponential multiplication of the Free Induction Decay: [194] This is used to improve the signal-to-noise ratio of spectra, but at the expense of resolution. The amounts used are given in the key to each spectrum.

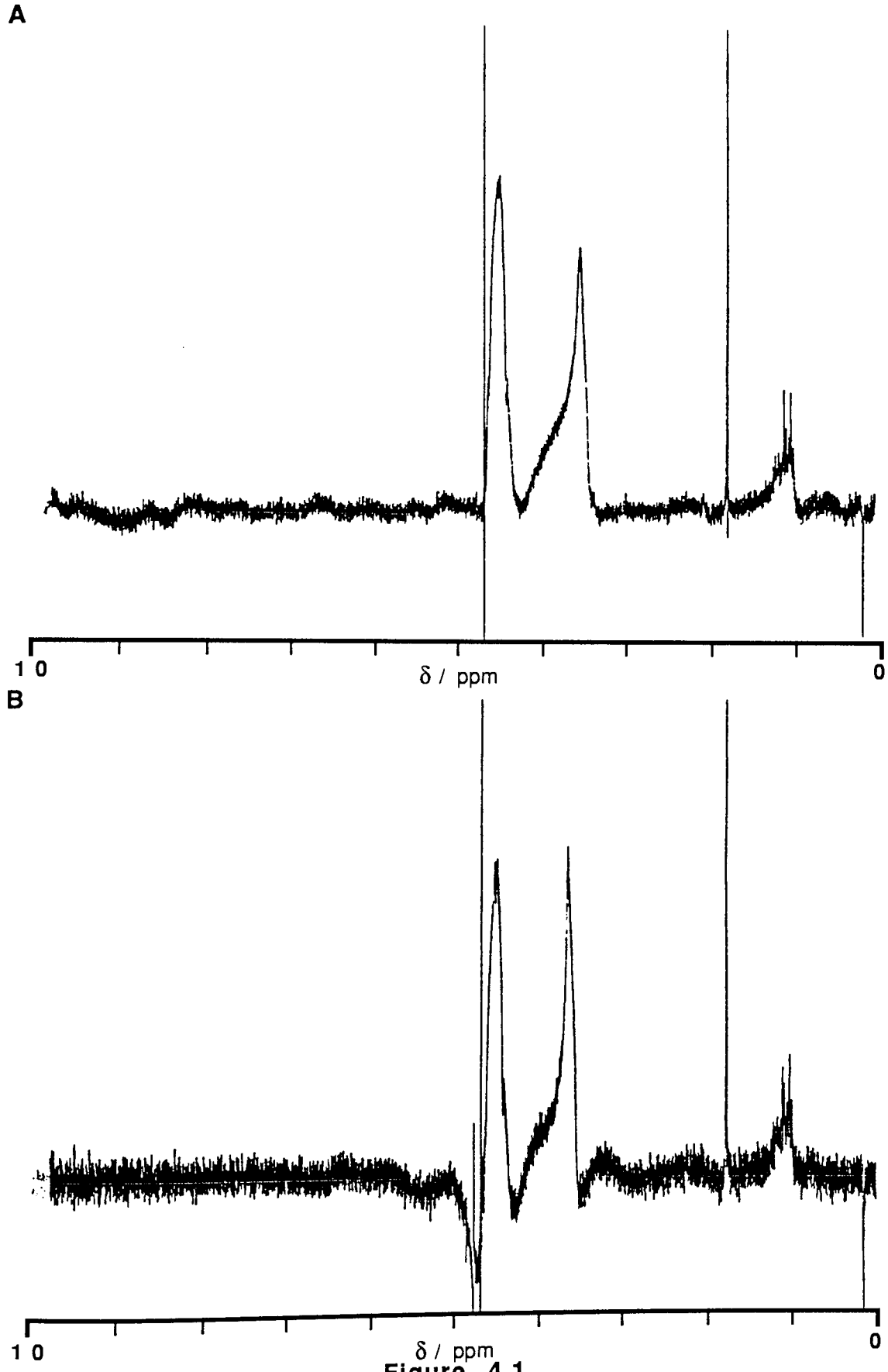

Figure 4.1

Proton NMR of Fluka Humic Acid v3 & Aldrich Humic Acid v1

Key: **A**–Fluka Humic Acid v3; **B**–Aldrich Humic Acid v1

Sample Details: Humic Acid Concentration 0.1 % w/v; Solvent 0.1 M NaOD in D_2O

*Spectral Acquisition Conditions: Nucleus 1H; Resonance Frequency 300 MHz; Presaturation of H-O-D at δ 4.7 ppm; Reference TMS; Scans **A**–442, **B**–148*

*Spectral Plotting Parameters: Line Broadening 0 Hz; Baseline Correction **A**–Spline Fitted*

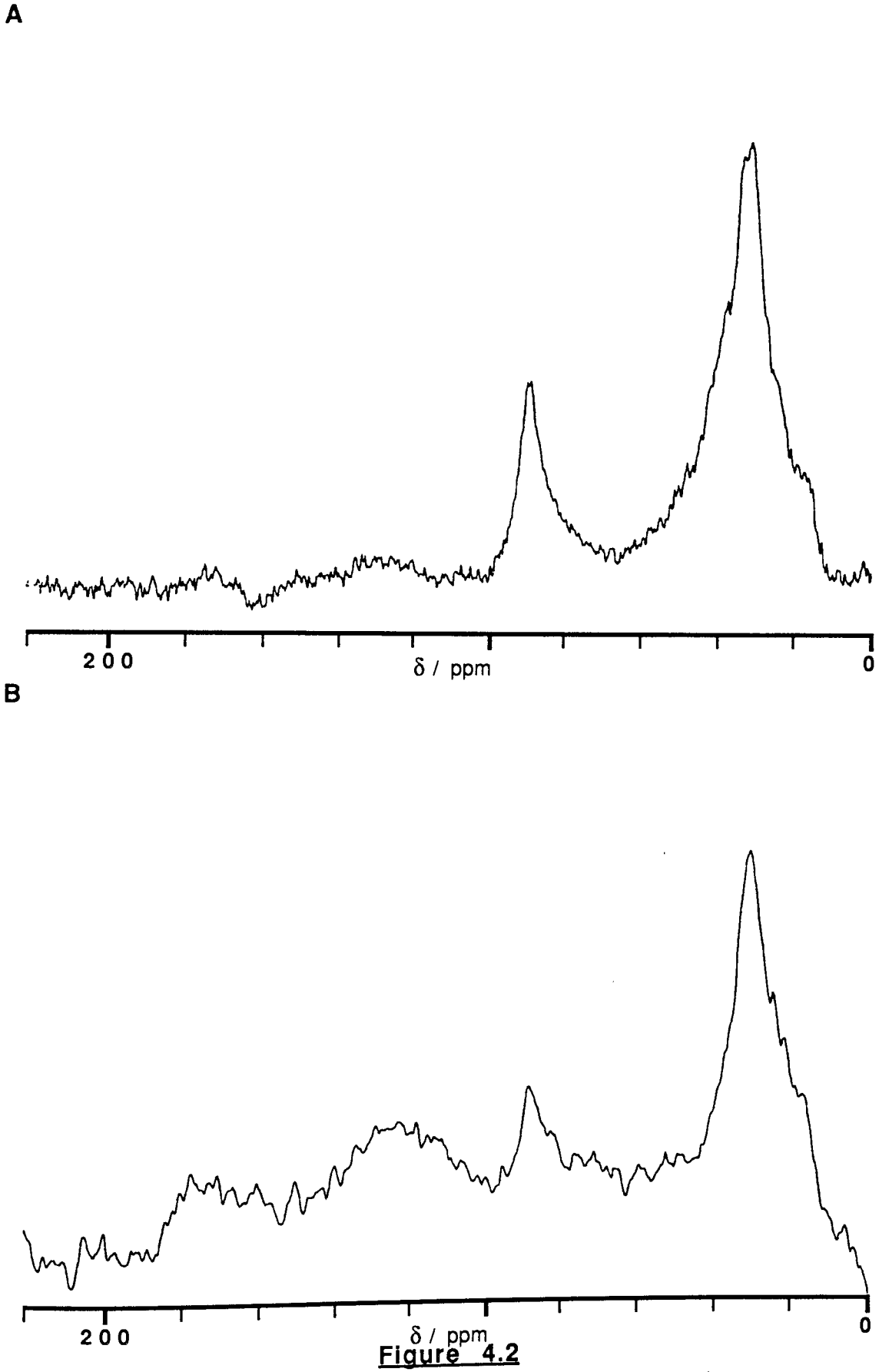

Figure 4.2

Carbon-13 Solid State CPMAS NMR of Fluka Humic Acid v1 & Aldrich Humic Acid v1

Key: **A**–Fluka Humic Acid v1; **B**–Aldrich Humic Acid v1

*Spectral Acquisition Conditions: Nucleus 13C; Resonance Frequency 76 MHz; CP Contact Time 3 ms; Delay 2 s; Scans **A**–22990, **B**–33600; Rotation Rate /Hz **A**–4600, **B**–4500*

*Spectral Plotting Parameters: Line Broadening /Hz **A**–30, **B**–100*

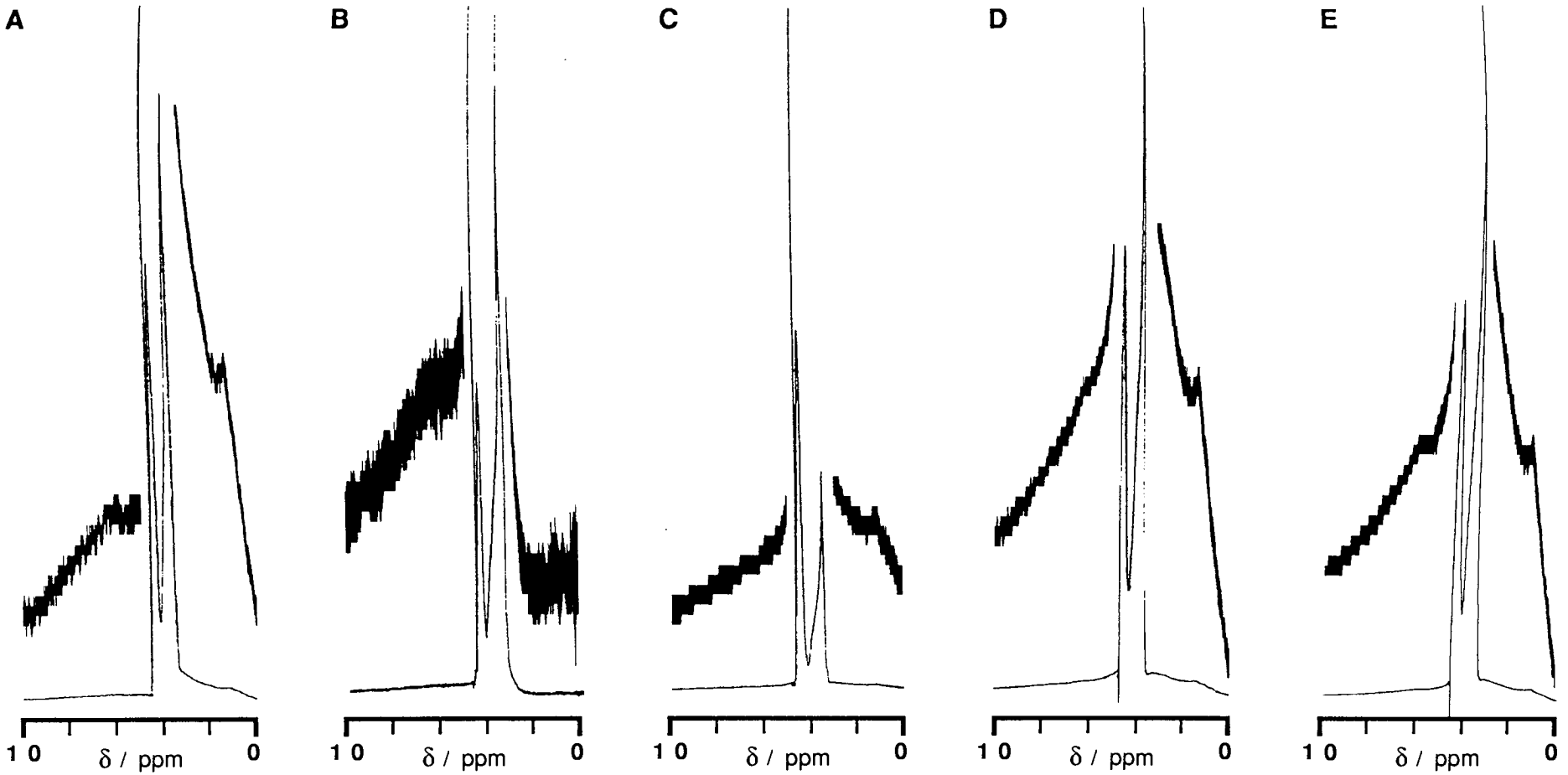

Figure 4.3

Proton NMR of Fluka Humic Acid v3 in the Presence of Lanthanide Metal Ions as Shift Reagents

Key: Trivalent Lanthanide Ion Complexes with Fluka Humic Acid: **A**–No Metal; **B**–Lanthanum; **C**–Praseodymium; **D**–Europium; **E**–Ytterbium

Sample Details: Fluka Humic Acid v3 Concentration 0.1 % w/v; Metal Ion Concentration 0.0004 M; Solvent D_2O; pH 7±0.1

Spectral Acquisition Conditions: Nucleus 1H; Resonance Frequency 300 MHz; Presaturation of H-O-D at δ 4.7 ppm; Reference TMS; Scans 500–2000

Spectral Plotting Conditions: Line Broadening 0 Hz; Inset Spectra x20 Ordinate Expansion

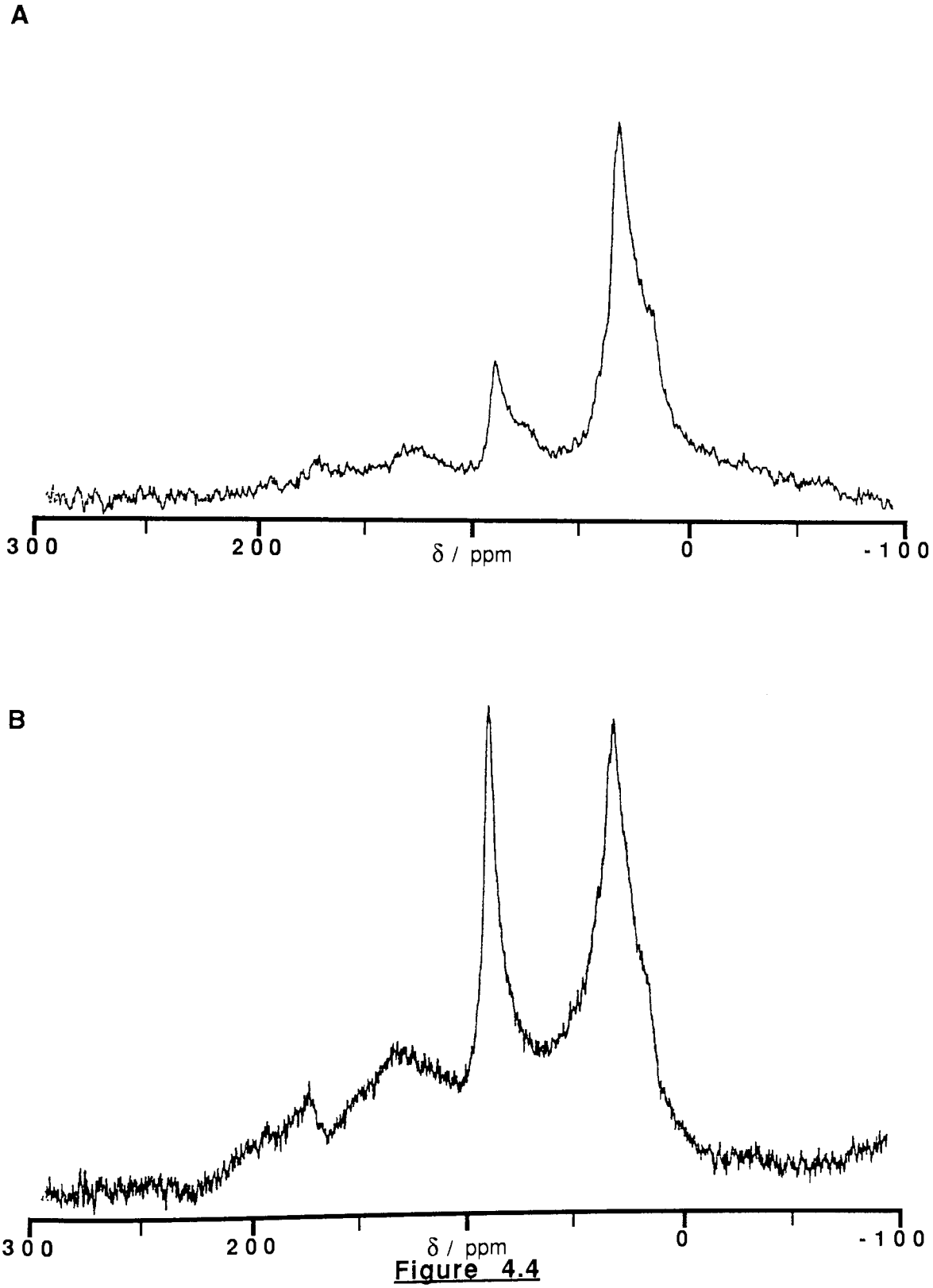

Figure 4.4

Carbon-13 Solid State CPMAS NMR of Europium(III) Complexes of Fluka Humic Acid v1 & Aldrich Humic Acid v1

Key: Europium(III) Complexes of: **A**–Fluka Humic Acid v1; **B**–Aldrich Humic Acid v1

Spectral Acquisition Conditions: Nucleus 13C; Resonance Frequency 76 MHz; CP Contact Time 3 ms; Delay 2 s; Scans ***A****–66872,* ***B****–35520; Rotation Rate /Hz* ***A****–4400,* ***B****–4800*

Spectral Plotting Parameters: Line Broadening /Hz ***A****–40,* ***B****–20*

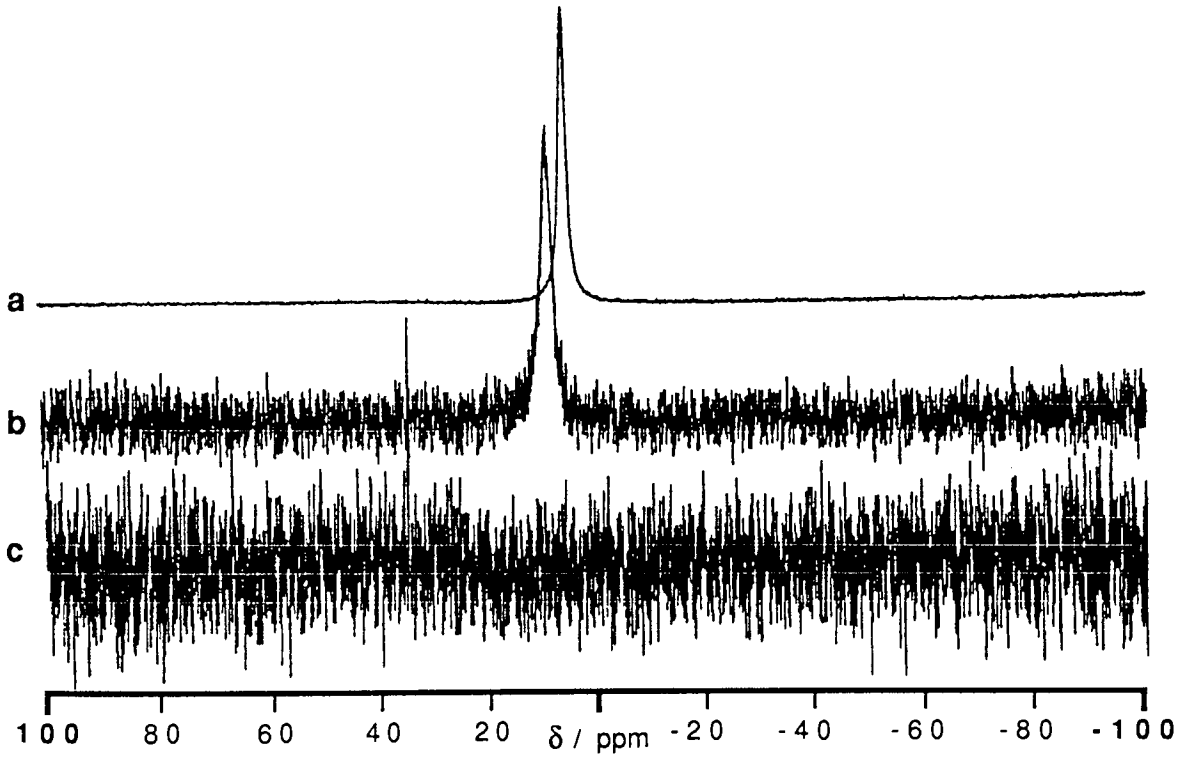

Figure 4.5

Scandium-45 NMR Concentration Sensitivity Assessment

Key: Scandium Chloride Concentration, [$ScCl_3$] / M: **a**–0.1, **b**–0.01, **c**–0.001
*Sample Details: Solvent Composition D_2O:H_2O **a**–1:10, **b**–1:100, **c**–1:1000*
Spectral Acquisition Conditions: Nucleus 45Sc; Resonance Frequency 73 MHz; Reference 1 M $ScCl_3$ in D_2O; Scans 1040
Spectral Plotting Parameters: Line Broadening 2 Hz

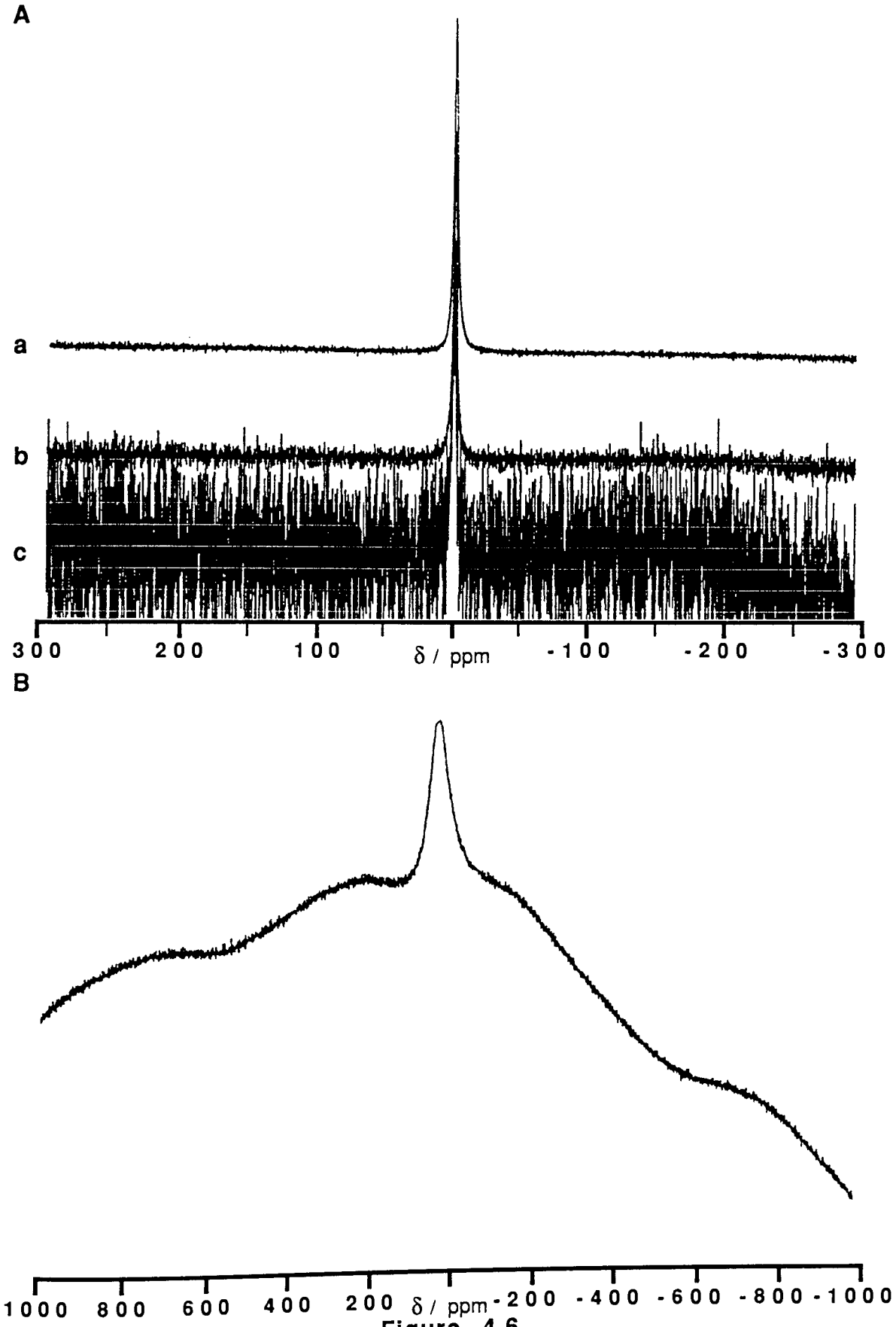

Figure 4.6

Lanthanum-139 NMR Concentration Sensitivity Assessment & Lanthanum Phthalate Complex

Key: **A**–Lanthanum Concentration Sensitivity Assessment: [$LaCl_3$] / M: **a**–0.05, **b**–0.01, **c**–0.0015; D_2O:H_2O **a**–1:0, **b**–1:10, **c**–1:10; **B**–Lanthanum Phthalate Complex

*Spectral Acquisition Conditions: Nucleus 139La; Resonance Frequency 42 MHz; Reference 0.05 M $LaCl_3$ in D_2O; Scans **A**–1000, **B**–64098; Line Broadening/ Hz **A**–0, **B**–6*

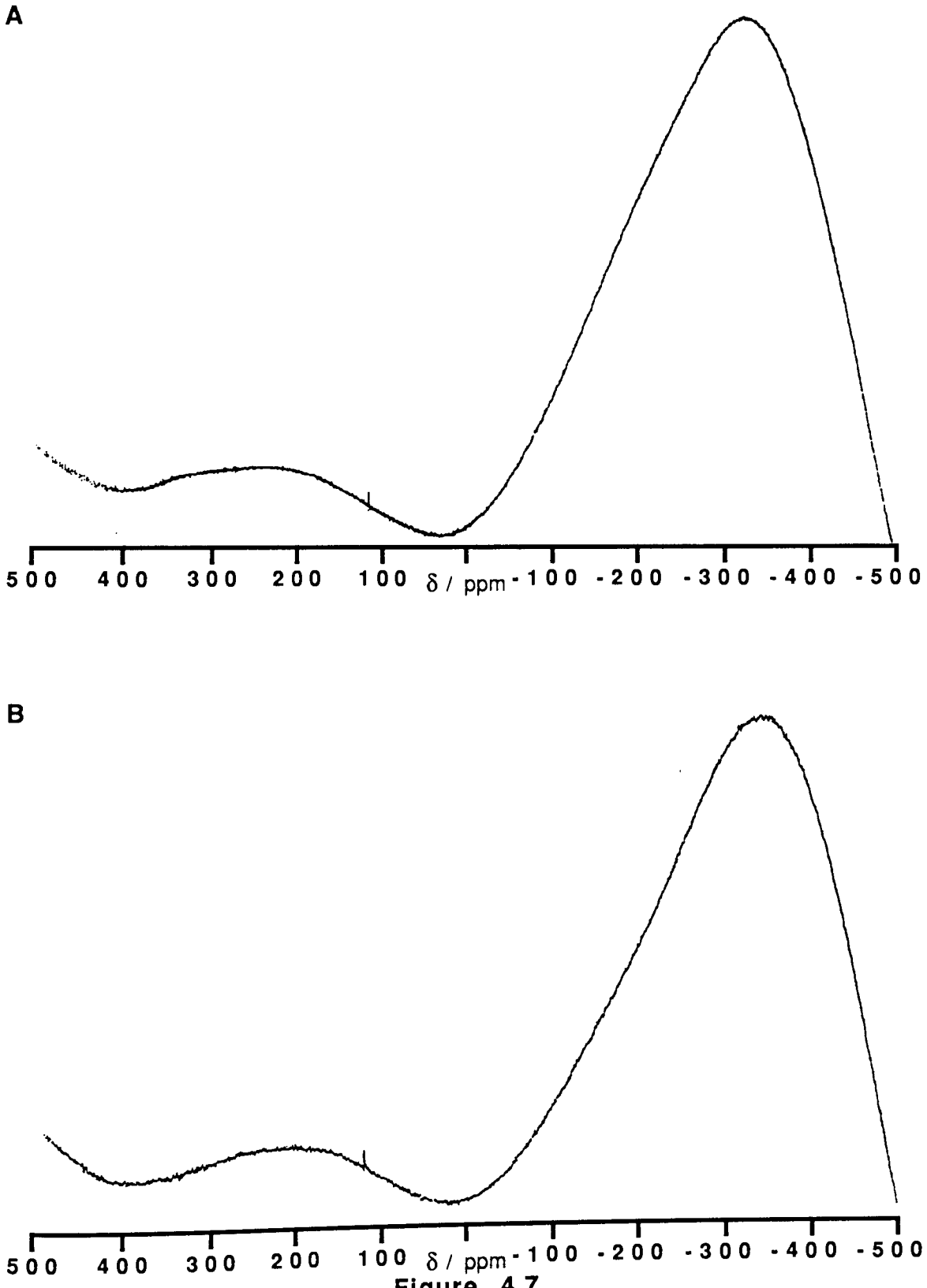

Figure 4.7

Zirconium-91 NMR of Zirconium(IV) Nitrate & Zirconium(IV)-Fluka Humic Acid v3 Complex

Key: Zirconium(IV) (in H_2O/D_2O): **A**–Nitrate; **B**–Fluka Humic Acid v3 Complex

*Spectral Acquisition Conditions: Nucleus 91Zr; Resonance Frequency 28 MHz; Reference Saturated (~9 % w/v) Cp_2ZrCl_2 in THF; Scans **A**–203000, **B**–30000: Line Broadening/ Hz **A**–2, **B**–8*

The proton spectrum of Figure 4.1A is presented with a fitted baseline obtained using a cubic spline algorithm available on the spectrometer computer. Sample spinning speeds are given for the solid state spectra of Figures 4.2 and 4.4 so that they can be analysed for the presence of spinning side-bands. The concentration sensitivity assessments of Figures 4.5 and 4.6A are presented with the same ordinate displacement but adjusted by different sensitivity factors; each is offset vertically.

4.4 Discussion

4.4.1 Proton and Carbon-13 Liquid State NMR

Liquid state proton spectra were obtained for the humic acids using sodium deutroxide as solvent and internal deuterium lock. Initial spectra (not presented here) were dominated by the resonance of protons in H–O–D groups; other resonances were not observed. These hydroxides derive from several sources, including the functional groups of the humic acids that are dissociated at the 'pH' used; the significant water content of the organic matter (see Section 2.2); and both the hydroxide groups and water content of the NaOH used to prepare the sodium deutroxide. To overcome this, the H–O–D peak (∂ 4·7 ppm) was irradiated using a gated sequence such that no irradiation occurred during the data acquisition stage of the cycle. Various levels of irradiation power were assessed, and the one selected gave maximum reduction of the H–O–D peak without inducing spectral distortions or heating the samples. This procedure revealed other peaks, as apparent in the spectra of Figure 4.1.

The aliphatic nature of both humic acids is clearly apparent from the band observed between 1·0 and 1·3 ppm. Although this lacks fine structure, its location implies that it corresponds to methylene protons, rather than those of methine or methyl units. The spectra show no evidence for protons directly attached to aromatic carbon nuclei (∂ 5·8–8·5 ppm) or for protons in alkyl groups bonded to aromatic cores (∂ 2·3–2·9 ppm). Schnitzer [1] also noted that spectra of (methylated) humic substances typically showed little aromatic or olefinic protons; This was explained by their aromatic cores being fully substituted by atoms other than hydrogen.

A broad peak is observed for both humic acids at ∂ 3·6 ppm. For Aldrich Humic Acid, and

to a lesser degree the Fluka sample, this appears to be superimposed on a broader feature located at lower field. These, and the resonance at ∂ 4·5 ppm, are attributable to the large variety of oxygen—and to a lesser extent nitrogen—functionality such as in carbohydrates, or alcoholic and phenolic protons. These may not be ionised at the alkalinity of the medium employed, but probably undergo rapid proton exchange with those of the solvent. Carboxyl protons are not apparent (∂ 9–12 ppm) due to their lower pK_a values (see Chapter 6).

The spectral resonances lack detail and show no coupling patterns. Rapid exchange on functions with labile protons, such as phenols, results in averaging of signals and no coupling with their neighbours as the residence time of a proton is less than the NMR time-scale. The signals observed are also broad as they represent the summation of responses from protons in many similar environments.

Attempts to record liquid state ^{13}C NMR spectra of Fluka Humic Acid and Aldrich Humic Acid had limited success, hence they are not presented here: The resultant spectra had very broad resonances of poor resolution, which in fact were broader than those obtained for solid state analysis of the humic acids discussed in the following Section. This may be attributed to the presence of partially dissolved or colloidal matter. Further, the amount of humic acid analysed (0·1 and 1·0 % w/v) is effectively smaller than that used in the solid state experiment. It is notable that carbon–13 NMR of methylated humic acid solutions tend to have considerable fine structure. [162]

4.4.2 Carbon–13 Solid State NMR

In contrast to pure organic substances of low to medium molecular weight that show well-defined sharp peaks in their ^{13}C spectra, those of humic substances given in Figure 4.2 are poorly resolved and show only bands rather than peaks; This arises since humic substances are complex mixtures. [157]

The solid state spectra of both humic acids suggest that they are predominantly aliphatic by the large envelopes centred at ∂ 31 ppm. However, this spectral region provides little information concerning the precise nature of the groups since resonances of different aliphatic structural units presumably overlap. A recent development in solid

state NMR of carbon is the dipolar dephasing sequence: [164,168] This enables the average degree of proton substitution on carbons to be determined. The method exploits differences in the relaxation rates of carbons with different $^{13}C-^{1}H$ dipolar interactions.

The broad band between 112 and 160 ppm represents aromatic structures and is observed in the spectra of both commercial humic acids. Its presence supports the comments made in the previous Section that these humic acids do have aromatic structures, but they are substituted by atoms or groups other than protons. It is notable that the intensity of the band is very low at ∂ 155 ppm, the resonance position for aromatic carbons directly bonded to an oxygen. This is unexpected since phenols are known to have a general occurrence in humic substances. [1]

The magnetic resonance of carbons in the rotor material at ∂ 89 ppm contribute to, and probably obscure, the expected resonance positions of aliphatic carbons bonded to oxygen atoms. A pulse sequence has been devised that selectively attenuates the delrin resonance. [195]

The absence of any resonances between 190 and 210 ppm in the spectrum of Fluka Humic Acid, and to a lesser degree Aldrich Humic Acid, implies that few carbonyls occur in aldehydic and ketonic groups. Most occur in carboxyl, ester, amide or quinone structures that resonate in the band centred at ∂ 173 ppm. The elemental analysis data of Section 2.2 showed that the proportion of nitrogen is low therefore amide structures are of little importance. Infrared spectra given in Section 2.3 suggest that carboxyl groups in their protonated and dissociated forms have the most significant contribution to the ∂ 173 ppm envelope.

Malcolm and MacCarthy [49,50] concluded their examination of the solid state ^{13}C NMR of several commercial humic acids by stating that their spectra were remarkably similar. They showed that the corresponding spectra of stream and soil humic substances were quite different in several respects including: peak maxima; numbers of peaks; and ratios of peak areas. This added weight to their criticisms concerning the use of commercial humic acids, referred to in Section 1.7.5.

The solid state spectra may contain side-bands. These are smaller signals equidistant from the main resonances that are caused by oscillations set up by irregularities in the

spinning of the sample tube; they act as modulators and produce side-bands above and below the frequency of a resonance (by addition and subtraction of the modulating frequency). They vary in position with the spinning rate of the sample tube. [64,194,196]

The solid state spectra were analysed for the presence of side-bands by checking for peaks at locations above and below the main resonances using the spinning speeds given on the spectra (Figure 4.2). The aliphatic resonance of both samples would produce a side-band slightly downfield from the region where the delrin rotor resonates, and vice versa. Neither sample appeared to have distortions of their peaks in these regions, and for the aromatic and carboxyl regions, analysing the spectra for side-bands is complicated by their own low intensities.

High spinning rates and use of precision sample tubes minimise the problem of side-bands. Pulse sequences have been devised that eliminate spinning side-bands (e.g., TOSS [197]), yet these may cause some distortion of the resonances. [163]

Quantitative interpretations of the ^{13}C CPMAS NMR spectra are not made here since a prerequisite is that all carbon atoms are detected in proportion to their abundance in the samples. The magnitude of the observed signal for each structural or functional group depends on the selected contact time which may vary for different ^{13}C nuclei because they have different proximities to protons, hence different T_1s. Ideally, the contact time—during which the energy levels are matched—and the pulse repetition time, should be optimised to allow for slower cross polarising and relaxing species. [197] Also, proton decoupling provides a further complication by distorting relaxation rates. [64] Some experiments have been reported that illustrate these points using ranges of contact and relaxation times to deduce their optimum values: For example, Leenheer *et al* [164] determined the proportions of carbons in different structural and functional units using various cross polarisation contact times (1–10 ms) but a constant relaxation delay (1·0 s). The proportions were quite sensitive to the contact time selected hence use of intensities without determination of the optimum acquisition parameters in solid state ^{13}C NMR was cautioned. Similarly, Barron *et al* [167] varied the relaxation delay time and the contact time in their CP NMR experiments. Recycle times of 0·5–2·0 s resulted in no differences in signals for specific carbon types. Also, no change in the relative enhancement of different carbon types was evident for $^{13}C-^{1}H$ contact times greater than 0·5 ms.

Short relaxation delays in solid state experiments are preferred since they reduce instrument time, but aromatic carbons, which have relatively long relaxation times, tend to be underestimated.[155] The optimum acquisition conditions were not determined in this study since relaxation parameters could not be determined directly. A series of experiments where the desired parameters are varied and the best values selected could have been performed, but this would be excessive in instrument time.

It is notable that the proportions of the structural and functional units in the two commercial samples are different from each other, although the same relaxation delay and contact time were used, thereby suggesting that this is a genuine effect. Although it is likely that the materials have mainly aliphatic cores, some caution must be attached to such as a statement based on the lower sensitivity of aromatic units for the reasons given.

4.4.3 Lanthanide Shift Reagents for Proton and Carbon–13 Liquid State NMR and Carbon–13 Solid State NMR

Proton spectra were acquired for both Fluka and Aldrich Humic Acids in the presence of several lanthanide ions; Spectra for the former are given in Figure 4.3, but those of the latter are not presented here as they show similar effects. Carbon–13 spectra were not obtained for solutions for the reasons given in Section 4.4.1. Note that spectrum A of Figure 4.3 is effectively the same as that of Figure 4.1A, but is presented with a different horizontal scaling factor that reflects the wider spectral window used during data acquisition.

The dominant features of the spectra of Figure 4.3 are the resonances at ∂ 3.6 ppm and ∂ 4.5 ppm, which are caused by protons attached to carbons also bearing an oxygen atom, as discussed in Section 4.4.1. Their larger intensities compared to Figure 4.1 reflects the greater proportion of H_2O:D_2O used in the solvent medium. It is notable that the relative intensities of these resonances change for the series of rare earth ions. The aliphatic resonance band is apparent in most spectra. Note that proton resonances were not observed outside the normal chemical shift range. Close examination of the spectra reveals some changes in the presence of the metal ions, but these are small. For the praseodymium and lanthanum complexes, the 3·6 ppm resonance is located some 0·2 ppm upfield of that in spectrum A; A similar effect is observed in the corresponding

Aldrich Humic Acid complex for praseodymium, but not lanthanum. The aliphatic resonance shifts some 0·2 ppm downfield for the europium complex, again a comparable effect is observed in the europium(III)-Aldrich Humic Acid complex. Little changes occurred in the line-widths of the samples.

Selection of lanthanum as a metal ion for this LSR study was intended to identify any complex formation shifts (see Section 4.1.6.1). Its shift with Fluka Humic Acid was upfield, and it was the same magnitude and direction as the chemical shift induced by praseodymium. This suggests that the latter was also a complex formation shift. However, no such LIS was observed for lanthanum in its complex with Aldrich Humic Acid, but a similar upfield shift occurred for praseodymium which correlated with the direction anticipated in Section 4.1.6.1. Europium gave downfield shifts with both humic acids, as expected. For Fluka Humic Acid, this presumably counteracts its complex formation shift. It is notable that ytterbium, which tends to give predominantly pseudo-contact interactions with resonant nuclei, resulted in no spectral changes, possibly due to its effects being cancelled as it usually gives downfield shifts.

It is not clear if the LIS were of a contact or pseudo-contact nature, although the results with ytterbium, and because the greatest shifts were observed for protons in the vicinity of oxygen atoms, both point to the former. The unreliability of the results prevents separation of the observed shifts into their components for extended analysis.

The solid state ^{13}C NMR spectra of Figure 4.4 were acquired under the same experimental conditions as those of the uncomplexed humic acids given in Figure 4.2, but are presented with an expanded chemical shift scale reflecting the wider spectral window employed. Also note that the spectra are not presented with the same line broadening factor.

The chemical shifts of the main resonances for the europium(III)-Fluka Humic Acid complex are quite similar to those of the humic acid itself. The only difference occurs in the methoxyl region which has a somewhat different shape than that of Figure 4.2A, even though this is obscured by the resonance of the rotor polymer. No other resonances are apparent outside the normal 0 – 220 ppm range.

For the Aldrich Humic Acid complex, the aliphatic envelopes are coincident, but the aromatic resonance is shifted some 9 ppm downfield. Also, there is some indication of a

shift for the carboxyl region, but this is not pronounced. The very weak resonance band located between –20 and –38 ppm coincides with the expected position for a spinning side-band (see Section 4.4.2). No other resonances or side-bands are observed outside the normal carbon chemical shift range.

Changes are apparent in the widths of some resonances for both samples: The aromatic and carboxyl regions in the spectrum of the Fluka complex are not clearly distinguished. This may be an artefact of the spectral magnification applied to the sample. The half-width of the aliphatic peak for the Fluka complex is some 220 Hz (~16 %) greater than that of humic acid itself. Similarly, the corresponding aliphatic peak in the Aldrich complex has a line-width increase of 620 Hz (~51 %).

Therefore, the paramagnetic ion appears to have some effect on the solid state carbon–13 spectra of the humic acids; both chemical shift and line-width effects occurred for selected regions of their spectra. The downfield shift induced by the europium ion with Aldrich Humic Acid is consistent with the LIS direction observed in proton spectra. Interestingly, it appears to be just the aromatic region that is affected.

An examination of published reports was carried out to locate citations of similar effects. None were found for the rare earth elements, but a few describing the effects of paramagnetic transition metal ions on the NMR spectra of humic substances (or similar fractions of organic matter) were located. For example, when lignite was ion exchanged with ferric ions to 3 % w/w, the fraction of carbon observed in ^{13}C CPMAS NMR dropped from 63–74 % to below 10 %. Vassallo *et al* [169] explained this phenomenon by the ferric ion shortening the spin-lattice relaxation time (in the rotating frame) of the carbon nuclei. It was not apparent from their work if the iron affected the chemical shifts or band-widths of the resonances, although the latter would be expected. Pfeffer *et al* [171] made similar observations with ferric ions and noted that the effects were greatest at the most acidic exchangeable proton sites. Preston *et al* [170] found that the rate of relaxation (in the rotating frame) increased in the presence of increasing proportions of cupric ions. The effects were largest for carbohydrates suggesting these had the greatest interaction with the paramagnetic ion. However, Preston and Schnitzer [172] found that the resolution of ^{13}C solution state spectra were not affected by metal ion proportions up to 0·8 % w/w co–extracted iron. Newman and Tate [173] made similar observations.

Since some effects have been observed in certain instances here, the proportions of the metal ions used were re–examined to check if they were within sensible limits. The amounts of metal ions used seem high in the first instance, if reported in the same manner used by Vassallo *et al* [169] and Preston and Schnitzer. [172] For the soluble complexes, they ranged from 5·5–6·9 % w/w, depending on the metal. Solids contained 4·9 % and 11·4 % europium by mass in the Fluka and Aldrich complexes respectively. However, if these masses of heavy metals are substituted by equivalent molar proportions of iron, the weight percentages for the soluble complexes would be 2·2 % w/w, and for the solid complexes, 1·8 and 4·2 % w/w. These values tend towards those that caused significant effects, [169] and from Section 4.2.2.3, they are of the correct order to ensure quantitative binding to the organic matter.

There is usually a considerable contact shift on nuclei of atoms or groups in the first co–ordination sphere of trivalent lanthanide ions. Similarly, the influence of the secondary magnetic field supplied by the lanthanide ion falls away sharply with distance, therefore pseudo-contact induced shifts are only significant if the nucleus is in proximity to the paramagnetic ion. [175,177] Failure of the ions to show definitive and reliable shifts in the proton spectra suggests that the interactions between the species were limited, probably as they were not close enough to each other. The lanthanide ions may still be co–ordinated to water and so there is no, or limited, inner-sphere co–ordination to the humic acids. [176] Similar conclusions were reached in a NMR study published by Gamble *et al* concerning the complexation of manganese(II) with fulvic acid. [198] This relied on the line broadening imparted by the paramagnetic Mn^{II} ion on the proton spectra of co–ordinating water molecules. Added fulvic acid had little effect on the line broadening, hence water ligands were not replaced from the inner co–ordination sphere and it was concluded that complexation with fulvic acid was only outer-sphere. For the solid complexes considered here, the europium ions had some effect on the half-widths of the peaks, but for the proton spectra, changes were small since the protons were probably undergoing rapid relaxation through other mechanisms.

In conclusion, some useful effects have been noted, but these need to be investigated more thoroughly by varying the amounts of metals in samples since this will permit analysis of the contact and pseudo-contact contributions of the LIS.

4.4.4 Metallic Nuclei Liquid State NMR

The scandium–45 NMR resonance was located using 1 M $ScCl_{3\ (D_2O)}$ and assigned a chemical shift of ∂ 0 ppm. A minor broad resonance observed by Rehder and Speh [186] at ∂ +33·1 ppm was not detected here. Others have recalculated the position of the main resonance by extrapolation to infinite dilution where the resonances for all scandium salts coincide, as they contain the same hydrated species; this would lead to a chemical shift of +1·5 ppm for the reference used here. [199,200] Although just one peak was observed here, several solution species may exist, [186] since scandium's resonances are usually time-averages for all species present as fast ligand exchange occurs. [200]

A concentration sensitivity assessment was carried out to deduce the practical levels of detection for the nucleus. The ^{45}Sc spectra of some scandium chloride dilutions are presented in Figure 4.5. Each sample is vertically offset for clarification and multiplied by a sensitivity factor to fill an ordinate scale. The 0·1 M Sc^{3+} sample clearly provides a sharp resonance, and dilution by an order of magnitude still results in a workable level. The sensitivity factor between these is around thirteen times; this is seen as different signal-to-noise effects in the spectra. A further ten-fold dilution to 0·001 M gave poor sensitivity. The chemical shift of the 0·01 M salt was displaced some 4 ppm downfield of the 0·1 M Sc^{3+} resonance. This reflects the different composition of the supporting medium both in chloride concentration and D_2O:H_2O ratio. The resonances of aqueous solutions of scandium are sensitive to media composition. [199,201]

The minimum concentration of scandium required for useful signals invoked difficulties in the preparation of complexes with humic acids. Ideally metal ion concentrations in complexes should cover a range equivalent to the cation exchange capacity of the humic acid. Use of 0·01 M Sc^{3+} lead to instant coagulation of added humic acids at any pH. Reduction of the amount of organic matter such that the metal ions were in excess resulted in a similar effect. Decreasing the scandium concentration by a factor of five gave humate complexes that had reasonable stability at near-neutral pH values, however the magnetic resonance of the scandium nucleus was undetectable. This situation was not resolved, therefore spectra of scandium complexes with humic acids are not presented here.

Some spectra were acquired immediately after preparing complexes containing detectable levels of scandium that were unstable over a longer time-scale. These were scanned at

intervals for 500 minutes. Although some chemical shifts were observed, these occurred instantly and can be accounted for by dilution effects since the medium supporting the complex had a different composition from that of the scandium ion source.

No further attention was given to the NMR of scandium, which is unfortunate as some useful studies have been reported with biomolecular systems, such as demonstration of temperature-dependent carboxylato exchange, [186] and with macrocyclic ligands; For example, concentration-dependent ^{45}Sc chemical shifts and line broadening were observed and related to the composition of the inner co–ordination sphere of the metal ion. [199]

NMR spectra are not presented for yttrium–89 since difficulties encountered in the initial setting-up of the spectrometer were not resolved. The small magnetic moment of the nucleus means that its interaction with its lattice is small therefore its T_1s are very long and the signal saturates easily. Use of strong magnetic fields tends to alleviate this problem since the dominant chemical shift anisotropy relaxation mechanism is dependent on the square of the magnetic field strength. [154] Special detection techniques have had some success in overcoming this sensitivity problem. A complex pulse sequence called Quadriga FT detects ^{89}Y with more success. [200] Use of the DEPT or INEPT pulse cycles may enhance the sensitivity of yttrium–89 through coupling to neighbouring abundant nuclei. This will enable a faster repetition rate since these pulse sequences are determined by the relaxation times of the nucleus used as a source for polarisation transfer, commonly protons. [154]

Bearing in mind the sensitivity problems encountered with scandium–45, then rather concentrated yttrium solutions would be required as its nuclear receptivity is much lower (see Table 4.1). This probably would prevent its study with humic acid complexes as coagulation of the organic matter would be likely. However, the nucleus remains a potentially useful probe of its interaction with large organic molecules as it gives large (negative) nuclear Overhauser enhancements. [179,182]

The lanthanum–139 NMR signal was located using a concentrated solution of its chloride and duly assigned a chemical shift of 0 ppm. A concentration sensitivity test was performed to assess the practical levels of detection for the nucleus. The greatest dilution used (0·0015 M) was at the limit of detection, and its spectrum was multiplied by a

sensitivity factor of nineteen compared to 0·05 M $LaCl_{3\ (aq)}$. A chemical shift occurs on dilution; for the 0·01 M sample this was +0·7 ppm, and for the greatest dilution, the peak occurred at ∂ +1·4 ppm.

Spectra of complexes with humic acids are not presented as signals were not detected when the lanthanum ion concentrations were at levels that prevented coagulation of the humic acids. Complexes made with high lanthanum concentrations and scanned immediately also gave no shifts. This situation is similar to that encountered with scandium.

A ^{139}La spectrum of a lanthanum phthalate complex is given in Figure 4.6; This was obtained after the solution was concentrated by rotary evaporation and many scans were taken. The chemical shift was +32 ppm and the peak had a line-width, $W_{1/2}$, of 2400 Hz. No indication of uncomplexed metal ion was observed; this may be due to use of quantitative proportions of the metal and ligand, and the high stability constants of the complex (Section 4.2.3.4), or the complex was undergoing rapid ligand exchange resulting in a single time-averaged resonance for all species present.[200,202] Vijverberg *et al*[203] also observed fast exchanging equilibria on addition of acetate, glycolate and oxydiacetate to aqueous lanthanum chloride. However, NTA gave resonances at 160 ppm and 0 ppm due to slow exchange, and similarly EDTA gave a very large chemical shift of 570 ppm, but some uncomplexed metal was observed at 0 ppm.[183] These chelating ligands presumably have stronger interactions with the metal ion that prevent rapid exchange.

Chemical shifts of ^{139}La are sensitive to inner- and outer-sphere complexation of the metal; They may be distinguished since the latter has little effect on chemical shifts as the ligands are separated from the metal by a solvation sphere.[183] This difference has been exploited with inorganic anions,[188] solvent mixtures[204] and simple ligands to determine if complexation was inner- or outer-sphere. For example, acetates form inner-sphere complexes with a chemical shift of +60 ppm.[183] Variations in chemical shifts with the mole-fraction of ligands has enabled determination of stability constants for complexation of the lanthanum nucleus.[205]

The intermediately valued quadrupole moment of ^{139}La (Table 4.1) makes its relaxation sensitive to changes in electric field gradients.[200] This sensitivity has been harnessed in the assessment of complex formation by La^{3+} since location of the nucleus in an

asymmetrical environment induces rapid quadrupolar relaxation that results in extensive line broadening.[183] The increase in line-width from 140 Hz in the reference to 2400 Hz for the phthalate complex suggests that such a study is possible if a range of metal-to-ligand ratios is employed. However, the problems in recording the NMR spectra of complexes with humic acids remain and need to be overcome first.

The ^{91}Zr NMR spectra given in Figure 4.7 show very broad resonances for the zirconium nitrate salt and a complex with Fluka Humic Acid v3. These have been referenced to zirconocene dichloride which itself lies some 122 ppm upfield from the commonly quoted dibromide reference. The half-width for the dichloride resonance was 351 Hz, whereas the high field resonances of the nitrate salt and humate complex were some twenty times greater. Although there is a chemical shift of some –19 ppm on complexation to –339 ppm, this is rather small compared to their band-widths. For comparison, these values are outside the limits determined for complex organometallic systems: Previous reported maxima were a high field chemical shift of –262 ppm (relative to Cp_2ZrCl_2) and a band-width, $W_{1/2}$ of 3100 Hz.[154]

The sharp peaks obtained for zirconocene dichloride, and for other simple organometallic compounds studied by McGlinchey and co–workers,[185] presumably arise from the symmetrical environment of the metallic nucleus; This results in a small or zero electric field gradient, and so inefficient quadrupolar relaxation. Replacement of the organic ligands with water molecules leads to the formation of hydrolysed species with co–ordination numbers of up to eight that are linked by oxygen or hydroxy bridges.[174] These create an asymmetric field around the metal ion which gives a resultant electric field gradient at the nucleus; Consequently, rapid quadrupolar relaxation occurs on its interaction with the large nuclear quadrupole moment (Table 4.1), and therefore a very broad resonance results. The band-width may be augmented by colloidal matter formed through further polymerisation of hydrolysed zirconium ions.

The ∂ 240 ppm and 210 ppm resonances of the nitrate salt and humate complex respectively may be tentatively assigned to different environments of the zirconium nucleus, but there is little chemical foundation for such comments as the aqueous solution chemistry of the metal hasn't been reported using NMR; Solution characterisation studies, similar to those performed for aluminium through ^{27}Al NMR, are required.[206] However, it is reasonable to assume that zirconium should bind to humic substances since

it forms complexes with oxygen-donor ligands, such as ß–diketonates and carboxylates. [117] It is not clear to what extent complexation has occurred since only one metal ion concentration was used; a series of concentrations should clarify this point.

4.5 Conclusions

A multinuclear approach to nuclear magnetic resonance spectroscopy has been applied to the study of humic acids and their complexes with heavy metals. A combination of the complimentary techniques of proton and carbon–13 NMR has provided some information concerning the structure and functionality of humic acids that supports the characterisation carried out in Chapter 2. Use of lanthanide ions as shift reagents to humic acids has shown some effects on the chemical shifts and line-widths of proton and carbon–13 spectra of their complexes. The reliability of the measurements was questioned, therefore the contact and pseudo-contact contributions to the chemical shifts were not separated. Some heavy metals were studied directly as NMR nuclei, however this approach had limited success. Although some chemical shift and line-width changes were observed for lanthanum–139 and zirconium–91, measurements were complicated by the sensitivity of the nuclei studied; The metal ion concentrations required for useful NMR signal strength tend to coagulate the humic acids. Fulvic acids may be more useful for such investigations as they have a lesser tendency to coagulate.

CHAPTER 5
LIGHT SCATTERING

5.1 Introduction

Dispersions of humic and fulvic acids contain some particles of colloidal dimensions. Studies described in this Chapter apply the colloidal characterisation technique of Laser Doppler Electrophoretic Light Scattering to determine the effect of various sample and supporting medium conditions on the light scattered by such dispersions. Analysis of the light scattering data provides electrophoretic mobilities, diffusion constants, particle sizes and zeta potentials for the humic materials. A brief investigation of the refractive indices of humic materials is undertaken to support the light scattering studies.

5.1.1 The Colloidal State and Light Scattering

The colloidal state represents a condition intermediate between true solutions, where the particles are of ionic or molecular dimensions, and particulate suspensions, where the particles are large enough to settle under gravity. [6] The colloidal particle diameter range is generally quoted as 1 nm to 1 μm. The diameter of dispersed humic materials lies around this range hence their classification as colloidal: Fulvic acids lie towards the true solubility limit and humic acids range up to particulate dimensions. Consideration of the composition and structure of humic materials suggests that they may behave as hydrophilic or hydrophobic colloids. Possession of colloidal characteristics permits application of light scattering techniques to the study of dispersions of these materials and derivation of several physical parameters.

5.1.2 Introduction to Experiments Conducted using Laser Doppler Electrophoretic Light Scattering

The investigations performed were to monitor the charge and size characteristics of humic materials as a function of dispersion conditions by the application of Laser Doppler Electrophoretic Light Scattering (LADELS). In this technique, light scattered from

colloidal substrates is used to determine their velocity under the influence of an applied electric field. Electrophoretic mobilities derived from such measurements can be used to provide information on the colloidal stability of the subject materials. The measurements can be further extended to indicate the sizes of the scattering particles.

5.1.3 Origin of the Technique of Laser Doppler Electrophoretic Light Scattering

The equipment employed in the Laser Doppler Electrophoresis technique is adapted from a combination of Laser Doppler Anemometry (LDA) apparatus and classical Microelectrophoresis apparatus. The former is normally used to measure the velocity of gases and liquids that have been seeded with scattering particles, whereas the latter is employed to determine the velocity of microscopically visible particles under the influence of an applied electric field. In experiments described herein, the LADELS apparatus has been used to measure accurately the velocity of small scattering particles in an electric field. Since the LADELS apparatus is rather unique, the origin of the component pieces of equipment will be detailed.

5.1.4 Laser Doppler Anemometry

The frequency analysis of (Rayleigh) scattered light was first reported by Cummins, Knable and Yeh: They showed that the spectrum of light scattered from a solution of macromolecules had a width proportional to the Brownian Diffusion Coefficient of the macromolecule.[207] This was later extended by Yeh and Cummins who used the Doppler shift of scattered laser light from particles carried in a water flow to measure their velocity. The technique was named Laser Doppler Anemometry.[208]

The method employs a laser as a light source since it produces very intense monochromatic coherent light. The name "Doppler" is derived from the Austrian scientist who first considered the phenomenon. Doppler Shifts arise when, in any form of wave propagation, there is movement of the source, receiver, propagating medium, or intervening reflector or scatterer. Here the shift is produced by the movement of a scattering particle across the path of the source and receiver. Since the velocities of the

particles commonly encountered are small (<10 m s^{-1}) compared to the velocity of light, the corresponding Doppler shifts are very small. The resolution of shifts as small as this is beyond the capability of the highest resolution optical spectrometers so direct optical measurement is not a practical method. The only technique suitable for measuring these small Doppler shifts uses the principle of "heterodyning" or "beating" of two frequencies. For optical velocity measurements, heterodyning occurs when two rays of equal light intensity are focussed at the same point of investigation. Scattered light from the cross-over is then focussed on the photomultiplier, which acts as the detector. The mixed output from the photomultiplier contains sum and difference frequencies and harmonics. This, the most common arrangement of the apparatus, is termed the Differential Doppler Technique (see Figure 5.1). Since scattered light from the two beams reaches the detector simultaneously, a beat is obtained of frequency equal to the difference in Doppler shifts corresponding to the angle of scattering, θ (see Figure 5.1).

A theoretical description of the technique has been given by Drain.[209] The Doppler shift frequency υ_D, is given as:

$$\upsilon_D = \frac{\kappa v}{2\pi (\cos \beta)} \qquad (1)$$

Where:

- v = Velocity of particles passing through the active region
- β = Angle of the path of the scatterer to the perpendicular of the cross-over of the incident laser beams
- κ = Scattering Vector, a function of the detection angle, θ, and the wavelength of the illuminating light, λ. It is given by:

$$\kappa = \frac{4\pi n \left(\sin \theta/2\right)}{\lambda} \qquad (2)$$

Substituting for the scattering vector in 2 gives:

$$\upsilon_D = \frac{2vn \left(\sin \theta/2\right)}{\lambda (\cos \beta)} \qquad (3)$$

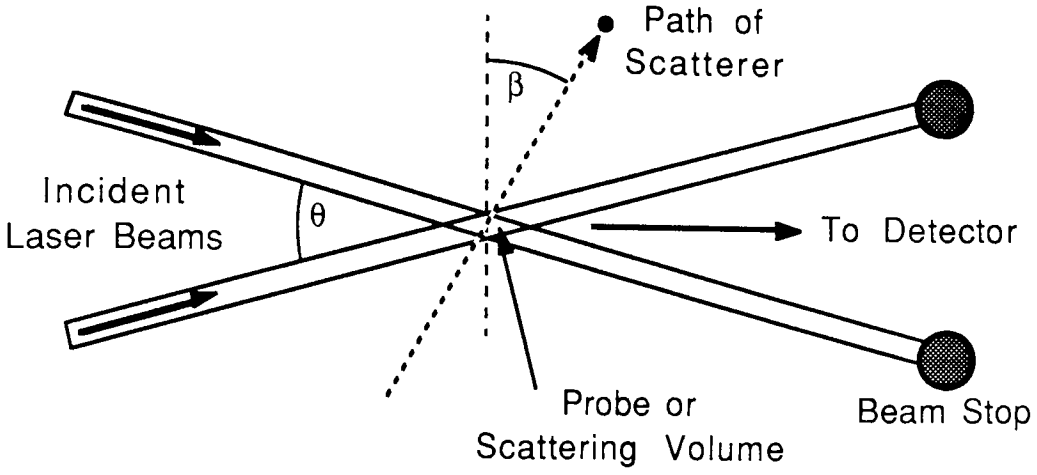

Figure 5.1
Arrangement of Light Beams in the Differential Doppler Technique

Where

n = Refractive index

An average flow of particles moving perpendicular to the axis of the cross-over will have $\cos \beta = 1$. Hence

$$\upsilon_D = \frac{2vn}{\lambda\left(\sin \theta/2\right)} \qquad (4)$$

The angle θ is generally small since this assists collection of more light at the detector. This, however, results in a rather elongated probe volume.

The origin of Doppler shifts also can be explained in terms of optical interference: The region where the two beams cross will contain Young's interference fringes of increased and reduced amplitude. As a particle crosses the fringe pattern it will block off some light from the fringes producing a modulated signal at the detector that depends on the velocity of the particle.

The main applications of the LDA apparatus have been in the determination of gas and liquid flows (e.g., Easson and Greated[210]) using seeded particles. For the samples studied here with the Laser Doppler Electrophoretic Light Scattering apparatus, the

subject materials *are* scatterers thus seeding is not necessary.

5.1.5 Electrophoresis

Electrophoresis involves the motion of dissolved or suspended material under the influence of an applied electric field.[211] It is one of four related electrokinetic phenomena that involve relative movement between rigid and mobile parts of an electrical double layer. Electrical Double Layer theories are associated with hydrophobic colloids.

5.1.5.1 Electrokinetic Phenomena and the Origin of the Electrical Double Layer

Most substances acquire an electrical surface charge when brought into contact with a polar medium, the possible charging mechanisms being dissociation, ion adsorption and dissolution. The surface charge influences the distribution of ions in the surrounding medium; ions of opposite charge (counter-ions) are attracted towards the surface, and ions of the same charge (co–ions) are repelled away from the surface. This leads to the formation of an electrical double layer made up of the charged surface and a neutralising excess of counter-ions distributed in a diffuse manner in the polar medium. If an electric field is applied tangentially along the charged surface a force is exerted on both parts of the double layer. The charged surface tends to move in one direction, whilst the ions in the mobile part of the double layer show a net migration in the opposite direction. Conversely, a potential gradient is created if the charged surface and the diffuse part of the double layer are made to move relative to one another.

The two major electrokinetic phenomena will be qualified:

Electrophoresis: The movement of a charged surface relative to stationary liquid by an applied electric field.

Electro-osmosis: The movement of liquid relative to a stationary charged surface (e.g., a wall) by an applied electric field. This is the complement of electrophoresis.

Electrokinetic phenomena thus depend on the nature of the electrical double layer:

Information available from electrokinetic experiments relate to the properties at a "surface of shear" between the two parts of the double layer. The electrical potential at the surface of shear is (approximately) equal to the electrokinetic or ζ (zeta) potential. The measurement of zeta potentials has proved useful in the assessment of colloidal stability.

5.1.6 Microelectrophoresis

The electrophoretic mobilities of microscopically visible particles can be measured directly by microelectrophoresis. This can be extended to smaller or dissolved particles if the material is adsorbed onto carrier particles.

The equipment required to make microelectrophoresis measurements consists of a cell, a power supply and an optical device to observe the particles, often a microscope. A diagram of a standard cell is given in Figure 5.2. Cells have a glass observation area, inlet and outlet taps, and a pair of electrodes. Note that the sample volume is quite large. The method relies on the visual observation of particles thus imposing several restrictions:

1 Particles must be coloured to be seen, and further, a different colour from the supporting medium.

2 Particles need to be large enough to be seen otherwise a strong scatterer must be added as a carrier for the subject particle.

If the sample is heterogeneous, the requirement for visual detection may well lead to selective sampling.

Microelectrophoresis measurements are complicated by the simultaneous occurrence of electro-osmosis. The internal surfaces of the glass cell are generally charged resulting not only in electrophoretic migration but also electro-osmotic flow near to the tube walls on application of the electric field. This is accompanied by a return flow of liquid with maximum velocity near to the centre of the tube giving a parabolic distribution of liquid speeds with depth. Thus the true electrophoretic velocity is only observed at the so-called "stationary levels" in the cell where the electro-osmotic flow and the return flow of liquid cancel (see Figure 5.3).

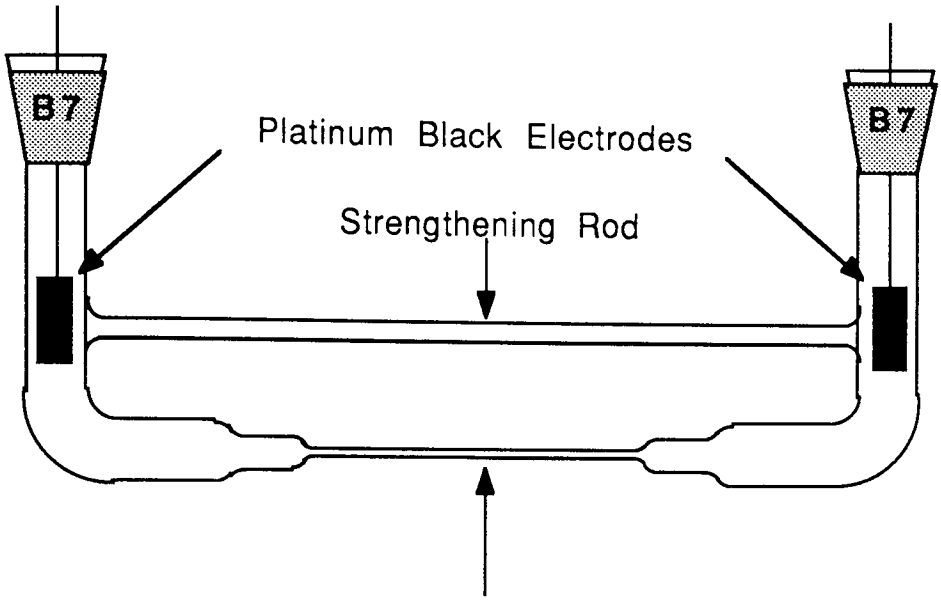

Figure 5.2
A van Gils Thin-Walled Microelectrophoresis Cell

5.1.6.1 Experimental Methodology for the Microelectrophoretic Determination of Electrophoretic Mobilities

Electrophoretic velocities are determined by timing individual particles over a fixed distance using an optical device, such as a microscope eyepiece scale. The particles are timed in alternate directions so that problems, such as those due to leakage and electrode polarisation, are largely eliminated.

5.1.7 Laser Doppler Electrophoretic Light Scattering (LADELS)

This may be considered as a combination of the techniques of Laser Doppler Anemometry and Microelectrophoresis: The hardware is similar to that of the LDA but a modified microelectrophoresis sample cell is inserted at the cross-over of the beams. Advantages over the traditional microelectrophoretic method are:

1 The size of the scatterers can range from sub–micronic to large thus carrier substrates are rarely required.

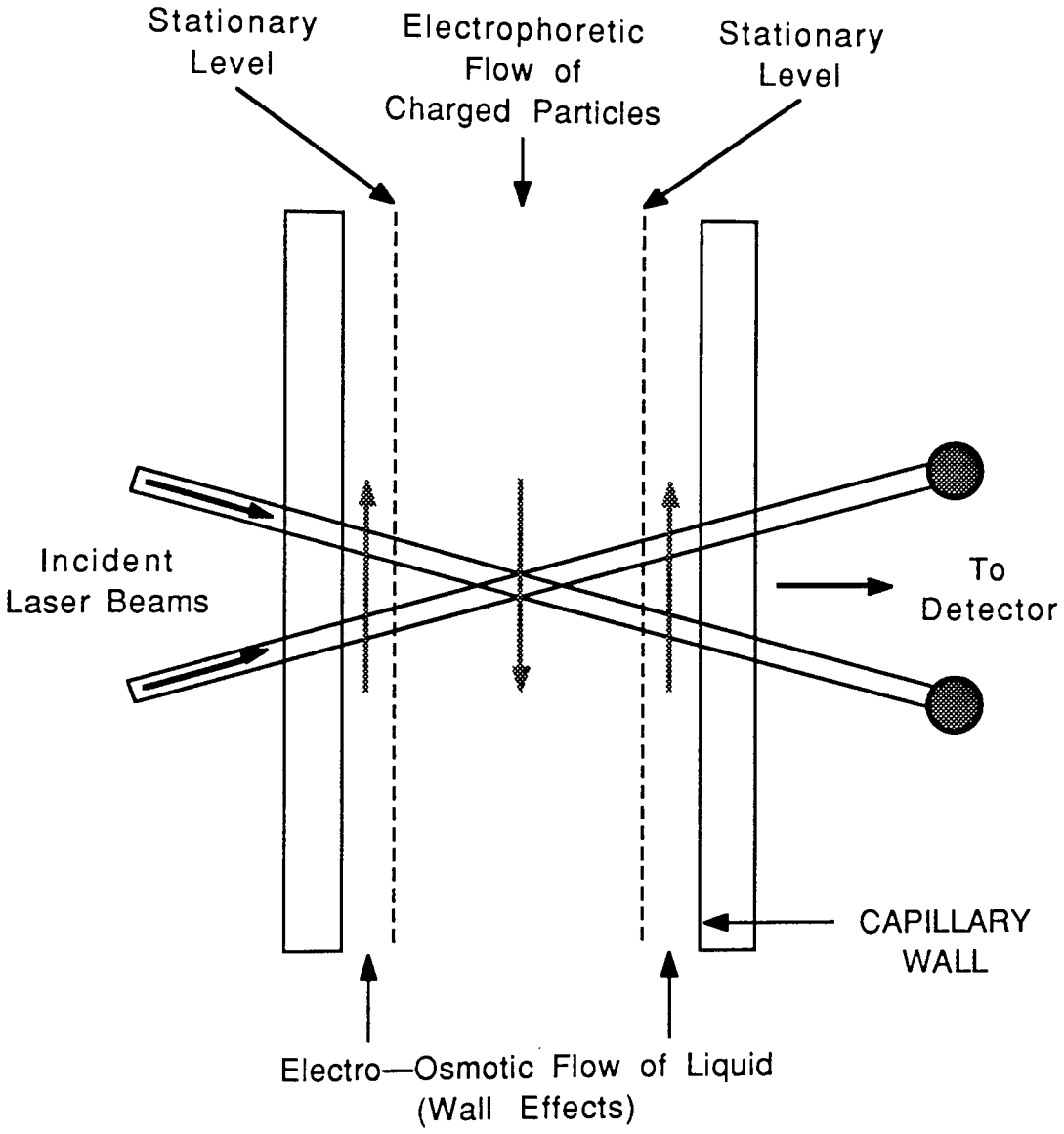

NOTE:
1. The directions of the Electrophoretic and Electro—Osmotic flows reverse when the polarity of the applied electric field reverses
2. The return flow of liquid occurs in the same direction as the electrophoretic flow of the charged particles

Figure 5.3
The Origin of Electrophoresis and Electro—Osmosis in the Capillary of a Laser Doppler Electrophoresis Sample Cell

2 The observations are made using a photosensitive detector thus avoiding selective observations within a sample.

3 The timing of the particle motion is automatic and statistically meaningful averages can be collected for the whole sample.

4 The measurements can be made over a wide range of concentration since there is no need to isolate a single particle for visual monitoring.

5 The technique can be applied to very small sample volumes.

6 The technique is less restrictive in refractive index considerations.

Ware and Flygare were the first to combine Laser Doppler Anemometry with electrophoresis: They measured the Doppler shift of (Rayleigh) scattered light from particles under the influence of electric fields. They showed that the Doppler width was proportional to the Brownian diffusion coefficient and that the magnitude of the Doppler shift was proportional to the electrophoretic mobility of the macromolecule.[212] Later, they extended their work to perform analytical separations of multicomponent systems containing a mixture of differently charged macromolecules.[213]

5.1.7.1 Theoretical Aspects of the Laser Doppler Electrophoretic Light Scattering Technique

In the LADELS system, charged macromolecules move towards the electrode of opposite polarity within the electrophoresis cell. From the magnitude of the Doppler shift the velocity of the particles is determined.[213] Equation 4 may be rearranged to:

$$v = \frac{\upsilon_D \lambda \left(\sin \theta/2\right)}{2\,n} \qquad (5)$$

This velocity divided by the electric field strength, E, gives the electrophoretic mobility, M, of the particles.

$$M = \frac{v}{E} \qquad (6)$$

$$\therefore M = \frac{\upsilon_D \lambda \left(\sin \alpha/2\right)}{2n\,E} \qquad (7)$$

Note that equation 7 suggests that spectral resolution is expected to increase with increasing field: In practice this is only realised to some extent since greater fields tend to lead to Joule heating of the sample, thence increased diffusion and broadening of the spectra.

The electric field strength is deduced from the magnitude of the potential difference, P.D., across the measurement points, divided by their separation, d:

$$E = \frac{P.D.}{d} \qquad (8)$$

The zeta potential, ζ, is related to the electrophoretic mobility, M, by the Henry equation: [214]

$$M = \frac{\varepsilon \zeta f(Kr)}{6\pi\eta} \qquad (9)$$

Where:

ε = Dielectric constant

K = Debye Hückel parameter, the inverse of which is termed the "thickness" of the electrical double layer.

At low values of Kr (for instance, small particles in a low ionic strength medium), $f(Kr) = 1{\cdot}0$ and the Henry equation reduces to the Hückel form:

$$M = \frac{\varepsilon \zeta}{6\pi\eta} \qquad (10)$$

In aqueous media of moderate to high ionic strength, $f(Kr) = 1{\cdot}5$ and the Smoluchowski form of the Henry equation operates:

$$M = \frac{\varepsilon \zeta}{4\pi\eta} \qquad (11)$$

Therefore, zeta potentials can be simply calculated from mobilities.

The random thermal motions of macromolecules result in their spectrum of scattered light being broadened with a width that is proportional to the diffusion coefficient of that macromolecule multiplied by the square of the scattering vector, κ. The Diffusion constant, D, can be determined both in the absence and presence of an electric field:

Field off:

$$\Delta \upsilon = \frac{D\kappa^2}{2\pi} \qquad (12)$$

Field on:

$$\Delta \upsilon = \frac{D\kappa^2}{\pi} \qquad (13)$$

Where

$\Delta\upsilon$ = Peak band-width at half-maximum height

κ = Scattering vector, as previously defined

The particle radius can be calculated from the diffusion constant by the Stokes-Einstein relationship:

$$D = \frac{k_B T}{6 \pi \eta r} \qquad (14)$$

Where

k_B = Boltzmann Constant

T = Absolute temperature

η = Viscosity of medium

r = Particle radius

The LADELS system thus allows the simultaneous determination of the electrophoretic mobility and the diffusion constant, and thence the zeta potential and particle radius.

5.2 Experimental

5.2.1 Laser Doppler Electrophoretic Light Scattering Apparatus

The components of the LADELS apparatus depicted in various diagrams will be detailed in the following Sections. The necessary procedures required to prepare the apparatus for routine use also will be described:

5.2.1.1 System Description

The main components of the LADELS apparatus depicted in the system diagram (Figure 5.4) are described here: A 5 mW Helium-Neon (λ = 622·8 nm) cylindrical laser, powered by a He–Ne Laser Power Supply was used to illuminate the sample cell. The cell was manufactured by Rank Brothers, Cambridge. Its features will be considered in the following Section. The electric field applied to the electrodes was supplied from a 500 V Square-Wave Generator. The potential difference across the terminals of known separation within the sample cell was measured using a Digital Voltmeter. A Nikon lens of focal length 50 mm was employed to focus an image of the cross-over of the laser beams onto the Thorn–EMI photomultiplier. The anode response of the photomultiplier was processed by a Schlumberger Solatron 1200 Signal Processor using a grounded input to a single channel. This was interfaced to a Digital Minc PDP–11 computer for data analysis and to a Hewlett-Packard Graphics Plotter for the production of spectral outputs.

5.2.1.2 Sample Cell Description

The main structural components of the sample cell were made from perspex: The two end blocks were recessed into the base and secured to it by a cemented threaded bar and small nuts (Figures 5.5 and 5.6). Each block was drilled and threaded at either end to permit attachment of the perspex electrode barrels. The blocks were also drilled to produce channels of small diameter that allowed the liquid samples to enter through the electrode barrels and flow towards the central sample capillary.

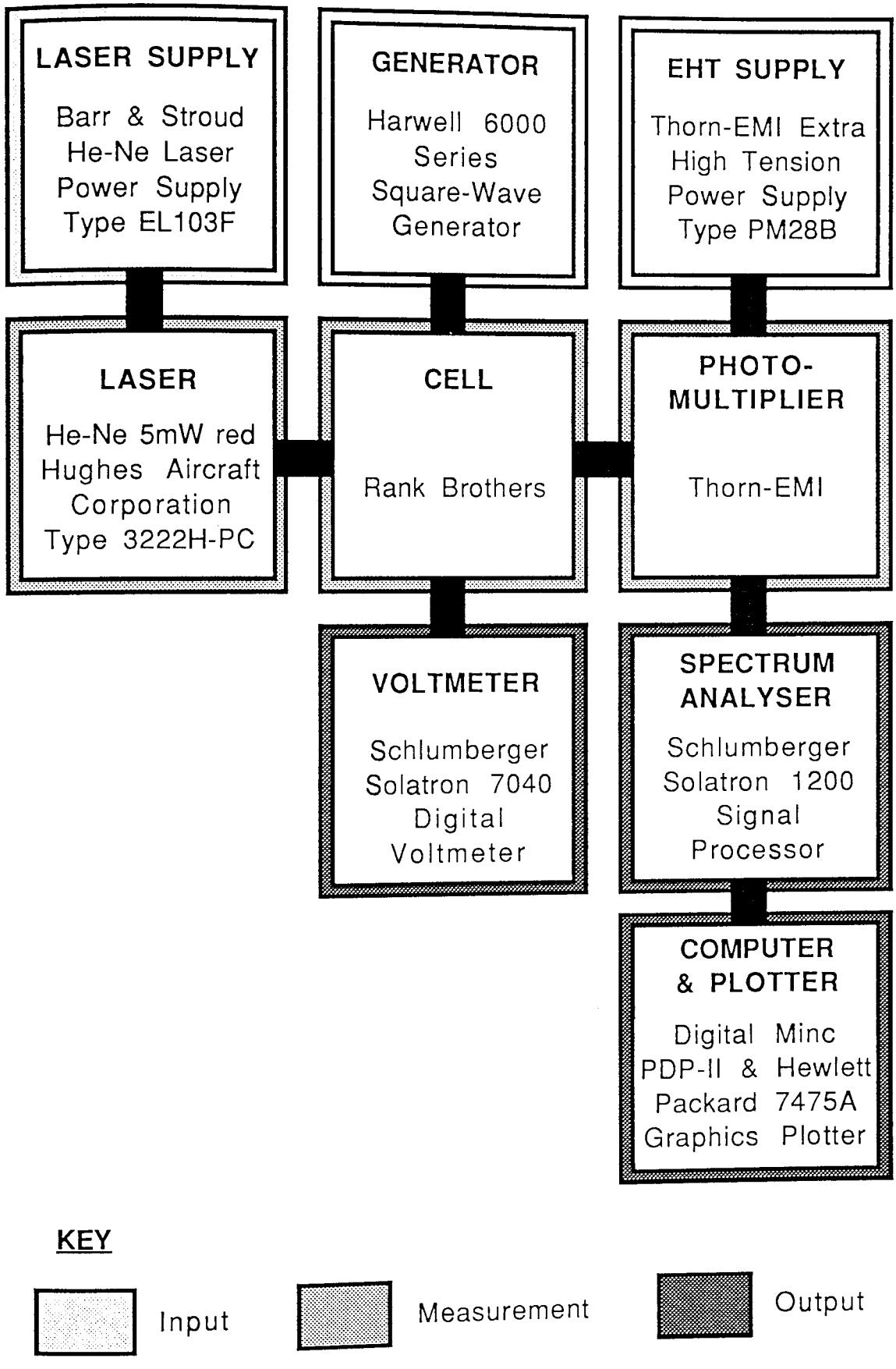

Figure 5.4
Laser Doppler Electrophoretic Light Scattering System Diagram

The quartz capillary, of external diameter 0·7 mm and length 23·5 mm, was mounted between two silicone rubber septums. The capillary served as the sampling area and so is much smaller than the sample volume employed in a standard microelectrophoresis cell. It was constructed from quartz to ensure optical purity and minimise complications due to "wall-effects" such as electro-osmosis and leaching. The capillary was surrounded by a high optical purity quartz jacket of side 1·0 cm. This was filled with distilled water (filtered to at least 0·10 μm, often 0·05 μm) to thermostat the sample thus avoiding convection-derived motion. The jacket was sealed at either end by a square rubber ring recessed into a polished perspex block and held in place by the two perspex blocks. The filtered water entered the quartz envelope through a polypropylene tube at the top of the blocks. These were connected to finely drilled bubble channels that served to remove air bubbles from the quartz envelope.

The electrode barrels consisted of a perspex body that was machined to assist hand-tightening into the end blocks. The barrels were hollow since the sample entered the cell through them when attached to a syringe using silicone rubber tubing. A similar exit for the liquid samples was provided at the other electrode. This was clipped to prevent transport of the sample during measurements. The platinised-black electrodes were housed within the perspex body. They were connected to the power supply by stiff wires that passed through the perspex barrel.

5.2.2 Laser Doppler Electrophoretic Light Scattering Optical Alignment Procedure

The LADELS apparatus was set up according to the following procedure ultimately resulting in the arrangement given in Figure 5.7. An Ealing-Beck triangular optical bench of length 2 metres was located on an Anaspec Zero G Vibration Isolation Table to provide stability. The bench incorporated a toothed track enabling translational motion of optical mounting stages using toothed wheels and a centimeter scale attached that permitted reproducible location of optical components and accurate measurement of positions when determining the cross-over angle. The optical components were attached to the bench using various sample stages. All stages permitted axial movement of the various components and some allowed small vertical or axially perpendicular adjustments using attached toothed tracks and wheels. Others had additional features, as necessary.

PLAN

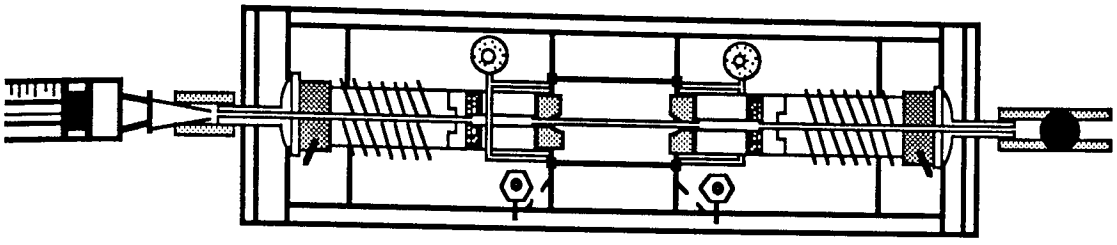

ELEVATION

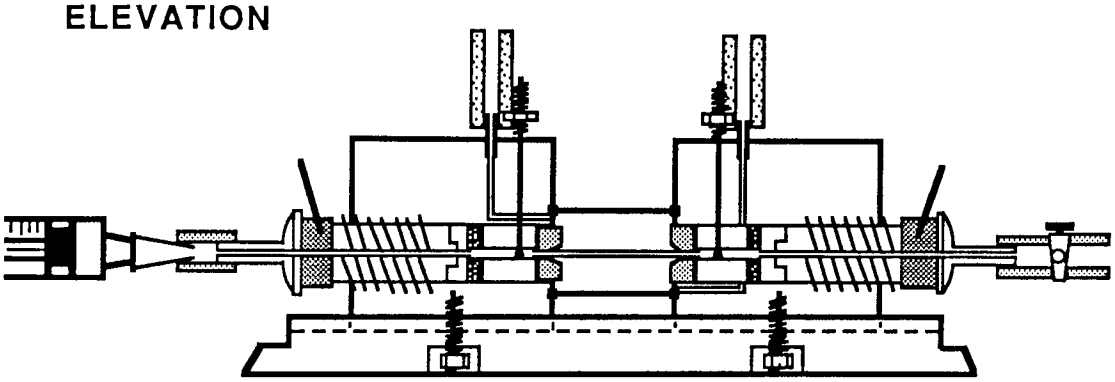

KEY

SCALE 1:1

MATERIALS:

- Polypropylene
- Rubber
- Knurled Perspex
- Glass or Perspex
- Silicone Rubber

Figure 5.5
Laser Doppler Electrophoretic Light Scattering Sample Cell Plan & Elevation

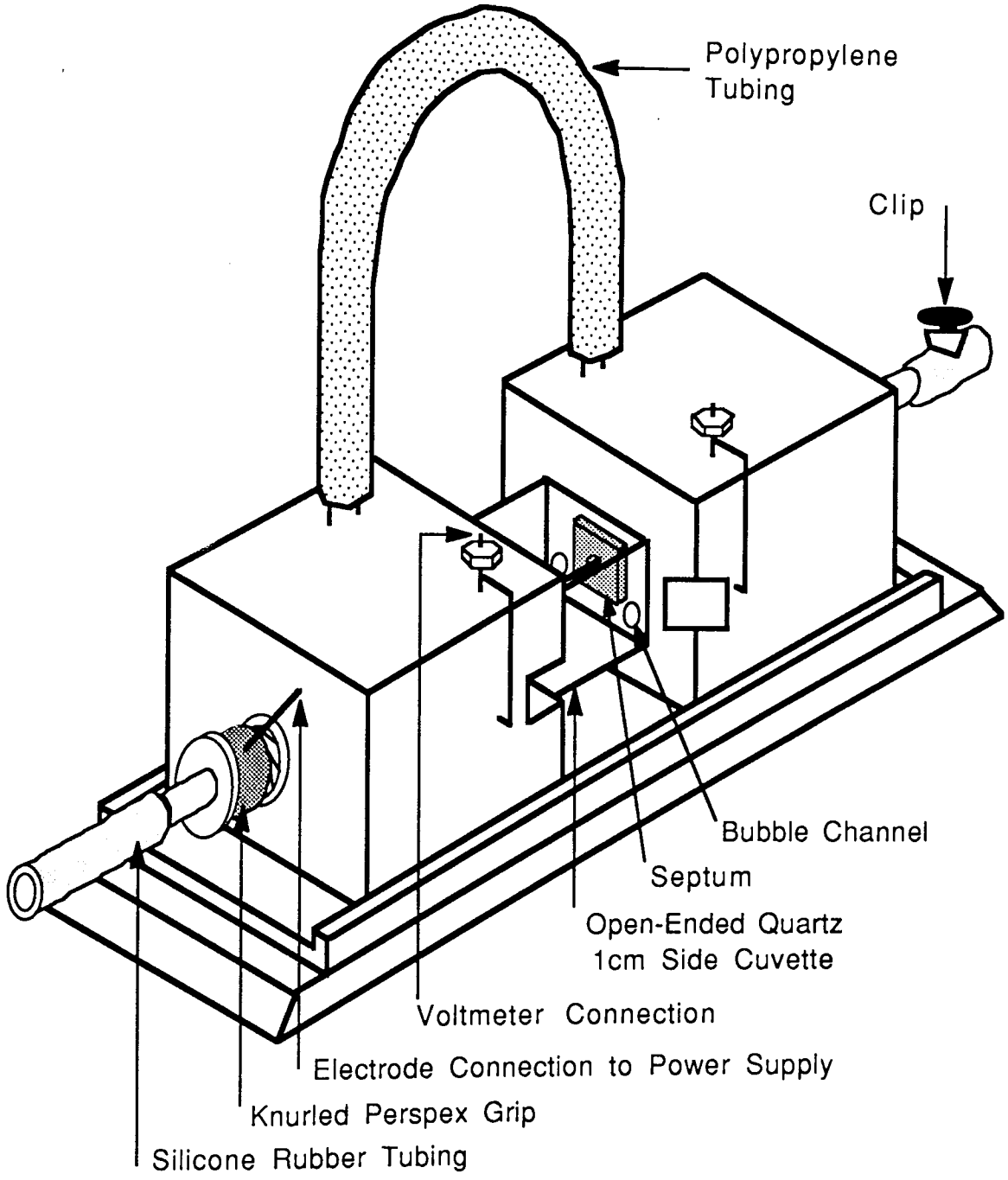

Figure 5.6
Laser Doppler Electrophoretic Light Scattering Sample Cell
Isometric View

The helium-neon laser was clamped in a suitable mounting stage and located at one end of the bench. This particular stage enabled precise motion in all directions. The laser beam was vertically polarised and collimated by the Beam Collimator Lens attached to the end of the laser body ensuring a beam of less than 1 mm diameter. The position of the laser in the vertical plane was crudely determined using a spirit level: Adjustments were made using the tilting mechanism. Precise vertical alignment was achieved with the assistance of a white card screen located in a simple optical mount.

The screen was positioned at the emergent beam and the vertical displacement marked. The screen was then moved some distance away along the optical bench and the laser tilt angle was adjusted to bring the beam back to the previous vertical mark. This ensured that the beam was parallel to the optical bench in the vertical plane. A neutral density filter was often placed in the light path to assist the precise location of the beam.

The laser body was offset by about 2 cm from the axis of the bench using a sideways adjustor on the stage. The horizontal alignment was checked by marking the emergent beam position on the screen, and then at some distance from the laser. Adjustments were made by rotation of the upper part of the optical stage after loosening a clamp. The beam was now parallel to the bench in the vertical and horizontal planes.

The diameter of the beam was further reduced using a concave lens of focal length 10 cm which was clamped to an optical stage and placed on the bench. Its axial position, and that of the screen, were varied until the best beam focus was obtained. Minor adjustment of the lens position located the focussed beam on the previous vertical and horizontal screen marks.

The beam splitter table was secured to an optical mount and placed on the triangular bench. With the assistance of a neutral density filter at the emergent beam, the axial displacement of the beam splitter table and the screen were adjusted to locate the position of maximum beam focus for both beams. The mirrors were then unclamped and rotated to merge the beams at the previous vertical displacement on the screen. This procedure ensured that the beam cross-over occurred at the best focussing condition. Note that the arrangement of the components on the beam splitter table removed the original laser offset and so produced a cross-over above the bench axis (see Figure 5.7).

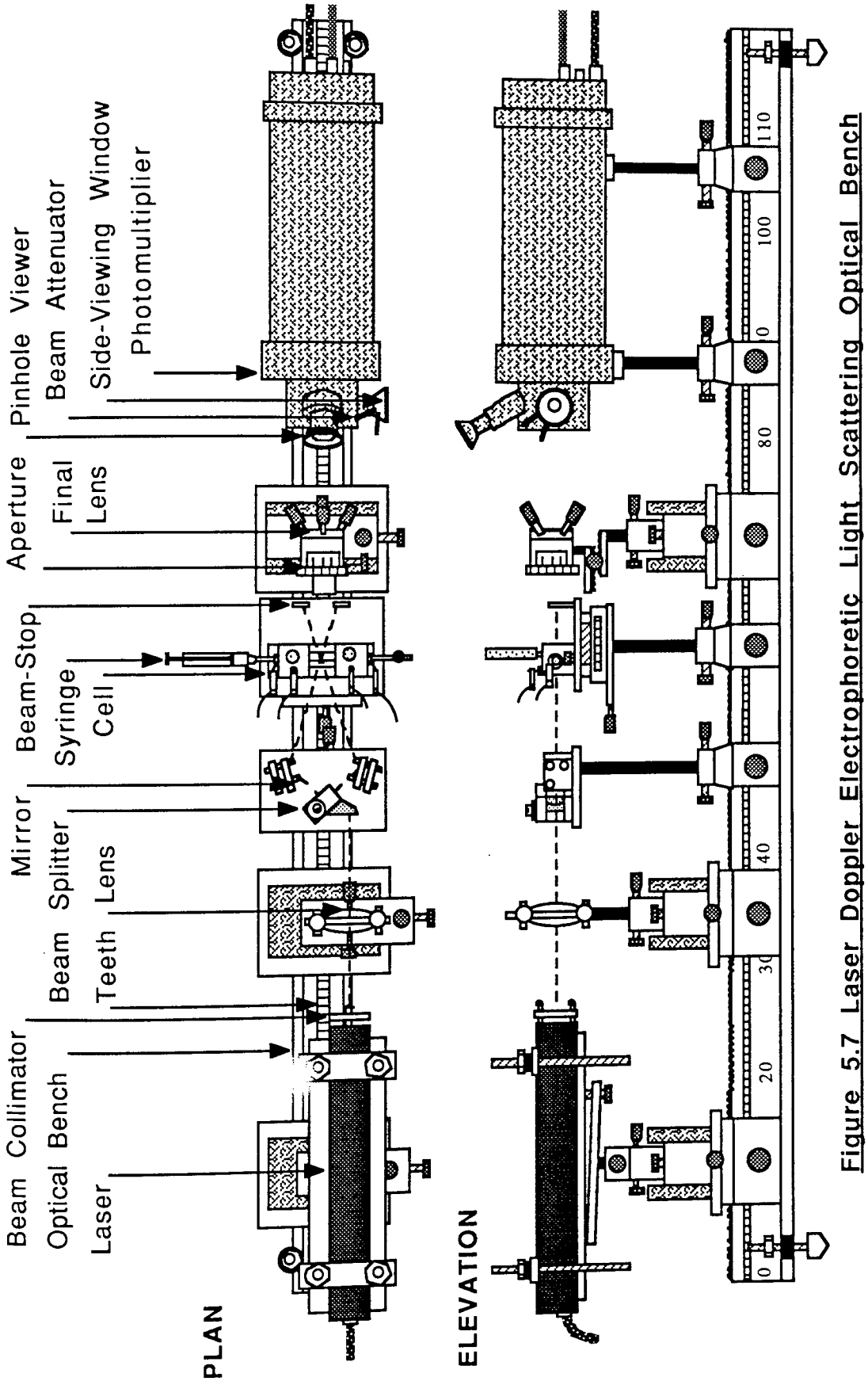

Figure 5.7 Laser Doppler Electrophoretic Light Scattering Optical Bench

SCALE ≈ 1:6

A clean quartz capillary was then inserted into the LADELS cell. The polypropylene tube at the top of the cell was then filled with 0·10 μm filtered distilled water and the whole cell tipped to and fro to permit air bubbles to escape. With the cell secured to an optical mount that allowed three-dimensional motion, a strong light scattering sample, such as polystyrene latex (¢055), was injected using a syringe. When sufficient sample had entered the capillary, it was sealed using a small clip. The position of the cell table was then moved along the axis of the optical bench until the capillary coincided with the focussed cross-over point. This was facilitated using a fine adjustment screw on the stage. Attainment of this condition was achieved using an Ealing-Beck travelling microscope that was attached to a retort stand using an appropriate clamp.

The final lens, a Nikon 50 mm focal length lens with a range of available apertures (f2·8, f4, f5·6, f8, f11 & f16), and the photomultiplier, were placed on the bench in their optical mounts. A spirit level was used to check crudely the horizontal level of the latter with necessary adjustments made on the stands under its body. The side window of the photomultiplier was then brought into use by rotation of a mirror inside the body and the attenuator was set to avoid damage to the eye. Whilst looking at the image of the sample cell, the lens and photomultiplier were moved along the axis of the optical bench using the gear wheels at the bottom of their mounts to give the best focus. As the sample cell was being viewed along the path of the optical bench, its stage was finely adjusted vertically to locate the centre of the capillary at the cross-over. Minor modifications were made to the two beams using the adjusting screws on the beam splitter mirrors, as necessary, to ensure the location of the capillary at the focussed beam cross-over.

Note that although it is possible to calculate the position of the stationary level within the capillary, it would be difficult to locate the beam cross-over at this point since the diameter of the capillary was rather small. This meant that the stationary level would be very near to the capillary wall and would tend to lead to reflections from that surface. To overcome this problem, measurements were always taken in the centre of the capillary since the particle velocity gradient at this point was minimised resulting in a less stringent focussing requirement and consequently a more reproducible cross-over location.

With the side-viewing mirror moved out of the path of the sample cell image, the image was then steered onto the pinhole of the photomultiplier by looking through the pinhole

viewing eyepiece above the body of the photomultiplier. Minor adjustments were made to axial and vertical positions of the final lens to locate precisely the image on the pinhole. Since improved signal-to-noise was realised when as much scattered light as possible was collected, the lens aperture was opened to at least a medium setting and the unscattered laser beams were attenuated using simple beam stops attached to the sample cell stage.

This completed the optical alignment resulting in the location of the sample capillary at the cross-over of the focussed beams. The image of the light scattered by the sample at the cross-over was focussed and steered onto the photomultiplier pinhole. This arrangement corresponded to that shown in Figure 5.7. The apparatus was ready for the determination of the cross-over angle, and then for use with samples for the measurement of electrophoretic mobilities.

5.2.2.1 Determination of the Cross-Over Angle

The cross-over angle, which is required in the calculation of electrophoretic mobilities, was determined in air to avoid contributions from refracting materials. The cell, its mounting stage, the final lens and the photomultiplier were removed from the optical bench after their optimum positions were noted, to facilitate access to the cross-over point.

The screen stage was placed on the optical bench. The location of the beam at the cross-over was noted on the card and the position of the stage on the optical bench was recorded. The screen was then moved some distance away and the positions of the divergent beams were marked on the card in the same way. Again the location of the stage on the optical bench was noted. A neutral density filter was often employed to assist the precise location of the divergent beams on the card due to the apparent loss of focus of the beams at large axial displacements. The cross-over angle was then determined by simple trigonometry using the axial displacement of the screen and the divergence of the beam.

5.2.3 Standard Operating Procedure

Once the optical adjustments were made and the cross-over angle determined, electrophoretic mobility measurements could commence. The following procedure was adhered to.

A clean capillary was inserted daily into the sample cell and the cell placed on its optical mount. The sample was then injected into the capillary using a syringe attached to the silicone rubber tubing. The waste tube was sealed once a little sample passed through and all bubbles were ejected. The optical alignment was generally confirmed by viewing the capillary with both the travelling microscope and the photomultiplier side-viewing window. The voltmeter and signal generator were then connected to their respective terminals. The latter was set to the required combination of applied potential difference, square-wave oscillation frequency and duty-cycle. Note that a driving current was not applied since this would cause Joule heating of the sample resulting in convectional transport. A low frequency square-wave potential was applied since this ensures that the applied voltage remains constant for a long period compared to the time for switch-over of the polarity. Also note that the reversal of potential was intended to overcome any possible problems due to leakage, electrode polarisation or the establishment of concentration gradients. Scattered light was recorded during both periods of electrical transport.

The Solatron signal processor—which converts the photomultiplier anode output from the time domain to the frequency domain by rapid Fourier Transformation—was set to acquire data by selection of the signal input channel and a wide-range Hanning spectral window. Following inspection of the spectra, progressively narrower windows could be chosen, as appropriate. An average of one thousand signals was generally acquired. Depending on the nature of the sample, the optical specifications and the size of the spectral window, the spectral recording times were generally of the order of several minutes. The data was displayed as a Power Spectrum of intensity squared against frequency.

The signal processor had a storage capacity of three spectra. These were transferred to the PDP–11 computer for extraction of the required information, and storage on disc. The electrophoretic mobilities were calculated using an in-house developed program that could display and store transferred spectra, locate the position of the Doppler shifted frequency, calculate the electrophoretic mobility and plot the spectra using a sub–program.

The LADELS equipment was generally tested daily for the reproducibility of standard samples. If the equipment was to be re-used that day, the capillary was rinsed with filtered distilled water by attaching a wash-bottle to the silicone rubber tubing. Otherwise, the cell was dismantled and the capillary discarded. Other components were rinsed. Polystyrene latex (¢055) was often used as a test sample. It contains spherical particles that are negatively charged in aqueous media over a wide pH range.[215]

5.2.4 Sample Preparation

The preparation of humic and fulvic acid samples for electrophoretic mobility determination will be outlined. Solutions of sodium hydroxide were prepared for the dispersion and pH adjustment of the humic and fulvic acid samples. A stock solution of hydrochloric acid was also made up for use in producing small adjustments in the acidity of the samples media.

A 0·10 M stock solution of sodium hydroxide was prepared by quantitatively diluting the contents of a BDH A.R. NaOH Convol (¢032) to 500·0 ml with distilled water that had been filtered through a 0·10 µm Millipore filter (¢056). Filtered water was employed since large particles can interfere with light scattering measurements. An aliquot of the alkali stock was diluted to 0·01 M using further 0·10 µm filtered distilled water and then making up to the appropriate mark in a suitable volumetric flask.

Similarly, a hydrochloric acid stock was prepared by quantitative dilution of a BDH Aristar 0·1 M Hydrochloric Acid Convol (¢057) using 0·10 µm filtered distilled water. Further dilutions giving 0·01 M and 0·001 M were made for use in fine pH adjustment.

A 0·2 % w/v stock of Fluka Humic Acid v3 was prepared by accurately weighing 1·00 g of the humic acid and dispersing it in 0·10 µm filtered water to which measured additions of 0·10 M $NaOH_{(aq)}$ were made. Dispersion was performed with the assistance of ultrasonic vibration and carried out under a simple tent filled with (oxygen-free) nitrogen (¢009). The pH was monitored during dispersion by a combination electrode (¢058) attached to a Phillips pH meter (¢059) that had been standardised with Kent EIL buffers (¢012) at pH 7·0 and 9·2. When a state of satisfactory visual

dispersion and medium pH were attained, the liquid was quantitatively transferred to a 500·0 ml volumetric flask and made up to the mark with further filtered distilled water. After an overnight equilibration period, the final pH of the solution was determined using the re–calibrated pH meter. The concentration of the humic acid based on the mass employed was 0·20 % w/v and the pH was measured as 8·3.

This humic acid stock was then diluted to produce a range of humic concentrations down to 0·0001 % w/v. This was achieved by pipetting an aliquot of the stock and diluting with filtered distilled water and appropriate volumes of sodium hydroxide and hydrochloric acid suggested by the pH meter. After making up to the mark in volumetric flasks, the pHs of these diluted samples were recorded. Note that if the $NaOH_{(aq)}$ or $HCl_{(aq)}$ additions became excessive and would possibly result in an undesirable ionic strength, the sample was discarded.

Two further samples were made at a concentration of 0·01 % w/v but with different pHs from the previous sample so that the variation of electrophoretic mobility with the acidity of the sample medium could be studied. The samples were prepared using the same dilutions but were pH adjusted with progressively larger volumes of 0·1 M $HCl_{(aq)}$ to produce samples with pH values of 5·9 and 3·9.

Filtered humic acid samples at approximately ~0·1 % w/v and ~0·001 % w/v were prepared by filtration of the above samples at the exact concentrations of 0·1 % w/v and 0·001 % w/v. Filtration was performed by attaching a 5 µm Gelman Sciences Acrodisc® (¢060) to the Luer fitting of a Sabre Sterile Plastic Syringe (¢061). The concentrations of the filtered samples were not re–determined.

Samples of the Fanay-Augéres Fulvic Acid were prepared in a less sophisticated manner due to the smaller amount of the solid available. The fulvic acid was accurately weighed into a small volumetric flask and filtered distilled water was added. The flask was subjected to ultrasonic vibration to assist dispersion. Unlike the humic acid, it was not necessary to add alkali to the fulvic acid since it is quite soluble in water. The contents were then made up to the volume mark giving a resultant concentration of 0·10 % w/v. After a period of equilibration, a final pH of 3·2 was recorded. Note that it was not possible to monitor the pH of the Fulvic Acid sample during dispersion due to the small volume involved.

Two diluted fulvic acid samples were prepared, each of final concentration 0·01 % w/v: The first was diluted just with filtered distilled water giving a pH of 4·0 and the second with a small aliquot of 0·1 M $NaOH_{(aq)}$ and further filtered distilled water giving a higher pH of 9·8. These samples were to be used for comparison of the effect of changes in pH of the medium upon the electrophoretic mobility of the fulvic acid particles at constant fulvic concentration.

Note that no specific attempt was made to control the ionic strength of the sample media. Additions of alkali and acid for dissolution and pH-adjustment provide counter-ions that contribute to the ionic strength. However, if it was felt that excessive additions of these were made then the sample was discarded.

5.3 Results

General comments concerning the presentation of spectral outputs will first be outlined. Then, various sample series will be considered and the required information of electrophoretic mobilities and band-widths will be derived from spectral outputs. Zeta potentials, diffusional constants and particle radii will be calculated from extracted information.

Raw spectral outputs are produced as power spectra of amplitude verses Doppler shift frequency. As an example, file EL 521 for an unfiltered aqueous dispersion of 0·010 % w/v Fluka Humic Acid v3 at pH 3·9 is provided in Figure 5.8. Since the magnitude of the electrophoretic mobilities corresponding to the various Doppler shifted peaks depend on several factors, as suggested by equation 7, such as the potential difference between the plates and observation angle, the spectra produced are not directly comparable in terms of electrophoretic mobility. However, to assist reader comparison of such outputs, they have been converted to yield identical electrophoretic mobility scales by appropriate data manipulation followed by superimposition of digitised spectra, compacted in one-dimension. This has been achieved without loss of spectral detail. It should, however, be noted that it is not possible to make direct comparisons between band-widths in this presentation format: These were determined from raw power spectra.

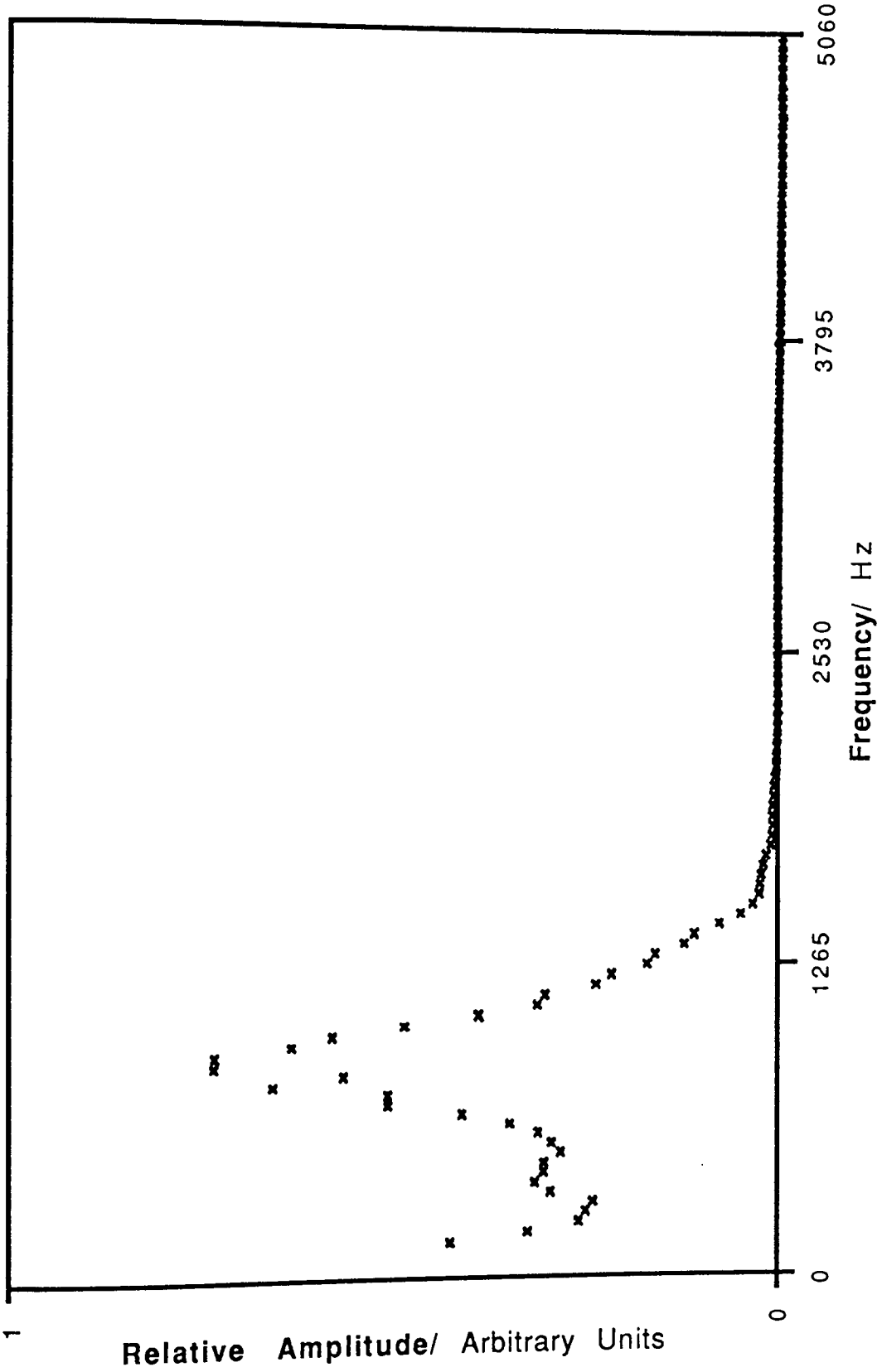

Figure 5.8

File EL521 Power Spectrum for
0.01 %w/v Unfiltered Fluka Humic Acid (pH=3.9)

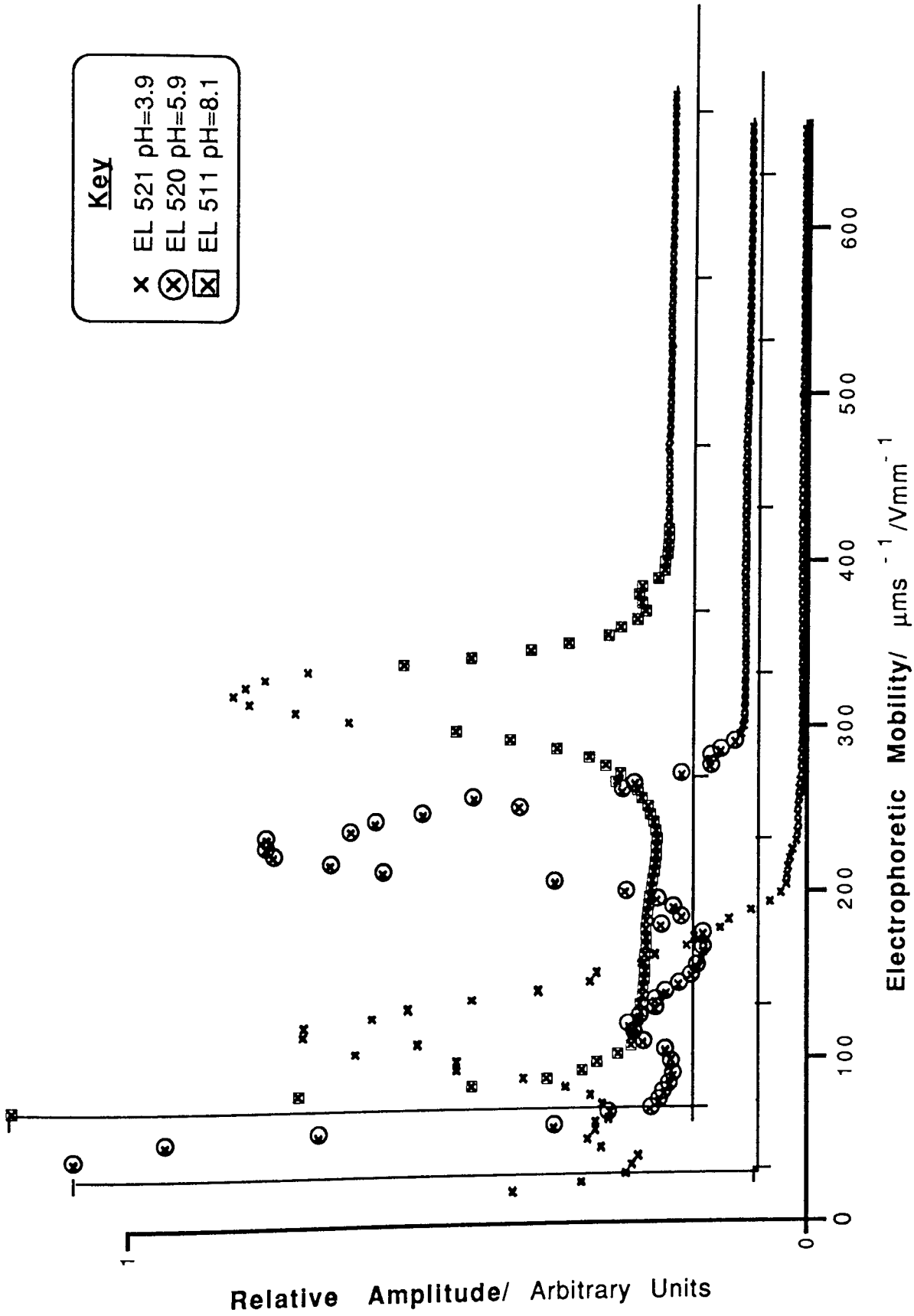

Figure 5.9

Electrophoretic Mobility Spectra for
0.01% w/v Unfiltered Fluka Humic Acid v3 pH Variation Series

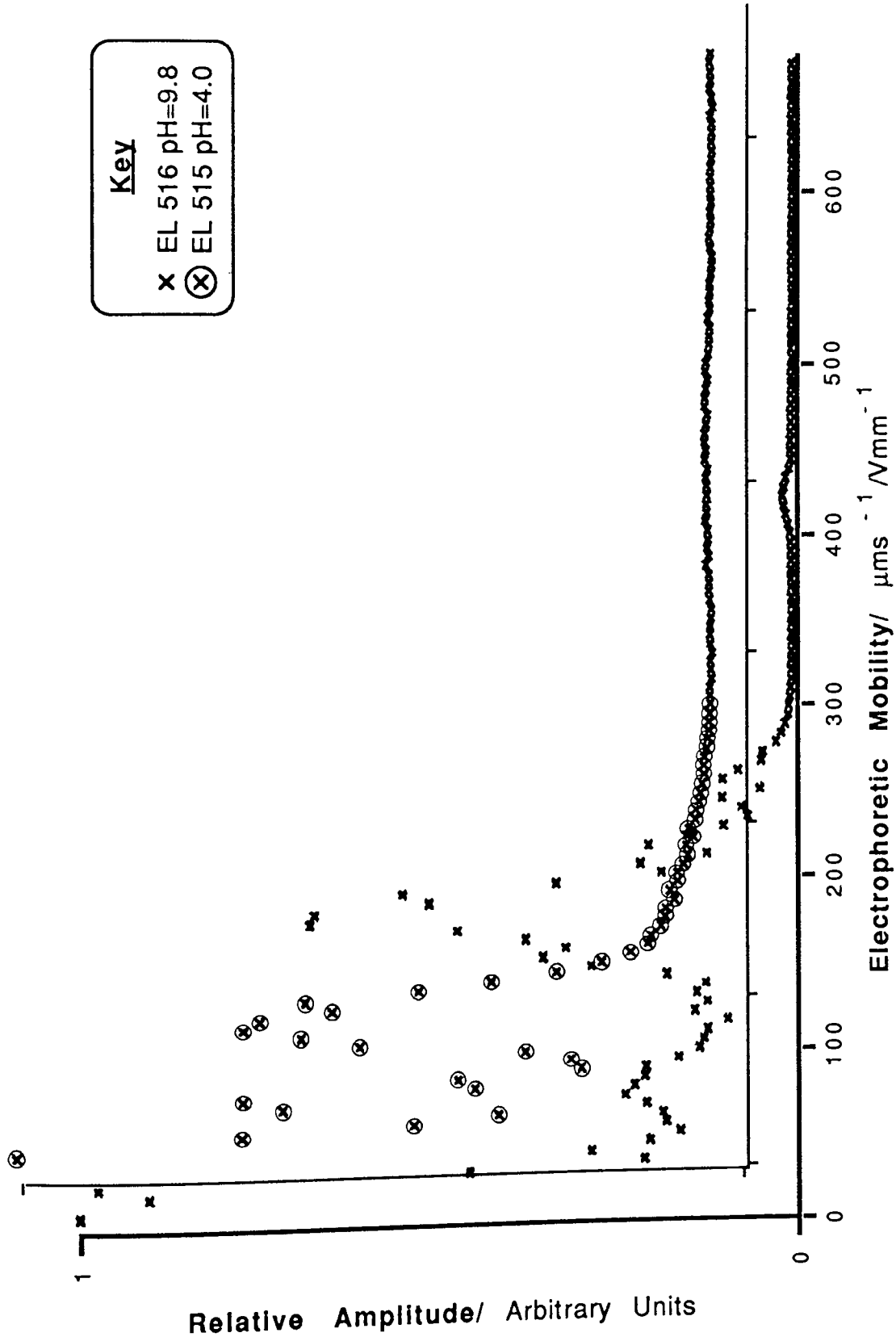

Figure 5.10
Electrophoretic Mobility Spectrum for
0.01% w/v Unfiltered Fanay—Augéres Fulvic Acid
pH Variation Series

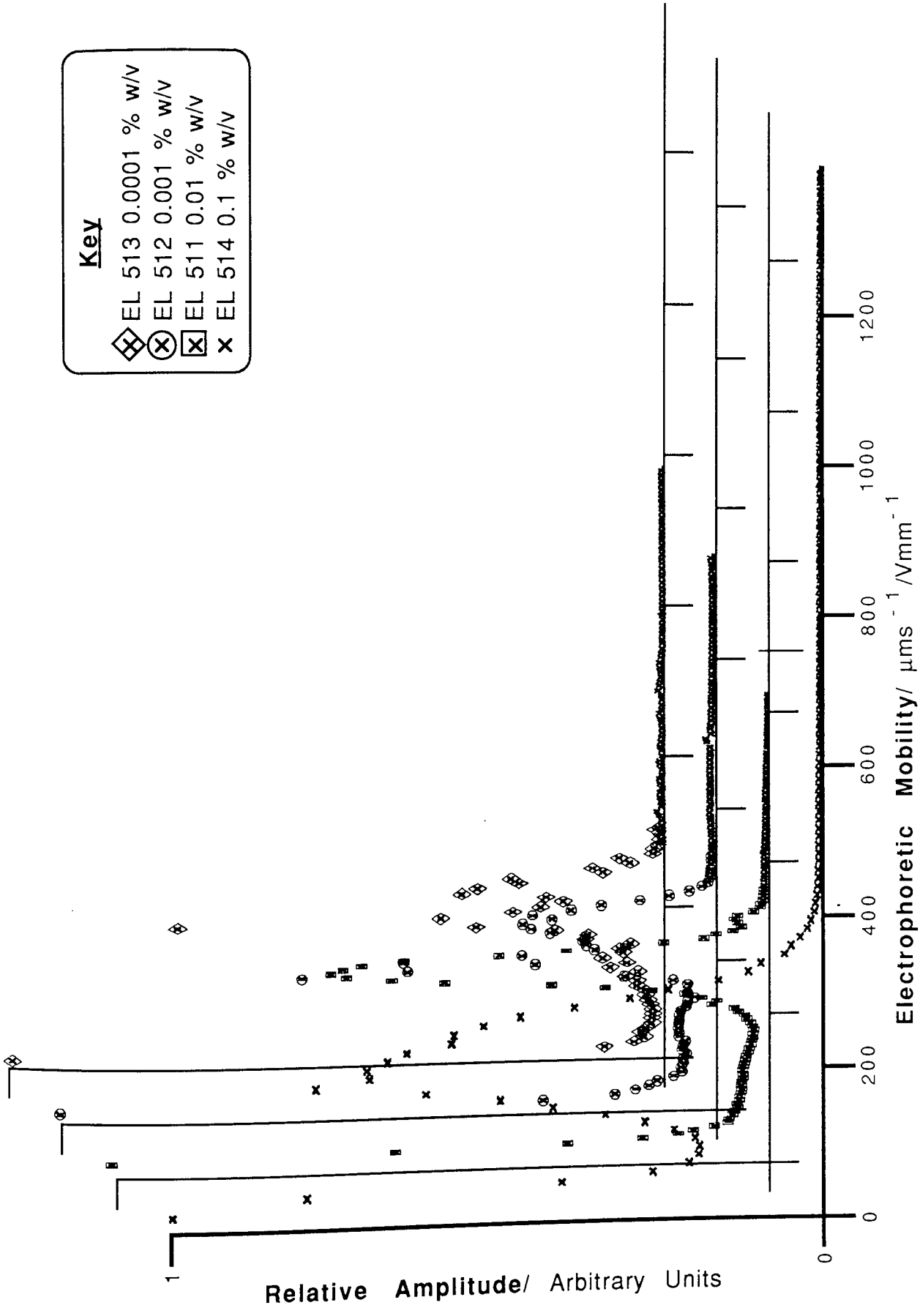

Figure 5.11
Electrophoretic Mobility Spectra for
Unfiltered Fluka Humic Acid v3 Concentration Variation Series

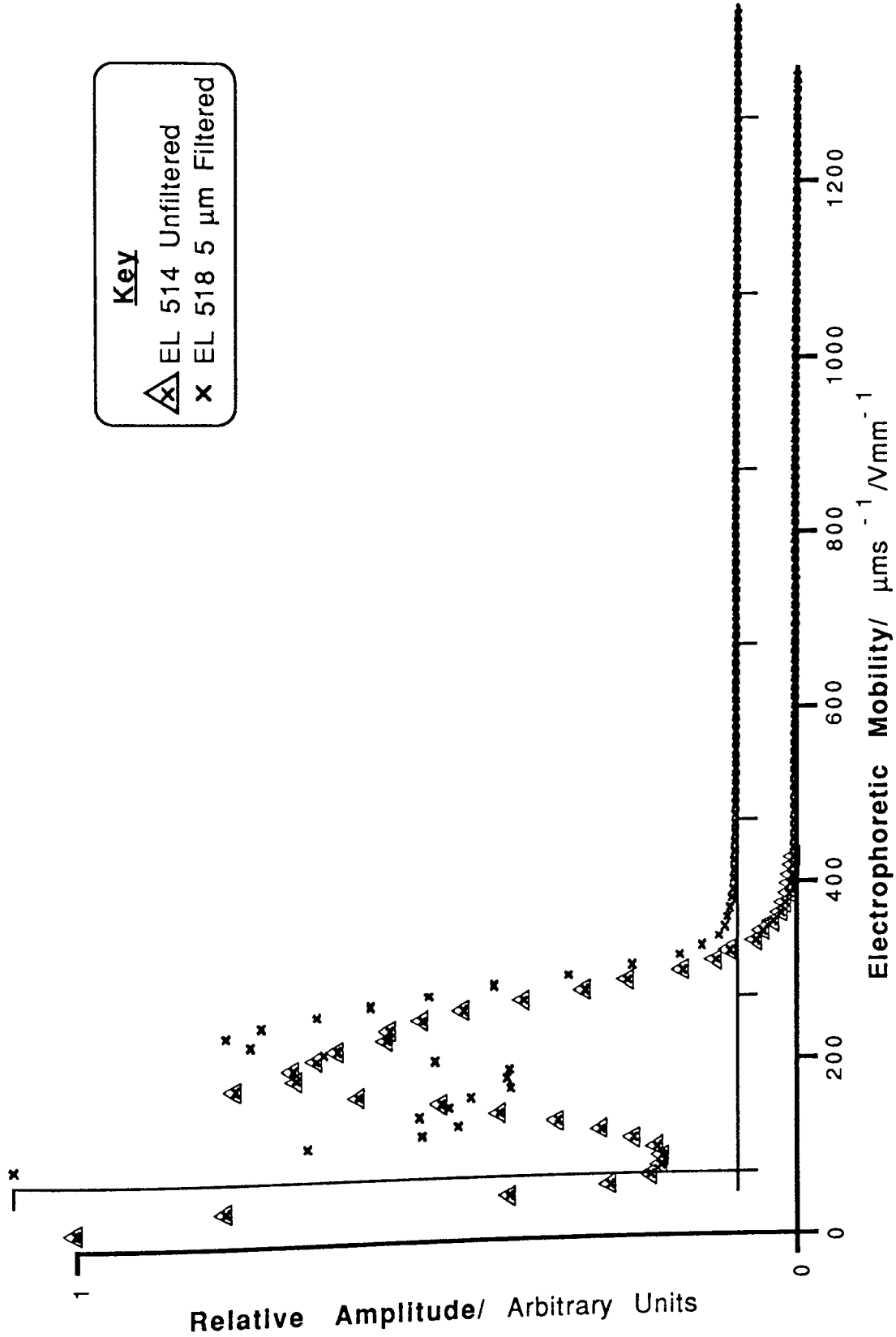

Figure 5.12
Electrophoretic Mobility Spectra for
0.1 %w/v Unfiltered & Filtered Fluka Humic Acid v3

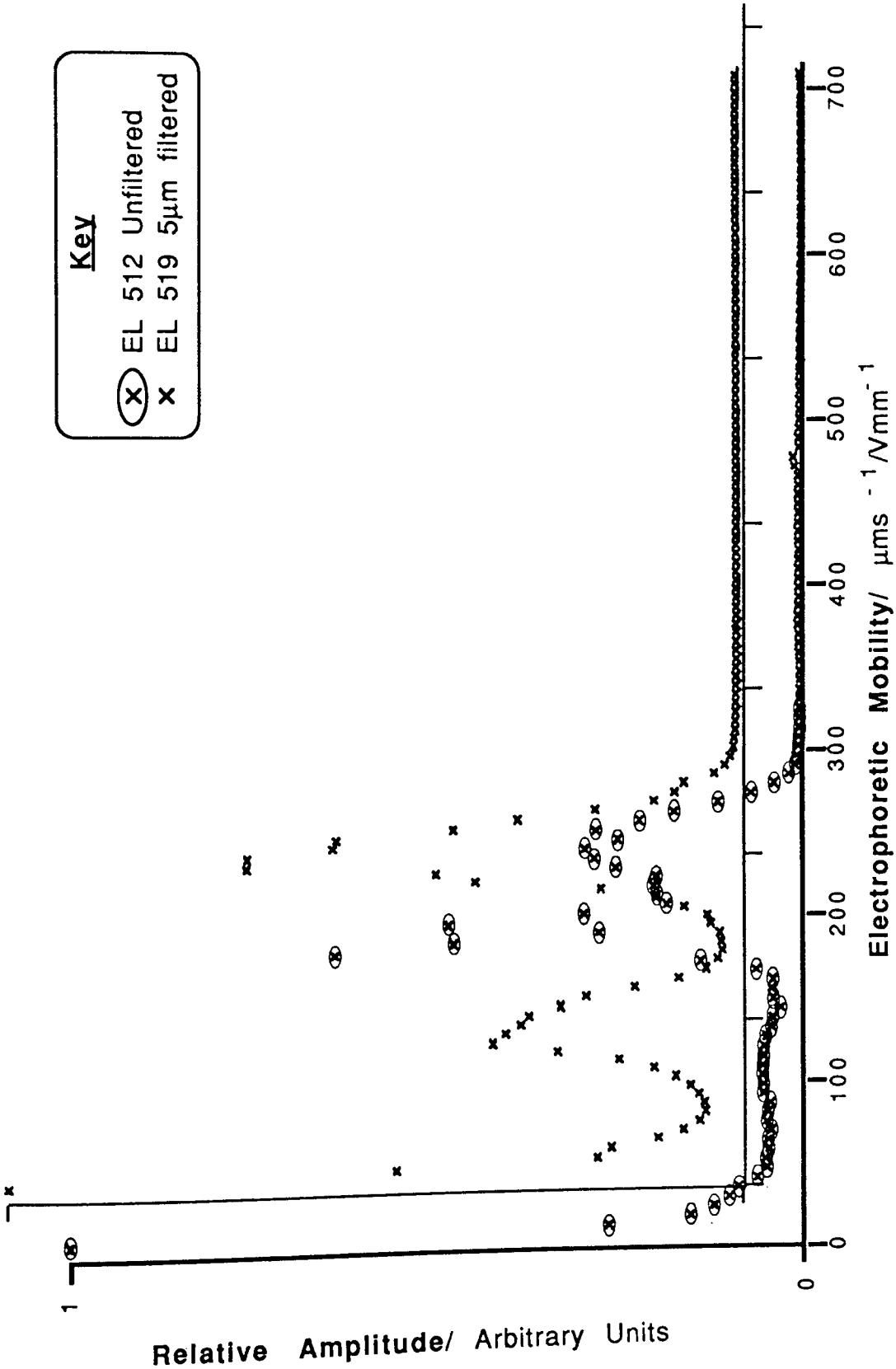

Figure 5.13

Electrophoretic Mobility Spectra for
0.001 %w/v Unfiltered & Filtered Fluka Humic Acid v3

Table 5.1
Sample and Electrophoretic Spectral Details for Fluka Humic Acid v3 pH Variation Series

SAMPLE NAME	FILE	CONCEN-TRATION /% w/v	pH	FILTER	P.D. / V	DOPPLER SHIFT /Hz	ELECTRO-PHORETIC MOBILITY /μms-1/Vmm-1	MAXIMUM AMPLITUDE OF PEAK Arbitrary Units	WIDTH AT HALF HEIGHT /Hz	SPECTRAL APPEARANCE
Fluka Humic Acid	EL 521	0.01	3.9	None	341	430	56	4E-08	?	Non-isolated, non-pronounced
						860	113	9E-08	438	Sharp & isolated.
Fluka Humic Acid	EL 520	0.01	5.9	None	357	710	89	7E-08	438	Moderately isolated.
						1570	196	3E-07	356	Sharp & isolated.
Fluka Humic Acid	EL 511	0.01	8.1	None	365	2070	253	3E-07	356	Very sharp & isolated.
						2590	317	2E-08	219	A relatively small feature.

Spectral Acquisition Parameters: Scattering Angle = 24.24°; Plate Separation = 29.6 mm; Wavelength = 632.8 nm; Final Lens Aperture = f11.

Table 5.2
Sample and Electrophoretic Spectral Details for Fanay—Augéres Fulvic Acid pH Variation Series

SAMPLE NAME	FILE	CONCEN-TRATION /% w/v	pH	FILTER	P.D. /V	DOPPLER SHIFT /Hz	ELECTRO-PHORETIC MOBILITY /μms-1/Vmm-1	MAXIMUM AMPLITUDE OF PEAK Arbitrary Units	WIDTH AT HALF HEIGHT /Hz	SPECTRAL APPEARANCE
Fanay-Augéres Fulvic Acid	EL 515	0.01	4.0	None	347	300	39	2.3E-10	136	Sharp but too close to the origin. Insufficient data.
						650	84	2.4E-10	327	Isolated.
Fanay-Augéres Fulvic Acid	EL 516	0.01	9.8	None	333	576	77	3.3E-10	488	Moderately isolated.
						1280	172	1.0E-09	299	Isolated: main peak.
						3121	419	1.9E-11	?	A relatively small feature.

Spectral Acquisition Parameters: Scattering Angle = 24.24°; Plate Separation = 29.6 mm; Wavelength = 632.8 nm; Final Lens Aperture = f11.

Table 5.3
Sample and Electrophoretic Spectral Details for Fluka Humic Acid v3 Concentration Variation Series

SAMPLE NAME	FILE	CONCEN-TRATION /% w/v	pH	FILTER	P.D. / V	DOPPLER SHIFT /Hz	ELECTRO-PHORETIC MOBILITY /µms-1/Vmm-1	MAXIMUM AMPLITUDE OF PEAK Arbitrary Units	WIDTH AT HALF HEIGHT /Hz	SPECTRAL APPEARANCE
Fluka Humic Acid	EL 514	0.1	8.9	None	170	770	203	1E-06	536	Isolated, intense, broad.
Fluka Humic Acid	EL 511	0.01	8.1	None	365	2070	253	3E-07	356	Sharp & isolated.
						2590	317	2E-08	219	A relatively small feature.
Fluka Humic Acid	EL 512	0.001	7.0	None	318	737	103	2E-09	?	Revealed on magnification.
						1332	187	1E-08	217	Half of a resolved doublet.
						1710	240	8E-09	326	Half of a resolved doublet.
Fluka Humic Acid	EL 513	0.0001	7.0	None	301	1169	173	2E-09	163	Half of a resolved doublet.
						1440	213	1E-09	190	Half of a resolved doublet.

Spectral Acquisition Parameters: Scattering Angle = 24.24°; Plate Separation = 29.6 mm; Wavelength = 632.8 nm; Final Lens Aperture = f11.

Table 5.4
Sample and Electrophoretic Spectral Details for Fluka Humic Acid v3 Filtration Variation Series

SAMPLE NAME	FILE	CONCEN-TRATION /% w/v	pH	FILTER	P.D. / V	DOPPLER SHIFT /Hz	ELECTRO-PHORETIC MOBILITY /μms-1/Vmm-1	MAXIMUM AMPLITUDE OF PEAK Arbitrary Units	WIDTH AT HALF HEIGHT /Hz	SPECTRAL APPEARANCE
Fluka Humic Acid	EL 514	0.1	8.9	None	170	770	203	1E-06	536	Isolated, intense, broad.
Fluka Humic Acid	EL 518	<0.1	≈8.9	5μm	170	630	166	4E-07	339	Isolated, intense, sharp.
Fluka Humic Acid	EL 512	0.001	7.0	None	318	737	103	2E-09	?	Revealed on magnification.
						1332	187	1E-08	217	Half of a resolved doublet.
						1710	240	8E-09	326	Half of a resolved doublet.
Fluka Humic Acid	EL 519	<0.001	≈7.0	5μm	357	732	97	1E-09	326	Isolated. Collapsed Doublet
						1510	200	3E-09	258	Isolated. Collapsed Doublet

Spectral Acquisition Parameters: Scattering Angle = 24.24°; Plate Separation = 29.6 mm; Wavelength = 632.8 nm; Final Lens Aperture = f11.

Table 5.5
Extracted Physical Parameters for Fluka Humic Acid v3 pH Variation Series

SAMPLE NAME	FILE	CONCEN-TRATION /% w/v	pH	FILTER	ELECTRO-PHORETIC MOBILITY /µms-1/Vmm-1	ZETA POTENTIAL /mV	WIDTH AT HALF HEIGHT /Hz	DIFFUSION CONSTANT /E-11 m2/s	PARTICLE RADIUS /nm
Fluka Humic Acid	EL 521	0.01	3.9	None	56	72	?	-	-
					113	145	438	7.92	3.1
Fluka Humic Acid	EL 520	0.01	5.9	None	89	114	438	7.92	3.1
					196	251	356	6.44	3.8
Fluka Humic Acid	EL 511	0.01	8.1	None	253	324	356	6.44	3.8
					317	406	219	3.96	6.2

Calculation Parameters: Scattering Constant = 4.17E+06 /m; Boltzmann Constant = 1.38066E-23 J/K; Temperature = 298 K; Viscosity = 8.909E-04 kg/ms; Relative Permittivity = 78.54

Note: Main peaks are shaded for clarification.

Table 5.6
Extracted Physical Parameters for Fanay—Augéres Fulvic Acid pH Variation Series

SAMPLE NAME	FILE	CONCEN-TRATION /% w/v	pH	FILTER	ELECTRO-PHORETIC MOBILITY /µms-1/Vmm-1	ZETA POTENTIAL /mV	WIDTH AT HALF HEIGHT /Hz	DIFFUSION CONSTANT /E-11 m2/s	PARTICLE RADIUS /nm
Fanay—Augéres Fulvic Acid	EL 515	0.01	4.0	None	39	50	136	2.46	10.0
					84	108	327	5.91	4.1
Fanay—Augéres Fulvic Acid	EL 516	0.01	9.8	None	77	99	488	8.82	2.8
					172	220	299	5.41	4.5
					419	537	?	-	-

Calculation Parameters: Scattering Constant = 4.17E+06 /m; Boltzmann Constant = 1.38066E-23 J/K; Temperature = 298 K; Viscosity = 8.909E-04 kg/ms; Relative Permittivity = 78.54

Note: Main peaks are shaded for clarification.

Table 5.7
Extracted Physical Parameters for Fluka Humic Acid v3 Concentration Variation Series

SAMPLE NAME	FILE	CONCEN-TRATION /% w/v	pH	FILTER	ELECTRO-PHORETIC MOBILITY /µms-1/Vmm-1	ZETA POTENTIAL /mV	WIDTH AT HALF HEIGHT /Hz	DIFFUSION CONSTANT /E-11 m2/s	PARTICLE RADIUS /nm
Fluka Humic Acid	EL 514	0.1	8.9	None	203	260	536	9.69	2.5
Fluka Humic Acid	EL 511	0.01	8.1	None	253	324	356	6.44	3.8
					317	406	219	3.96	6.2
Fluka Humic Acid	EL 512	0.001	7.0	None	103	132	?	-	-
					187	240	217	3.92	6.2
					240	307	326	5.89	4.2
Fluka Humic Acid	EL 513	0.0001	7.0	None	173	222	163	2.95	8.3
					213	273	190	3.44	7.1

Calculation Parameters: Scattering Constant = 4.17E+06 /m; Boltzmann Constant = 1.38066E-23 J/K; Temperature = 298 K; Viscosity = 8.909E-04 kg/ms; Relative Permittivity = 78.54

Note: Main peaks are shaded for clarification.

Table 5.8
Extracted Physical Parameters for Fluka Humic Acid v3 Filtration Variation Series

SAMPLE NAME	FILE	CONCEN-TRATION /% w/v	pH	FILTER	ELECTRO-PHORETIC MOBILITY /μms-1/Vmm-1	ZETA POTENTIAL /mV	WIDTH AT HALF HEIGHT /Hz	DIFFUSION CONSTANT /E-11 m2/s	PARTICLE RADIUS /nm
Fluka Humic Acid	EL 514	0.1	8.9	None	203	260	536	9.69	2.5
Fluka Humic Acid	EL 518	<0.1	≈8.9	5μm	166	213	339	6.13	4.0
Fluka Humic Acid	EL 512	0.001	7.0	None	103	132	?	-	-
					187	240	217	3.92	6.2
					240	418	326	5.89	4.2
Fluka Humic Acid	EL 519	<0.001	≈7.0	5μm	97	124	326	5.89	4.2
					200	256	258	4.67	5.3

Calculation Parameters: Scattering Constant = 4.17E+06 /m; Boltzmann Constant = 1.38066E-23 J/K; Temperature = 298 K; Viscosity = 8.909E-04 kg/ms; Relative Permittivity = 78.54

Note: Main peaks are shaded for clarification.

Figure 5.14
Variation of Electrophoretic Mobility with pH for Fluka Humic Acid v3 and Fanay-Augéres Fulvic Acid

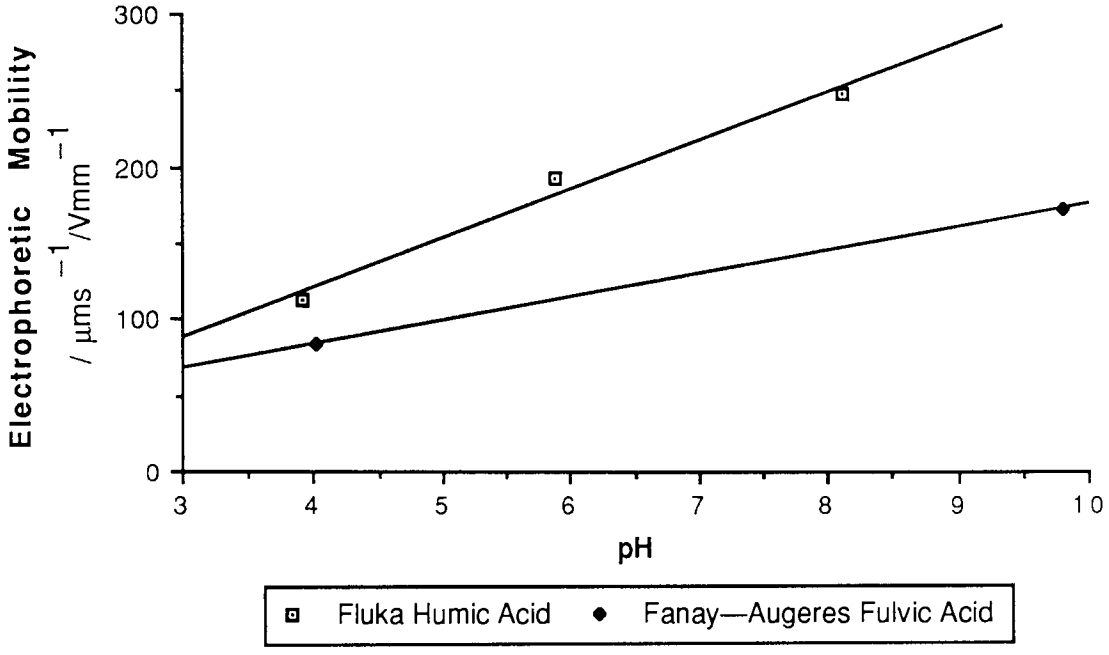

An unspecified combination of ordinate scales are generally used in the mobility overlay spectra since normalisation would tend to suppress spectral details for many samples. Note that differences in amplitude give little useful information concerning the samples. When comparisons have been made between amplitudes the samples have been run using identical spectral acquisition conditions and only qualitative comparisons are made. Spectra for the various sample series are provided in Figures 5.9–5.13.

Note that the spectral windows employed on the Solatron spectrum analyser have excluded the first sixty hertz. This is because of a mains interference problem that swamps the whole spectrum resulting in a very intense peak at 50 Hz but no Doppler shifted features except under very high magnification. Also, since the bulk of the spectrum would be due to this interference signal, the magnified Doppler peaks tend to be poorly shaped since their acquisition statistics would be poor. Unfortunately, this meant that it was not possible to analyse the Doppler spectra under conditions where the electric field was switched off to determine diffusional coefficients and hence information concerning the size of the particles. However, it is still possible to extract this information when the field is on by analysing band-widths (see Section 5.1.7.1).

Spectral information is tabulated for the various sample series in Tables 5.1–5.4.

Parameters derived from these by appropriate calculation are given in Tables 5.5–5.8. Mobility-pH relationships are plotted in Figure 5.14 for Fluka Humic Acid v3 and Fanay-Augéres Fulvic Acid.

5.4 Discussion

Spectral features of sample series will be described and patterns in their characteristics will be considered. Attention will then be paid to information calculated from extracted spectral parameters.

5.4.1 Variation of Electrophoretic Mobility with pH: Fluka Humic Acid

The mobility spectra for the three samples of concentration 0·01 % w/v at various acidity conditions are given in Figure 5.9 with the resulting extracted data quoted in Table 5.1. The spectra are presented using the same abscissa scale of Electrophoretic Mobility but the ordinate scales are different to avoid suppression of spectral details.

The trend from the spectra is clear: The electrophoretic mobilities increase with a rise in the pH of the systems. Thus the particles are more mobile under alkaline conditions.

Each spectrum contains a sharp, isolated peak and a smaller feature. For EL 520 and EL 521 the latter occurs interestingly at nearly half the frequency of the main one. This could be a harmonic artefact which would suggest that similar peaks of different orders may be present. This is, however, not realised implying that the effects are genuine and so are due to a different species of lower mobility present in a lower proportion or having a reduced light scattering ability. EL 511 also shows a second peak but with a relatively minor displacement from the main one. This suggests the presence of a species of similar mobility to that of the main peak but in a smaller proportion or with a reduced ability to scatter.

Observation of multiple peaks in spectra is not unusual: Ware and Flygare studied commercial preparations of Bovine Serum Albumin (B.S.A.) by LADELS. They reported

the presence of B.S.A. dimers and analytically separated the various components in mixtures of B.S.A. and fibrinogen. The composition determined from integrated peak areas reflected the concentrations of the components in the mixture.[213]

The spectral changes observed for the humic acid may be due to acid-induced aggregation resulting in a structure which contains components that assume a greater variety of identities at higher alkalinity. This is consistent with the changes in the mobilities: a reduced electrophoretic mobility is realised on compression of the structure due to a decreased particulate charge. Detailed comments concerning the particle sizes will be made in a later Section, still it is apparent from equations 12–14 that spectral band-widths are inversely proportional to the particle radii. From the data in Table 5.1, the band-widths of these spectral peaks decrease with increasing pH, hence the particle radii increase with pH. This supports the theory of acid-induced aggregation.

5.4.2 Variation of Electrophoretic Mobility with pH: Fanay-Augéres Fulvic Acid

The mobility spectra for the pH variation samples at constant fulvic acid concentration are given in Figure 5.10 with the relevant sample and spectral information tabulated in Table 5.2.

The limited availability of the Fanay-Augéres Fulvic Acid meant that only two conditions have been studied. However, the trend is clearly similar to that observed with Fluka Humic Acid v3: Increased electrophoretic mobility parallels increased alkalinity. Thus the particles are more mobile under high pH conditions and structural aggregation occurs on reducing the pH of the medium. It is recognised that some consideration must be attached to this statement based on the statistics of the sampling, however the behaviour is similar to that of the humic acid sample.

The band-widths of the main peaks in both spectra are quite similar: The spectral width for the higher pH sample is slightly lower than that of the more acidic sample thus implying that the particle radius increases to some extent with increased pH of the supporting medium. This supports the model of fulvic acid undergoing some aggregation when acidified. Changes in heterogeneity in response to the changing conditions of the

dispersions may also affect the peak width.

The EL 515 spectrum for the pH 4·0 sample reveals a second feature, as shown in Figure 5.10. EL 516, the spectrum recorded for fulvic acid in the more alkaline medium, shows a reasonably sharp main peak along with a low frequency peak and an additional feature at 3121 Hz.

Note that the maximum amplitudes of the main peaks were around two orders of magnitude less for the Fanay-Augéres Fulvic Acid compared to Fluka Humic Acid at the same concentration. This seems to imply that the humic structures are better at scattering light than the fulvic structures. This will be considered in greater detail in Section 5.6.

Figure 5.14 displays graphically the mobilities of Fluka Humic Acid v3 and Fanay-Augéres Fulvic Acid plotted against pH of the media. Changes in the medium acidity induces changes in the degree of ionisation of the samples which are revealed as modified electrophoretic mobilities. Other factors, such as size and conformation, probably contribute to these effects. Although Figure 5.14 is based on just a few data points, it does reveal that the humic acid sample has a greater electrophoretic mobility than the fulvic acid sample over the acidity range studied. However, it is recognised that further studies on these samples under other media conditions are necessary for an absolute verification of this statement.

Underdown *et al* applied Rayleigh scattering considerations in several studies of the behaviour of aqueous dispersions of fulvic acid: Light scattering was similarly revealed to be a function of the degree of ionisation, but aggregation of the fulvic acid was not pronounced on acidification except in the presence of large salt concentrations. The mechanism that they believe to operate is a balance of the disaggregation of large units and the opening of smaller units due to increased surface charge. Their studies also considered aggregation and binding by polyvalent metal ions.[216–218]

5.4.3 Variation of Electrophoretic Mobility with Concentration: Fluka Humic Acid

The mobility spectra for the series of aqueous dispersions in which the concentration of

Fluka Humic Acid v3 is varied are given in Figure 5.11. Note that pHs were constant only for the two samples of lowest humic concentration (see Table 5.3), thus attention will be paid to both dilution- and acidity-derived processes.

Figure 5.14 reveals changes in both the appearance of the spectra and in the magnitude of the electrophoretic mobilities of the humic acid samples. The two highest concentration samples produced a broad peak. For the 0·1 % w/v sample (EL 514), this was the only spectral feature. Dilution to 0·01 % w/v revealed a minor feature at higher mobility. It is possible that this secondary feature arose from the variation of the pHs of these samples (see Table 5.3) rather than from the change in concentration. However, such effects were not revealed in the pH-variation series for Fluka Humic Acid v3 discussed previously thus they must result from the dilution of the samples. Dilution by a further order of magnitude accompanied by a pH change of a unit resulted in an increased emergence of the second peak at higher mobility. Maintenance of acidity but reduction in concentration of the humic acid from 0·001 % w/v to 0·0001 % w/v in samples did not affect the relative spectral proportions of the two peaks to a great extent. The effect of dilution may not be apparent in this concentration range possibly since condition-induced structural rearrangements are complete.

Analysis of the trend in electrophoretic mobility with humic acid concentration is complicated by the variation in the acidity of the higher concentration samples. The mobility increases on dilution from 0·1 to 0·01 % w/v, whilst the pH drops by nearly one unit. In Section 5.4.1 mobilities were found to decrease with reduced pH thus the mobility rise on dilution from 0·1 to 0·01 % w/v must be due to dilution effects in the samples that outweigh pH effects. This may be accounted for by consideration of a given mass of humic acid: Dilution permits expansion of the structure into the greater physical space thus some separation of the humic nuclei occurs. Expansion is accompanied by the exposition of further charged surface groups resulting in an increased electrophoretic mobility. Further dilution to 0·001 % w/v accompanied by a fall of one pH unit results in a large drop in the electrophoretic mobilities of the samples. The increased importance attached to the higher mobility peak in the power spectrum can only be accounted for by the occurrence of other processes, presumably dilution-induced. Progressing to the lowest concentration sample, smaller reductions in mobilities are apparent with the acidity of the media remaining constant.

Consideration of the band-widths of the spectral peaks from the power spectra suggests

that particle radii increase on dilution. It is notable that for the two most dilute samples, the most mobile species in each has the greatest band-width, thus implying that these species are small sized but of high charge. Reduction in band-widths also could be due to the formation of a more homogeneous particle size distribution on dilution. Particle sizes will be considered in further detail in Section 5.4.7. Note that the amplitudes of the peaks show a gradual decrease (see Table 5.3) reflecting a decrease in the concentration of the scattering species.

5.4.4 Variation of Electrophoretic Mobility with Filtration: Fluka Humic Acid

The humic acid concentrations and acidities of the filtrates were not re–determined following filtration since the volumes used were too small. Attempts to measure the concentration of the filtrate by weighing the residue retained by the filter are complicated by the Acrodisc's design: The membrane is sealed within a plastic support preventing removal of the filter membrane for drying. Desiccation is unlikely to dehydrate adequately the humic matter. Concentrations of humic matter can only be assumed to be less than the original values due to the appearance of brown-coloured matter on the filters. This observation suggests the presence of large particles in the samples: This has been discussed in Section 2.7 which considered size-specific filtration of the humic acids.

Filtration of 0·1 % w/v Fluka Humic Acid v3 resulted in several changes in the electrophoretic mobility spectra as revealed in Figure 5.12 and detailed in Table 5.4: Both the width of the peak and its amplitude were reduced on filtering due to removal of some humic particles. The electrophoretic mobility of the filtrate determined from the position of this peak was reduced suggesting that the large particles removed by the filtration process were the more mobile components of the sample. Filtration of the sample effectively reduced the humic acid concentration to some extent: The effects of this were not similar to those observed when the 0·1 % w/v Fluka Humic Acid v3 sample was diluted by an order of magnitude, as discussed in Section 5.4.3. In the latter case, an increased mobility and the emergence of a secondary spectral feature was observed suggesting compositional changes occurred on dilution of the sample. However, filtration of the 0·1 % w/v sample involves the selective removal of large components in the

sample, and so the sample must be heterogeneous.

The changes in the spectral widths at half-maximum height for the 0·1 % w/v sample and for the higher mobility peak of the less concentrated sample do not reflect the anticipated reduction in particle size expected from filtration. Another factor, possibly the reduction in the heterogeneity of the sample, presumably dominates over size-derived effects.

The maximum amplitude of the peaks for these samples decreases on filtration. No attempt has been made to quantify this change in terms of a concentration reduction since scattering ability depends not only on the concentration of the scattering species but also the size and number of the scattering particles (molar mass), their polarisability and the extent of ordering of the scattering centres within the sample.[85] Filtration will change the molar mass distribution of the filtrate as a specific size-range of particles are removed.

Filtration of the more dilute 0·001 % w/v Fluka Humic Acid v3 sample similarly resulted in reduced mobilities and a large decrease in the amplitudes of the peaks. The doublet feature of EL 512 collapsed to a singlet and the minor peak at low frequency in the former increased in relative importance in EL 519. This further reflects the removal of large-sized mobile charge carriers and relatively increased importance of the smaller-sized less mobile ones. The emergence of the smaller frequency feature was quite different from the spectral changes that occurred on dilution of the 0·001 % w/v Fluka Humic Acid v3 to 0·0001 % w/v discussed previously. Again this is due to the effect of removing specific components of a sample rather than diluting the whole sample.

Similar band-width effects to those encountered with the 0·1 % w/v sample are realised for the higher mobility peak of the spectrum: The reduction in the width of this Doppler shifted peak is probably caused by a reduction in the sample heterogeneity. For the lower mobility peak, particle size reduction dominates. Underdown *et al* also found that the light scattered from samples decreased as a result of filtration. They proposed that the large particles removed by filtration were aggregates rather than covalently-bonded polymers.[216]

Note that size-specific sieving of humic acids, with particular respect to molecular

weight distributions, has been addressed in Section 2.7.

5.4.5 Interpretation of Electrophoretic Mobilities

In general, there have been few reports of electrophoretic studies on humic substances, and those that have appeared in the literature tend to be of a rather empirical nature focussing on the use of electrophoresis to assist the analytical or preparative separation of various fractions, rather than having the intention of studying the colloidal characteristics of the materials. Thus, few electrophoretic mobilities have been reported. An exception to this is the work of MacKenzie and Dawson who quoted mobilities of sodium pyrophosphate extracts of various peats and muck following electrophoretic fractionation on a cellulose column. The fractions identified were polysaccharide, organic matter and coloured matter. Three sub-fractions were noted for each of low, medium and high mobilities. The electrophoretic mobilities of the most mobile components of the latter were $-54{\cdot}7\ \mu m\ s^{-1}/V\ mm^{-1}$, when averaged for all samples studied.[219] Another series of microelectrophoresis studies have concentrated on the role of humic substances in stabilising particulate metal oxides thus preventing their aggregation.[220,221] The adsorbed organic matter tends to control the surface chemistry of the resultant species.[222]

Kononova and Titova used paper electrophoresis to fractionate soil humic materials; the number of fractions revealed was dependent on the specific material and the operating conditions employed. It was noted that the materials travelled towards the anode.[223] Varney *et al* studied fulvic acid electrophoretically using cellulose paper strips. The fulvic acid front migrated towards the anode but was rather diffuse. Migration decreased with increased acidity and the particles became immobile at pH 1·0 to 1·2. This condition in which the material is electrostatically discharged was equated with the Point of Zero Charge (P.Z.C.). The reduction of electrostatic free energy on expansion of the structure was considered.[224] Other workers have used 2D-Polyacrylamide Gel Electrophoresis (2D-PAGE)[225] and Isoelectric Focussing (IEF)[226] to study electrophoretic fractionation of humic substances.

Table 5.9
Some Electrophoretic Mobility Data

Sample	Electrophoretic Mobility $\mu m\ s^{-1}/V\ mm^{-1}$	Reference
Fluka Humic Acid *	56 to 253	This study
Fanay—Augéres Fulvic Acid *	39 to 172	This study
Silica Sols (Ludox HS Grade)	–13 to –35	227
Bovine Serum Albumin	18	212
Bovine Serum Albumin Dimers	17	213
Lymphocytes	24	228
Erythrocytes	28	228
Polystyrene latex/polyethyleneimine mixes	–63 to +27	215
Hydrocarbon Oil Droplets	0 to –60	211

Note:
** = The values quoted are for the most significant peaks*
($1\ \mu m\ s^{-1}/V\ mm^{-1} = 10^{-5}\ cm^2/V\ s$)

The magnitudes of the electrophoretic mobilities determined in these studies are rather large compared with those reported for other systems in the literature. Table 5.9 lists some electrophoretic mobility data for a diverse selection of materials obtained under various sampling conditions. It is notable that the study of silica sols was carried out on the same equipment as employed in the experiments described herein. [227]

Some attention must be paid to possible reasons for the very large values of electrophoretic mobilities derived in this study to decide upon their significance. One likely cause of error originates from the manner in which the measurements of the velocity of the mobile species were made: It was stated in Section 5.2.2 that the centre of the capillary used in the sample cell was located at the focussed cross-over of the laser beams in the LADELS apparatus. However, it would have been preferable to locate the cell such that the cross-over coincided with the stationary level of liquid flow in the capillary since this is a requirement in the definition of electrophoresis (Section 5.1.5.1). The internal surfaces of electrophoresis sample containers (such as capillaries) are generally charged during measurements, thus the applied electric field causes not only the electrophoretic migration of the particles but also the electro-osmotic flow of liquid near to the walls of the capillary and a return flow at the centre of the volume. The latter flow tends to reinforce the electrophoretic migration of the particles if the velocity is

measured at the centre of the capillary. By definition, it is strictly only at the stationary level, where the effects of the liquid flow cancel, that the true electrophoretic mobility can be determined. It is thus likely that the results reported here are enhanced because of this problem, but the extent of its contribution is not known.

The reason for using the centre of the capillary as the measurement zone originates in the difficulty of bringing the stationary level of the capillary to the focussed laser beams. Shaw calculated that the stationary level for a cylinder is located at 0·146 of the internal diameter from the cell wall.[211] This would lead to a very stringent focussing condition, and recalling that the diameter of the capillary is around 0·7 mm, the beams would be very close to the quartz walls possibly resulting in reflections of the beams from the walls.

"True" electrophoretic mobilities could be determined from the data acquired in this study if the extent of charging of the walls was known so that the contribution of electro-osmosis, could be assessed. Note that quartz capillaries were employed in these studies to assist the alleviation of such problems. If "true" electrophoretic mobilities were measured rather than mobilities that may have some electro-osmosis-derived contribution, then the measurement would be solely of electric field induced motion. However, as the mobilities were not measured at the stationary levels and were presumably affected to some extent by the flow of liquid in the capillary, then flow dynamics of the charged particles should become a consideration.

The definition of electrophoretic mobility provided in Section 5.1.5.1 refers to the speed that a charged surface moves relative to a stationary layer of liquid in response to an applied electric field. Thus a high mobility implies that the sample has a highly charged surface. Based on knowledge of the functionality of humic and fulvic acid (see Chapters 2 and 4), the main mechanism for the generation of a surface charge is probably through ionisation of these functional groups. Thus, both the Fluka Humic Acid v3 and Fanay-Augéres Fulvic Acid are extensively functionalised with ionisable groups, the former structure somewhat more so than the latter.

Some contribution to the negative surface charge of the particles may originate from a mechanism involving the specific adsorption of ions in a manner similar to that encountered with hydrophobic particles, such as oil droplets:[211] Adsorption of negative

hydroxyl ions rather than the more hydrated protons or sodium ions from the supporting medium onto the hydrophobic bulk humic or fulvic structures would augment the surface charges (revealed, approximately, as zeta potentials) and thence, their electrophoretic mobilities. This effect would be enhanced at increasing alkalinity, although other factors such as steric-based repulsions between adsorbed charges may limit the effect.

Some deliberation may have to be given to the presence of impurities in the samples (see Chapter 2) that may produce contributary effects. For example, trace amounts of transition metals may undergo some changes in the extent of their complexation or hydrolysis upon dispersion resulting in contributions to the observed mobilities.

Changes in electrophoretic mobilities with decreasing acidity of the supporting medium have been noted for several sample types using the microelectrophoretic technique.[211] For example, the increased mobility of pectic acid with increased alkalinity has been accounted for structurally by the ionisation of carboxyl groups. Complete ionisation is deduced from the constancy of the mobility above pH 5. This situation was not realised for both the Fluka Humic Acid v3 and the Fanay-Augéres Fulvic Acid, yet it has been shown that the mobilities increase with pH and the acquisition of further data may reveal an approach to this condition. This may mitigate the problems encountered in resolving end points of potentiometric titrations and so would permit the determination of a true acidity function, pK_a, for the humic material. Shaw has paid some attention to the difficulties in using electrophoretic mobility data to determine pK_a values.[211]

In Section 5.2.4 it was stated that no specific attempt was made to control the ionic strength of the humic and fulvic acid sample media. The use of both acid and alkali to adjust the pH of the samples provides counter-ions that contribute to the ionic strength. Counter-ions also would be generated from dissolution of components of the ash content of the samples (see Sections 2.2 and 2.4). However, ionic strength is quite difficult to control without creating a high concentration when other media parameters are also being monitored. In this work it was attempted to maintain their values. Shaw stated that in general, electrophoretic behaviour has a complex dependence on the ionic strength of the medium.[211]

5.4.6 Determination of Zeta Potentials from Electrophoretic Mobilities

The electrophoretic mobilities of the samples have been used to determine zeta potentials according to the theory presented in Section 5.1.7.1: In aqueous media of moderate to high ionic strength the Smoluchowski equation operates and zeta potentials can be simply calculated from mobilities by rearrangement of equation 11 to:

$$\zeta = \frac{4\pi\eta M}{\varepsilon} \qquad (15)$$

Substitution of the following values for aqueous media at 25 °C:

η_{H_2O} = $8{\cdot}909 \times 10^{-3}$ kg m^{-1} s^{-1}

ε_o = $8{\cdot}854 \times 10^{-12}$ J^{-1} C^2 m^{-1}

ε_r = 78·54

yields:

$$\zeta = 1{\cdot}28M \text{ mV} \qquad (16)$$

The Electrophoretic Mobility, M, is given in units of $\mu m\ s^{-1}/V\ mm^{-1}$. Zeta potentials calculated in this way are presented in Tables 5.5–5.8.

Note that, unlike the classical microelectrophoresis apparatus where it is possible to see the direction of motion of particles relative to the polarity of electrodes, the sign of the charges on the particles cannot be determined from the LADELS equipment as employed in the studies described herein. McFayden has described a method to determine the sign of the charge by application of a modulation to one of the laser beams.[214] However, there is little doubt that both the humic and fulvic acid particles are negatively charged over the pH ranges studied based on the behaviour of their electrophoretic mobilities with changes in the acidity of the medium and knowledge of their functional groups (Chapters 2 and 4).

Since the zeta potentials are directly derived from the electrophoretic mobilities, their magnitudes will reflect those of the mobilities. Presentation of zeta potentials as single value parameters suggests that their interpretation is simple. However, it should be

recalled that the parameter is associated with the potential at the surface of shear in an electrical double layer, the location of which is rather vague due to the rapidly changing viscosity of the region.[211] Some consideration needs to be given to the polydisperse nature of the particle and its shape, especially in the region of the surface of shear, as this has not been accounted for. Calculation of surface charges from zeta potentials is complicated by the incorporation of the complications inherent in the evaluation of ζ and additional restrictions of low potentials and spherical particles.[229]

5.4.7 Determination of Diffusion Coefficients and Particle Radii from Band-Widths

The band-widths of the spectral peaks will be examined according to the theory presented in Section 5.1.7.1 since they can provide potentially useful information concerning diffusional characteristics and sizes of particles in the samples.

Band-widths have been interpreted from spectra that were recorded with the electric field switched on. In this mode, the Doppler shifted peaks are well isolated from the low-frequency mains interference problem thus band-width determination is facilitated providing peak shapes are uniform. However, it would have been preferable to determine diffusional characteristics from band-widths in the absence of the added influence of an applied electric field: This was impossible since the unshifted peak would be superimposed on the mains interference peak and would be insignificant compared to it.

Diffusion constants have been determined from the band-widths at half-maximum height, $\Delta\upsilon$, and the scattering constant, κ, using the condition where the electric field is switched on:

$$\Delta\upsilon = \frac{D\kappa^2}{\pi} \qquad (13)$$

The scattering vector for the optical arrangement employed was previously defined in equation 2. Taking the refractive index as unity (since the cross-over angle was determined in air), then the scattering vector for a cross-over angle of $\theta = 24{\cdot}24\,°$, and use of a red laser ($\lambda = 632{\cdot}8$ nm) is, by substitution:

$$\kappa = \frac{4\pi \left(\sin 24.24/2\right)}{632.8E\text{-}09}$$

$$\therefore \kappa = 4.17 \times 10^{6}\ m^{-1}$$

Thus diffusion constants can be determined by rearrangement of equation 13 to:

$$D = \frac{\Delta\upsilon\pi}{\kappa^2}$$

Substituting for κ yields:

$$D = 1.80 \times 10^{-13}\ \Delta\upsilon$$

Particle radii have been calculated from extracted diffusion constants by the Stokes-Einstein equation:

$$D = \frac{k_B T}{6\pi\eta r} \qquad (14)$$

Where

k_B = Boltzmann Constant

T = Absolute Temperature

η = Viscosity of medium

r = Radius of particle

Rearranging for r gives:

$$r = \frac{k_B T}{6\pi\eta D} \qquad (17)$$

Substitution of the following values:

k_B = $1.38066 \times 10^{-23}\ J\ K^{-1}$

T = $298\ K$

η_{H_2O} = $8.909 \times 10^{-4}\ kg\ m^{-1}\ s^{-1}$

yields:

$$r = \frac{1.38066 \times 10^{-23} \times 298}{6\pi \times 8.909 \times 10^{-4} \times D}$$

$$\therefore r = \frac{2.45 \times 10^{-19}}{D} \qquad (18)$$

Substitution for D into this equation gives the particle radius under the above experimental conditions. The band-widths, diffusional constants and particle radii for the Fluka Humic Acid v3 and Fanay-Augéres Fulvic Acid samples are given in Tables 5.5–5.8.

The magnitude of the calculated diffusion constants can be compared to values for water (in water) and the hydroxyl ion in water of $2{\cdot}26 \times 10^{-9}$ and $5{\cdot}30 \times 10^{-9}$ $m^2\ s^{-1}$ respectively at 25 °C, [119] and more realistically, the value of $6(\pm 1) \times 10^{-11}$ $m^2\ s^{-1}$ for Bovine Serum Albumin at an ionic strength of 0·1. [212] The value determined for B.S.A. decreased to some extent at lower ionic strengths. Note that the Stokes-Einstein relation assumes that the particle causing viscous drag is spherical.

The particle radii calculated for the samples of humic and fulvic acid are less than anticipated. For example, 0·1 % w/v Fluka Humic Acid v3 which had a large fraction removed by filtration with a 5 µm filter revealed a particle radius of just 2·5 nm. The largest radius recorded for the humic acid was 8·3 nm for the most dilute sample. Similarly, the Fanay-Augéres Fulvic Acid gave values of 4·1 nm at pH 4·0, and 4·5 nm at pH 9·8. These sizes are probably too small to account for the strength of the scattering from the samples.

It is notable that the maximum amplitudes of the main peaks were around two orders of magnitude less for the Fanay-Augéres Fulvic Acid compared to Fluka Humic Acid v3 at the same concentration. This implies that the humic structures are better at scattering light than the fulvic structures. This is not compatible with the rather similar particle radii extracted by this method.

Several experimental approaches have been described in the literature to determine size

information on humic substances. Lindqvist [230] reported a radius of gyration—which is the root mean square distance of the electrons in the particle from the centre of charge [231]—of 1·8–1·9 nm for a hydrolysed sample of sodium humate from Small Angle X–Ray Scattering (S.A.X.S.). The sample was degraded by the acid treatment. Wershaw *et al*, using the same technique, discussed the existence either of particles of two or more sizes, or of particles that were the same size but consisting of a dense core with a less dense outer shell of electron density for their soil-derived sodium humate solutions. The former conclusion was favoured and radii of gyration were quoted as 11·0 nm for the ellipsoidal large particles and 3·8 nm for the nearly spheroidal smaller ones. [232] Thurman *et al*, again employing the S.A.X.S. technique, reported the presence of two fractions in the aquatic humic material: A colloidal humic acid fraction was said to be polydisperse and the dissolved fulvic component monodisperse. Radii of gyration were in the range of 0·47–3·3 nm. [231]

Studies by Olson *et al* have employed Low Angle Laser Light Scattering to determine the molecular weight distribution of their coal derived samples that were fractionated by Size Exclusion Chromatography (SEC). Polydispersity ratios were reported to be quite low. [233–235] Hombach *et al* reported that particle scattering functions indicated that their coal derivatives contained spherically shaped scatterers. [236] This was a rather rare comment on the shape of particles of humic materials in light scattering studies. Others, using techniques such as Scanning and Transmission Electron Microscopy, [53,220] Surface Tension, [237] Gel Filtration Chromatography, [224] Surface Pressure and Viscosity, [11] and Ultra-violet and Visible Absorption Spectroscopy, [79] have commented on the shapes of humic materials.

The particle sizes derived in these studies reflect factors besides the actual sizes of the humic macromolecules. Several reasons will be presented to explain the discrepancies, most of which involve other mechanisms that may contribute to the band-width of the peaks from which the particle sizes are derived:

1 The assumption that the particles undergo the same Brownian motion in the absence and presence of the electric field, resulting in the shifting of the peak with retention of its width, may be incorrect. Asymmetry of the particle may be an important factor resulting in preferential orientation under the applied electric field. [213]

2 Heterogeneity of the samples broadening the peaks resulting in a distribution of

mobilities rather than peaks broadened only by diffusion. Ware and Flygare identified separate Bovine Serum Albumin (B.S.A.) components in their mobility spectra.[212] Similarly, it is likely that some of spectral width for humic and fulvic acid samples has contributions from sample size and charge-based heterogeneity that is unresolved by this technique. This is supported by some of the changes in band-widths that occur on filtration of Fluka Humic Acid v3.

3 Transit Time Broadening: This arises because of the finite transit time of particles through the illuminated volume.[209]

4 Scattering Angle Variation: This is due to the spread in the direction of the illuminated focussed beam and the receiving angle.[209]

5 Variation in the driving potential difference: This arises from the change-over in polarity of the P.D. every ten seconds which produces a period in which the particles are reversing direction or being driven at low P.D.

6 Some heating of the sample resulting in temperatures above 25 °C.

7 The presence of electro-osmosis may result in the broadening of spectral peaks due to the distribution of velocities that it creates within the sampling area.[238]

8 Viscosities, which are used in the calculation step, were not determined for individual samples and have only been assumed to equal that of water.

Assessment of the contributions of these factors would be highly speculative, however it is likely that heterogeneity and electro-osmosis do affect the experimental observations. Attention needs to be paid to the meaning of the particle radii calculated using this method: Since the samples are heterogeneous (see Section 2.7) the calculated result incorporates this heterogeneity and reveals a particle radius as a single value that does not indicate the extent of this disparity.

5.4.8 Mixture Analysis by Laser Doppler Electrophoresis Light Scattering

Some of the results obtained from power spectra point towards the heterogeneous composition of the samples. Ware and Flygare extended their LADELS studies to perform a mixture analysis of bovine serum albumin and fibrinogen: They reported the analytical separation of the constituent components based on the appearance of separate peaks in the spectra for the species.[213] Similarly, Ware studied several biological mixtures and

identified components in several mixtures from multi-peak spectra.[239]

5.4.9 Accuracy and Reproducibility of Laser Doppler Electrophoresis Light Scattering Measurements

Some brief comments will be made concerning the reproducibility and accuracy of LADEL measurements. Some element of inconsistency between repetitive measurements was suspected. This may arise to some extent as a consequence of the difficulty in locating both the centre and width of the shifted peaks due to the irregular shapes frequently displayed. A curve-fitting routine may assist the elimination of these problems as they are somewhat subjective. Note that any uncertainties in the accuracy of peak locations and widths will be proportionately transferred to the Electrophoretic Mobilities, ζ Potentials, Diffusion Constants and Particle Radii determined in these studies.

5.5 Conclusions

Parameters derived for the materials studied are sensitive to the conditions of their supporting medium and their concentration and particle size distribution.

Both Fluka Humic Acid v3 and Fanay-Augéres Fulvic Acid were found to be highly charged at the surface of shear in their electrical double layers; the humic acid somewhat more-so than the fulvic acid studied. A comparison of the electrophoretic mobilities of the humic and fulvic versions of the same sample would assist the determination of this as a general property or otherwise. It was also noted that the scattering from the fulvic acid studied was much less than that of the humic acid.

Electrophoretic mobilities and particle radii were found to increase with the pH of the medium. Such changes are probably due to the dissociation of acidic functional groups and structural changes. This implies that the structure possesses some flexibility that permits such changes to occur. Dilution of the Fluka Humic Acid v3 and the Fanay-Augéres Fulvic Acid produced a large decrease in the amplitude of light scattered in Power Spectra and increased particle radii. Filtration of the samples revealed the presence of some large particles (diameter >5 μm) in the samples implying that they are

polydisperse. Effects of reduced heterogeneity were apparent in the band-widths of the spectra. Reductions in the electrophoretic mobility were noted suggesting that the large particles removed may be the more electrophoretically mobile components of the humic acid. A reduction in light scattering amplitude was also observed. Particle radii determined in these studies are probably underestimated considering the strength of the scattering from the materials, and because some component can be removed with a filter of nominal diameter 5 μm. It should be stressed that the radii determined mask the polydisperse nature of the samples but provide an indication of some average particle size, and the effect of sample and media conditions on particle sizes.

5.6 Refractive Index and Specific Refractive Index Considerations

5.6.1 Introduction

The light scattering intensity observed in the LADELS experiments for Humic Materials was noted to be rather large. In this Section, the factors that cause this observation will be examined, and experiments performed to investigate its origin will be described.

A simple model for light scattering can be derived if the dispersion is considered to consist of point scattering centres which obey Rayleigh-type scattering.[85] According to Rayleigh, the intensity of scattering of a non–polarised beam of light is given by:

$$i_\theta = \frac{8\pi^4 \alpha^2 I_0 n \left(1+\cos^2\theta\right)}{r^2 \lambda^4} \qquad (19)$$

Where:

- i_θ = Scattering intensity for non–polarised light
- α = Polarisability of the material
- I_0 = Intensity of incident radiation
- n = Number of scattering centres
- θ = Scattering angle, with respect to the transmitted light direction

r = Distance of the detector from the centre of the scattering cell

λ = Wavelength of incident radiation

If the assumption is made of a dispersion of independent monodisperse scatterers in an appropriate medium, then the number of scattering centres per unit volume can be related to the molar mass of the dispersed material, whilst the polarisability of the material can be related to the refractive index of the dispersion. Application of this model leads to the simple equation:

$$R_\theta = M\,c\,K^* \qquad (20)$$

Where:

R_θ = Excess scattering from the sample relative to pure dispersion medium

M = Molar mass of the dispersed material

c = Concentration of the dispersed material (mass per unit volume)

K^* = Optical constant, defined by:

$$K^* = \frac{2\pi^2 n_0^2}{\lambda^4 N_A}\left(\frac{\delta n}{\delta c}\right)^2 \qquad (21)$$

Where:

n_0 = Refractive index of the dispersion medium

N_A = Avogadro's Constant

$\left(\frac{\delta n}{\delta c}\right)$ = Specific Refractive Index Increment, S.R.I.I., for the sample

It should be appreciated that this model is an over-simplification since it takes no account of the effects of external interference in the reduction of the scattering intensity. Although humic and fulvic acids are unlikely to consist of small monodisperse molecules that act as point scattering centres, the theory has been presented since an appreciation of the most important factors that determine scattering intensity can be gained.

From equations 20 and 21 it is apparent that the intensity of light scattering is proportional to several factors, namely:

The molar mass of the dispersed material, M

The concentration of the species, c

The optical constant, K*, which is itself proportionately dependant on:

The square of the refractive index of the dispersion medium, n_0

The inverse fourth power of the wavelength, λ

The square of the S.R.I.I., $\left(\frac{\delta n}{\delta c}\right)$

Thus for a given wavelength of light employed in the light scattering measurements and a chosen dispersion medium, then scattering is dependant on the molar mass of the material, concentration of the species and the square of the S.R.I.I.

Brief experiments will be detailed that investigate these dependencies with the aim of determining the dominant factor that controls the strength of humic- and to a lesser extent fulvic-acid scattering. These experiments involve the determination of refractive indices of the materials using an Abbé Refractometer and thence an estimate of their S.R.I.I.s. It was realised that the latter measurement should be determined using a specialised instrument that permits accurate determination of the rather small increment; however, access to such equipment was not available. This was not deemed essential to the semi-quantitative intentions of this short investigation.

5.6.2 Experimental

The samples chosen for refractive index determination were the humic and fulvic acid employed in the LADELS experiments, two other humic acids, and two colloidal silica samples for comparison, since these are well-characterised strong scatterers.[227,240,241]

The samples were prepared by appropriate quantitative dilutions of stocks, if previously prepared, or by dispersion. For the Fanay-Augéres Fulvic Acid, dispersion was accomplished in distilled water, but for the corresponding Humic Acid, dispersion did not occur to any visible extent, even in dilute alkali. This sample was not considered further. A range of concentrations were employed in measurements to gain an appreciation of the concentration dependance of the refractive index.

Table 5.10
Refractive Indices and Specific Refractive Index Increments for Humic Materials and Colloidal Silica

Sample	Concentration / % w/v	pH	Deviation Angle	Refractive Index (293 K, 589 nm)	Specific Refractive Index Increment (293 K, 589 nm) / ml/g	Comments
Fluka Humic Acid v3	0.002	–	3°7'	1.3321	0.354	
	0.050	6.9	3°8'	1.3323		
Aldrich Humic Acid v1	0.002	–	3°7'	1.3321		
	0.020	–	3°7'	1.3321		
	2.000	7.0	–	–		Too diffuse to measure deviation
Fanay—Augéres Fulvic Acid	0.002	–	3°7'	1.3321		
Fanay—Augéres Humic Acid	–	–	–	–		Material not dispersable
Syton W30 Colloidal Silica	0.002	–	3°7'	1.3321		
	0.950	–	3°9'	1.3325	0.060	S.R.I.I. calculated from highest
	9.500	8.9	3°46'	1.3386		concentration pair
Ludox TM Colloidal Silica	0.002	–	3°7'	1.3321		
	0.350	–	3°8'	1.3323	0.062	S.R.I.I. calculated from highest
	35.000	8.5	5°18'	1.3538		concentration pair
Ludox Colloidal Silica	–	–	–	–	0.061	Huglin [242] (Ludox grade not quoted)
Distilled Water	1.000	–	3°7'	1.3321		
	1.000	–	3°12'	1.3330		Source: Abbé Manufacturer's Tables

Measurement Parameters: Wavelength = 589 nm; Temperature = 293 K
All samples were dispersed with, and diluted by, distilled water

Refractive Index Measurements were made on an Abbé Refractometer (¢063) using a sodium lamp for illumination at 589·6 nm. Angular deviations from individual samples, including water as a reference material, were recorded.

5.6.3 Results

The measured angular displacements and the corresponding refractive indices determined from the manufacturer's data tables are quoted in Table 5.10. S.R.I.I.s are quoted where sufficient data is available to permit their calculation.

5.6.4 Discussion

It is evident from Table 5.10 that Fluka Humic Acid v3 has a refractive index increment of similar order to those calculated and quoted for the colloidal silica samples. The Fluka Humic Acid v3 S.R.I.I. is derived from an extra deviation of one minute from that observed with the more dilute sample or the solvent. This places much weight on the reliability of this measurement. Olson and Diehl reported large S.R.I.I. values for lignites in the range 0·16 to 0·25, depending on the sample-solvent pair employed.[233] Note that the wavelength of light and the specific grade of Ludox Colloidal Silica employed in the Specific Refractive Index Increment measurements reported in Huglin and quoted in Table 5.10 are not apparent.[242]

It is thus likely, based on these rather simple measurements, that the humic and fulvic acid samples have high S.R.I.I.s, thus causing the high scattering observed in the LADELS experiments. The source of the high scattering intensity also could be molar mass-derived implying that the masses of the samples are large since Rayleigh scattering is proportional to molar mass. This contribution would contradict the particle radii determined by the LADELS method but reinforce those suggested by the specific size filtration discussed in Section 2.7.

Refractive indices at optical frequencies can be simply related to polarisabilities.[119] The latter depends on the atomic number, atomic size and the ease of excitation of constituent atoms of materials. In reality it is the strength by which the nuclei of atoms

control their electrons thus preventing distortion in an electric field that determines the magnitude of the polarisability. Thus if polarisabilities are large, the electrons are rather loosely held in applied electric fields. For the humic and fulvic acid samples studied, this is probably due to the high charges located at the plane of shear that were measured in the electrophoresis experiments.

5.6.5 Conclusions

The intensity of light scattered by the humic and fulvic acid samples was quite large. A combination of refractive index and molecular mass considerations account for this.

CHAPTER 6
KINETICS, BUFFERING and MECHANISMS of the POTENTIOMETRIC TITRATIONS of HUMIC ACIDS

6.1 Introduction

The chemical structure of humic materials (outlined in Chapters 1 and 2) has an aromatic or aliphatic backbone substituted by functional groups, the most abundant of which are carboxyls and phenolic hydroxyls. [1,6] These groups are believed to be the main cause of the acidity of humic materials and their ability to bind metal ions on substitution, both of which are of environmental importance. Attempts have been made to quantify the abundances and acidities of these functional groups by potentiometric titrations. Despite the widespread use of this method few researchers have monitored or commented upon the rate of equilibration following acid or alkali additions during such titrations. Experimental studies described in this Chapter investigate the approach to equilibrium in potentiometric titrations of humic acids since this is believed to be a slow process compared to the rate of simple neutralisation reactions. The potentiometric behaviour is analysed by applying chemical kinetics, and mechanistic implications of humic acid protonation are considered.

6.1.1 Environmental Effects of Humic Materials

The environmental significance of humic materials, as a major segment of the world's surface organic carbon, is the cause of much of the research activity directed at these substances. Of particular interest is their ability to influence terrestrial and aquatic acidity, the availability of micronutrients to vegetation, soil and water quality, and geochemistry. These properties arise from the chemical structure of humic materials. [243]

A strong interrelationship exists between soil pH and humic materials through a buffering mechanism that maintains the neutrality of soils. [244,245] The acid-base properties of dissolved humic materials are believed to be responsible for controlling the pH of some organically-rich fresh waters. [224,246] Humics contribute to the regulation

of metal ion toxicity in soils, rivers and lake waters.[244] Their ion exchange properties play a significant role in determining the availability of micronutrients to plants.[245]

These properties have prompted many investigations of the functional groups that cause the acidity and ion exchange behaviour of the materials. Potentiometric titrations have been applied to characterise proton and metal ion binding to humic substances.

6.1.2 Potentiometric Titrations of Humic Materials

Potentiometric titrations have frequently been used to quantify the abundances and acidities of humic functional groups. Some workers have monitored proton release on metal ion binding, or directly monitored metal ion concentrations by ion-sensitive electrode potentiometry to determine conditional stability constants for complexation of metal ions with humic materials. Other studies have included detailed theoretical analysis of proton and/or metal ion binding whilst some have been further extended to model complex chemical systems. Representative experimental approaches applied to potentiometric titrations and typical information derived will be outlined.

The parameters derived in studies of the potentiometric properties of a fulvic acid using aqueous titrations with standard alkali by Gamble, are typical. The fulvic acid had two types of carboxyl group; one was ortho to a phenolic –OH group. The number of each type per gram was quantified. The acid ionisation equilibrium of both substituents was calculated as a function of their respective degrees of ionisation in 0·1 *m* $KCl_{(aq)}$ at 25 °C: In both cases acid strength decreased with increasing degree of ionisation. The sample studied showed the potentiometric behaviour typical of a low molecular weight polyelectrolyte.[247,248] Choppin and Kullberg's experiments used both potentiometric and calorimetric titrations to determine thermodynamic parameters for the protonation of soil humic acids. These involved titration with mineral acid of basic media containing humic acids. The pK_a values determined were compared to typical values for simple organic acids to suggest the identity of the acidic humic functional groups; these were believed to be benzoate, salicylate and phenolate.[249]

Ephraim performed potentiometric titrations on fulvic acids from two sources. His experimental approaches used continuous (stepwise) and discontinuous (batchwise)

titrations in aqueous media, and non-aqueous titrations with *t*-n-butlyammonium hydroxide in dimethylformamide. The results showed that the protonation behaviour of these fulvic acids was a reflection of their polyelectrolytic nature and their site heterogeneity.[244] Marinsky and Ephraim paid particular attention to the potentiometric properties of humic substances in the presence and absence of salts. This aimed to determine the permeability of the polymer matrix to electrolyte, and explain the high sensitivity of the potentiometric properties of weakly acidic polyelectrolytes to medium ionic strength.[250] Marinsky, Gupta and Schindler carried out potentiometric titrations to prove the validity and applicability of their theory on the protolytic behaviour of humic acid gels.[251] Many other potentiometric studies have been reported.[25,243,245,252-263]

Many theoretical models described in the literature consider the complexation of humic materials by metal ions. Some experiments apply metal ion potentiometry using ion-selective electrode measurements. Marinsky and co-workers have paid much attention to theoretical considerations of protonation and metal ion complexation of humic materials in a series of reports.[243-245,150,251,259,260] However, some of their work has been challenged resulting in revised interpretations.[264,265] The report by Marinsky, Gupta and Schindler included a theoretical analysis of the protolytic and metal ion complexation behaviour of humic acid gels.[260] Marinsky and Ephraim quantitatively explained the high sensitivity of the potentiometric properties of humic materials to medium ionic strength through theoretical considerations of protonation.[250] Potentiometric titration results were analysed by Ephraim with a unified physico-chemical protonation model that accommodated the main complications associated with humic materials; their polyelectrolytic nature and site heterogeneity.[244] Further development of the model enabled interpretation of metal ion binding to a fulvic acid in every conceivable experimental situation. The model predicts the binding of macro quantities of copper(II) to a fulvic acid as a function of the degree of neutralisation, ionic strength, and concentrations of metal ions and fulvic acid.[259]

Dzombak *et al* analysed the theory underlying discrete and continuous multiligand models for metal ion-humate binding using synthetic and experimental data.[266,267] The binding of copper(II) and fulvic acid was considered by Gamble *et al*: The theory of polyelectrolyte titration was applied to provide a complete description of ion-sensitive electrode and spectrophotometric data.[268] In a further study, they presented a theoretical description of multiple metal ion-humic acid cation exchange.[269] Tipping

and Hurley produced a quantitative chemical model of organic soils that incorporates complexation by humic functional groups and non-specific ion exchange reactions. The model accounted satisfactorily for the results of acid-base titration experiments giving reasonable simultaneous predictions of soil pH and aluminium concentrations.[270] Metal to fulvic acid ion-sensitive electrode titration data was analysed by Turner *et al*: Five binding models were used; each was summarised and reviewed.[271]

Theoretical models of protonation and complexation may also be based on methods other than potentiometry: For example, Dobbs *et al* made luminescence measurements and described a pH–dependent multiligand model derived from the Gaussian distribution model that was previously used independently to describe proton or metal ion binding to humic substances. The applicability of the model was extended to account for competitive binding of the metalated and protonated ligand species.[134,135]

6.1.3 Observations in the Preparation of Fluorescence Samples

During the preparation of samples for fluorescence studies described in Chapter 3, it was noticed that the chemical system—consisting of humic acid at a given ionic strength either in the presence or absence of europium(III) ions—displayed a slow response to acid or alkali aliquots used to adjust the pH to a specified value. Also, the pH changes were not as large as expected based on the magnitude of the additions. This prompted a detailed analysis of the literature to locate citations of similar effects. Most attention was focussed on potentiometric titrations although some was paid to articles on metal ion complexation.

6.1.4 Reported Equilibration Time-Scales and Buffering in Potentiometric Titrations and Metal Ion Complexation of Humic Materials

Examination of the literature has revealed occasional references to the time-scale of equilibration in potentiometric titrations, but few detailed studies. Similarly, a few reports on metal ion complexation have mentioned the rate of formation of complexes. Comments concerning buffering in potentiometric titrations are also rare. Examples of

representative work will be described.

Most reports of potentiometric titrations do not comment on the equilibration time following addition of a titrant. Some make unqualified statements; for example, Ephraim determined the pH in his discontinuous titration of fulvic acid in an aqueous medium "after equilibrium was reached."[244] Others have quoted a response time but offered no justification for its selection: Varney *et al* allocated two and a half minutes for equilibration,[224] whereas Wilson and Kinney allowed ten minutes after each titrant addition.[261] A few reports have offered some explanation for their choice of titrant response time. In Choppin and Kullberg's potentiometric titrations the pH was measured between thirty and sixty minutes after each addition of titrant. It was stated that "the system was very close to equilibrium by then and further waiting would have resulted in additional errors." Measurement of the pH after the quoted equilibration time revealed a maximum drift of 0·1 unit.[249] However, that this can be a relatively large error in hydrogen ion concentration, depending on the prevailing pH. In contrast, their calorimetric experiments showed that the protonation reactions were fast with heat release complete within a minute after each addition. In the acidic region, the reaction was somewhat slower.[249] Their work suggests that the actual proton-hydroxide neutralisation reaction is fast, but other processes that accompany this change occur over a much longer time-scale. Mathuthu considered that pH equilibrium was reached in aqueous potentiometric titrations when the potential drift was less than 0·1 V in ten minutes.[245] Marinsky, Gupta and Schindler justified their selection of equilibration times: In potentiometric titrations of a dissolved humic acid with standard base, equilibration took ninety to one hundred and twenty minutes, as indicated by attainment of a constant potential. They also examined copper(II) binding with humic acid by equilibration of mixtures at defined ionic strengths under nitrogen. The equilibrium condition was characterised by small positive and negative fluctuations in electrode measurements of pH and pCu in supernatant solutions.[251]

Comments concerning the rate of attainment of equilibrium in metal ion complexation studies are rare, and of those that suggest a suitable time-scale, few justify its selection. Dobbs *et al* stated that complexation between europium(III) and fulvic acid occurred rapidly, therefore enabling their spectroscopic measurements to commence immediately after sample preparation.[134] A fixed five minute equilibration period was allocated by Turner *et al* before reading the potential in their measurements of lead(II) and copper(II) binding by fulvic acid using ion-sensitive electrodes.[271] Frizado titrated

humic acids with metal hydroxides potentiometrically: It was found that monovalent metal ions (Na^+, K^+) produced a constant pH after around fifteen minutes, whereas divalent cations (Mg^{2+}, Ca^{2+}) required around forty five minutes to reach this condition.[258] In Marinsky, Gupta and Schindler's study of copper(II) binding with humic acid, a period of thirty days was required to reach equilibrium: Reasons for this slow rate were not identified.[251] Although it is appreciated that the rates of complexation reactions are themselves dependent on the rate of ligand exchange on the cation, the specific nature of the humic material employed, and media conditions, the marked differences between the times used in work of Dobbs *et al*[134] and by Marinsky and co-workers[251] imply that clarification of the criteria for the selection of equilibration times is required.

A few studies have reported and explained buffering effects in potentiometric titrations and complexation reactions. Ephraim observed buffering over a wide range of titration conditions and accounted for it through the heterogeneity of the samples.[244] Wilson and Kinney detected a buffering effect between pH 12 and the equivalence point that was caused by protonation of phenolic groups in their dissolved organic matter samples.[261] Buffering in Mathuthu's titrations of fulvic acid was accounted for by the presence of functional groups with different acidities. It was also observed in titrations with copper(II) and europium(III) ions and duly explained by the hydrolysis equilibria of these cations.[245]

Occasional reports have commented on other changes involving humic substances over time. These have generally been coincidental observations rather than studies directed at such effects. An illustrative selection will be described. In Choppin and Kullberg's work on the protonation of soil humic acids, discrepancies were observed between forward and reverse titrations when samples were equilibrated for periods up to six days: The extent of the reduction in the required alkali titre increased with storage time. This was explained by the uptake of carbon dioxide by the alkaline solutions, or the occurrence of changes in the chemical structure of the humic acid.[249] They do not appear to have taken steps to exclude CO_2 from their apparatus. Choppin and Kullberg also observed that the exchange capacity of the humic acid increased from a value of 2·95 meq g^{-1} to 4·16 meq g^{-1} over a year reflecting slow changes during storage.[249] Pommer and Breger also noted changes in exchange capacities from their discontinuous titration results. The capacity of a peat humic acid had changed by 27 %, fifty days after dissolution. Evidence from Infrared Spectroscopy suggested that the humic material had

probably condensed with the loss of carbonyl groups. Analysis of the solutions used in potentiometric experiments showed that acidic solutions tended to drift to a higher pH, alkaline solutions drifted to a lower one, and an intermediate region showed no change with time. The rate of pH drift decreased as the solutions approached the intermediate region.[253,254] Posner noted that the pH of humic acid dispersions dropped when greater than 8. It was proposed that this was due to consumption of alkali through aerial oxidation of the humic material, yet a similar pH decrease was observed with acetic acid that cannot be explained by an oxidative mechanism.[272] The consumption of alkali by reaction with carbon dioxide presumably accounts for these changes.

The work of Borggaard is unique since it is a detailed study of some factors affecting the rate of equilibration.[263] He recommended that alkaline humate solutions should be stored in sealed, sterile containers under nitrogen since these conditions produce insignificant pH changes with time. Under such conditions, protolytic equilibrium is established instantly and potentiometric titrations of humic materials can be performed as normal acid-base titrations. Borggaard reached these conclusions by measuring the protolytic equilibration time in samples of three dissolved humic acids in various container types, at different initial pH's in the range 4–11. The samples were only opened when a pH measurement was to be made and then they were discarded. The pH of samples after various equilibration times depended on the initial pH value, the container material and whether the contents were sealed under nitrogen or air. Using sterile ampoules under nitrogen, pH changes were always less than 0·3 units over a twenty eight day storage period, whatever the initial pH value, and generally less than 0·1 unit. With sterile ampoules under air or glass tubes under air, pH changes of up to 2 units were observed. Other equilibria or reactions are involved in these latter cases, such as aerial oxidation. From Borggaard's work it seems likely that the response of the humic material to the prevailing acidity was rapid since this was a genuine neutralisation reaction, but secondary processes were slow thereby giving the impression of slow pH changes overall.

In summary, few workers have quoted equilibration time-scales for neutralisation and complexation reactions involving humic substances. Of those that have, there is little consensus and justification of selected equilibration periods. The work detailed on the rates of complexation reactions illustrates this point with time-scales varying from instantaneous[134] up to thirty days.[251] This immense disparity suggests that the basic phenomena underlying the selection of equilibration periods require clarification. Also, some citations of other slow changes involving humic substances in media of differing

acidity were located. For these reasons, and as some relevant observations were made during the preparation of samples for fluorescence analysis (see Chapter 3), a co–ordinated investigation of these effects was initiated.

6.1.5 Introduction to Experimental Work

The aim of the experimental work is to study the approach to equilibrium in potentiometric titrations of humic acids under various conditions. The experimental approach involves monitoring the pH of alkaline humic acid dispersions during additions of mineral acid through hydrogen ion potentiometry. Chemical kinetic considerations are applied to the results obtained and mechanistic implications of the protonation behaviour are discussed. The protonation results are also analysed for buffering effects.

6.2 Experimental

6.2.1 Introduction

Initial considerations suggested that a useful approach to the kinetic analysis of potentiometric titrations was to study the acidification of alkaline dispersions of humic acids. This is favoured since the organic matter would be in its anionic humate form and therefore in a reasonable state of dispersion. Humic acid samples were subjected to various conditions to study factors that may influence their protonation equilibration times. The initial humic acid concentrations covered a wide range up to a limit of ~2 % w/v. The humic stocks prepared contained various concentrations of an alkaline dispersant. The acid additions used to protonate the humate dispersions were intended to produce different ultimate pH values and traverse the likely equivalence points of the constituent functional groups.

6.2.2 Preparation of Chemicals

Sodium hydroxide for dispersion of the humic acids was prepared by dissolution of B.D.H. A.R. pellets (¢010) in distilled water. Hydrochloric acid for protonation of the

alkaline humate samples was diluted from a F.S.A. A.R. concentrate (¢011). Serial dilutions of these were made following standardisation of the alkali with potassium hydrogen phthalate (¢036) using phenolphthalein (¢037) as indicator, and subsequent titration of the mineral acid with the standardised alkali.

The humic acid stocks were prepared differently to those described elsewhere in this thesis. Instead of dispersing a given mass of the humic acid in the minimum alkali volume and making up to an appropriate volume with distilled water, all the liquid additions were of that alkali. Therefore, the dispersions tended not to be nearly-neutral but alkaline. The preparation procedure involved agitation under a nitrogen atmosphere followed by quantitative transfer of the alkaline dispersion to an appropriate volumetric flask. The humic acids used in these experiments were Aldrich Humic Acid v1 (¢004) and Fluka Humic Acid v3 (¢003).

6.2.3 Experimental Procedure for Potentiometric Titrations

An aliquot of an alkaline dispersion of a humic acid was dispensed into a round-bottomed multi-necked flask. The dispersion was diluted as necessary with distilled water to give the required initial humic acid concentration. A small positive pressure of oxygen-free nitrogen (¢009) was established within the flask to prevent ingress of atmospheric gases that may alter the pH of the medium or encourage oxidation of the organic matter. The flask was placed in a Grant constant temperature bath (¢062) thermostatted to 25 °C. A doubly-calibrated combination pH electrode (¢016) was inserted into one neck of the flask and both supported and sealed by an appropriate bung. The pH of the humic acid dispersion was measured using a pH meter (¢017) and recorded by an attached Perkin-Elmer chart recorder (¢031). The initial temperature of the dispersion was determined using the temperature probe attached to the pH meter. The dispersion was agitated by a magnetic stir-bar inside the flask that was driven by a similar magnet attached to a rotary stirrer outside the glass vessel. Some agitation was also provided by the nitrogen bleed. Once a condition of constant initial temperature and pH was attained, the acid was added. This was performed rapidly using a burette, micropipette or fast-flow pipette. The pH of the dispersion was monitored and occasional temperature measurements were made. Data collection was terminated once a condition of constant acidity appeared to be reached.

The range of humic acid concentrations and acid additions that were used in the kinetic runs are given in Table 6.1. The initial humic acid concentration quoted has been compensated for any dilution of a stock by distilled water before acidification. The final concentration value has been adjusted to account for the volume of acid used to protonate the humate dispersion. The alkali concentration given is that used to disperse the humic acid. Its volume quoted therefore represents the amount of the alkaline humate dispersion used. The concentration and volume of the hydrochloric acid added at the start of the potentiometric titration are given. The selected volume and concentration was a compromise between a fast addition and rapid distribution in the sample. The temperatures quoted are averages of values determined during a protonation titration. Temperature deviations from the quoted mean within a given cycle tended to be small, even during the initial mixing stage.

6.3 Results

Table 6.2 provides some analysis of the alkaline humic acid samples that were protonated. The initial pH is that of the humic acid dispersion before acidification but following any dilution by distilled water. The final pH noted is the last one recorded in the protonation process; this was the lowest pH observed. The anticipated final pH has been calculated by assuming that the hydrochloric acid aliquot simply neutralises all the sodium hydroxide present in a given volume and that the humic acid does not affect this.

The buffering effect—given in mol dm^{-3} of hydrogen ion concentration—represents the difference between the measured and anticipated final pH values. The buffering effect is also quoted relative to the final humic acid concentration in Table 6.2.

A sample raw chart of pH against time for Aldrich humic acid is given in Figure 6.1. For this and other humic acid samples, charts have been analysed and data has been noted from them to facilitate calculations and presentation in more useful formats. In the initial protonation stages, data has generally been read at more frequent intervals. Raw data is given for four samples in Tables 6.3–6.6.

Table 6.1
Composition of Humic Acid Acidification Samples

Humic Acid	Humic Acid Concentration		Alkali, $NaOH_{(aq)}$		Acid, $HCl_{(aq)}$		Temperature
	Initial / % w/v	Final / % w/v	Concentration / mol dm^{-3}	Volume / cm^3	Concentration / mol dm^{-3}	Volume / cm^3	/ °C
Fluka Humic Acid v3	0.020	0.019	0.0055	100.0	0.1166	7.0	23.8
	0.029	0.025	0.0078	70.0	0.1166	9.0	23.6
	2.005	1.671	0.0948	50.0	1.166	10.0	24.7
Aldrich Humic Acid v1	0.040	0.040	0.0011	50.0	0.1166	0.8	23.6
	0.100	0.086	0.0011	50.0	0.01166	8.0	22.9
	0.100	0.088	0.0011	50.0	0.01166	7.0	23.2
	0.100	0.089	0.0011	50.0	0.01166	6.0	23.0
	0.200	0.143	0.0011	50.0	0.1166	20.0	23.3
	0.200	0.191	0.0011	50.0	0.1166	2.3	23.6
	2.000	1.754	0.0948	50.0	1.166	7.0	24.9

Notes:

The initial humic acid concentration accounts for any dilution to the humic stock using distilled water before acidification. The final concentration takes account of the volume of acid added. The alkali concentration and volume relate to the humic acid dispersion medium; the volume quoted is that of the alkaline humic acid dispersion employed. The concentration and volume of hydrochloric acid that was used to rapidly acidify the humic acid dispersion are quoted. Temperatures are presented as averages of values determined during the course of humic acid acidification.

Table 6.2
Anticipated Acidities, Measured Acidities and Buffering Effects for Humic Acid Acidification

Humic Acid	Final Humic Acid Concentration, HA_f / %w/v	Measured Initial pH	Measured Final pH	Anticipated Final pH	Buffering Effect in $[H^+_{(aq)}]$ / $moldm^{-3}$	Buffering Effect in $[H^+_{(aq)}]$ relative to HA_f / $moldm^{-3}\%w/v^{-1}$
Fluka Humic Acid v3	0.019	11.29	3.33	2.60	2.067E-03	0.10878
	0.025	11.20	2.20	2.19	5.372E-05	2.1487E-03
	1.671	12.62	0.19	0.94	*none*	*none*
Aldrich Humic Acid v1	0.040	9.99	5.53	3.12	7.604E-04	1.901E-02
	0.086	9.63	6.93	3.17	6.685E-04	7.773E-03
	0.088	9.79	7.53	3.32	4.758E-04	5.406E-03
	0.089	9.90	7.95	3.56	2.761E-04	3.102E-03
	0.143	9.77	2.25	1.49	2.674E-02	0.1870
	0.191	9.42	5.92	2.39	4.073E-03	2.132E-02
	1.754	11.85	2.35	1.22	5.56E-02	3.168E-02

Notes:

The anticipated final pH is calculated by assuming that the hydrochloric acid simply neutralises the sodium hydroxide present as the humic acid dispersant. The residual hydrogen ions lead to the anticipated pH. The buffering effect is calculated as the difference between the anticipated and measured hydrogen ion concentrations. This represents the amount of hydrogen ions consumed by the humate on acidification to its protonated form.

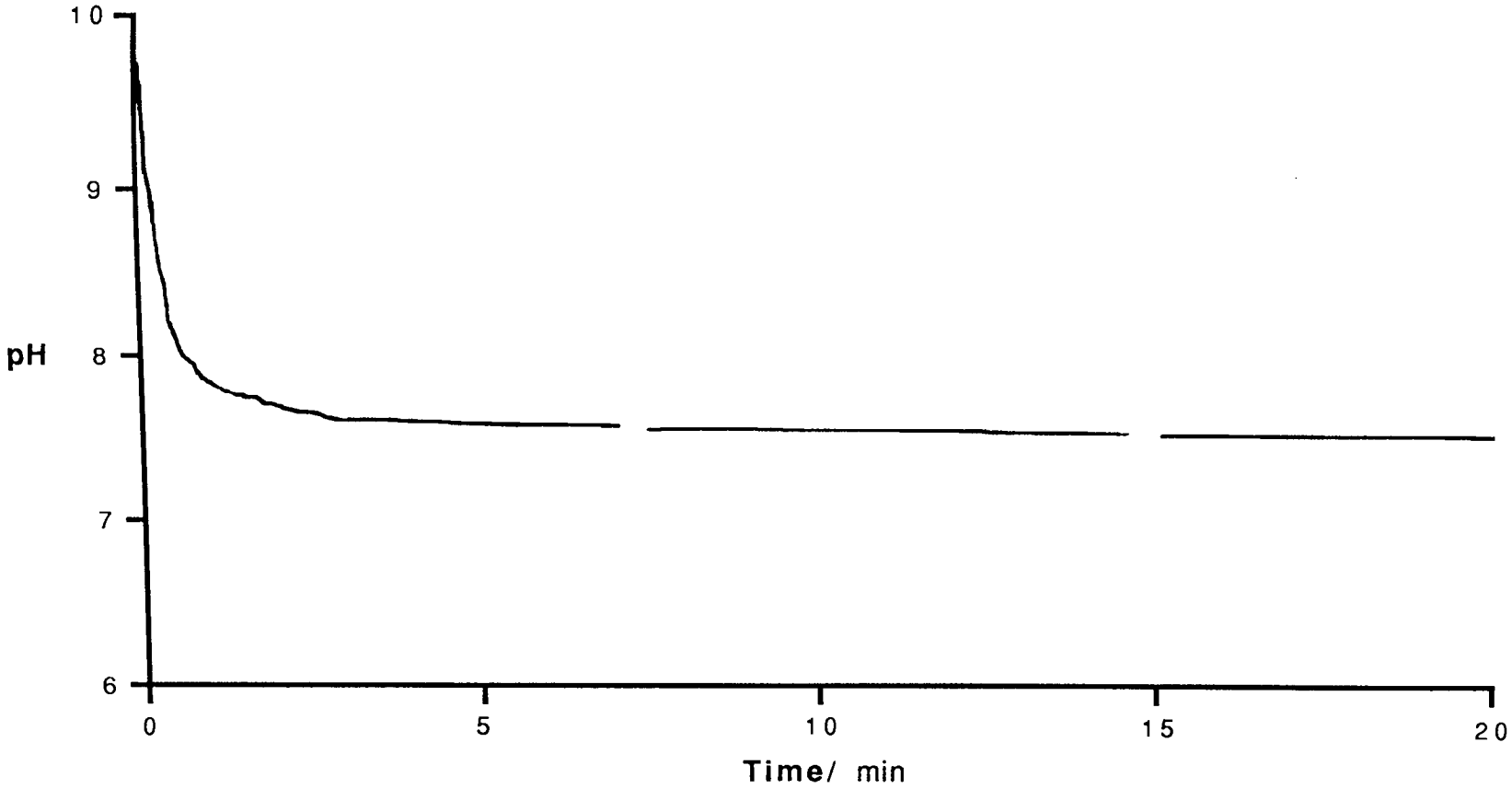

Figure 6.1

Acidification Kinetics of 0.088 %w/v Aldrich Humic Acid in 0.001 M NaOH (aq)

Sample Conditions: Initial Humic Acid Concentration = 0.100 %w/v, Final Humic Acid Concentration = 0.086 %w/v
Acid: 8.0 ml of 0.01166 M HCl (aq); Average temperature = 22.9 °C

Table 6.3

Experimental and Calculated Acidification Kinetics Data for 0.019 % w/v Fluka Humic Acid v3

Time / min	Experimental pH	Experimental ln Δ	Calculated $\ln\alpha - k_1 t$	Experimental ∂ ln Δ	Calculated ∂ ln Δ	Calculated ln Δ	Calculated pH
0.0	11.29	0.000	-1.340	1.340	1.250	-0.090	4.38
0.2	4.00	-0.228	-1.348	1.120	0.997	-0.351	3.84
0.4	3.58	-0.770	-1.356	0.586	0.795	-0.561	3.68
0.6	3.52	-0.959	-1.364	0.406	0.635	-0.730	3.60
0.8	3.52	-0.959	-1.372	0.414	0.506	-0.866	3.55
1.0	3.51	-0.997	-1.380	0.384	0.404	-0.977	3.52
1.2	3.49	-1.081	-1.388	0.308	0.322	-1.066	3.49
1.4	3.48	-1.127	-1.396	0.269	0.257	-1.139	3.48
1.6	3.47	-1.177	-1.404	0.227	0.205	-1.200	3.47
1.8	3.47	-1.177	-1.413	0.236	0.164	-1.249	3.46
2.0	3.46	-1.231	-1.421	0.190	0.130	-1.290	3.45
2.2	3.45	-1.289	-1.429	0.140	0.104	-1.325	3.44
2.4	3.45	-1.289	-1.437	0.148	0.083	-1.354	3.44
2.6	3.44	-1.352	-1.445	0.093	0.066	-1.379	3.44
2.8	3.43	-1.421	-1.453	0.032	0.053	-1.400	3.43
3.0	3.43	-1.421	-1.461	0.040	0.042	-1.419	3.43
3.2	3.43	-1.421	-1.469	0.048	0.034	-1.435	3.43
3.4	3.42	-1.497	-1.477	-0.020	0.027	-1.450	3.43
3.6	3.42	-1.497	-1.485	-0.012	0.021	-1.464	3.42
3.8	3.42	-1.497	-1.493	-0.004	0.017	-1.476	3.42
4.0	3.42	-1.497	-1.501	0.004	0.014	-1.488	3.42
5.0	3.41	-1.581	-1.542			-1.542	3.41
6.0	3.41	-1.581	-1.582			-1.582	3.41
7.0	3.40	-1.676	-1.622			-1.622	3.41
8.0	3.40	-1.676	-1.662			-1.662	3.40
9.0	3.39	-1.782	-1.703			-1.703	3.40
10.0	3.39	-1.782	-1.743			-1.743	3.39

11.0	3.39	-1.782	-1.783			-1.783	3.39
12.0	3.38	-1.904	-1.824			-1.824	3.39
13.0	3.37	-2.047	-1.864			-1.864	3.38
14.0	3.37	-2.047	-1.904			-1.904	3.38
15.0	3.36	-2.218	-1.945			-1.945	3.38
16.0	3.36	-2.218	-1.985			-1.985	3.37
17.0	3.37	-2.047	-2.025			-2.025	3.37
18.0	3.37	-2.047	-2.065			-2.065	3.37
19.0	3.37	-2.047	-2.106			-2.106	3.37
20.0	3.37	-2.047	-2.146			-2.146	3.36
21.0	3.37	-2.047	-2.186			-2.186	3.36
22.0	3.37	-2.047	-2.227			-2.227	3.36
23.0	3.37	-2.047	-2.267			-2.267	3.36
24.0	3.37	-2.047	-2.307			-2.307	3.36
25.0	3.36	-2.218	-2.348			-2.348	3.35
26.0	3.36	-2.218	-2.388			-2.388	3.35
27.0	3.36	-2.218	-2.428			-2.428	3.35
28.0	3.36	-2.218	-2.468			-2.468	3.35
29.0	3.36	-2.218	-2.509			-2.509	3.35
30.0	3.36	-2.218	-2.549			-2.549	3.35
31.0	3.36	-2.218	-2.589			-2.589	3.34
32.0	3.34	-2.706	-2.630			-2.630	3.34
33.0	3.33	-3.100	-2.670			-2.670	3.34
34.0	3.33	-3.100	-2.710			-2.710	3.34
35.0	3.33	-3.100	-2.751			-2.751	3.34
36.0	3.33	-3.100	-2.791			-2.791	3.34
37.0	3.34	-2.706	-2.831			-2.831	3.34
38.0	3.34	-2.706	-2.871			-2.871	3.34
39.0	3.33	-3.100	-2.912			-2.912	3.33
40.0	3.33	-3.100	-2.952			-2.952	3.33

Table 6.4

Experimental and Calculated Acidification Kinetics Data for 1.67 % w/v Fluka Humic Acid v3

Time / min	Experimental pH	Experimental ln Δ	Calculated $\ln\alpha - k_1 t$	Experimental ∂ ln Δ	Calculated ∂ ln Δ	Calculated ln Δ	Calculated pH
0	12.62	0.000	-0.167	0.167	0.190	0.023	
2	1.90	-0.019	-0.181	0.162	0.149	-0.032	1.67
3	1.70	-0.030	-0.189	0.159	0.133	-0.056	1.43
5	1.19	-0.100	-0.203	0.103	0.104	-0.099	1.20
7	1.03	-0.149	-0.218	0.069	0.082	-0.136	1.07
9	0.97	-0.173	-0.232	0.060	0.065	-0.168	0.98
11	0.89	-0.211	-0.247	0.035	0.051	-0.196	0.92
13	0.88	-0.217	-0.261	0.045	0.040	-0.222	0.87
15	0.84	-0.241	-0.276	0.036	0.031	-0.245	0.83
17	0.80	-0.267	-0.291	0.024	0.025	-0.266	0.80
19	0.78	-0.282	-0.305	0.024	0.019	-0.286	0.77
21	0.73	-0.322	-0.320			-0.320	0.73
23	0.71	-0.340	-0.334			-0.334	0.72
25	0.69	-0.360	-0.349			-0.349	0.70
27	0.66	-0.391	-0.364			-0.364	0.69
29	0.62	-0.438	-0.378			-0.378	0.67
31	0.61	-0.451	-0.393			-0.393	0.66
33	0.60	-0.465	-0.407			-0.407	0.65
35	0.60	-0.465	-0.422			-0.422	0.63
37	0.60	-0.465	-0.437			-0.437	0.62
39	0.59	-0.478	-0.451			-0.451	0.61
41	0.58	-0.493	-0.466			-0.466	0.60
43	0.57	-0.508	-0.480			-0.480	0.59
45	0.56	-0.523	-0.495			-0.495	0.58
47	0.55	-0.539	-0.509			-0.509	0.57
49	0.55	-0.539	-0.524			-0.524	0.56
51	0.55	-0.539	-0.539			-0.539	0.55

53	0.54	-0.556	-0.553			-0.553	0.54
55	0.53	-0.574	-0.568			-0.568	0.53
57	0.52	-0.592	-0.582			-0.582	0.53
59	0.52	-0.592	-0.597			-0.597	0.52
61	0.51	-0.611	-0.612			-0.612	0.51
63	0.51	-0.611	-0.626			-0.626	0.50
65	0.51	-0.611	-0.641			-0.641	0.50
69	0.50	-0.631	-0.670			-0.670	0.48
73	0.49	-0.651	-0.699			-0.699	0.47
77	0.46	-0.719	-0.728			-0.728	0.46
81	0.43	-0.798	-0.757			-0.757	0.44
85	0.42	-0.826	-0.787			-0.787	0.43
89	0.41	-0.857	-0.816			-0.816	0.42
93	0.40	-0.889	-0.845			-0.845	0.41
97	0.40	-0.889	-0.874			-0.874	0.40
101	0.40	-0.889	-0.903			-0.903	0.40
105	0.39	-0.923	-0.932			-0.932	0.39
109	0.38	-0.959	-0.962			-0.962	0.38
113	0.37	-0.997	-0.991			-0.991	0.37
117	0.37	-0.997	-1.020			-1.020	0.36
121	0.36	-1.038	-1.049			-1.049	0.36
125	0.35	-1.081	-1.078			-1.078	0.35
129	0.32	-1.231	-1.107			-1.107	0.34
133	0.31	-1.289	-1.137			-1.137	0.34
137	0.31	-1.289	-1.166			-1.166	0.33
141	0.30	-1.352	-1.195			-1.195	0.33
145	0.29	-1.422	-1.224			-1.224	0.32
149	0.28	-1.498	-1.253			-1.253	0.32
153	0.25	-1.783	-1.282			-1.282	0.31
157	0.22	-2.220	-1.312			-1.312	0.31
161	0.21	-2.432	-1.341			-1.341	0.30
165	0.21	-2.432	-1.370			-1.370	0.30
169	0.20	-2.709	-1.399			-1.399	0.29
173	0.19	-3.104	-1.428			-1.428	0.29
177	0.19	-3.104	-1.457			-1.457	0.29
181	0.19	-3.104	-1.487			-1.487	0.28

Table 6.5

Experimental and Calculated Acidification Kinetics Data for 0.088 % w/v Aldrich Humic Acid v1

Time / min	Experimental pH	Experimental ln Δ	Calculated $\ln\alpha - k_1 t$	Experimental ∂ ln Δ	Calculated ∂ ln Δ	Calculated ln Δ	Calculated pH
0.0	9.79	-0.006	-1.560	1.554	1.720	0.160	
0.1	9.38	-0.014	-1.569	1.555	1.626	0.058	
0.2	9.02	-0.033	-1.578	1.545	1.538	-0.040	8.94
0.3	8.59	-0.091	-1.586	1.495	1.454	-0.132	8.44
0.4	8.33	-0.173	-1.595	1.423	1.375	-0.220	8.23
0.5	8.11	-0.305	-1.604	1.299	1.300	-0.304	8.11
0.6	8.01	-0.402	-1.613	1.211	1.229	-0.384	8.03
0.7	7.97	-0.451	-1.622	1.171	1.162	-0.459	7.96
0.8	7.91	-0.539	-1.630	1.091	1.099	-0.531	7.91
0.9	7.87	-0.611	-1.639	1.029	1.039	-0.600	7.88
1.0	7.83	-0.695	-1.648	0.953	0.982	-0.666	7.84
1.1	7.81	-0.744	-1.657	0.913	0.929	-0.728	7.82
1.2	7.79	-0.797	-1.666	0.868	0.878	-0.787	7.79
1.3	7.78	-0.826	-1.674	0.848	0.831	-0.844	7.77
1.4	7.76	-0.888	-1.683	0.795	0.785	-0.898	7.76
1.5	7.75	-0.922	-1.692	0.770	0.743	-0.949	7.74
1.6	7.74	-0.958	-1.701	0.743	0.702	-0.999	7.73
1.7	7.74	-0.958	-1.710	0.751	0.664	-1.046	7.72
1.8	7.71	-1.080	-1.718	0.638	0.628	-1.091	7.71
1.9	7.70	-1.127	-1.727	0.600	0.594	-1.134	7.70
2.0	7.70	-1.127	-1.736	0.609	0.561	-1.175	7.69
2.1	7.68	-1.230	-1.745	0.515	0.531	-1.214	7.68
2.2	7.67	-1.288	-1.754	0.465	0.502	-1.252	7.68
2.3	7.66	-1.351	-1.762	0.411	0.474	-1.288	7.67
2.4	7.66	-1.351	-1.771	0.420	0.449	-1.323	7.66
2.5	7.65	-1.420	-1.780	0.360	0.424	-1.356	7.66
2.6	7.64	-1.496	-1.789	0.293	0.401	-1.388	7.65

2.7	7.63	-1.580	-1.798	0.217	0.379	-1.418	7.65
2.8	7.62	-1.675	-1.806	0.132	0.359	-1.448	7.65
2.9	7.61	-1.781	-1.815	0.034	0.339	-1.476	7.64
3.0	7.61	-1.781	-1.824			-1.824	7.61
4.0	7.60	-1.903	-1.912			-1.912	7.60
5.0	7.59	-2.046	-2.000			-2.000	7.59
6.0	7.59	-2.046	-2.088			-2.088	7.59
7.0	7.58	-2.217	-2.176			-2.176	7.58
8.0	7.57	-2.428	-2.264			-2.264	7.58
9.0	7.57	-2.428	-2.352			-2.352	7.57
10.0	7.57	-2.428	-2.440			-2.440	7.57
11.0	7.57	-2.428	-2.528			-2.528	7.57
12.0	7.57	-2.428	-2.616			-2.616	7.56
13.0	7.56	-2.703	-2.704			-2.704	7.56
14.0	7.56	-2.703	-2.792			-2.792	7.56
15.0	7.55	-3.095	-2.880			-2.880	7.55
16.0	7.54	-3.771	-2.968			-2.968	7.55
17.0	7.54	-3.771	-3.056			-3.056	7.55
18.0	7.53	-8.225	-3.144			-3.144	7.55
19.0	7.53	-8.225	-3.232			-3.232	7.55
20.0	7.53	-8.225	-3.320			-3.320	7.55
21.0	7.53	-8.225	-3.408			-3.408	7.54
22.0	7.53	-8.225	-3.496			-3.496	7.54
23.0	7.53	-8.225	-3.584			-3.584	7.54
24.0	7.53	-8.225	-3.672			-3.672	7.54
25.0	7.53	-8.225	-3.760			-3.760	7.54
26.0	7.53	-8.225	-3.848			-3.848	7.54
27.0	7.53	-8.225	-3.936			-3.936	7.54
28.0	7.53	-8.225	-4.024			-4.024	7.54
29.0	7.53	-8.225	-4.112			-4.112	7.54
30.0	7.53	-8.225	-4.200			-4.200	7.54

Table 6.6

Experimental and Calculated Acidification Kinetics Data for 1.75 % w/v Aldrich Humic Acid v1

Time / min	Experimental pH	Experimental ln Δ	Calculated $\ln\alpha - k_1 t$	Experimental ∂ ln Δ	Calculated ∂ ln Δ	Calculated ln Δ	Calculated pH
0.0	11.85	0.000	-0.445	0.445	0.450	0.005	
0.2	5.30	-0.001	-0.448	0.447	0.403	-0.045	3.70
0.4	4.90	-0.003	-0.452	0.449	0.361	-0.091	3.41
0.6	4.50	-0.007	-0.455	0.448	0.324	-0.131	3.26
0.8	4.10	-0.018	-0.458	0.440	0.290	-0.168	3.16
1.0	4.00	-0.023	-0.462	0.439	0.260	-0.202	3.09
1.2	3.98	-0.024	-0.465	0.441	0.233	-0.232	3.03
1.4	3.95	-0.025	-0.468	0.443	0.208	-0.260	2.99
1.6	3.93	-0.027	-0.472	0.445	0.187	-0.285	2.96
1.8	3.89	-0.029	-0.475	0.446	0.167	-0.308	2.93
2.0	3.76	-0.040	-0.478	0.439	0.150	-0.328	2.90
2.2	3.71	-0.045	-0.482	0.437	0.134	-0.347	2.88
2.4	3.60	-0.058	-0.485	0.427	0.120	-0.365	2.86
2.6	3.52	-0.070	-0.488	0.418	0.108	-0.380	2.85
2.8	3.48	-0.077	-0.491	0.415	0.096	-0.395	2.84
3.0	3.40	-0.093	-0.495	0.402	0.086	-0.408	2.82
3.2	3.32	-0.113	-0.498	0.385	0.077	-0.421	2.81
3.4	3.25	-0.134	-0.501	0.367	0.069	-0.432	2.80
3.6	3.19	-0.156	-0.505	0.349	0.062	-0.443	2.80
3.8	3.04	-0.228	-0.508	0.280	0.056	-0.452	2.79
4.0	2.99	-0.260	-0.511	0.251	0.050	-0.462	2.78
4.2	3.02	-0.240	-0.515	0.274	0.045	-0.470	2.78
4.4	3.05	-0.222	-0.518	0.296	0.040	-0.478	2.77
4.6	2.99	-0.260	-0.521	0.261	0.036	-0.486	2.76
4.8	2.97	-0.274	-0.525	0.251	0.032	-0.493	2.76

5.0	2.96	-0.281	-0.528	0.247	0.029	-0.499	2.76
5.2	2.89	-0.340	-0.531	0.191	0.026	-0.506	2.75
5.4	2.82	-0.413	-0.535	0.121	0.023	-0.512	2.75
5.6	2.80	-0.438	-0.538	0.100	0.021	-0.517	2.74
5.8	2.78	-0.464	-0.541	0.077	0.019	-0.523	2.74
6.0	2.77	-0.478	-0.545	0.067	0.017	-0.528	2.74
7.0	2.75	-0.507	-0.561			-0.561	2.72
8.0	2.74	-0.523	-0.578			-0.578	2.71
9.0	2.72	-0.556	-0.594			-0.594	2.70
10.0	2.71	-0.573	-0.611			-0.611	2.69
11.0	2.70	-0.591	-0.628			-0.628	2.68
12.0	2.70	-0.591	-0.644			-0.644	2.67
13.0	2.68	-0.630	-0.661			-0.661	2.67
14.0	2.66	-0.672	-0.677			-0.677	2.66
15.0	2.65	-0.695	-0.694			-0.694	2.65
16.0	2.64	-0.718	-0.711			-0.711	2.64
17.0	2.63	-0.743	-0.727			-0.727	2.64
18.0	2.62	-0.769	-0.744			-0.744	2.63
19.0	2.61	-0.797	-0.760			-0.760	2.62
20.0	2.59	-0.856	-0.777			-0.777	2.62
22.0	2.58	-0.888	-0.810			-0.810	2.61
24.0	2.57	-0.922	-0.843			-0.843	2.59
26.0	2.57	-0.922	-0.877			-0.877	2.58
28.0	2.56	-0.958	-0.910			-0.910	2.57
30.0	2.56	-0.958	-0.943			-0.943	2.56
32.0	2.55	-0.996	-0.976			-0.976	2.56
34.0	2.54	-1.036	-1.009			-1.009	2.55
36.0	2.53	-1.079	-1.043			-1.043	2.54
38.0	2.52	-1.126	-1.076			-1.076	2.53
40.0	2.52	-1.126	-1.109			-1.109	2.52
42.0	2.51	-1.176	-1.142			-1.142	2.52
44.0	2.50	-1.229	-1.175			-1.175	2.51
46.0	2.50	-1.229	-1.209			-1.209	2.50

48.0	2.50	-1.229	-1.242			-1.242	2.50
50.0	2.50	-1.229	-1.275			-1.275	2.49
52.0	2.49	-1.287	-1.308			-1.308	2.49
54.0	2.49	-1.287	-1.341			-1.341	2.48
56.0	2.48	-1.350	-1.375			-1.375	2.48
58.0	2.48	-1.350	-1.408			-1.408	2.47
60.0	2.47	-1.419	-1.441			-1.441	2.47
62.0	2.47	-1.419	-1.474			-1.474	2.46
64.0	2.46	-1.495	-1.507			-1.507	2.46
66.0	2.46	-1.495	-1.541			-1.541	2.45
68.0	2.45	-1.579	-1.574			-1.574	2.45
70.0	2.44	-1.673	-1.607			-1.607	2.45
72.0	2.43	-1.779	-1.640			-1.640	2.44
74.0	2.42	-1.901	-1.673			-1.673	2.44
76.0	2.42	-1.901	-1.707			-1.707	2.44
78.0	2.41	-2.043	-1.740			-1.740	2.43
80.0	2.41	-2.043	-1.773			-1.773	2.43
90.0	2.39	-2.423	-1.939			-1.939	2.42
100.0	2.38	-2.697	-2.105			-2.105	2.41
110.0	2.36	-3.753	-2.271			-2.271	2.40
120.0	2.36	-3.753	-2.437			-2.437	2.39
130.0	2.36	-3.753	-2.603			-2.603	2.38
140.0	2.36	-3.753	-2.769			-2.769	2.38
150.0	2.36	-3.753	-2.935			-2.935	2.37
160.0	2.36	-3.753	-3.101			-3.101	2.37

Figure 6.2
Acidification Kinetics for 0.019 % w/v Fluka Humic Acid v3
Experimental and Calculated ln Δ Against Time
(Straight Section Analysis, Partial Data Set)

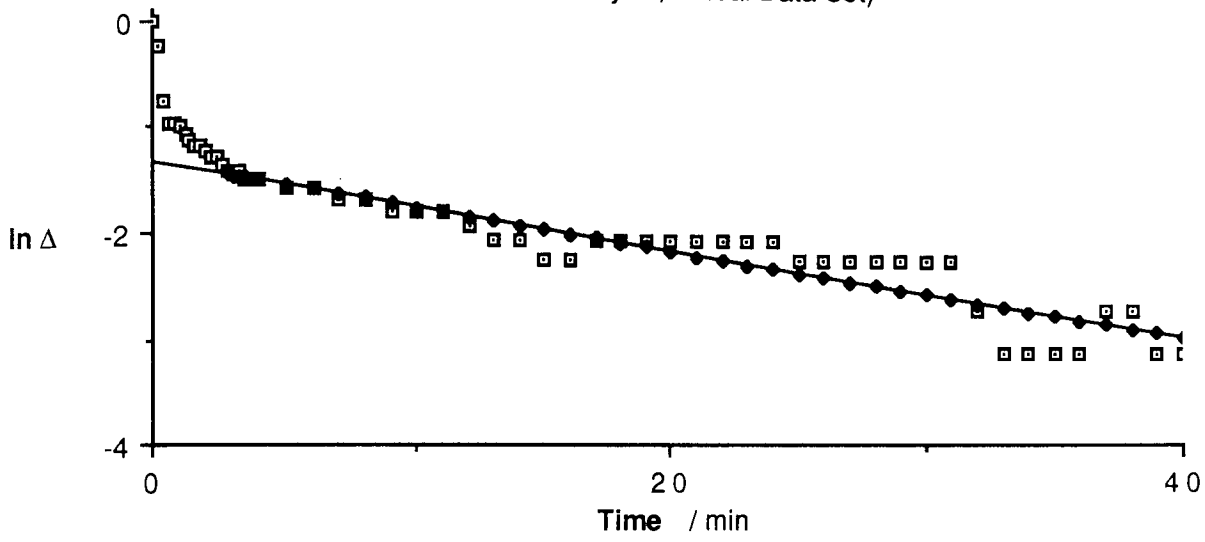

Constants: [H+]∞ = 4.90e-4; a = 0.262; k1 = 0.0403

Experimental ln Δ ◆ Calculated ln Δ

Figure 6.3
Acidification Kinetics for 0.019 % w/v Fluka Humic Acid v3
Experimental and Calculated ∂ ln Δ Against Time
(Curved Section Analysis, Partial Data Set)

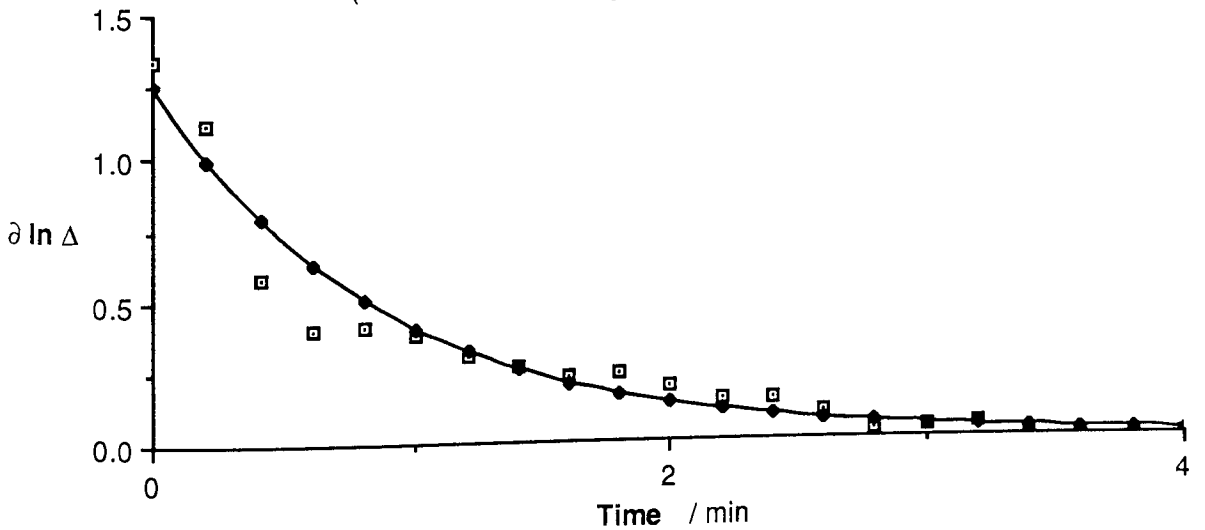

Constants: [H+]∞ = 4.90e-4; a = 0.262; β = -0.328; k1 = 0.0403; k2 = 1.17

Experimental ∂ ln Δ ◆ Calculated ∂ ln Δ

Figure 6.4
Acidification Kinetics for 0.019 % w/v Fluka Humic Acid v3
Experimental and Calculated ln Δ Against Time
(Straight and Curved Section Analyses, Full Data Set)

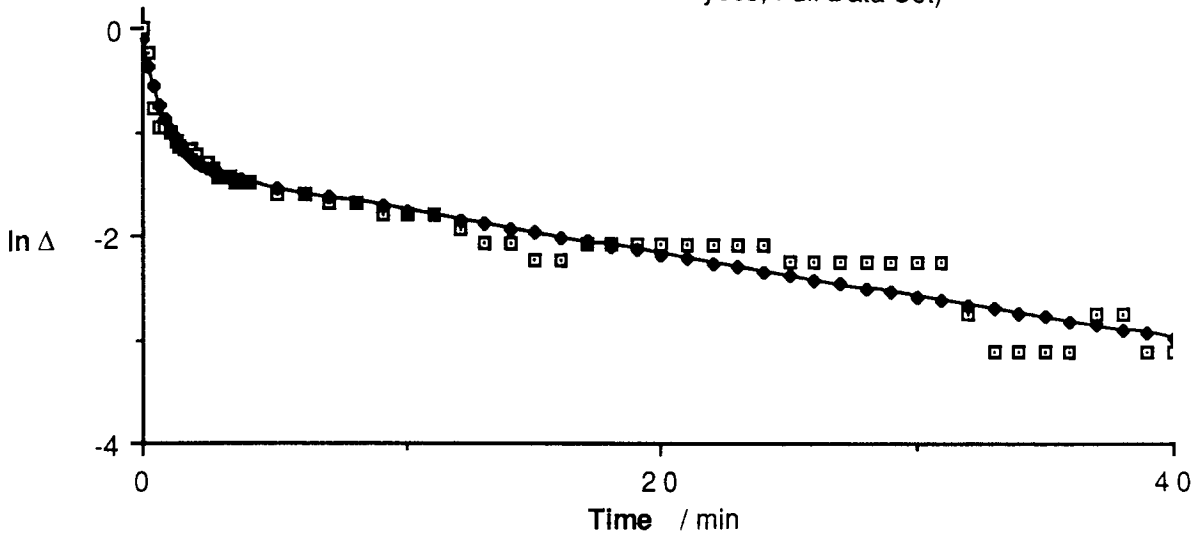

Constants: [H+]∞ = 4.90e-4; a = 0.262; ß = -0.328; k1 = 0.0403; k2 = 1.17

Experimental ln Δ ◆ Calculated ln Δ

Figure 6.5
Acidification Kinetics for 0.019 % w/v Fluka Humic Acid v3
Experimental and Calculated pH Against Time
(Partial Data Set)

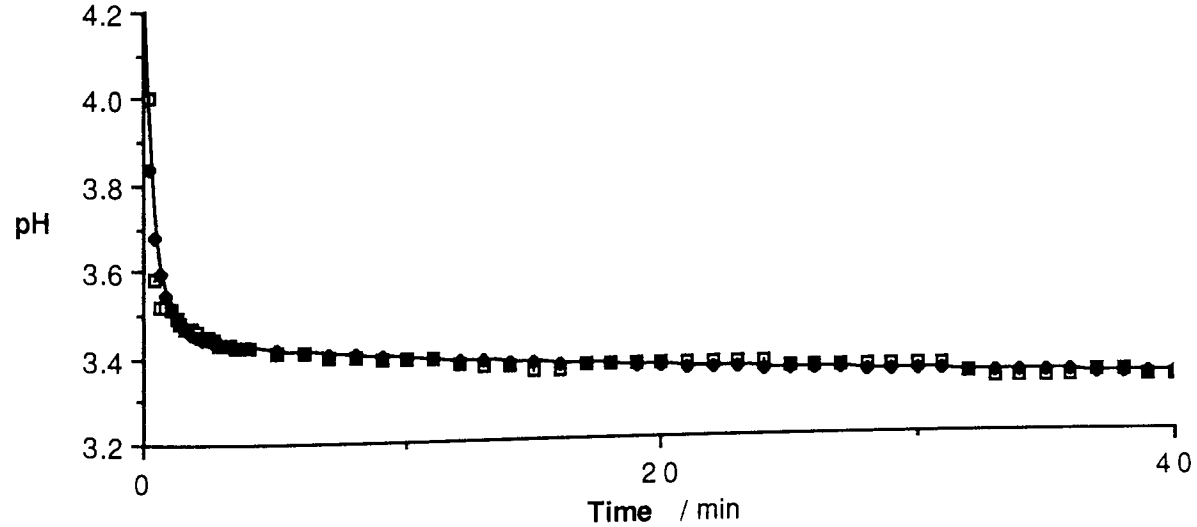

Constants: [H+]∞ = 4.90e-4; a = 0.262; ß = -0.328; k1 = 0.0403; k2 = 1.17

Experimental pH ◆ Calculated pH

Figure 6.6
Acidification Kinetics for 1.67 % w/v Fluka Humic Acid v3
Experimental and Calculated ln Δ Against Time
(Straight Section Analysis, Full Data Set)

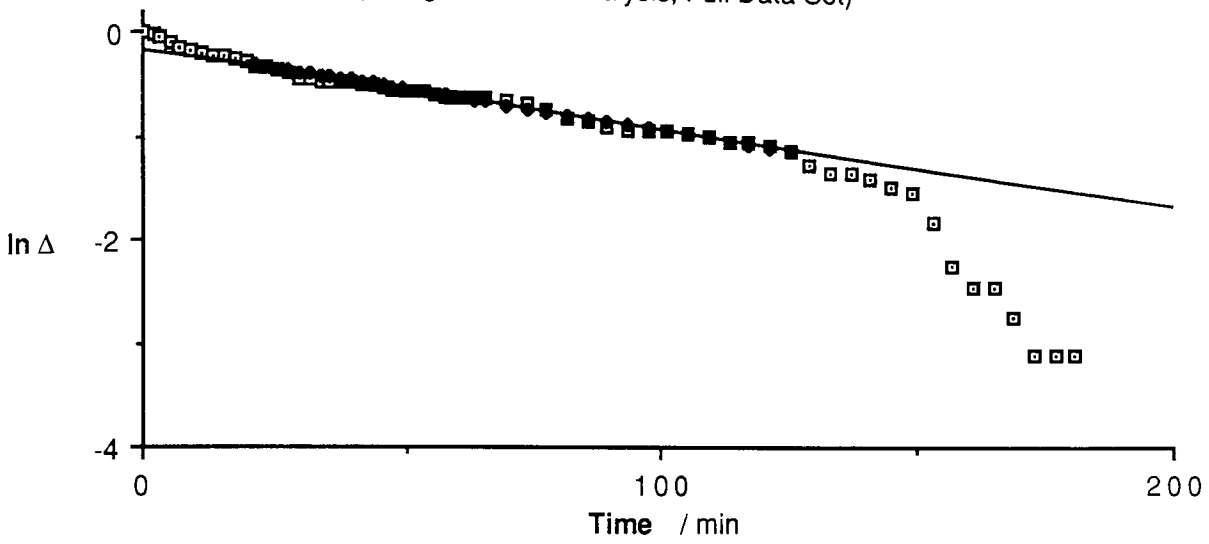

Constants: [H+]∞ = 0.676; a = 0.846; k1 = 0.00729

Experimental ln Δ Calculated ln Δ

Figure 6.7
Acidification Kinetics for 1.67 % w/v Fluka Humic Acid v3
Experimental and Calculated ∂ ln Δ Against Time
(Curved Section Analysis, Partial Data Set)

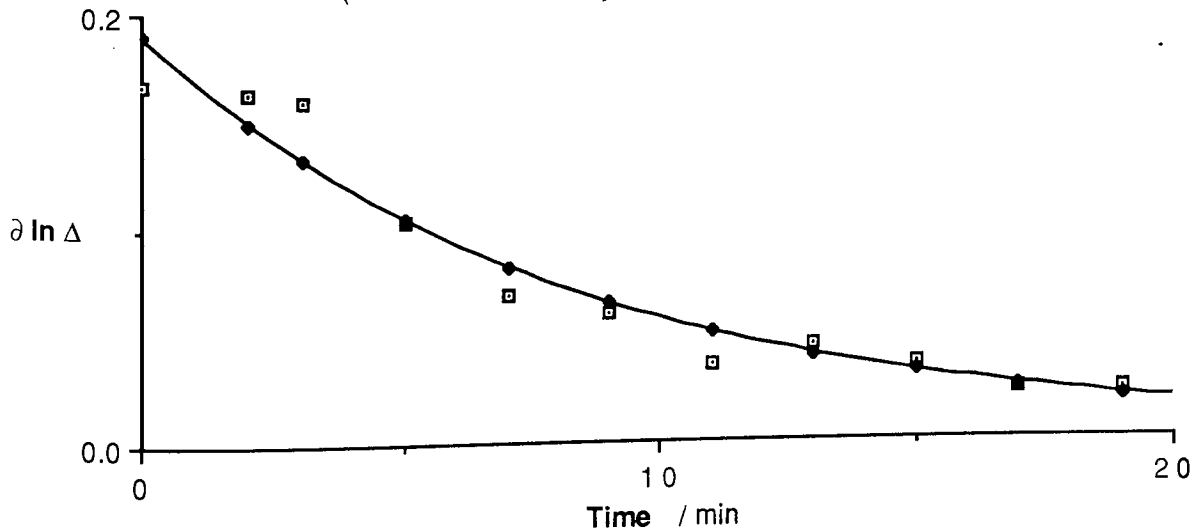

Constants: [H+]∞ = 0.676; a = 0.846; ß = -0.161; k1 = 0.00729; k2 = 0.127

Experimental ∂ ln Δ Calculated ∂ ln Δ

Figure 6.8
Acidification Kinetics for 1.67 % w/v Fluka Humic Acid v3
Experimental and Calculated ln Δ Against Time
(Straight and Curved Section Analyses, Partial Data Set)

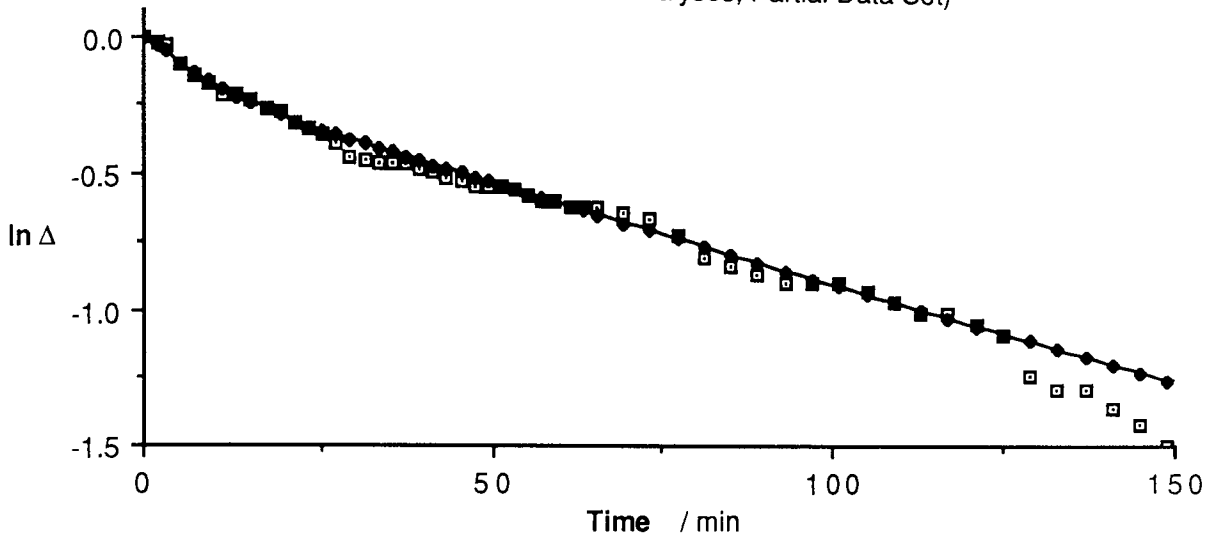

Constants: [H+]∞ = 0.676; a = 0.846; ß = -0.161; k1 = 0.00729; k2 = 0.127

Experimental ln Δ ◆ Calculated ln Δ

Figure 6.9
Acidification Kinetics for 1.67 % w/v Fluka Humic Acid v3
Experimental and Calculated pH Against Time
(Partial Data Set)

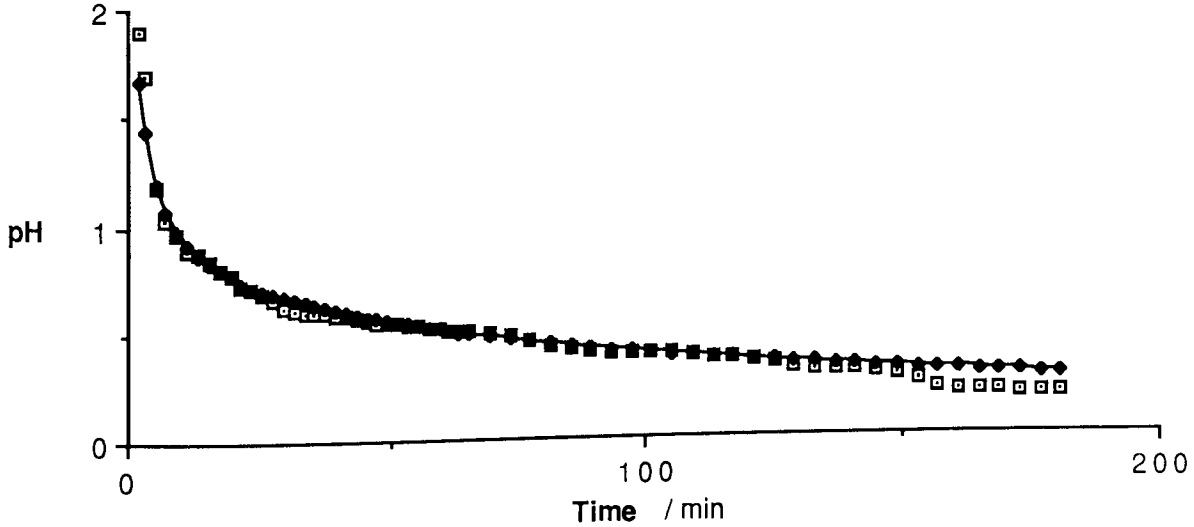

Constants: [H+]∞ = 0.676; a = 0.846; ß = -0.161; k1 = 0.00729; k2 = 0.127

Experimental pH ◆ Calculated pH

Figure 6.10

Acidification Kinetics for 0.088 % w/v Aldrich Humic Acid v1

Experimental and Calculated ln Δ Against Time

(Straight Section Data Analysis, Partial Data Set)

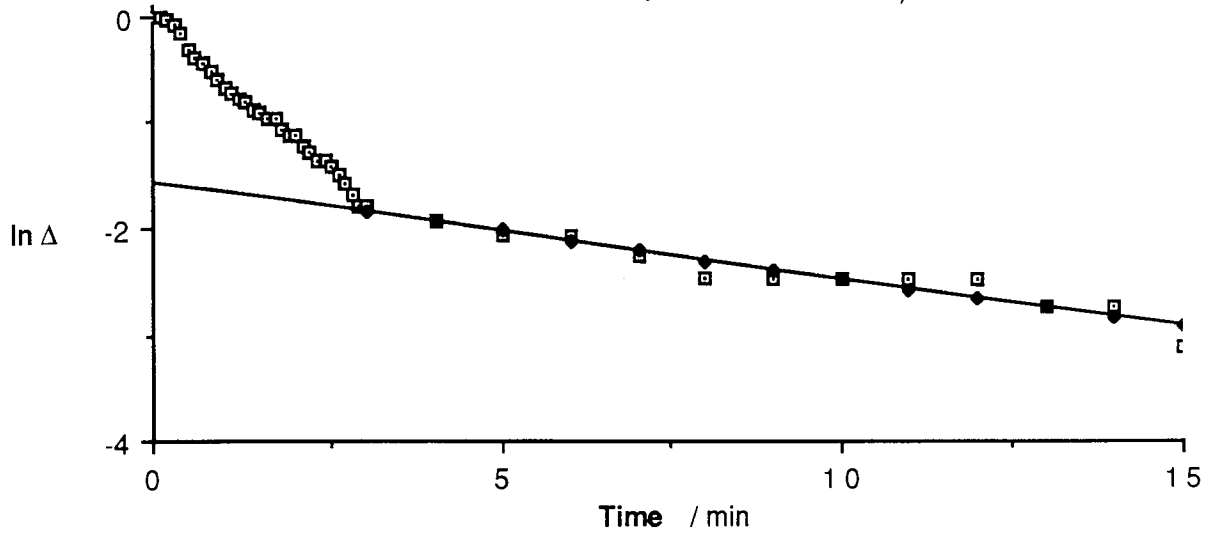

Constants: [H+]∞ = 2.95e-8; a = 0.210; k1 =0.088

Experimental ln Δ ◆ Calculated ln Δ

Figure 6.11

Acidification Kinetics for 0.088 % w/v Aldrich Humic Acid v1

Experimental and Calculated ∂ ln Δ Against Time

(Curved Section Analysis, Partial Data Set)

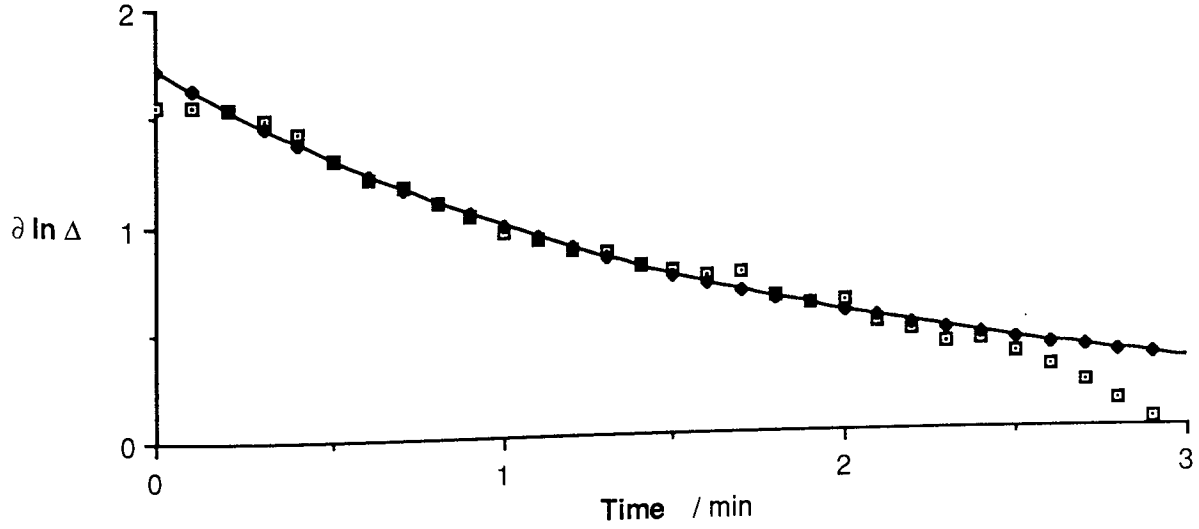

Constants: [H+]∞ = 2.95e-8; a = 0.210; β = -0.36; k1 = 0.088; k2 = 0.648

Experimental ∂ ln Δ ◆ Calculated ∂ ln Δ

Figure 6.12

Acidification Kinetics for 0.088 % w/v Aldrich Humic Acid v1

Experimental and Calculated ln Δ Against Time

(Straight and Curved Section Analyses, Partial Data Set)

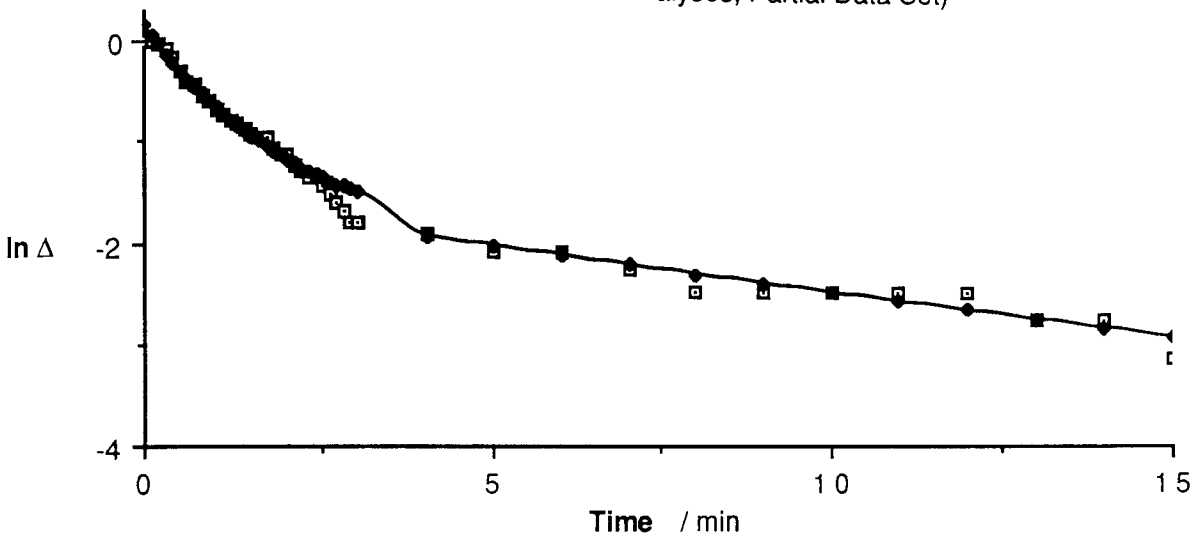

Constants: [H+]∞ = 2.95e-8; a = 0.210; ß = -0.36; k1 = 0.088; k2 = 0.648

Experimental ln Δ ◆ Calculated ln Δ

Figure 6.13

Acidification Kinetics for 0.088 % w/v Aldrich Humic Acid v1

Experimental and Calculated pH Against Time

(Partial Data Set)

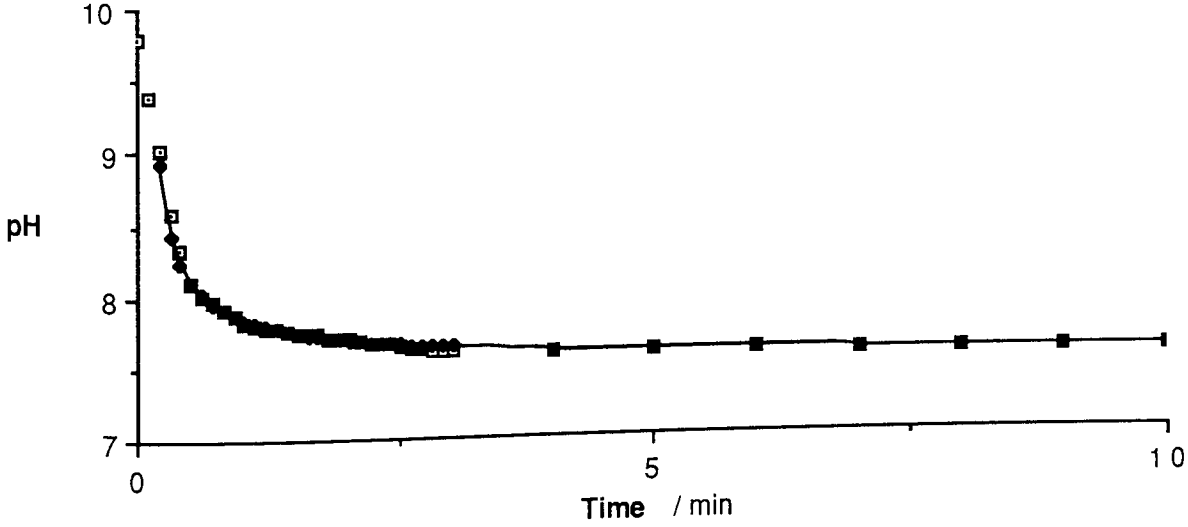

Constants: [H+]∞ = 2.95e-8; a = 0.210; ß = -0.36; k1 = 0.088; k2 = 0.648

Experimental pH ◆ Calculated pH

Figure 6.14
Acidification Kinetics for 1.75 % w/v Aldrich Humic Acid v1
Experimental and Calculated ln Δ Against Time

(Straight Section Analysis, Partial Data Set)

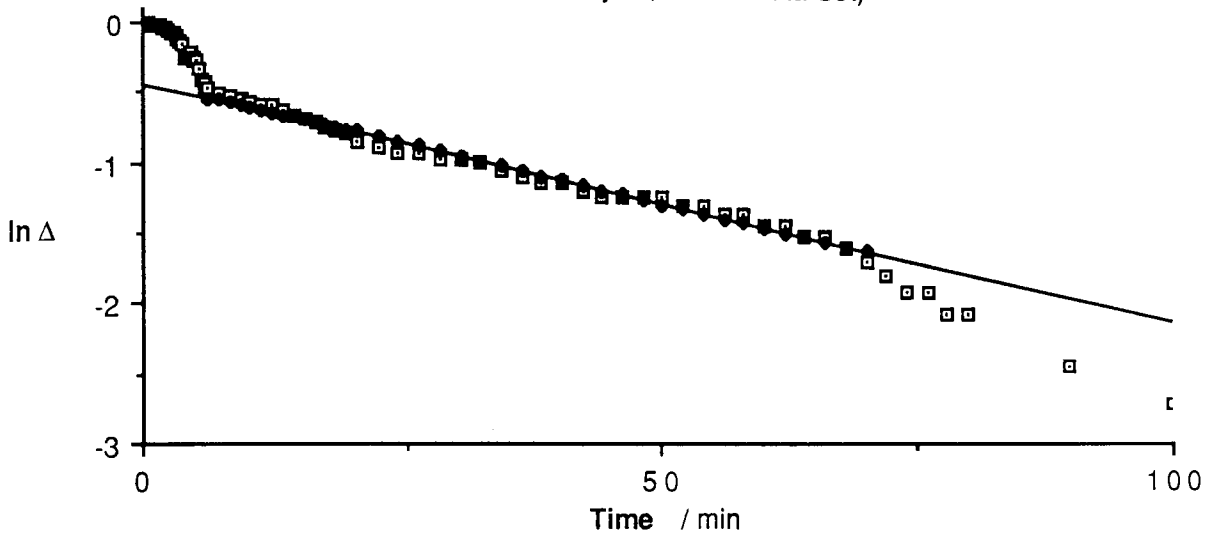

Constants: [H+]∞ = 4.47e-3; a = 0.641; k1 = 0.0166

Experimental ln Δ Calculated ln Δ

Figure 6.15
Acidification Kinetics for 1.75 % w/v Aldrich Humic Acid v1
Experimental and Calculated ∂ ln Δ Against Time

(Curved Section Analysis; Partial Data Set)

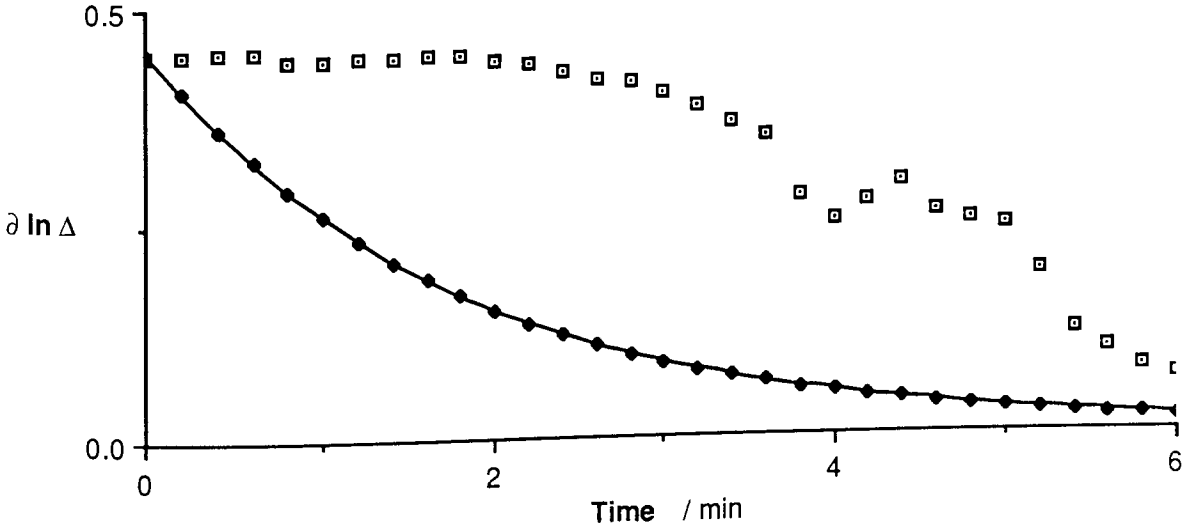

Constants: [H+]∞ = 4.47e-3; a = 0.641; ß = -0.288; k1 =0.0166; k2 = 0.567

Experimental ∂ ln Δ Calculated ∂ ln Δ

Figure 6.16
Acidification Kinetics for 1.75 % w/v Aldrich Humic Acid v1
Experimental and Calculated ln Δ Against Time
(Straight and Curved Section Analyses, Partial Data Set)

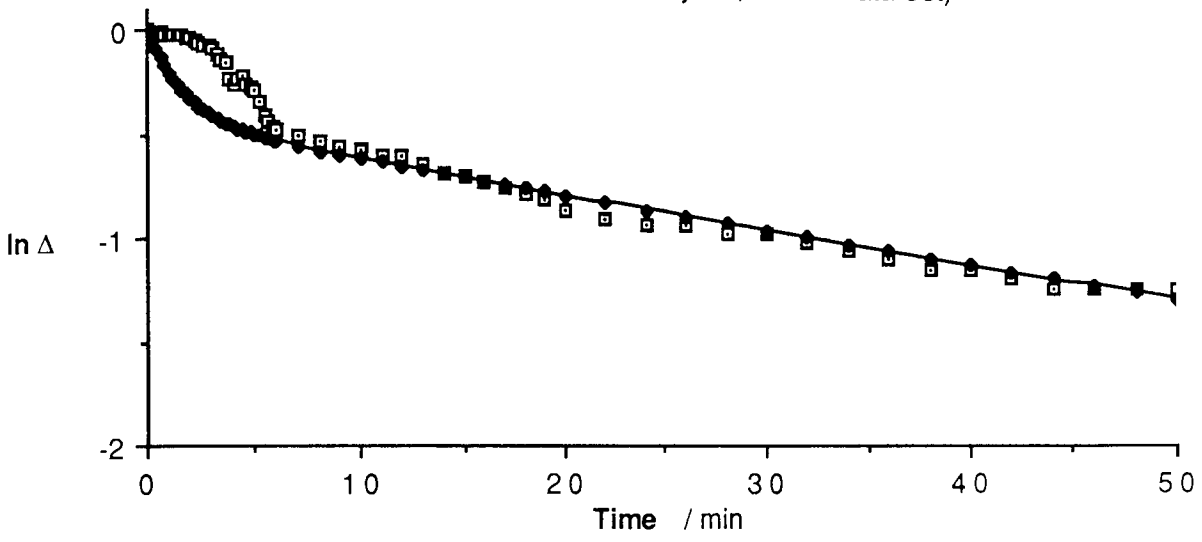

Constants: [H+]∞ = 4.47e-3; a = 0.641; ß = -0.288; k1 =0.0166; k2 = 0.567

Experimental ln Δ ◆ Calculated ln Δ

Figure 6.17
Acidification Kinetics for 1.75 % w/v Aldrich Humic Acid v1
Experimental and Calculated pH Against Time
(Partial Data Set)

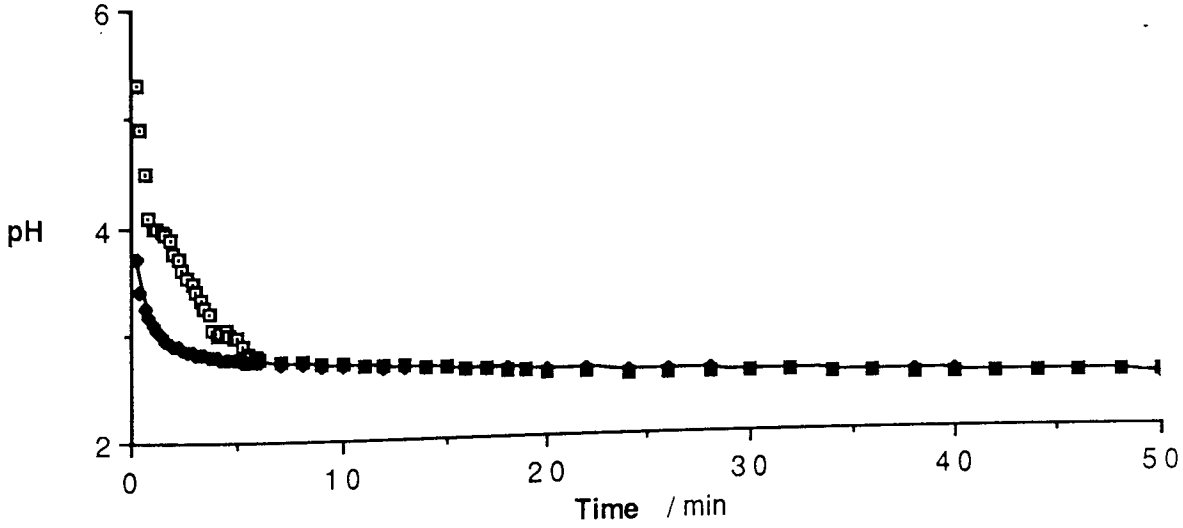

Constants: [H+]∞ = 4.47e-3; a = 0.641; ß = -0.288; k1 = 0.0166; k2 = 0.567

Experimental pH ◆ Calculated pH

The graphs presented in Figures 6.2–6.17 are of various functions derived from the protonation data to enable derivation of kinetic parameters. The origins of the plotted functions are discussed in Section 6.4.4. All plotted data is unsmoothed although some partial sets have been used to highlight relevant features. Note that Figures 6.5, 6.9, 6.13 and 6.17 are graphs of the experimentally determined pH against time with the corresponding calculated pH's superimposed. The humic acid concentrations given on the graphs are final concentrations and may be correlated with the sample compositions given in Table 6.1.

6.4 Discussion

6.4.1 General Points Concerning Potentiometric Titrations

All graphs of pH against time for the protonation of both Fluka and Aldrich humic acids under various media conditions show similar characteristics, namely a rapid decrease in pH following addition of acid to the alkaline medium, and a slower change in pH with a variable time-scale ranging from several minutes to a few hours. All but one of the sample conditions studied displayed a marked buffering effect with anticipated pH values not realised experimentally.

For Fluka Humic Acid, the effect of its concentration on equilibration times is not clear since both a low and high humic acid concentration produced prolonged pH changes. Further, there appears to be no relationship between the acid dosages applied to the samples and equilibration times. The time-scales observed are much greater than those discussed in Section 6.1.4, however the equilibration time is dependent on the experimental conditions selected and the point at which it is decided that equilibrium has been reached.

Despite studying more samples and conditions for Aldrich humic acid, the general kinetic behaviour is again unclear. The effect of high humic acid concentrations is not apparent since the most concentrated sample produced prolonged changes in pH, but the second-most concentrated sample resulted in very rapid equilibration. This created some doubt in the reliability and reproducibility of the pH measurements and prompted a re–examination of experimental methodology.

6.4.2 Reliability and Reproducibility of Measurements

Some doubt exists concerning the reliability and reproducibility of the pH measurements in potentiometric titrations. It is suspected that selection of a set of experimental conditions for a given humic acid sample may not necessarily result in reproducible effects. Although no samples were repeated using exactly the same conditions, one set of Aldrich humic acid samples using a slight gradation in acidification dosage produced similar effects in both the shape and duration of the pH against time graphs, and the magnitude of the buffering effect. However, although reproducibility is evident in this case, it cannot be stated with certainty that this was general. Most of the likely sources of problems identified focus on measurement of the acidity of the medium, hence several experiments are briefly described that investigate the pH measurement. Some attention is also paid to other matters concerned with the experimental techniques and design.

The response time of the pH electrode and meter was assessed by monitoring a simple neutralisation in which excess mineral acid was added to some dilute alkali. An instantaneous pH change was registered on the pH meter following addition of the acid implying that the response of the electrode and meter was not suspect. The electrode electrolyte was replaced in case this was the origin of the problem. A repeat of the simple neutralisation described above also produced an instantaneous response.

During potentiometric titrations, the pH electrode was continually immersed in the humic acid dispersion for periods of up to three hours. In this time it is possible that some acidified humic material may have been deposited on the surface of the glass electrode thus affecting the sensitivity of the electrode membrane to protons. Following one such prolonged kinetic run, the combination electrode was transferred to a beaker containing the minimum volume of dilute sodium hydroxide to immerse the electrode membrane. The contents of the beaker were then agitated by ultrasonic vibration (¢042) for several minutes to assist desorption of any humic matter from the electrode. The resultant solution was analysed optically by transferring it to a 4 cm path length quartz cuvette and assessing its ultra-violet absorbance against a dilute sodium hydroxide reference on the Pye-Unicam SP8–100 Spectrophotometer (¢029). Despite selecting the most sensitive range for absorption of radiation by humic acid (see Section 2.5), no

absorbance above background levels was observed. Therefore adsorption of humic matter on the pH electrode was not a source of problems.

The possibility of atmospheric gases affecting the samples and their supporting media in the same way as others noted [249,263,272] was discounted since the samples were maintained under an inert atmosphere during pH measurements. However, one related refinement not considered in the experimental design was that the bleed of nitrogen may have assisted the loss of water from the dispersion medium since the equilibrium vapour pressure of water would have been continually reduced by its removal. This would have an effect on the pH of the medium since its total volume would be reduced, although it is likely that this effect is unimportant since the dispersions were maintained at 25 °C.

A possible complication that derives from the preparation of the stock dispersions from the Aldrich and Fluka humic acid solids is that the dispersions were not necessarily of the same age when protonation experiments were carried out on them. Although samples were equilibrated at least overnight before use, some of the dispersion may not have been used until several days after preparation. Bearing in mind the results described in this Chapter, it is possible that the samples underwent some equilibration changes during this standing time. The preparation and usage dates of the samples were not recorded.

Non-humic components of the samples may be the origin of some effects. These may arise since the samples contain residual amounts of non-organic matter (see Sections 1.7, 2.2 & 2.4). The presence of multivalent cations could provide a contribution to the buffering effect through their hydrolysis, although it is unlikely that they would exist independently from the humic material. It is doubtful that non-humic matter would have a marked effect on the protonation behaviour since it accounts for only a small proportion of the mass. Mathuthu attributed some of the buffering effects in potentiometric titrations in the presence of europium ions to hydrolysis equilibria of the metal ion. Similar observations were made with the cupric ion. [245]

Some sources of problems considered above can therefore be discounted but there is some doubt concerning the role of water vapour in the nitrogen gas flow, and the extent of aging in the samples. However, it appears that the experimental observations genuinely derive from the humic acid samples rather than from experimental artifacts. This has prompted the derivation of a kinetic scheme to model experimental data and the proposal of a

mechanism to account for the experimental observations.

6.4.3 Buffering Effects on Protonation

All but one of the sample conditions studied displayed a marked buffering effect with anticipated pH values not realised experimentally. The extent of the buffering effect is given in Table 6.2 in terms of undetected hydrogen ions. The final column also provides this measure relative to the humic acid concentration.

One Fluka humic acid sample does not appear show a buffering effect. Its final pH value is too low considering the magnitude of the acid addition. The problem probably arises from incorrect calibration of the pH meter. With an initial Aldrich humic acid concentration of 0·100 % w/v, an increase in the volume of acid added to three separate samples resulted in an increased buffering effect whilst the final humic acid concentration was nearly constant. The extra acid added was not proportionately realised in the pH measurement since more protons were retained by the organic matter. Here, buffering occurs in the near-neutral pH region and may be accounted for by carboxylate to carboxyl protonation equilibria. The acid additions were sufficient to protonate the carboxylate groups since the pK_a's of carboxyls are typically above the anticipated pH's. [6]

Calculation of the amount of hydrogen ions required to protonate the carboxylate and other anionic humic acid functional groups accounts for around half the buffering effect of Aldrich humic acid, based on typical functional group analyses. [6] The calculation makes an assumption of the existence of a direct relationship between the humic acid concentration and the proton requirements. Note that the rest of the protons retained by the organic matter may be accounted for by the mechanism discussed in Section 6.4.5.

Analysis of the buffering data for Aldrich humic acid in Table 6.2 reveals that the buffering effect is closely related to the anticipated pH. Extensive buffering is noted with large hydrochloric acid additions that would be expected to result in low pH values. There is less correlation between buffering and the humic acid concentration, as suggested by data in the last column of Table 6.2. Therefore the dominant effect in determining the extent of the buffering action is the amount of acid that is added, rather than the concentration of the humic acid.

Buffering by humic matter relies on equilibria involving the protonation of anionic functional groups, particularly the abundant carboxylates. Mathuthu correlated buffering in the potentiometric titrations of fulvic acid with the presence of functional groups of different acidities.[245] Ephraim explained the buffering in his non-aqueous titration of fulvic acid by the heterogeneity of the samples.[244] Wilson and Kinney attributed their observation of a buffering effect between pH 12 and the equivalence point to the protonation of the phenolate anion.[261] Gamble stated that once all the ion exchange sites had been converted to their protonated form, the pH buffering capacity of humic acid would be lost.[269]

6.4.4 Analysis Scheme for Protonation Data

The nature of the changes observed in the pH of the media supporting the humic acids with time has prompted a kinetic analysis of the data to determine if the hydrogen ion concentrations can be modelled and kinetic parameters derived. A scheme is presented that attempts to model these changes. Typical graphs of pH against time (see Figures 6.5, 6.9, 6.13, 6.17) suggest that two processes may operate, and that the pH tends to an equilibrium value. The scheme incorporates these observations by proposing three forms of humic acid, A, B and C, and two equilibria in which they interconvert and release protons. Species A is the first protonated form of the humic acid following acidification of the medium. Note that involvement of three humic species and release of protons in each stage is not a requirement, but the scheme is capable of accounting for this. Since only protons were measured experimentally, the scheme is directed towards a model that uses proton concentration data.

Consider a humate dispersion that has been rapidly acidified and is undergoing slower step-wise changes with concomitant release of some protons in each forward reaction. This is represented by the following two-step scheme:

$$A \underset{k_{-1}}{\overset{k_1}{\rightleftharpoons}} B + x\,H^+ \qquad (1)$$

$$B \underset{k_{-2}}{\overset{k_2}{\rightleftharpoons}} C + (y - x)\,H^+ \qquad (2)$$

The number of protons produced in each stage is represented by x and (y – x), and the forward rate constants by k_1 and k_2. The values of the rate constants determine the shape of plots of pH against time. Typical experimental graphs tend towards an equilibrium pH condition that may correspond to the conversion of all A to C. If so, the reactions 1 and 2 could be summarised as an overall equation:

$$A \rightarrow C + y\,H^+ \qquad (3)$$

Attainment of this condition enables the proton concentration at infinite time, $[H^+]_\infty$ to be related to $[A]_0$, the initial concentration of species A:

$$[H]_\infty = y\,[A]_0 \qquad (4)$$

To enable development of equations that model the behaviour observed experimentally, the system needs to be simplified, therefore only the forward reactions of equations 1 and 2 are considered. The concentrations of A, B and C at any time t, can be represented by standard kinetic integrals:

$$[A]_t = [A]_0\, e^{-k_1 t} \qquad (5)$$

$$[B]_t = \frac{k_1\,[A]_0}{k_2 - k_1}\left(e^{-k_1 t} - e^{-k_2 t}\right) \qquad (6)$$

$$[C]_t = [A]_0\left(1 - \frac{k_2\,e^{-k_1 t} - k_1\,e^{-k_2 t}}{k_2 - k_1}\right) \qquad (7)$$

The instantaneous proton concentration $[H^+]_t$, is related to the concentrations of species B and C by:

$$[H^+]_t = x\,[B]_t + y\,[C]_t \qquad (8)$$

Substitution of the integrals for $[B]_t$ and $[C]_t$ from equations 6 and 7 leads to:

$$[H]_t = x\frac{k_1[A]_0}{k_2 - k_1}\left(e^{-k_1 t} - e^{-k_2 t}\right) + y[A]_0\left(1 - \frac{k_2 e^{-k_1 t} - k_1 e^{-k_2 t}}{k_2 - k_1}\right) \qquad (9)$$

Recalling equation 4 enables the initial concentration of A to be replaced in equation 9 by $[H]_\infty$, a measurable value:

$$y\frac{[H^+]_t}{[H^+]_\infty} = x\frac{k_1}{k_2 - k_1}\left(e^{-k_1 t} - e^{-k_2 t}\right) + y\left(1 - \frac{k_2 e^{-k_1 t} - k_1 e^{-k_2 t}}{k_2 - k_1}\right)$$

Therefore:

$$(k_2 - k_1)y\left(\frac{[H^+]_\infty - [H^+]_t}{[H^+]_\infty}\right) = x k_1\left(e^{-k_2 t} - e^{-k_1 t}\right) + y\left(k_2 e^{-k_1 t} - k_1 e^{-k_2 t}\right)$$

This may be simplified to yield equation 10, a two part expression for the proton concentration as a function of time:

$$\left(\frac{[H^+]_\infty - [H^+]_t}{[H^+]_\infty}\right) = \frac{(y k_2 - x k_1)}{y(k_2 - k_1)}e^{-k_1 t} - \frac{k_1(y - x)}{y(k_2 - k_1)}e^{-k_2 t} \qquad (10)$$

Consideration of the shape of the plots of pH against time suggests that one exponential term dominates and controls the overall kinetics. This one will have the smallest rate constant, and in the first instance it will be *assumed* that $k_1 < k_2$, although the treatment applies equally for the converse. Equation 10 is simplified by defining the function as Δ in terms of the constants α and β, which are multipliers of the two exponentials:

$$\Delta = \left(\frac{[H^+]_\infty - [H^+]_t}{[H^+]_\infty}\right) \qquad (11)$$

$$\alpha = \frac{(y k_2 - x k_1)}{y(k_2 - k_1)} \qquad (12)$$

$$\beta = \frac{k_1(y - x)}{y(k_2 - k_1)} \qquad (13)$$

Therefore,

$$\Delta = \alpha e^{-k_1 t} - \beta e^{-k_2 t} \qquad (14)$$

Since the aim is to produce an equation that models the protonation data, the last equation is simplified in the following sequence, first by factorisation:

$$\Delta = \alpha e^{-k_1 t}\left(1 - \frac{\beta}{\alpha} e^{-(k_2 - k_1)t}\right)$$

$$\therefore \ln\Delta = \ln\alpha - k_1 t + \ln\left(1 - \frac{\beta}{\alpha} e^{-(k_2 - k_1)t}\right) \qquad (15)$$

Secondly, the final term of the expression can be simplified by applying the following general approximation (in which c is a small variable):

$$\ln(1 - c) \approx -c$$

Therefore:

$$\ln\Delta = \ln\alpha - k_1 t - \frac{\beta}{\alpha} e^{-(k_2 - k_1)t} \qquad (16)$$

Equation 16 represents a useful form for modelling the proton concentration data. This has been applied to four humic acid samples resulting in the graphs of Figures 6.2–6.17 and the calculated data presented in Tables 6.3–6.6. The calculation procedures used to derive these are described and then the results for individual samples are discussed.

The function Δ is defined using the proton concentration at a given time, $[H+]_t$ and that at infinite time, $[H+]_\infty$. Experimental values for the latter are available as pH_∞ from the raw pH against time charts; these are given in Table 6.2. Since some samples appeared

not to have reached an equilibrium condition their values were extrapolated, but the modifications required were small. Those for the four samples that are treated with the kinetic scheme are given in Table 6.7. Experimental data of pH against time is provided in Tables 6.3–6.6 for the four samples. The $\ln \Delta$ functions for the experimental data were calculated from equation 11. In the first instance, $\ln \Delta$ can be considered as a linear function of time and equation 16 can be simplified to:

$$\ln \Delta = \ln \alpha - k_1 t \qquad (17)$$

Values for α and k_1 were assessed by fitting equation 17 to experimental $\ln \Delta$ against time plots which typically have a near-linear section. The best α and k_1 values were selected and data was calculated for the whole time span. This is given in the fourth column of Tables 6.3–6.6 and is plotted together with the experimental data in Figures 6.2, 6.6, 6.10 and 6.14. Note that the graphs only show some calculated data points to enable identification of the region of the experimental data that they were modelled to. All four samples clearly deviate from the $\ln \Delta$ linearity approximation in the initial stages of protonation. This region can be used to derive further parameters once modelled. Subtraction of equation 17 from equation 16 allows the contribution of the curvature to the $\ln \Delta$ against time plots be determined. This is defined as $\partial \ln \Delta$ in equation 18:

$$\partial \ln \Delta = - \frac{\beta}{\alpha} e^{-(k_2 - k_1)t} \qquad (18)$$

Experimental $\partial \ln \Delta$ values are given in the data Tables and are plotted in Figures 6.3, 6.7, 6.11 and 6.15 against time for the initial stages of protonation. Superimposed are calculated $\partial \ln \Delta$ data that has been derived by fitting exponentials to the experimental data using the parameters $-\beta/\alpha$ and $-(k_2-k_1)$.

The graphs given in Figures 6.4, 6.8, 6.12 and 6.16 represent experimental and calculated $\ln \Delta$ data where this is defined by equation 16 and therefore accounts for both the linear and curved sections of the data. These may be regarded as a summation of the previous two plots for each sample. Similarly, pH data has been derived from the calculated $\ln \Delta$ data using equation 11; This is given in Tables 6.3–6.6 and plotted with the corresponding experimental data in Figures 6.5, 6.9, 6.13 and 6.17.

Table 6.7
Calculation Parameters for Acidification Kinetics

Concentration /% w/v	$[H^+]_\infty$ /mol dm^{-3}	α	β	k_1 /min^{-1}	k_2 /min^{-1}	x:y
0.019 FHA	4.90×10^{-4}	0.262	-0.328	0.0403	1.17	16.6:1
1.67 FHA	0.676	0.846	-0.161	0.00729	0.127	3.6:1
0.088 AHA	2.95×10^{-8}	0.210	-0.36	0.088	0.648	5.0:1
1.75 AHA	4.47×10^{-3}	0.641	-0.288	0.0166	0.567	11.3:1

Note:
The terms used in this Table are defined in Section 6.4.4

The curve-fitting calculation parameters for the four samples are collated in Table 6.7; they are discussed in the following Section.

6.4.5 Mechanistic Interpretations of Protonation Kinetics

Some mechanistic information concerning the protonation of the humic acid samples is available from the data analysis and modelling derived in the previous Section. The nature of the plots are first described.

Both Fluka Humic Acid samples studied gave very good fits to the linear and curved sections of the $\ln \Delta$ data, and therefore close correlations with the complete $\ln \Delta$ plots and the corresponding pH against time graphs. For the Aldrich Humic Acid samples, the linear sections of the $\ln \Delta$ data were modelled well, but the initial stages of the $\partial \ln \Delta$ data were not exponential and parameters derived from this region of the data are probably inaccurate. However, the $\partial \ln \Delta$ contributions were included in the overall $\ln \Delta$ data since they provide some improvement over the linear approximation defined in equation 17.

Calculation parameters derived from modelling of the protonation kinetics of the four

samples are given in Table 6.7; Of particular interest are the values of the rate constants k_1 and k_2, and the x:y ratio. Initially it was *assumed* that $k_1 < k_2$; this effectively results in k_1 being assigned to the linear sections of the ln Δ plots since the smaller rate constant controls the overall kinetic behaviour. For all four samples, the k_1 values determined were less than those of k_2, as expected from the initial assumption. The k_1 values should be more accurate than the k_2's since the former are calculated from regression analysis applied to near-linear data, whereas the latter are deduced from curve-fits applied to data that for the Aldrich Humic Acid samples, were non-exponential.

Inspection of the pH against time graphs of Figures 6.5, 6.9, 6.13 and 6.17 shows that each is characterised by an initial region of rapid pH change and a slower region extending over a longer time. Correlation of these sections with the rate constants suggests that k_2 should be assigned to the former and k_1 to the latter. However, since the reaction scheme of equations 1&2 would not be feasible, then the initial assumption of $k_1 < k_2$ must be incorrect. The kinetic analysis can be equally derived using the assumption $k_1 > k_2$; this would lead to k_2 being assigned to the linear region and k_1 to the initial rapid stage. The x:y ratio deduced from equations 12 and 13 gives the numbers of protons released in each step of the proposed scheme. Although these and the rate constants are different for each sample, it is notable that the ratio of the rate constants for a given sample has a smaller variance with a factor of five between the largest and smallest.

It is likely that the proposed scheme cannot fully account for all kinetic data since several assumptions made initially, particularly that the reverse reactions are insignificant, are not strictly true. However, the general behaviour is clear. Mechanistically, reaction 1 may not be the true first reaction of the protonation process; it is only the first relatively slow step that can be observed. Faster processes, such as titration of residual hydroxide ions and the initial protonation of the humic matter, are not observable. Reaction 1 of the scheme is slow by comparison, and reaction 2 even slower. The values of the x:y ratio suggest that the second reaction was incomplete since it should produce more protons than the first.

Form A is produced by rapid aggregation of the humate structure resulting in protonation of most anionic humate functional groups. Species A undergoes some configurational changes involving the more flexible parts of the humic structure, and converts to form B; This is accompanied by a rapid release of some protons that may have been

trapped when the structure was initially aggregated. The second change—from species B to C—is slower since it involves movement of the less flexible parts of the humic structure to a more thermodynamically stable conformation. This may involve size changes and the separation of the hydrophobic and hydrophilic components to enable each to associate with its own kind. Since processes involving the movement of structural units are likely to be slow, then this presumably controls the rate of release of protons in this stage.

The mechanism probably would be influenced by factors that encourages aggregation, such as high concentrations of humic matter and large acidification dosages. The experimental dependence of the slow potentiometric effects on humic acid concentration is not clear (see Section 6.4.1), although it is notable that the most concentrated samples of both humic acids had long equilibration times. The strongly acidic conditions employed in many protonation runs may have resulted in some precipitation of the organic matter as well as the formation of dispersed aggregates. This can be accommodated by the mechanism described since these may also undergo configurational rearrangements resulting in elimination of some protons.

Evidence for configurational changes in humic materials when maintained in media of different pH is provided by the work of Varney and co–workers who observed that during a potentiometric titration of fulvic acid, marked conformational changes occurred with the molecular radius increasing from 6·5 Å at pH 1·15 to 13·2 Å at pH 9·26. These conformational changes were believed to arise because of intramolecular electrostatic repulsive forces associated with the build up of charge on the flexible fulvate polyanion.[224] Further evidence is provided by Yonebayashi and Hattori who noted changes in some humic acid fractions during gel permeation chromatography. More of the excluded fraction was observed if the sample stood in a weakly acidic or neutral buffer solution. This was explained by the association of smaller molecules to form micelle-like aggregates that cannot permeate the column material.[273] Choppin and Kullberg[249] explained some unusual behaviour in a potentiometric titration by the occurrence of a change in the chemical structure of the humic acid whilst stored in the alkaline dispersion medium, however this may have arisen from some oversight in their experimental methodology.

The consumption of protons not accounted for by the protonation of carboxylate and other functional groups in the buffering effect discussed in Section 6.4.3 may be explained by

the proposed mechanism. The initial aggregation traps some protons that are not subsequently released by the structural rearrangements, and therefore, they do not return to the bulk of the aqueous medium. It is notable that if the potentiometric titrations were carried out in a stepwise manner using small additions of acid, buffering may not have been observed to the same extent since the structures would be less aggregated and protons not associated with anionic functional groups may have been able to diffuse away from the humic matter.

6.4.6 Alternative Experimental Monitoring Techniques

The mechanism described to explain the slow pH changes could have been monitored using other experimental methods. The requirements are for techniques that provide continuous monitoring of a parameter that indicates a change occurring on acidification (in a similar manner to pH), or for methods that permit repeated determinations of some parameter with a short data acquisition time.

Light scattering provides suitable monitoring techniques since sizes and shapes of submicronic particles may be determined. This would require rapid measurement compared to the experimental time-scale. It probably would not be possible to monitor the initial fast acidification. Studies described previously in this thesis (see Chapter 5) have successfully monitored the light scattered by humic acids under various equilibrated acidity conditions. These studies were not carried out continuously although data acquisition is fast enough to permit that.

Some consideration was given to the use of proton nuclear magnetic resonance spectroscopy to monitor protonation titrations (see Chapter 4). This was not implemented due to difficulties encountered in acquiring the proton spectra rapidly, and complications in detecting labile protons whilst the aqueous solvent is irradiated.

6.4.7 Implications of the Buffering and Kinetic Behaviour in Potentiometric Titrations

The origin of the buffering and slow pH changes observed in the preparation of samples

for fluorescence studies that prompted the investigations described in this Chapter have been explained. In Chapter 3, it was stated that the preparation of the europium(III)-Fluka Humic Acid v3 "complexes," involved making no further adjustments to their composition once a condition of constant pH was attained. However, from the experiments described in this Chapter, it is possible that pH changes did occur since the samples would be sensitive to such changes across the region of neutrality (pH 7·0 ± 0·1) that they were restricted to. Note that it is likely that the europium ion used in those samples also contributes to these effects through its hydrolysis equilibria caused by the polarising effect of its high charge density. These effects may have caused some of the variance in the measured fluorescence of samples that was not accounted for by the precision prescribed to their preparation. Slow changes may have occurred that disturbed their composition and therefore the nature of the interaction between metal and the organic matter. A wide time span (of weeks) was spent preparing the samples, but their ages were not recorded when their fluorescence was determined. Some samples may have been fully equilibrated whereas this may not have been true for others.

This work has important implications to the detection and selection of end points in potentiometric titrations and deciding the attainment of equilibrium in metal ion complexation. End point usage and equilibration is therefore debatable and considerable justification should be given to their selection.

6.5 Conclusions

Potentiometric titrations of humic acids have been performed by rapid acidification of alkaline humate media using a wide range of conditions. The organic matter usually responded by buffering the mineral acid addition and producing both a rapid and slow pH change.

The proton concentration data was analysed and modelled by applying chemical kinetic considerations. Most of the likely sources of experimental artifacts were discounted and despite concern over the reliability and reproducibility of the results, a mechanism that accounts for the experimental observations was proposed. The protonated forms of the humic acids undergo two configurational changes, one of which is much faster than the other, but both result in release of protons to the medium.

This mechanism explains the buffering and slow response to pH changes that was observed in the preparation of europium(III)-Fluka Humic Acid v3 "complexes" described in Chapter 3. This work has important implications for the selection of end points in potentiometric titrations and the recognition of equilibration in metal ion complexations.

CHAPTER 7
CONCLUSIONS and EVALUATION

7.1 Conclusions

Several samples of humic substances were studied in this thesis. All but one were humic acids, and those that were studied most extensively were obtained commercially. Some characterisation techniques were applied to them.

Elemental analysis of Fluka and Aldrich humic acids revealed high proportions of carbon relative to other elements implying that they are aromatic. Infrared spectroscopy contradicted this since spectra implied that the samples studied are predominantly aliphatic, although some evidence for aromatic and alkene carbons was observed. The samples are functionalised mainly with oxygen-containing groups. Little information concerning the precise chemical structure of the humic and fulvic nuclei was derived.

Compositional analysis showed that moisture and ash form a large proportion of the samples. Purification of Fluka Humic Acid by the classical alkaline dissolution/acid precipitation procedure reduced the ash content of the sample and resulted in the conversion of carboxylate to carboxyl groups. Complexation of Fluka Humic Acid produced an opposite infrared spectral effect. Infrared spectra of a fulvic and humic acid derived from the same source were compared; these had similar structures, but the fulvic acid is more functionalised than the corresponding humic acid.

Thermal analysis of humic acids revealed that some components of the samples are quite thermally stable resulting in significant ash contents. Pyrolysis-induced decomposition of humic acids occurred over a wide temperature span but uniquely defined processes were not identified. Infrared spectroscopy suggested that pyrolysis residues were mainly siliceous matter derived from the source, but some evidence for carbonaceous matter was observed.

Although humic substances are coloured, their ultra-violet and visible absorption spectra are featureless. Yet, both Fluka and Aldrich humic acids fluoresce over a wide range of wavelengths with maximised efficiency following irradiation at low wavelengths.

Fluorescence spectra show little resemblance to ultra-violet/visible absorption spectra, suggesting that fluorescence is not the most likely mechanism for degrading the absorbed radiation, possibly since the fluorophores are present in a small concentration.

Photophysical processes occurring in an aqueous medium containing Fluka Humic Acid and europium(III) were studied and experimental data was modelled. The enhanced fluorescence on addition of the luminescent lanthanide ion to humic acid was accounted for by an energy transfer process in the photophysical model from the irradiated humic acid to the metal ion. Several feasible energy transfer mechanisms were forwarded, the most probable of which is of a non–radiative nature and does not require complexation of the metal ion and humic acid since it can occur over large distances.

A multinuclear nuclear magnetic resonance spectroscopy approach was applied to the study of humic acids and their complexes with heavy metals. Proton and carbon–13 NMR of humic acids provided some structural and functionality information that supports the other characterisation studies. The presence of paramagnetic lanthanide ions as shift reagents showed some effects in the chemical shifts and line-widths of proton and carbon–13 spectra of their humic acid complexes. The reliability of these measurements was questioned and the contact and pseudo-contact contributions to the chemical shifts were not separated. Some heavy metals were studied directly as NMR nuclei to gain information about their local environments, however this approach had limited success. Some chemical shift and line-width changes were observed for lanthanum–139 and zirconium–91, but measurements were restricted by the sensitivity of the nuclei studied; The metal ion concentrations required for useful NMR signal strength tend to coagulate humic acids. Fulvic acids may be more useful for such investigations as they are somewhat more stable in aqueous media.

An aqueous dispersion of Aldrich humic acid was fractionated by ultrafiltration to yield a weight average molecular weight of 170000 daltons from a broad molecular weight distribution. The E_4:E_6 absorbance ratio was sensitive to fractionation.

Laser Doppler Electrophoretic Light Scattering was applied to probe the colloidal characteristics of humic substances. Parameters derived were sensitive to the conditions of their supporting media, and their concentration and particle size distribution. Both Fluka Humic Acid and Fanay-Augéres Fulvic Acid are highly charged at the surface of shear in their electrical double layers; the humic acid somewhat more-so than the fulvic

acid studied. The large intensity of light scattered by the humic and fulvic acid samples was explained by consideration of refractive indices and molecular masses. Scattering from the fulvic acid studied was much less than that of the humic acid.

Electrophoretic mobilities and particle radii increased with the pH of the medium. These changes are probably due a combination of the dissociation of acidic functional groups and some macromolecular structural rearrangements. Dilution of Fluka Humic Acid and Fanay-Augéres Fulvic Acid produced a large decrease in the light scattered but increased particle radii. Filtration affected the band-widths of the spectra and the light scattered was again reduced. Electrophoretic mobilities were reduced implying that the large particles removed are the more electrophoretically mobile components of the humic acid.

During the preparation of europium(III)-Fluka Humic Acid "complexes" for fluorescence studies, the chemical system responded slowly to pH changes induced by acid or alkali additions, and their magnitude was not as extensive as anticipated. Inspection of the literature of potentiometric titrations and metal ion complexation located few citations of equilibration times and even fewer instances where their selection was justified. This prompted an investigation of these effects. Potentiometric titrations of humic acids were performed by rapid acidification of alkaline humate media under a range of conditions. The organic matter usually responded by buffering the mineral acid addition and producing a slow pH change. The proton concentration data was analysed and modelled by applying chemical kinetic considerations. Despite concern over the reliability and reproducibility of the results, a mechanism that accounts for the experimental observations was proposed. Newly protonated humic acids undergo conformational changes in response to the acidity of the medium. Two separate changes were modelled that both result in proton release after sometime, however one is much faster than the other. The mechanism explains the buffering and slow pH changes that were observed in the preparation of europium(III)-Fluka Humic Acid "complexes." It has important implications for the selection of end points in potentiometric titrations and recognition of equilibration in metal ion complexations.

7.2 Evaluation

The studies described in this thesis have focussed on selected aspects of the

characteristics and properties of humic substances. The aim was not to provide a comprehensive coverage of the subject, but to probe some areas that have received little attention. The main Chapters (2–6) have each included some novel approaches to experimental studies or data analysis and modelling.

Progress in the understanding of the properties and characteristics of humic substances will always be limited by their inherent complexity and diversity from various sources. The question "What is Humic Acid?" [10] will remain unanswered for sometime in the future.

REFERENCES

1 Schnitzer, M.
Humic Substances: Chemistry and Reactions
Ch 1, pp 1–64, in
Schnitzer, M. & Khan, S.U. (Eds.)
Soil Organic Matter
Developments in Soil Science 8
Elsevier, Amsterdam (1978)

2 Aiken, G.R.; McKnight, D.M.; Wershaw, R.L. & MacCarthy, P.
Ch. 1, pp 1–9, in
Aiken, G.R.; McKnight, D.M.; Wershaw, R.L. & MacCarthy, P. (Eds.)
Humic Substances in Soil, Sediment and Water (Geochemistry, Isolation and Characterisation)
Wiley-Interscience, New York (1985)

3 Stumm, W. & Morgan, J.J.
Aquatic Chemistry: An Introduction Emphasising Chemical Equilibria in Natural Waters
2nd Edition, Wiley-Interscience, New York (1981)

4 Schnitzer, M.
Binding of Humic Substances by Soil Mineral Colloids
Ch. 4, pp 77–101, in
Huang, P.M. & Schnitzer, M. (Eds.)
Interactions of Soil Minerals with Natural Organics and Microbes
S.S.S.A. Special Publication No. 17, Soil Science Society of America, Madison (1986)

5 Schnitzer, M. & Khan, S.U.
Humic Substances in the Environment
Marcel Dekker, New York (1972)

6 Stevenson, F.J.
Humus Chemistry: Genesis, Composition, Reactions
Wiley-Interscience, New York (1982)

7 Buffle, J.
Natural Organic Matter and Metal-Organic Interactions in Aqueous Systems
Ch. 6, pp 165–221, in
Sigel, H. (Ed.)
Metal Ions in Biological Systems, Volume 18: Circulation of Metals in the Environment
Marcel Dekker, New York (1985)

8 Olofson, U. & Allard, B.
Complexes of Actinides with Naturally Occurring Organic Substances- Literature Survey
Svensk Kaernbraenslefoersoerjning AB, SKBF–KBS–TR–83–09, Stockholm (1983)

9 Hänninen, K.I.; Klöcking & Helbig, B.
Synthesis and Characterisation of Humic Acid-Like Polymers

Becher, G. (Ed.)
Advances in Humic Substances Research
Proceedings of the Third International Meeting of the International Humic Substances Society
Oslo, Norway, 4–8 August 1986
Sci. Tot. Env., 62, 201–210 (1987)

10 Steelink, C.A.
What is Humic Acid?
J. Chem. Ed., 40(7), 379–384 (1963)

11 Ghosh, K. & Schnitzer, M.
Macromolecular Structures of Humic Substances
Soil Sci., 129(5), 266–276 (1980)

12 Chen, Y. & Schnitzer, M.
Scanning Electron Microscopy of a Humic Acid and of a Fulvic Acid and its Metal and Clay Complexes
Soil Sci. Soc. Am. Proc., 40, 682–686 (1976)

13 Boggs, S., Jr.; Livermore, D. & Seitz, M.G.
Humic Substances in Natural Waters and their Complexation with Trace Metals and Radionuclides: A Review
Argonne National Laboratory, ANL–84–78 (1985)

14 Ong, H.L. & Bisque, R.F.
Coagulation of Humic Colloids by Metal Ions
Soil Sci., 106, 220–224 (1968)

15 Langford, C.H.; Gamble, D.S.; Underdown, A.W. & Lee, S.
Interaction of Metal Ions with a Well Characterised Fulvic Acid
Ch. 11, pp 219–237, in
Christman, R.F. & Gjessing, E.T. (Eds.)
Aquatic and Terrestrial Humic Materials
Ann Arbor, Michigan (1983)

16 Khan, S.U.
The Interaction of Organic Matter with Pesticides
Ch. 4, pp 137–172, in
Schnitzer, M. & Khan, S.U. (Eds.)
Soil Organic Matter
Developments in Soil Science 8
Elsevier, Amsterdam (1978)

17 Stevenson, F.J. & Fitch, A.
Chemistry of Complexation of Metal Ions with Soil Solution Organics
Ch. 2, pp 29–58, in
Huang, P.M. & Schnitzer, M. (Eds.)
Interactions of Soil Minerals with Natural Organics and Microbes
S.S.S.A. Special Publication No. 17, Soil Science Society of America, Madison (1986)

18 Prakash, A. & MacGregor, D.J.
Environmental and Human Health Significance of Humic Materials: An Overview
Ch. 25, pp 481–494, in
Christman, R.F. & Gjessing, E.T. (Eds.)

Aquatic and Terrestrial Humic Materials
Ann Arbor, Michigan (1983)

19 Tucker, A.
Browned Off at the Taps
The Guardian, (May 3, 1988)

20 Tan, K.H.
Degradation of Soil Minerals by Organic Acids
Ch. 1, pp 1–27, in
Huang, P.M. & Schnitzer, M. (Eds.)
Interactions of Soil Minerals with Natural Organics and Microbes
S.S.S.A. Special Publication No. 17, Soil Science Society of America, Madison (1986)

21 Mattigod, S.V.; Sposito, G. & Page, A.L.
pp 203–221, in
Dowdy, R.H. (Ed.)
Chemistry in the Soil Environment
Special Publication No. 40, American Society of Agronomy and Soil Science Society of America, Madison (1981)

22 Purdue, E.M. & Lytle, C.R.
A Critical Examination of Metal-Ligand Complexation Models: Application to Defined Multiligand Mixtures
Ch. 14, pp 295–313, in
Christman, R.F. & Gjessing, E.T. (Eds.)
Aquatic and Terrestrial Humic Materials
Ann Arbor, Michigan (1983)

23 Tuschall, J.R. & Brezonik, P.L.
Complexation of Heavy Metals by Aquatic Humus: A Comparative Study of Five Analytical Techniques
Ch. 13, pp 275–294, in
Christman, R.F. & Gjessing, E.T. (Eds.)
Aquatic and Terrestrial Humic Materials
Ann Arbor, Michigan (1983)

24 Weber, J.R.
Metal Ion Speciation Studies in the Presence of Humic Materials
Ch. 15, pp 315–331, in
Christman, R.F. & Gjessing, E.T. (Eds.)
Aquatic and Terrestrial Humic Materials
Ann Arbor, Michigan (1983)

25 van Dijk, H.
Cation Binding by Humic Acids
Geoderma, 5, 53–67 (1971)

26 Carlsen, L.
The Role of Organics on the Migration of Radionuclides in the Geosphere
Report No. EUR 12024 EN, Commission of the European Communities (C.E.C.), Luxembourg (1989)

27 Ewart, F.T. & Williams, S.J.
A Literature Survey of the Possible Effects of Humic and Fulvic Acids on the Disposal of LLW and ILW

U.K. At. Energy Res. Estab., [Rep.], AERE–R 12033 (1986)

28 Kim, J.I.; Buckau, G.; Baumgärtner, F.; Moon, H.C. & Lux, D.
Colloid Generation and the Actinide Migration in Gorleben Groundwaters
pp 31–40, in
McVay, G.L. (Ed.)
Scientific Basis for Nuclear Waste Management VII
Materials Research Society Symposia Proceedings, 26 (1984)

29 Kim, J.I.; Buckau, G. & Zhuang, W.
Humic Colloid Generation of Transuranic Elements in Groundwater and Their Migration Behaviour
pp 747–756, in
Bates, J.K. & Seefeldt, W.B. (Eds.)
Scientific Basis for Nuclear Waste Management X
Materials Research Society Symposia Proceedings, 84 (1987)

30 Warnecke, E.; Hollmann, A. & Stier-Friedland, G.
Migration of Radionuclides: Experiments Within the Site Investigation Program at Gorleben
pp 41–48, in
McVay, G.L. (Ed.)
Scientific Basis for Nuclear Waste Management VII
Materials Research Society Symposia Proceedings, 26 (1984)

31 Ivanovich, M. & Hardy, C.J.
Identification and Measurement of Colloids in Groundwater
pp 227–260, in
Come, B. & Chapman, N.A., (Eds.)
Commission of the European Communities: Nuclear Science and Technology, Natural Analogues Working Group, Final Report, EUR 10671 EN (1986)
Interlaken, June 17–19 (1986)
Commission of the European Communities (1986)

32 Krauskopf, K.B.
Thorium and Rare-Earth Metals as Analogs for Actinide Elements
Chapman, N.A. & Smellie, J.A.T. (Eds.)
Natural Analogues to the Conditions Around a Final Repository for High-Level Radioactive Waste
Chem. Geol., 55, 323–335 (1986)

33 Torres, R.A. & Choppin, G.R.
Europium(III) and Americium(III) Stability Constants with Humic Acid
Radiochim. Acta, 35(3), 143–148 (1984)

34 Torres, R.A.
Humic Acid Complexation of Europium, Americium and Plutonium
PhD Thesis, Florida State University (1982)

35 Bertha, E.L. & Choppin, G.R.
Interaction of Humic and Fulvic Acids with Eu(III) and Am(III)
J. Inorg. Nucl. Chem., 40, 655–658 (1978)

36 Marinsky, J.A.
The Complexation of Europium(III) by Fulvic Acid

Svensk Kaernbraenslefoersoerjning AB, SKBF-KBS-TR-83-14, Stockholm (1983)

37 Choppin, G.R.
Speciation of Trivalent f-Elements in Natural Waters
J. Less Common Met., 126, 307-313 (1986)

38 Maes, A. & Cremers, A.
Radionuclide Sorption in Soils and Sediments: Oxide-Organic Matter Competition
pp 93-100, in
Bulman, R.A. & Cooper, J.R. (Eds.)
Proceedings of the Seminar on Speciation of Fission and Activation Products in the Environment
Oxford, April 1985
Elsevier Applied Science, Amsterdam (1986)

39 Caceci, M.S.
The Interaction of Humic Acid with Europium(III): Complexation Strength as a Function of Load and pH
Radiochim. Acta, 39(1), 51-56 (1985)

40 Carlsen, L.; Bo, P. & Larsen, G.
Radionuclide-Humic Acid Interactions Studied by Dialysis
Ch. 10, pp 167-178, in
Barney, G.S.; Navratil, J.D. & Schulz, W.W. (Eds.)
Geochemical Behaviour of Disposed Radioactive Waste
ACS Symposium Series, 246, American Chemical Society, Washington D.C. (1984)

41 Choppin, G.R.
Binding of Actinides by Humic Acid
Thalassia Jugoslavica, 16(2-4), 243-247 (1980)

42 Musani-Marazovic, L.; Faguet, D. & Konrad, Z.
The Interaction of Trace Metal Radionuclides with Humic Substances
Ch. 24, pp 389-412, in
Organic Marine Geochemistry
ACS Symposium Series, 305, American Chemical Society, Washington D.C. (1986)

43 Mikheev, N.B.; Spitsyn, V.I.; Ionova, G.V.; Auérman, L.N. & Korshunov, B.G.
Patterns in the Stability of the Lower Oxidation States of Actinides and Lanthanides
Soviet Radiochemistry, 28(1), 71-77 (1986)

44 Bulman, R.A.; Baker, T.E. & Baker, S.T.
Investigations of Interactions of Transuranics and Cerium with Humates
Becher, G. (Ed.)
Advances in Humic Substances Research
Proceedings of the Third International Meeting of the International Humic Substances Society
Oslo, Norway, 4-8 August 1986
Sci. Tot. Env., 62, 213-218 (1987)

45 Then, G.M.; Appel, H.; Duffield, J.; Taylor, D.M. & Thies, W.-G.
In Vivo and In Vitro Studies of Hafnium-Binding to Rat Serum Transferrin
J. Inorg. Biochem., 27, 255-270 (1986)

46 Hodgkinson, D.P.; Robinson, P.C.; Tasker, P.W. & George, D.
The Objectives of NIREX Research in Support of Post-Closure Radiological

Assessments for LLW and ILW Disposal
U.K. At. Energy Res. Estab., [Rep.], AERE–R 12219 (1986)

47 Aldrich Chemical Catalog

48 Chapman, N.A. & McKinley, I.G.
The Geological Disposal of Nuclear Waste
Wiley, Chichester (1987)

49 Malcolm, R.L. & MacCarthy, P.
Limitations in the Use of Commercial Humic Acids in Water and Soil Research
Environ. Sci. Technol., 20, 904–911 (1986)

50 MacCarthy, P. & Malcolm, R.L.
The Nature of Commercial Humic Acids
Ch. 4, pp 55–63, in
Suffet, I.H. & MacCarthy, P. (Eds.)
Aquatic Humic Substances: Influence on Fate and Treatment of Pollutants
Advances in Chemistry Series, 219, American Chemical Society, Washington D.C. (1989)

51 Calderoni, G. & Schnitzer, M.
Effects of Age on the Chemical Structure of Paleosol Humic Acids and Fulvic Acids
Geochim. Cosmochim. Acta, 48, 2045–2051 (1984)

52 Alberts, J.J. & Dickson, T.J.
Organic Carbon and Cation Associations in Humic Material from Pond Water and Sediment
Proceedings of the First Meeting of the International Humic Substances Society
Estes Park, Colorado, August 1983
Org. Geochem., 8(1), 55–64 (1985)

53 Yong, R.N. & Mourato, D.
Extraction and Characterisation of Organics from the Champlain Sea Subsurface Soils
Can. Geotech. J., 25(3), 599–607 (1988)

54 Theng, B.K.G.; Wake, J.R.H. & Posner, A.M.
The Humic Acids Extracted by Various Reagents From a Soil
J. Soil Sci., 18, 349–363 (1976)

55 Gregor, J.E. & Powell, H.K.J.
Acid Pyrophosphate Extraction of Soil Fulvic Acids
J. Soil Sci., 37(4), 577–585 (1986)

56 Gregor, J.E. & Powell, H.K.J.
Effects of Extraction on Fulvic Acid Properties
Becher, G. (Ed.)
Advances in Humic Substances Research
Proceedings of the Third International Meeting of the International Humic Substances Society
Oslo, Norway, 4–8 August 1986
Sci. Tot. Env., 62, 3–12 (1987)

57 Midwood, R.B. & Felbeck, G.T., Jr.
Analysis of Yellow Organic Matter from Fresh Water
J., Am. Water Works Assoc., 60, 357–366 (1968)

58 Montgomery, W.J.
Standard Laboratory Test Methods for Coal and Coke
Ch. 6, pp 195–246, in
Karr, C., Jr. (Ed.)
Analytical Methods for Coal and Coal Products Volume 1
Academic Press, New York (1978)

59 Allardice, D.J. & Evans, D.G.
Moisture in Coals
Ch. 7, pp 247–278, in
Karr, C., Jr. (Ed.)
Analytical Methods for Coal and Coal Products Volume 1
Academic Press, New York (1978)

60 Balkas, T.I.; Bastürk, Ö.; Gaines, A.F.; Salihoglu, I. & Yilmaz, A.
Comparison of Five Humic Acids
Fuel, 62, 373–379 (1983)

61 Weber, J.H. & Wilson, S.A.
The Isolation and Characterisation of Fulvic Acid and Humic Acid From River Water
Water Res., 9, 1079–1084 (1975)

62 Huffman, E.W.D., Jr. & Stuber, H.A
Ch. 17, pp 433–455, in
Aiken, G.R.; McKnight, D.M.; Wershaw, R.L. & MacCarthy, P. (Eds.)
Humic Substances in Soil, Sediment and Water (Geochemistry, Isolation and Characterisation)
Wiley-Interscience, New York (1985)

63 Kumada, K.
Chemistry of Soil Organic Matter
Developments in Soil Science 17, Elsevier, Amsterdam (1987)

64 Kemp, W.
Organic Spectroscopy
2nd Edition, MacMillan, Basingstoke (1987)

65 MacKenzie, M.W.
Advances in Applied Fourier Transform Infrared Spectroscopy
Wiley, Chichester (1988)

66 MacCarthy, P. & Rice, J.A.
Ch. 21, pp 527–559, in
Aiken, G.R.; McKnight, D.M.; Wershaw, R.L. & MacCarthy, P. (Eds.)
Humic Substances in Soil, Sediment and Water (Geochemistry, Isolation and Characterisation)
Wiley-Interscience, New York (1985)

67 Schnitzer, M. & Calderoni, G.
Some Chemical Characteristics of Paleosol Humic Acids
Chem. Geol., 53(3–4), 175–184 (1985)

68 Byler, D.M.; Gerasimowicz, W.V.; Susi, H. & Schnitzer, M.
FT–IR Spectra of Soil Constituents: Fulvic Acid and Fulvic Acid Complex with Ferric Ions
Appl. Spectrosc., 41(8), 1428–1430 (1987)

69 Gerasimowicz, W.V.; Byler, D.M.; Susi, H. &

Resolution-Enhanced FT-IR Spectra of Soil Constituents: Humic Acid
Appl. Spectrosc., 40(4), 504-507 (1986)

70 Tan, K.H.
Formation of Metal-Humic Acid Complexes by Titration and their Characterisation by Differential Thermal Analysis and Infrared Spectroscopy
Soil Biol. Biochem., 10, 123-129 (1978)

71 Boyd, S.A.; Sommers, L.E. & Nelson, D.W.
Copper(II) and Iron(III) Complexation by the Carboxylate Group of Humic Acid
Soil Sci. Soc. Am. J., 45, 1241-1242 (1981)

72 Harrison, R.D. (Ed.)
Book of Data
Nuffield Foundation, Penguin Books, Harmondsworth (1972)

73 Duval, C.
Inorganic Thermogravimetric Analysis
Second and Revised Edition, Elsevier, Amsterdam (1963)

74 Schnitzer, M. & Kodama, H.
Differential Thermal Analysis of Metal-Fulvic Acid Salts and Complexes
Geoderma, 7, 93-103 (1972)

75 Schnitzer, M. & Hoffman, I.
Thermogravimetry of Soil Humic Compounds
Geochim. Cosmochim. Acta, 29, 859-870 (1965)

76 Black, A.P. & Willems, D.G.
Electrophoretic Studies of Coagulation for Removal of Organic Colour
J., Am. Water Works Assoc., 53, 589-604 (1961)

77 Packham, R.F.
Studies of Organic Colour in Natural Water
Proc. Soc. Water Treat. Exam., 13, 316-334 (1964)

78 Frimmel, F.H. & Bauer, H.
Influence of Photochemical Reactions on the Optical Properties of Aquatic Humic Substances from Fall Leaves
Becher, G. (Ed.)
Advances in Humic Substances Research
Proceedings of the Third International Meeting of the International Humic Substances Society
Oslo, Norway, 4-8 August 1986
Sci. Tot. Env., 62, 139-148 (1987)

79 Ghosh, K. & Schnitzer, M.
UV and Visible Absorption Spectroscopic Investigations in Relation to Macromolecular Characterisation of Humic Substances
J. Soil Sci., 30(4), 735-745 (1979)

80 Dkhar, G.D.; Prasad, B & Sinha, M.K.
Characterisation of Humic and Fulvic Acids of Forest and Cultivated Soils
J. Indian Soc. Soil Sci., 34(1), 29-37 (1986)

81 Donard, O.F.X.; Belin, C. & Ewald, M.
Corrected Fluorescence Excitation Spectra of Fulvic Acids. Comparison with U.V./Visible Absorption Spectra
Becher, G. (Ed.)

Advances in Humic Substances Research
Proceedings of the Third International Meeting of the International Humic Substances Society
Oslo, Norway, 4–8 August 1986
Sci. Tot. Env., 62, 157–161 (1987)

82 Greenland, D.J. & Hayes, M.H.B.
Chemistry of Soil Constituents
Wiley, Chichester (1978)

83 Mori, S.
Derivative Ultraviolet and Visible Spectrophotometry: Applications to Polymer Analysis
J. Appl. Polym. Sci., 33(6), 1923–1931 (1987)

84 Moulin, V.; Robouch, P.; Vitorge, P. & Allard, B.
Spectrophotometric Study of the Interaction between Americium(III) and Humic Materials
Inorg. Chim. Acta, 140(1–2), 303–306 (1987)

85 Billingham, N.C.
Molar Mass Measurements in Polymer Science
Kogan Page, London (1977)

86 Visser, S.A.
Fluorescence Phenomena of Humic Matter of Aquatic Origin and Microbial Cultures
Ch. 9, pp 183–202, in
Christman, R.F. & Gjessing, E.T. (Eds.)
Aquatic and Terrestrial Humic Materials
Ann Arbor, Michigan (1983)

87 Datta, C.; Ghosh, K. & Mukherjee, S.K.
Fluorescence Excitation Spectra of Different Fractions of Humus
J. Indian Chem. Soc., 48(3), 279–287 (1971)

88 Seal, B.K.; Roy, K.B. & Mukherjee, S.K.
Fluorescence Emission Spectra and Structure of Humic and Fulvic Acids
J. Indian Chem. Soc., 41(3), 212–214 (1964)

89 Miano, T.M.; Sposito, G. & Martin, J.P.
Fluorescence Spectroscopy of Humic Substances
Soil Sci. Soc. Am. J., 52(4), 1016–1019 (1988)

90 Lévesque, M.
Fluorescence and Gel Filtration of Humic Compounds
Soil Sci., 113, 346–353 (1972)

91 Goldberg, M.C. & Negomir, P.M.
Characterisation of Aquatic Humic Acid Fractions by Fluorescence Depolarisation Spectroscopy
Ch. 11, pp 180–205, in
Luminescence Applications in Biological, Chemical, Environmental and Hydrological Sciences
ACS Symposium Series, 383, American Chemical Society, Washington D.C. (1989)

92 Milne, P.J.; Odum, D.S. & Zika, R.G.
Time Resolved Fluorescence Measurements on Dissolved Marine Organic Matter
Ch. 10, pp 132–140, in
Zika, R.G. & Cooper, W.J. (Eds.)

Photochemistry of Environmental Aquatic Systems
ACS Symposium Series, 327, American Chemical Society, Washington D.C. (1987)

93 Buffle, J.; Deladoey, P.; Zumstein, J. & Haerdi, W.
Schweiz. Z. Hydrol., 44, 326–361 (1982)

94 Power, J.F.; Sharma, D.K.; Langford, C.H.; Bonneau, R. & Joussot-Dubien, J.
Laser Flash Photolytic Studies of a Well Characterised Soil Humic Substance
Ch. 12, pp 157–173, in
Zika, R.G. & Cooper, W.J. (Eds.)
Photochemistry of Environmental Aquatic Systems
ACS Symposium Series, 327, American Chemical Society, Washington D.C. (1987)

95 Amy, G.L.; Collins, M.R.; Kuo, C.J. & King, P.H.
A Comparison of Gel Permeation Chromatography and Ultrafiltration for Molecular Weight Characterisation of Aquatic Organic Matter and Humic Substances
Proc.–AWWA Annu. Conf., 1347–1361 (1985)

96 Rashid, M.A.
Role of Humic Acids of Marine Origin and their Different Molecular Weight Fractions in Complexing Di– and Tri–valent Metals
Soil Science, 111(5), 298–306 (1971)

97 Biederbeck, V.O. & Paul, E.A.
Fractionation of Soil Humate with Phenolic Solvents and Purification of the Nitrogen-Rich Portion with Polyvinylpyrrolidone
Soil Sci., 115(5), 357–366 (1973)

98 Kerr, R.A. & Quinn, J.G.
Chemical Studies on the Dissolved Organic Matter in Sea Water. Isolation and Fractionation
Deep Sea Res., 22, 107–116 (1975)

99 Ogner, G.
Fractionation of Humus Hydrolysates by Ion Exchange Resins
Soil Sci., 110(2), 86–92 (1970)

100 Swift, R.S.; Thornton, B.K. & Posner, A.M.
Spectral Characteristics of a Humic Acid Fractionated with respect to Molecular Weight using an Agar Gel
Soil Sci., 110(2), 93–99 (1970)

101 Gjessing, E.T.
Physical and Chemical Characteristics of Aquatic Humus
Ann Arbor Science, Michigan (1976)

102 Gjessing, E.T.
Gel and Ultramembrane Filtration of Aquatic Humus: A Comparison of the Two Methods
Schw. Z. Hydrol, 35, 286–294 (1973)

103 Amicon Corp.
Products for Separations Technology
Publication 553, Amicon Corp., Massachusetts (1983)

104 Brock, T.D.
Membrane Filtration: A User's Guide and Reference Manual
Springer-Verlag, Berlin (1983)

105 Amicon Corp.

Salt Removal by Diafiltration
Publication 446C, Amicon Corp., Massachusetts (1981)

106 Collins, M.R.; Amy, G.L. & Steelink, C.
Molecular Weight Distribution, Carboxylic Acidity and Humic Substances Content of Aquatic Organic Matter: Implications for Removal During Water Treatment
Environ. Sci. Technol., 20(10), 1028–1032 (1986)

107 Dobbs, R.A.; Wise, R.H. & Dean, R.B.
The Use of Ultraviolet Absorbance for Monitoring the Total Organic Carbon Content of Water and Waste Water
Water Res., 6, 1173–1180 (1972)

108 Buffle, J.; Deladoey, P. & Haerdi, W.
The Use of Ultrafiltration for the Separation and Fractionation of Organic Ligands in Fresh Waters
Anal. Chim. Acta, 101, 339–357 (1978)

109 Chen, Y.; Senesi, N. & Schnitzer, M.
Information Provided on Humic Substances by E_4:E_6 Ratios
Soil Sci. Soc. Am. J., 41, 352–358 (1977)

110 Andreux, F.
Genesis and Properties of Humic Molecules
Ch. 6, pp 109–139, in
Bormeau, M. & Souchiet, B.
Constituents and Properties of Soils
Academic Press, London (1982)

111 Amicon Corp.
Operating Instructions for Diaflo® Ultrafilters
Publication I–101M, Amicon Corp., Massachusetts (1981)

112 Jeffrey, P.D.
Biochem., 13, 4441–4444 (1974)

113 Richardson, F.S.
Terbium(III) and Europium(III) Ions as Luminescent Probes and Stains for Biomolecular Systems
Chem. Rev., 82, 541–552 (1982)

114 Wybourne, B.G.
Spectroscopic Properties of Rare Earths
Interscience, New York (1965)

115 Hufner, S.
Optical Properties of Transparent Rare Earth Compounds
Academic Press, New York (1978)

116 Hufner, S.
Ch. 8, pp 313–388, in
Sinha, S.P. (Ed.)
Systematics and Properties of The Lanthanides
NATO ASI Series C No.109, D.Reidel Publishing Company, Dordrech (1983)

117 Sharpe, A.G.
Inorganic Chemistry
Longman, London (1981)

118 Thompson, L.C.

Ch. 25, pp 209–297, in
Gschneidner, K.A. & Eyring, L. (Eds.)
Handbook on the Physics and Chemistry of the Rare Earths, Volume 3
North-Holland Publishing Company, Amsterdam (1979)

119 Atkins, P.W.
Physical Chemistry
2nd Edition, Oxford University Press, Oxford (1982)

120 Förster, T.
Transfer Mechanisms of Electronic Excitation
Disc. Faraday Soc., (27), 7–17 (1959)

121 McCapra, F.
Shining a Light on Medical Diagnostics
Chem. Br., 25(2), 139–144 (1989)

122 Li, W.; Mishima, T.; Adachi, G.–Y. & Shiokawa, J.
The Fluorescence of Transparent Polymer Films of Rare Earth Complexes
Inorg. Chim. Acta, 121, 97–101 (1986)

123 Okamoto, Y.; Wang, S.S.; Zhu, K.J.; Banks, E.; Garetz, B. & Murphy, E.K.
Synthesis, Characterisation and Applications of Rare Earth Metal Ion Chelating Polymers
pp 425–450, in
Sheats, J.E.; Pittman, C.U., Jr. & Carraller, C.E., Jr. (Eds.)
Metal Containing Polymeric Systems
Plenum Press, New York (1985)

124 Alpha, B.; Lehn, J.–M. & Mathis, G.
Energy Transfer Luminescence of Europium(III) and Terbium(III) Cryptates of Macrobicyclic Polypyridine Ligands
Angew. Chem. Int. Ed. Engl., 26(3), 266–267 (1987)

125 Zepp, R.G.; Schlotzhauer, P.F. & Sink, R.M.
Photosensitised Transformations Involving Electronic Energy Transfer in Natural Waters: Role of Humic Substances
Environ. Sci. Technol., 19, 74–81 (1985)

126 Fischer, A.M.; Winterle, J.S. & Mill, T.
Primary Photochemical Processes in Photolysis Mediated by Humic Substances
Ch. 10, pp 132–140, in
Zika, R.G. & Cooper, W.J. (Eds.)
Photochemistry of Environmental Aquatic Systems
ACS Symposium Series, 327, American Chemical Society, Washington D.C. (1987)

127 Chapman, R.D.; Loda, R.T.; Riehl, J.P. & Schwartz, R.W.
Spectroscopic Investigation of the Multidentate Coordination Equilibrium among Conformational Isomers of Tris(2,2',2"–terpyridyl)europium(III) Perchlorate in Acetonitrile
Inorg. Chem., 23, 1652–1657 (1984)

128 Hilmes, G.L. & Riehl, J.P.
Circularly Polarized Luminescence from Racemic Lanthanide(III) Complexes with Achiral Ligands in Aqueous Solution using Circularly Polarized Excitation
Inorg. Chem., 25, 2617–2622 (1986)

129 *Fluorescence Spectrometer 3000 Operation Manual*

Perkin Elmer

130 Ismail, K.Z. & El-Bayoumi, M.A.
Intramolecular Energy-Transfer in a Europium(III) Chelate with Salicylidene-Valinate Schiff Base
Transition Met. Chem., 9, 335-337 (1984)

131 Hwang, Y.T.; Andrews, L.J. & Solomon, E.I.
Resonant Fluorescence Study of the Eu^{3+}-Substituted Ca^{2+} Site in Busycon Hemocyanin: Structural Coupling between the Heterotrophic Allosteric Effector and the Coupled Binuclear Copper Active Site
J. Am. Chem. Soc., 106, 3832-3838 (1984)

132 Crosby, G.A.; Whan, R.E. & Alire, R.M.
J. Chem. Phys., 34, 743-745 (1961)

133 Power, J.F.; Sharma, D.K.; Langford, C.H.; Bonneau, R. & Joussot-Dubien, J.
Photophysics of a Well-Characterised Humic Substance
Photochem. Photobiol., 44(1), 11-13 (1986)

134 Dobbs, J.C.; Susetyo, W.; Knight, F.E.; Castles, M.A.; Carreira, L.A. & Azarraga, L.V.
Characterisation of Metal Binding Sites in Fulvic Acids by Lanthanide Ion Probe Spectroscopy
Anal. Chem., 61(4), 483-488 (1989)

135 Dobbs, J.C.; Susetyo, W.; Carreira, L.A. & Azarraga, L.V.
Competitive Binding of Protons and Metal Ions in Humic Substances by Lanthanide Ion Probe Spectroscopy
Anal. Chem., 61(14), 1519-1524 (1989)

136 Hercules, D.M.
Theory of Luminescence Processes
Ch. 1, pp 1-40, in
Hercules, D.M. (Ed.)
Fluorescence and Phosphorescence Analysis: Principles and Applications
Interscience, New York (1966)

137 Ohnesorge, W.E.
Fluorescence of Metal Chelate Compounds
Ch. 4, pp 151-167, in
Hercules, D.M. (Ed.)
Fluorescence and Phosphorescence Analysis: Principles and Applications
Interscience, New York (1966)

138 Ryan, D.K.; Thompson, C.P. & Weber, J.H.
Comparison of Mn^{2+}, Co^{2+} and Cu^{2+} Binding to Fulvic Acid as Measured by Fluorescence Quenching
Can. J. Chem., 61, 1505-1509 (1983)

139 Saar, R.A. & Weber, J.H.
Comparison of Spectrofluorometry and Ion-Sensitive Electrode Potentiometry for Determination of Complexes between Fulvic Acid and Heavy-Metal Ions
Anal. Chem., 52, 2095-2100 (1980)

140 Gauthier, T.D.; Shane, E.C.; Guerin, W.F.; Seitz, W.R. & Grant, C.L.

Fluorescence Quenching Method for Determining Equilibrium Constants for Polycyclic Aromatic Hydrocarbons Binding to Dissolved Humic Materials
Environ. Sci. Technol., 20(11), 1162–1166 (1986)

141 Berger, P.; Ewald, M.; Liu, D. & Weber, J.H.
Application of the Fluorescence Quenching Titration Method to the Complexation of Copper(II) in the Gironde Estuary (France)
Mar. Chem., 14, 289–295 (1984)

142 Blaser, P. & Sposito, G.
Spectrofluorometric Investigation of Trace Metal Complexation by an Aqueous Chestnut Leaf Litter Extract
Soil Sci. Soc. Am. J., 51(3), 612–619 (1987)

143 Cabaniss, S.E. & Shuman, M.S.
Combined Ion Sensitive Electrode and Fluorescence Quenching Detection for Copper-Dissolved Organic Matter Titrations
Anal. Chem., 58(2), 398–401 (1986)

144 Cabaniss, S.E.
A Potentiometric and Fluorometric Study of Copper Complexation by Dissolved Organic Matter
PhD Thesis, University of North Carolina at Chapel Hill (1986)

145 Cabaniss, S.E. & Shuman, M.S.
Fluorescence Quenching Measurements of Copper-Fulvic Acid Binding
Anal. Chem., 60(21), 2418–2421 (1988)

146 Fish, W. & Morel, F.M.M.
Propagation of Error in Fulvic Acid Titration Data: A Comparison of Three Analytical Methods
Can. J. Chem., 63, 1185–1193 (1985)

147 Frimmel, F.H. & Hopp, W.
Stability Spectra for the Description of Copper-Humic Acid Complexes: A Fluorescence Quench Study
Fressenius Z. Anal. Chem., 325(1), 68–72 (1986)

148 Ryan, D.K. & Weber, J.H.
Copper(II) Complexing Capacities of Natural Waters by Fluorescence Quenching
Environ. Sci. Technol., 16, 866–872 (1982)

149 Ryan, D.K. & Weber, J.H.
Fluorescence Quenching Titration for Determination of Complexing Capacities and Stability Constants of Fulvic Acid
Anal. Chem., 54(6), 986–990 (1982)

150 Underdown, A.W.; Langford, C.H. & Gamble, D.S.
The Fluorescence and Visible Absorbance of Cu(II) and Mn(II) Complexes of Fulvic Acid: The Effect of Metal Ion Loading
Can. J. Soil Sci., 61, 469–474 (1981)

151 Waite, T.D. & Morel, F.M.M.
Ligand Exchange and Fluorescence Quenching Studies of the Fulvic Acid-Iron Interaction: Effects of pH and Light
Anal. Chim. Acta, 162, 263–274 (1984)

152 Ebsworth, E.A.V.; Rankin, D.W.H. & Cradock, S.
Structural Methods in Inorganic Chemistry
Blackwell Scientific, Oxford (1987)

153 Paudler, W.W.
Nuclear Magnetic Resonance: General Concepts and Applications
Wiley, Chichester (1987)

154 Benn, R. & Rufínska, A.
High-Resolution Metal-NMR Spectroscopy of Organometallic Compounds
Angew. Chem. Int. Ed. (Engl.), 25, 861–881 (1986)

155 Wilson, M.A.
Applications of Nuclear Magnetic Resonance Spectroscopy to the Study of the Structure of Soil Organic Matter
J. Soil Sci., 32, 167–186 (1981)

156 Bronnimann, C.E.; Hawkins, B.L.; Zhang, M. & Maciel, G.E.
Combined Rotation and Multiple Pulse Spectroscopy as an Analytical Proton Nuclear Magnetic Resonance Technique for Solids
Anal. Chem., 60(17), 1743–1750 (1988)

157 Dereppe, J.–M.; Moreaux, C. & Debyser, Y.
Investigation of Marine and Terrestrial Humic Substances by ^{1}H and ^{13}C Nuclear Magnetic Resonance and Infrared Spectroscopy
Org. Geochem., 2, 117–124 (1980)

158 Hatcher, P.G.; Rowan, R. & Mattingly, M.A.
^{1}H and ^{13}C NMR of Marine Humic Acids
Org. Geochem., 2, 77–85 (1980)

159 Hatcher, P.G.; Maciel, G.E. & Dennis, L.W.
Aliphatic Structure of Humic Acids: A Clue to Their Origin
Org. Geochem., 3, 43–48 (1981)

160 Wilson, M.A.; Collin, P.J. & Tate, K.R.
^{1}H–Nuclear Magnetic Resonance Study of a Soil Humic Acid
J. Soil Sci., 34, 297–304 (1983)

161 Poutanen, E.L.
Characterisation of Humic and Fulvic Acids Isolated from Baltic Sea Sediments using ^{13}C and ^{1}H Nuclear Magnetic Resonance Spectra
Org. Geochem., 9(4), 163–170 (1986)

162 Bartle, K.D.; Pomfret, A.; Pappin, A.J.; Mills, D.G. & Evliya, H.
Analysis of Methylated Humic Acids from Fossil Fuels by Size Exclusion Chromatography and NMR
Org. Geochem., 11(3), 139–149 (1987)

163 Fründ, R.; Gonzalez-Vila, F.J.; Lüdemann, H.–D. & Martin, F.
Comparison of the Solid State CPMAS and Solution Carbon–13–NMR Spectra of Humic Acids Extracted from Composted Municipal Refuse
Z. Naturforsch., C: Biosci., 42(3), 205–208 (1987)

164 Leenheer, J.A.; Wilson, M.A. & Malcolm, R.L.
Presence and Potential Significance of Aromatic-Ketone Groups in Aquatic Humic Materials
Org. Geochem., 11(4), 273–280 (1987)

165 Newman, R.H.; Tate, K.R.; Barron, P.F. & Wilson, M.A.
Towards a Direct, Non–Destructive Method of Characterising Soil Humic Substances Using ^{13}C NMR

J. Soil Sci., 31, 623–631 (1980)

166 Schnitzer, M. & Preston, C.M.
Analysis of Humic Acids by Solution and Solid-State Carbon–13 Nuclear Magnetic Resonance
Soil Sci. Soc. Am. J., 50(2), 326–331 (1986)

167 Barron, P.F.; Wilson, M.A.; Stephens, J.F.; Cornell, B.A. & Tate, K.R.
Cross Polarisation ^{13}C NMR Spectroscopy of Whole Soils
Nature, 286, 585–587 (1980)

168 Hatcher, P.G.; Schnitzer, M.; Vassallo, A.M. & Wilson, M.A.
The Chemical Structure of Highly Aromatic Humic Acids in Three Volcanic Ash Soils as Determined by Dipolar Dephasing NMR Studies
Geochim. Cosmochim. Acta, 53(1), 125–130 (1989)

169 Vassallo, A.M.; Wilson, M.A.; Collin, P.J.; Oades, J.M.; Waters, A.G. & Malcolm, R.L.
Structural Analysis of Geochemical Samples by Solid-State Nuclear Magnetic Resonance Spectrometry. Role of Paramagnetic Material
Anal. Chem., 59(4), 558–562 (1987)

170 Preston, C.M.; Dudley, R.L.; Fyfe, C.A. & Mathur, S.P.
Effects of Variations in Contact Times and Copper Contents in a ^{13}C CPMAS NMR Study of Samples of Four Organic Soils
Geoderma, 33(3), 245–253 (1984)

171 Pfeffer, P.E.; Gerasimowicz, W.V. & Piotrowski, E.G.
Effect of Paramagnetic Iron on Quantitation in Carbon–13 Cross Polarisation Magic Angle Spinning Nuclear Magnetic Resonance Spectrometry of Heterogeneous Environmental Matrices
Anal. Chem., 56, 734–741 (1984)

172 Preston, C.M. & Schnitzer, M.
^{13}C NMR of Humic Substances: pH and Solvent Effects
J. Soil Sci., 38(4), 667–678 (1987)

173 Newman, R.H. & Tate, K.R.
Use of Alkaline Soil Extracts for ^{13}C NMR Characterisation of Humic Substances
J. Soil Sci., 35, 47–54 (1984)

174 Greenwood, N.N. & Earnshaw, A.
Chemistry of the Elements
Pergamon Press, Oxford (1984)

175 Cockerill, A.F.; Davies, G.L.O.; Harden, R.C. & Rackham, D.M.
Lanthanide Shift Reagents for Nuclear Magnetic Resonance Spectroscopy
Chem. Rev., 73(6), 553–588 (1973)

176 Williams, R.J.P.
The Chemistry of Lanthanide Ions in Solution and Biological Systems
Struc. Bond., 50, 79–119 (1982)

177 Inagaki, F. & Miyazawa, T.
NMR Analyses of Molecular Conformations and Conformational Equilibria with the Lanthanide Probe Method
Prog. N.M.R. Spectroscopy, 14, 67–111 (1981)

178 Nieboer, E.

The Lanthanide Ions as Structural Probes in Biological and Model Systems
Struc. Bond., 22, 1–47 (1975)

179 Rehder, D.
Early Transition Metals, Lanthanides and Actinides
Ch. 19, pp 479–519, in
Mason, J. (Ed.)
Multinuclear NMR
Plenum, New York (1987)

180 Pommery, J.; Ebenga, J.P.; Imbenotte, M.; Palavit, G. & Erb, F.
Determination of the Complexing Ability of a Standard Humic Acid Towards Cadmium Ions
Water Res., 22(2), 185–189 (1988)

181 Schebetkovskii, V.N. & Bochkov, A.A.
Behaviour of Radioactive Elements in Sorption Systems with Humus Substances. IV Sorption of $^{239}Pu^{IV}$ from Acid Solutions by Peat
Soviet Radiochemistry, 17(1), 13–18 (1975)

182 Dechter, J.J.
NMR of Metal Nuclides. Part II. The Transition Metals
Progress in Inorganic Chemistry, 33, 393–507 (1985)

183 Rinaldi, P.L.; Khan, S.A.; Choppin, G.R. & Levy, G.C.
Lanthanum–139 Nuclear Magnetic Resonance Chemical Shifts
J. Am. Chem. Soc., 101(5), 1350–1351 (1979)

184 Thompson, A.R. & Oldfield, E.
Solid-State Scandium–45, Yttrium–89, and Lanthanum–139 Nuclear Magnetic Resonance Spectroscopy
J. Chem. Soc. Chem. Commun., (1), 27–29 (1987)

185 Sayer, B.G.; Hao, N.; Dénès, G.; Bickley, D.G. & McGlinchey, M.J.
Zirconium–91 Nuclear Magnetic Resonance Spectroscopy: The First Chemical Study
Inorg. Chim. Acta, 48, 53–55 (1981)

186 Rehder, D. & Speh, M.
An Exploratory Scandium–45 NMR Study into the Complexation of Alanine and Oligopeptides
Inorg. Chim. Acta, 135, 73–79 (1987)

187 Reuben, J. & Luz, Z.
Longitudinal Relaxation in Spin 7/2 Systems. Frequency Dependence of Lanthanum–139 Relaxation Times in Protein Solutions as a Method of Studying Macromolecular Dynamics
J. Phys. Chem., 80, 1357–1361 (1976)

188 Reuben, J.
Lanthanum–139 as a Nuclear Magnetic Resonance Probe of Macromolecular Dynamics
J. Am. Chem. Soc., 97, 3823–3824 (1975)

189 Kidd, R.G.
Quadrupolar and Other Types of Relaxation
Ch. 5, pp 103–131, in
Laszlo, P. (Ed.)
NMR of Newly Accessible Nuclei, Volume 1: Chemical and

Biochemical Applications
Academic Press, London (1983)

190 Wehrli, F.W.
Nuclear Magnetic Resonance of the Less Common Quadrupolar Nuclei
Annual Reports on NMR Spectroscopy, 9, 125–219 (1979)

191 Brevard, C. & Granger, P.
Handbook of High Resolution Multinuclear NMR
Wiley, New York (1981)

192 Sillén, L.G. & Martell, A.E. (Eds.)
Stability Constants of Metal-Ion Complexes Supplement No. 1
Special Publication No. 25, The Chemical Society, London (1971)

193 Weast, R.C. (Ed.)
Handbook of Chemistry and Physics
53rd Edition, The Chemical Rubber Co., CRC Press, Cleveland (1972)

194 Wilson, M.A.
NMR Techniques and Applications in Geochemistry and Soil Chemistry
Pergamon Press, Oxford (1987)

195 Zumbulyadis, N.
Suppression of the Spinner Signal in Magic-Angle-Spinning NMR
J. Magn. Reson., 49, 329–331 (1982)

196 Blümich, B. & Spiess, H.W.
Two-Dimensional Solid-State NMR Spectroscopy: New Possibilities for the Investigation of the Structure and Dynamics of Solid Polymers
Angew. Chem. Int. Ed. Engl., 27, 1655–1672 (1988)

197 Dixon, W.T.; Schaefer, J.; Sefcik, M.D.; Stejskal, E.O. & McKay, R.A.
Total Suppression of Sidebands in CPMAS C–13 NMR
J. Magn. Reson., 49, 341–345 (1982)

198 Gamble, D.S.; Langford, C.H. & Tong, J.P.K.
The Structure and Equilibria of a Manganese(II) Complex of Fulvic Acid Studied by Ion Exchange and Nuclear Magnetic Resonance
Can. J. Chem., 54, 1239–1245 (1976)

199 Melson, G.A.; Olszanski, D.J. & Rahimi, A.K.
Coordination Chemistry of Scandium. VIII[1] Detection of Complex Formation in Solution by ^{45}Sc NMR Spectroscopy
Spectrochim. Acta, 33A, 301–309 (1977)

200 Kidd, R.G.
Nuclear Shielding of the Transition Metals
Annual Reports on NMR Spectroscopy, 10A, 1–79 (1980)

201 Drakenberg, T.
Nuclear Magnetic Resonance of Less Common Quadrupolar Nuclei
Annual Reports on NMR Spectroscopy, 17, 231–283 (1986)

202 Vickery, R.C.
Scandium, Yttrium and Lanthanum
Ch. 31, pp 329–353 in
Bailar, J.C., Jr.; Emeléus, H.J.; Nyholm, Sir R. & Trotman-Dickenson, A.F. (Eds.)

Comprehensive Inorganic Chemistry Volume 3
Pergamon Press, Oxford (1973)

203 Vijverberg, C.A.M.; Peters, J.A.; Kieboom, A.P.G. & van Bekkum, H.
The Use of Lanthanum–139 NMR in the Study of Complexation Behaviour of (Hydroxy)Carboxylate Anions
Rec. Trav. Pays–Bas, 99(9), 287–288 (1980)

204 Tarasov, V.P.; Kirakosyan, G.A.; Yu, A.B.; Trots, S.V. & Panyushkin, V.T.
Investigation of Water-Dimethylformamide Solutions of Lanthanum(III) by ^{139}La NMR
Soviet Journal of Co–ordination Chemistry, 11(7), 514–518 (1985)

205 Bünzli, J.–C.G.; Merbach, A.E. & Nielson, R.M.
^{139}La NMR and Quantitative FT–IR Investigation of the Interaction between Ln(III) Ions and Various Anions in Organic Solvents
Inorg. Chim. Acta, 139, 151–152 (1987)

206 Akitt, J.W.
Aluminium, Gallium, Indium and Thallium
Ch. 9, pp 259–292, in
Mason, J. (Ed.)
Multinuclear NMR
Plenum, New York (1987)

207 Cummins, H.Z.; Knable, N. & Yeh, Y.
Observation of Diffuse Broadening of Rayleigh Scattered Light
Phys. Rev. Lett., 12(6), 150–155 (1964)

208 Yeh, H. & Cummins, H.Z.
Localised Fluid Flow Measurements with an He–Ne Laser Spectrometer
Appl. Phys. Lett., 4, 176–178 (1964)

209 Drain, L.E.
The Laser Doppler Technique
John Wiley and Sons, Chichester (1980)

210 Easson, B. & Greated, C.
Breaking Waves
Physics World, (4), 36–40 (1990)

211 Shaw, D.J.
Electrophoresis
Academic Press, London (1969)

212 Ware, B.R. & Flygare, W.H.
The Simultaneous Measurement of the Electrophoretic Mobility and Diffusion Coefficient in Bovine Serum Albumin Solutions by Light Scattering
Chem. Phys. Lett., 12(1), 81–85 (1971)

213 Ware, B.R. & Flygare, W.H.
Light Scattering in Mixtures of BSA, BSA Dimers, and Fibrinogen Under the Influence of Electric Fields
J. Colloid Interface Sci., 39(3), 670–675 (1972)

214 M^{c}Fayden, P.
Electrophoretic Mobility and Zeta Potential of Colloidal Particles
International Laboratory, 32–42 (September 1986)

215 Uzgiris, E.E. & Costaschuk, F.M.

Investigation of Colloid Stability in Polyelectrolyte Solutions by Laser Doppler Spectroscopy
Nature (Phys. Sci.), 242, 77–79 (1973)

216 Underdown, A.W.; Langford, C.H. & Gamble, D.S.
Light Scattering of a Polydisperse Fulvic Acid
Anal. Chem., 53(13), 2139–2140 (1981)

217 Underdown, A.W.; Langford, C.H. & Gamble, D.S.
Light Scattering Studies of the Relationship between Cation Binding and Aggregation of a Fulvic Acid
Environ. Sci. Technol., 19(2), 132–136 (1985)

218 Gamble, D.S.; Langford, C.H. & Underdown, A.W.
Light Scattering Measurements of Cu(II)–Fulvic Acid Complexing: The Interdependence of Apparent Complexing Capacity and Aggregation
Proceedings of the First Meeting of the International Humic Substances Society
Estes Park, Colorado, August 1983
Org. Geochem., 8(1), 35–39 (1985)

219 MacKenzie, A.F. & Dawson, J.E.
A Study of Organic Soil Horizons using Electrophoretic Techniques
J. Soil Sci., 13(2), 160–166 (1962)

220 Cameron, A.J. & Liss, P.S.
The Stabilisation of "Dissolved" Iron in Freshwaters
Water Res., 18(2), 179–185 (1984)

221 Tipping, E. & Cooke, D.
The Effects of Adsorbed Humic Substances on the Surface Charge of Goethite (α–FeOOH) in Freshwaters
Geochim. Cosmochim. Acta, 46, 75–80 (1982)

222 Hunter, K.A.
Microelectrophoretic Properties of Natural Surface Active Organic Matter in Coastal Seawater
Limnol. Oceanogr., 25(5), 807–822 (1980)

223 Kononova, M.M. & Titova, N.A.
Use of Paper Electrophoresis for Fractionation of the Humic Substances of Soil and for Study of their Complex Compounds with Iron
Soviet Soil Sci., 1230–1237 (1961)

224 Varney, M.S.; Mantoura, R.F.C.; Whitfield, M.; Turner, D.R. & Riley, J.P.
Potentiometric and Conformational Studies of the Acid-Base Properties of Fulvic Acid from Natural Waters
pp 751–772, in
Wong, C.S.; Boyle, E.; Bruland, K.W.; Burton, J.D. & Goldberg, E.D. (Eds.)
Trace Metals in Sea Water
Proceedings of a NATO Advanced Research Institute on Trace Metals in Sea Water
30 March–3 April 1981, Errice, Sicily
NATO Conference Series, IV, Marine Sciences, 9, Plenum Press, New York (1983)

225 DeNobili, M.; Leita, L. & Sequi, P.
2D Electrophoresis of Humic Substances: Application of a High Resolution

Technique to Polyanionic Polydisperse Systems
Becher, G. (Ed.)
Advances in Humic Substances Research
Proceedings of the Third International Meeting of the International **Humic Substances Society**
Oslo, Norway, 4–8 August 1986
Sci. Tot. Env., 62, 85–88 (1987)

226 Zhang, D. & Lu, S.
An Assessment of the Separation and Analysis of Humic Substances by Isoelectric Focussing (IEF) Method
Becher, G. (Ed.)
Advances in Humic Substances Research
Proceedings of the Third International Meeting of the International **Humic Substances Society**
Oslo, Norway, 4–8 August 1986
Sci. Tot. Env., 62, 89–96 (1987)

227 Ramsay, J.D.F. & Scanlon, M.
Structure and Interactions in Aqueous Colloidal Dispersions of Oxide Particles
Colloids and Surfaces, 18, 207–221 (1986)

228 Uzgiris, E.E. & Kaplan, J.H.
Protein Coated Electrodes
Rev. Sci. Instrum., 45(1), 120–121 (1974)

229 Hieminz, P.C.
Principles of Colloid and Surface Chemistry
2nd Edition, Marcel Dekker Inc., New York (1986)

230 Lindqvist, I.
A Small Angle X–Ray Scattering Study of Sodium Humate Solutions
Acta Chem. Scand., 24(8), 3068–3069 (1970)

231 Thurman, E.M.; Wershaw, R.L.; Malcolm, R.L. & Pinckney, D.J.
Molecular Size of Humic Substances
Org. Geochem., 4, 27–35 (1982)

232 Wershaw, R.L.; Burcar, P.J.; Sutula, C.L. & Wiginton, B.J.
Sodium Humate Solution Studied with Small Angle X–Ray Scattering
Science, 157, 1429–1431 (1967)

233 Olson, E.S. & Diehl, J.W.
Size Exclusion Chromatography-Low Angle Laser Light Scattering Photometry of Lignite Macromolecules
J. Chromatog., 349(2), 337–346 (1985)

234 Olson, E.S.; Diehl, J.W. & Froehlich, M.L.
Molecular Weights of Lignite Macromolecules
ACS Fuel Division Preprints, 31(1), 102–106 (1985)

235 Olson, E.S.; Diehl, J.W. & Froehlich, M.L.
Structural Features of Low-Rank Coals Important in Liquefaction, Bioconversion and Gasification
Fuel Process. Technol., 15, 319–326 (1987)

236 Hombach, H.–P.; Collins, C.J.; Maxwell, B.E. & Benjamin, B.M.
Scattering of Radiation by Coal

Paper A3, pp 16–21, in
Proceedings of an International Conference on Coal Science
Sponsored by the International Energy Agency, Dusseldorf, September 1981, Verlag Glückauf GmbH, Essen (1981)

237 Hayase, K. & Tsubota, H.
Sedimentary Humic Acid and Fulvic Acid as Surface Active Agents
Geochim. Cosmochim. Acta, 47, 947–952 (1983)

238 Haas, D.D. & Ware, B.R.
Design and Construction of a New Electrophoretic Light Scattering Chamber and Applications to Solutions of Hemoglobin
Anal. Biochem., 74, 175–188 (1976)

239 Ware, B.R.
The Study of Biological Surfaces by Laser Electrophoretic Light Scattering
Ch. 7, pp 102–117, in
New Applications of Lasers in Chemistry
American Chemical Society, Washington D.C (1978)

240 Ramsay, J.D.F. & Poinsignon, C.
Neutron Scattering Investigations of Porous Silicas and Water/Silica Interfaces
Langmuir, 3(3), 320–326 (1987)

241 Ramsay, J.D.F.
Recent Developments in the Characterisation of Oxide Sols using Small Angle Neutron Scattering Techniques
Chem. Soc. Rev., 15, 335–371 (1986)

242 Huglin, M.B. (Ed.)
Light Scattering from Polymer Solutions
Academic Press, London (1972)

243 Ephraim, J.; Alegret, S.; Mathuthu, A.; Bicking, M.; Malcolm, R.L. & Marinsky, J.A.
A Unified Physicochemical Description of the Protonation and Metal Ion Complexation Equilibria of Natural Organic Acids (Humic and Fulvic Acids). 2. Influence of Polyelectrolyte Properties and Functional Group Heterogeneity on the Protonation Equilibria of Fulvic Acid.
Environ. Sci. Technol., 20(4), 354–366 (1986)

244 Ephraim, J.H.
Studies of the Protonation and Metal Ion Complexation Equilibria of Natural Organic Acids: Fulvic Acids
PhD Thesis, State University of New York at Buffalo (1985)

245 Mathuthu, A.S.
A Unified Physicochemical Description of the Protonation and Metal Ion Complexation Equilibria of Natural Organic Acids (Fulvic Acid) in Ionic Media.
PhD Thesis, State University of New York at Buffalo (1987)

246 Shapiro, J.
Chemical and Biological Studies on the Yellow Organic Acids of Lake Water
Limnol. Oceanogr., 2(3), 161–179 (1957)

247 Gamble, D.S.
Titration Curves of Fulvic Acid: The Analytical Chemistry of a Weak Acid Polyelectrolyte

Can. J. Chem., 48, 2662–2669 (1970)

248 Gamble, D.S.
Potentiometric Titration of Fulvic Acid: Equivalence Point Calculations and Acidic Functional Groups
Can. J. Chem., 50, 2680–2690 (1972)

249 Choppin, G.R. & Kullberg, L.
Protonation Thermodynamics of Humic Acid
J. Inorg. Nucl. Chem, 40, 651–654 (1978)

250 Marinsky, J.A. & Ephraim, J.
A Unified Physicochemical Description of the Protonation and Metal Ion Complexation Equilibria of Natural Organic Acids (Humic and Fulvic Acids). 1. Analysis of the Influence of Polyelectrolyte Properties on Protonation Equilibria in Ionic Media: Fundamental Concepts.
Environ. Sci. Technol., 20(4), 349–354 (1986)

251 Marinsky, J.A.; Gupta, S. & Schindler, P.
The Interaction of Cu(II) Ion with Humic Acid
J. Coll. Interfac. Sci., 89(2), 401–411 (1982)

252 Lamy, I.; Cromer, M. & Scharff, J.P.
Comparative Study of Copper(II) Interactions with Monomeric Ligands and Synthetic or Natural Organic Materials from Potentiometric Data
Anal. Chim. Acta, 212(1–2), 105–122 (1988)

253 Pommer, A.M. & Breger, I.A.
Potentiometric Titration and Equivalent Weight of Humic Acid
Geochim. Cosmochim. Acta, 20, 30–44 (1960)

254 Pommer, A.M. & Breger, I.A.
Equivalent Weight of Humic Acid from Peat
Geochim. Cosmochim. Acta, 20, 45–50 (1960)

255 van Dijk, H.
Electrometric Titrations of Humic Acids
Sci. Proc. R. Dub. Soc., Ser. A1: 4, 163–176 (1960)

256 Yonebayashi, K. & Hattori, T.
Non–Aqueous Titration of Functional Groups in Humic Acid
Proceedings of the First Meeting of the International Humic Substances Society
Estes Park, Colorado, August 1983
Org. Geochem., 8(1), 47–54 (1985)

257 Huizenga, D.L. & Kester, D.R.
Protonation Equilibria of Marine Dissolved Organic Matter
Limnol. Oceanogr., 24(1), 145–150 (1979)

258 Frizado, J.P.
Ion Exchange on Humic Materials– A Regular Solution Approach
Ch. 7, pp 133–145, in
Jenne, E.A. (Ed.)
Chemical Modelling in Aqueous Systems
ACS Symposium Series, 93, American Chemical Society, Washington D.C. (1979)

259 Ephraim, J. & Marinsky, J.A.
A Unified Physicochemical Description of the Protonation and Metal Ion

Complexation Equilibria of Natural Organic Acids (Humic and Fulvic Acids). 3. Influence of Polyelectrolyte Properties and Functional Group Heterogeneity on the Copper(II) Ion Binding Equilibria in an Armadale Horizons Bh Fulvic Acid Sample.
Environ. Sci. Technol., 20(4), 367–376 (1986)

260 Marinsky, J.A.; Gupta, S. & Schindler, P.
A Unified Physicochemical Description of the Equilibria Encountered in Humic Acid Gels.
J. Coll. Interfac. Sci., 89(2), 412–426 (1982)

261 Wilson, D.E. & Kinney, P.
Effects of Polymeric Charge Variations on the Proton-Metal Ion Equilibria of Humic Materials
Limnol. Oceanogr., 22(2), 281–289 (1977)

262 Borggaard, O.K.
Titrimetric Determination of Acidity and pK Values of Humic Acid
Acta Chem. Scand., A28(1), 121–122 (1974)

263 Borggaard, O.K.
Experimental Conditions Concerning Potentiometric Titration of Humic Acid
J. Soil Sci., 25, 189–195 (1974)

264 Cabaniss, S.E. & Morel, F.M.M.
Comment on "A Unified Physicochemical Description of the Protonation and Metal Ion Complexation Equilibria of Natural Organic Acids (Humic and Fulvic Acids)"
Environ. Sci. Technol., 23(6), 746–747 (1989)

265 Marinsky, J.A.
Rebuttal to Comment on "A Unified Physicochemical Description of the Protonation and Metal Ion Complexation Equilibria of Natural Organic Acids, Parts 1 and 2"
Environ. Sci. Technol., 23(6), 747–748 (1989)

266 Dzombak, D.A.; Fish, W. & Morel, F.M.M.
Metal-Humate Interactions: 1. Discrete Ligand and Continuous Distribution Models
Environ. Sci. Technol., 20(7), 669–675 (1986)

267 Fish, W.; Dzombak, D.A. & Morel, F.M.M.
Metal-Humate Interactions: 2. Application and Comparison of Models
Environ. Sci. Technol., 20(7), 676–683 (1986)

268 Gamble, D.S.; Underdown, A.W. & Langford, C.H.
Copper(II) Titration of Fulvic Acid Ligand Sites with Theoretical, Potentiometric and Spectroscopic Analysis
Anal. Chem., 52, 1901–1908 (1980)

269 Gamble, D.S.; Schnitzer, M.; Kerndorff, H. & Langford, C.H.
Multiple Metal Ion Exchange Equilibria with Humic Acid
Geochim. Cosmochim. Acta, 47, 1311–1323 (1983)

270 Tipping, E. & Hurley, M.A.
A Model of Solid-Solution Interactions in Acid Organic Soils Based on the Complexation Properties of Humic Substances.
J. Soil Sci., 39(4), 505–519 (1988)

271 Turner, D.R.; Varney, M.S.; Whitfield, M.; Mantoura, R.F.C. & Riley, J.P.
Electrochemical Studies of Copper and Lead Complexation by Fulvic Acid. 1. Potentiometric Measurements and a Critical Comparison of Metal Binding Models.

Geochim. Cosmochim. Acta, 50(2), 289–297 (1986)

272 Posner, A.M.
Titration Curves of Humic Acid
Trans. 8th Int. Congress Soil Sci. Comm., 2, 161–174 (1964)

273 Yonebayashi, K. & Hattori, T.
Surface Active Properties of Soil Humic Acids
Becher, G. (Ed.)
Advances in Humic Substances Research
Proceedings of the Third International Meeting of the International Humic Substances Society
Oslo, Norway, 4–8 August 1986
Sci. Tot. Env., 62, 55–64 (1987)

APPENDIX 1

CHEMICALS and EQUIPMENT INDEX

Table A1.1

Chemicals Index

Reference	Chemical	Supplier	Grade	Product Number	Other Information
¢001	Fluka Humic Acid v1 (s)	Fluka		53680	FHA v1, Lot No. 33828 1084
¢002	Fluka Humic Acid v2 (s)	Fluka		53680	FHA v2
¢003	Fluka Humic Acid v3 (s)	Fluka		53680	FHA v3, Lot No. 33980 1086
¢004	Aldrich Humic Acid, Sodium Salt v1 (s)	Aldrich	Technical	H1,675-2	AHA v1, Batch 54975
¢005	Aldrich Humic Acid, Sodium Salt v2 (s)	Aldrich	Technical	H1,675-2	AHA v2, Batch 8860 3
¢006	Fanay-Augéres Fulvic Acid (s)	Donation			FAFA
¢007	Fanay-Augéres Humic Acid (s)	Donation			FAHA
¢008	Gorleben Gohy 573 Humic Acid (s)	Donation			GGHA 573
¢009	Nitrogen (g)	B.O.C.	Oxygen-Free		
¢010	Sodium Hydroxide pellets	B.D.H.	A.R.		Assay > 98 %; Na_2CO_3 = 1 %
¢011	Concentrated Hydrochloric Acid (aq)	F.S.A.	A.R.	H/1200	~35-38 % w/v HCl
¢012	Buffer Sachets	Kent EIL			
¢013	Buffer Mixture pH 4.0 (s)	B.D.H.		331892 M	
¢014	Buffer Mixture pH 7.0 (s)	B.D.H.		331902 U	
¢015	Buffer Mixture pH 9.2 (s)	B.D.H.		33191 2 W	
¢018	Silver Nitrate (s)	B.D.H.	A.R.	10233	Assay > 99.9 %
¢019	Phosphorus Pentoxide (s)	Aldrich		21,470-1	
¢022	Potassium Bromide (s)	F.S.A.	Spectrograde	P/4020/48	
¢023	Potassium Bromide (s)	Aldrich	Infrared	22,186-4	
¢028	Sulphur Flowers (s)	Hopkin & Williams	G.P.R.	8338	Ash < 0.2 %
¢032	Sodium Hydroxide (aq) Convol	B.D.H.	A.R.		
¢035	Europium Nitrate Pentahydrate (s)	Aldrich		20,791-8	
¢036	Potassium Hydrogen Phthalate (s)	Aldrich	Gold Label	17,992-2	Assay 99.95-100.05 %
¢037	Phenolphthalein (s)	Aldrich	A.C.S. Reagent	10,594-5	

¢038	Concentrated Nitric Acid $_{(aq)}$	F.S.A.	A.R.	N/2300	~70 % w/v HNO_3, Na < 3 ppm
¢039	Sodium Nitrate $_{(s)}$	B.D.H.	Lab. Reagent	30187	Assay > 98 %
¢044	Deuterium Oxide $_{(D_2O)}$	Aldrich	Gold Label	15,188-2	99.8 atom % D
¢045	Lanthanum Chloride Heptahydrate $_{(s)}$	B.D.H.	Lab. Reagent	29008	
¢046	Praseodymium Perchlorate Hexahydrate $_{(s)}$	Alfa Products	Ventron	87971	
¢047	Ytterbium Ingot	Rare Earth Products			
¢048	Sodium Hydroxide Pellets	May & Baker	Lab. Reagent		
¢049	Concentrated Nitric Acid $_{(aq)}$	F.S.A.	S.L.R.		
¢050	Scandium Chloride Hexahydrate $_{(s)}$	Johnson Matthey	REacton	532759	Oxides/ppm: Lu = 50; Yb = 30
¢051	Yttrium Nitrate Hexahydrate $_{(s)}$	Aldrich		23,795-7	Assay = 99.9 %
¢052	Zirconocene Dichloride $_{(s)}$	Aldrich		19,621-5	Assay > 98 %
¢053	Phthalic Acid $_{(s)}$	B.D.H.	Lab. Reagent	29539	
¢054	Zirconium Nitrate $_{(s)}$	B.D.H.	Technical		
¢055	Polystyrene Latex $_{(aq)}$	Biorad			
¢057	0.1 M Hydrochloric Acid $_{(aq)}$ Convol	B.D.H.	Aristar	18007	

Table A1.2
Equipment Index

Reference	Manufacturer	Item	Product Number
¢016	Uniprobe Instruments	Combination pH Electrode	15-201
¢017	Jennings	Universal Digital pH Meter	P.T.I.-6
¢020	Carlo Erba Strumentazione	Elemental Analyser	1106
¢021	Electrothermal	Electric Bunsen	
¢024	Perkin-Elmer	Fourier Transform Infrared Spectrometer	1710
¢025	Perkin-Elmer	Plotter Printer	PP1
¢026	Perkin-Elmer	Infrared Data Station	
¢027	Stanton	Automatic Thermo-Recording Balance	
¢029	Pye-Unicam	Ultra-violet Spectrophotometer	SP8-100
¢030	Perkin-Elmer	Fluorescence Spectrometer	3000
¢031	Perkin-Elmer	Flat-Bed Recorder	
¢033	Amicon	Diaflo Ultrafilters: XM300; XM100A; XM50; YM30; YM10; YM5; YM2	
¢034	Amicon	400 ml Stirred Cell	8400
¢040	Finnpipette	Finnpipette, 5–50 µl & 1-5 ml	
¢041	Agla	All-Glass Micrometer Syringe (0-0.5 ml)	
¢042	L & R	Maxomatic Ultrasonic Bath (48 W)	
¢043	Bruker	300 MHz NMR Spectrometer	ACE 300
¢056	Millipore	0.10 µm Pore Size Filter	
¢058	Kent EIL	Standard Combination Electrode	
¢059	Phillips	pH Meter	PW 9418
¢060	Gelman Sciences	5 µm Acrodisc®	
¢061	Sabre	Sterile Plastic Syringe	
¢062	Grant	Thermostatted Bath	
¢063	Bellingham and Stanley	Abbé '60' High Accuracy Refractometer	

APPENDIX 2

T.G.A. DATA for PURIFIED FLUKA HUMIC ACID v1

Table A2.1
T.G.A. Data for Purified Fluka Humic Acid v1

Data Operation	Temperature / °C	Sample Weight Loss / mg	Crucible Weight Loss / mg	True Sample Weight Loss / mg	True Sample Weight Loss / mg	% Weight Loss / %	Derivitive Weight Loss / mg/°C
Data Smoothing	None	None	Least Squares Fitted	None	Seven Points	Seven Points	Seven Points
Data Truncation	None	None	None	0 ≥ Data	0 ≥ Data	0 % ≥ Data ≥ -100 %	None
	20	0.00	-5.17	0.00			
	30	0.00	-5.56	0.00			
	40	0.00	-5.95	0.00			
	50	-3.04	-6.34	0.00	0.00	0.00	
	60	-3.90	-6.73	0.00	0.00	0.00	-0.05
	70	-4.40	-7.12	0.00	0.00	0.00	-0.06
	80	-5.60	-7.51	0.00	0.00	0.00	-0.04
	90	-6.00	-7.90	0.00	0.00	0.00	-0.03
	100	-6.40	-8.28	0.00	0.00	0.00	-0.03
	110	-6.70	-8.67	0.00	0.00	0.00	-0.03
	120	-7.90	-9.06	0.00	0.00	0.00	-0.04
	130	-8.30	-9.45	0.00	0.00	0.00	-0.05
	140	-9.00	-9.84	0.00	0.00	0.00	-0.05
	150	-11.20	-10.23	-0.97	-0.38	-0.85	-0.06
	160	-11.90	-10.62	-1.28	-0.99	-2.22	-0.06
	170	-12.60	-11.01	-1.59	-1.60	-3.59	-0.06
	180	-13.35	-11.40	-1.95	-2.28	-5.10	-0.06
	190	-14.90	-11.79	-3.12	-2.82	-6.32	-0.05

200	-15.30	-12.17	-3.13	-3.32	-7.43	-0.05
210	-16.45	-12.56	-3.89	-3.83	-8.58	-0.05
220	-17.73	-12.95	-4.78	-4.29	-9.62	-0.04
230	-18.09	-13.34	-4.75	-4.69	-10.51	-0.04
240	-18.90	-13.73	-5.17	-5.09	-11.40	-0.04
250	-19.33	-14.12	-5.21	-5.42	-12.15	-0.03
260	-20.41	-14.51	-5.90	-5.65	-12.66	-0.03
270	-20.80	-14.90	-5.90	-5.95	-13.33	-0.03
280	-21.49	-15.29	-6.20	-6.23	-13.97	-0.03
290	-22.05	-15.68	-6.38	-6.55	-14.68	-0.03
300	-22.92	-16.06	-6.86	-6.78	-15.20	-0.02
310	-23.60	-16.45	-7.15	-7.03	-15.76	-0.03
320	-24.30	-16.84	-7.46	-7.28	-16.32	-0.03
330	-24.74	-17.23	-7.51	-7.52	-16.86	-0.03
340	-25.28	-17.62	-7.66	-7.78	-17.45	-0.02
350	-25.95	-18.01	-7.94	-7.99	-17.92	-0.02
360	-26.46	-18.40	-8.06	-8.19	-18.36	-0.03
370	-27.49	-18.79	-8.70	-8.55	-19.18	-0.03
380	-27.78	-19.18	-8.60	-8.84	-19.82	-0.03
390	-28.42	-19.57	-8.86	-9.07	-20.34	-0.03
400	-30.00	-19.95	-10.05	-9.39	-21.06	-0.02
410	-30.00	-20.34	-9.66	-9.55	-21.41	-0.02
420	-30.31	-20.73	-9.58	-9.88	-22.15	-0.03
430	-31.43	-21.12	-10.31	-10.16	-22.77	-0.03
440	-31.30	-21.51	-9.79	-10.38	-23.28	-0.03
450	-32.80	-21.90	-10.90	-10.78	-24.17	-0.04
460	-33.09	-22.29	-10.80	-11.08	-24.84	-0.03
470	-34.33	-22.68	-11.65	-11.28	-25.30	-0.03
480	-35.50	-23.07	-12.43	-11.59	-26.00	-0.03
490	-35.10	-23.46	-11.65	-11.78	-26.41	-0.02

500	-35.60	-23.84	-11.76	-12.02	-26.94	-0.02
510	-36.20	-24.23	-11.97	-12.12	-27.18	0.00
520	-36.83	-24.62	-12.21	-12.05	-27.01	0.00
530	-37.45	-25.01	-12.44	-12.07	-27.07	-0.02
540	-37.80	-25.40	-12.40	-12.35	-27.70	-0.03
550	-37.70	-25.79	-11.91	-12.68	-28.43	-0.04
560	-38.00	-26.18	-11.82	-13.09	-29.34	-0.04
570	-40.29	-26.57	-13.72	-13.52	-30.31	-0.05
580	-41.20	-26.96	-14.24	-14.01	-31.41	-0.06
590	-42.40	-27.35	-15.06	-14.75	-33.07	-0.07
600	-43.20	-27.73	-15.47	-15.46	-34.66	-0.06
610	-43.95	-28.12	-15.83	-15.92	-35.70	-0.05
620	-45.63	-28.51	-17.12	-16.47	-36.94	-0.06
630	-45.67	-28.90	-16.77	-17.17	-38.50	-0.07
640	-46.25	-29.29	-16.96	-17.91	-40.16	-0.07
650	-47.80	-29.68	-18.12	-18.59	-41.67	-0.06
660	-50.00	-30.07	-19.93	-19.19	-43.04	-0.07
670	-51.11	-30.46	-20.65	-19.98	-44.80	-0.09
680	-51.40	-30.85	-20.55	-20.91	-46.88	-0.09
690	-52.60	-31.24	-21.37	-21.83	-48.95	-0.09
700	-53.90	-31.62	-22.28	-22.78	-51.08	-0.11
710	-55.48	-32.01	-23.47	-24.01	-53.83	-0.13
720	-56.96	-32.40	-24.56	-25.45	-57.07	-0.15
730	-59.40	-32.79	-26.61	-27.06	-60.68	-0.16
740	-62.42	-33.18	-29.24	-28.71	-64.38	-0.18
750	-64.21	-33.57	-30.64	-30.73	-68.89	-0.20
760	-66.60	-33.96	-32.64	-32.78	-73.50	-0.22
770	-68.18	-34.35	-33.83	-35.13	-78.76	-0.24
780	-72.29	-34.74	-37.55	-37.53	-84.15	-0.24
790	-74.08	-35.13	-38.96	-39.89	-89.44	-0.23

800	-78.53	-35.51	-43.02	-42.06	-94.29	-0.21
810	-81.98	-35.90	-46.08	-44.05	-98.77	-0.17
820	-83.43	-36.29	-47.14	-45.48	-100.00	-0.13
830	-84.49	-36.68	-47.81	-46.67	-100.00	-0.09
840	-84.87	-37.07	-47.80	-47.24	-100.00	-0.04
850	-85.03	-37.46	-47.57	-47.40	-100.00	-0.01
860	-85.12	-37.85	-47.27	-47.43	-100.00	0.00
870	-85.28	-38.24	-47.04	-47.33	-100.00	0.01
880	-85.80	-38.63	-47.17	-47.25	-100.00	0.01
890	-86.35	-39.02	-47.34	-47.19	-100.00	0.00
900	-86.51	-39.40	-47.11	-47.21	-100.00	-0.01
910	-87.06	-39.79	-47.27	-47.30	-100.00	-0.01
920	-87.31	-40.18	-47.13	-47.38	-100.00	-0.01
930	-87.96	-40.57	-47.39	-47.47	-100.00	-0.01
940	-88.67	-40.96	-47.71	-47.58	-100.00	-0.01
950	-89.07	-41.35	-47.72	-47.61	-100.00	0.00
960	-89.70	-41.74	-47.96	-47.65	-100.00	0.00
970	-90.00	-42.13	-47.87	-47.66	-100.00	
980	-90.00	-42.52	-47.48			
990	-90.34	-42.91	-47.44			
1000	-90.70	-43.29	-47.41			

APPENDIX 3

"IONSTG" COMPUTER PROGRAM

A3.1 Introduction

The program "IONSTG" was written (in BASIC) for both the Apple IIe and BBC microcomputers to relieve the necessity for repetitive ionic strength calculations during the preparation of samples for fluorescence studies (see Chapter 3). The program calculates the ionic strength of a multi-component system and suggests electrolyte additions required to attain a user-defined ionic strength within the experimental constraints of a given total volume and acidity of the supporting medium.

A3.2 Calculation Procedures

The calculation of ionic strength is based on the equation: [119]

$$I = \frac{1}{2} \sum_{i} c_i z_i^2 \qquad \text{(A3.1)}$$

Where:

I	=	Ionic strength of the system
c_i	=	Concentration in mol dm^{-3} on the i^{th} ion
z_i	=	Charge on the i^{th} ion

Strictly, the concentrations should be expressed as molalities.

A3.2.1 Contributions to the Ionic Strength

For the system under consideration, the program assesses the charges and concentrations of the ionic components of the fluorescence sample series. The europium(III) ions and humic acid (probably partially dissociated and thus existing as humate anions) are excluded from the calculation since these are the subject species.

Sodium nitrate solution, which was used as the ionic strength adjustor, provides a cation and anion pair. For added acid and alkali, the contribution of "free" protons and hydroxide ions to the ionic strength are obtained from the prevailing pH using the dissociation constant of water. Calculation in this manner also accounts for protons stemming from the dissociation of the humic acid, protons from hydrolysis of the trivalent metal ion and excess hydroxide ions used to disperse the humic acid. The total contribution of protons and hydroxide ions to the ionic strength is small since the pH of the samples was controlled to within a narrow deviation from neutrality. The acid and alkali counter-ions are estimated from the volume of a given concentration added. Sodium ions from the alkali used to disperse the humic acid are considered in the calculation but those associated with Fluka Humic Acid v3 in the solid phase are not since their contribution is minimal due to the low humic acid concentration utilised. Note that europium salt provides three nitrate counter-ions per mole of the salt added. The ionic contributions are summarised in Table A3.1.

All the ionic species discussed are monovalent thus equation A3.1 may be simplified to:

$$I = \frac{1}{2}\sum_i q \qquad \text{(A3.2)}$$

The ionic contributions of Table A3.1 can be substituted into equation A3.2 to yield:

$$I = \frac{1}{2}\sum\left([Na^+]_1 + [NO_3^-]_1 + [Na^+]_2 + [NO_3^-]_2 + [Na^+]_3 + [NO_3^-]_3 + [H^+]_T + [OH^-]_T\right) \qquad \text{(A3.3)}$$

The subscripts employed in equation A3.3 correlate with the ionic species of Table A3.1. The protons and hydroxide ions have several sources that are not distinguished in the calculation since their concentrations are calculated from the prevailing pH rather than individual additions. Thus $[H^+]_T$ and $[OH^-]_T$ imply the total proton and hydroxide concentrations respectively in the equations:

$$[H^+]_T = \sum_i [H^+]_i$$

Table A3.1
Ionic Contributions to Fluorescence Samples

Source	Cation Produced	Anion Produced
$NaNO_3$ (aq)	$[Na^+]_1$	$[NO_3^-]_1$
FHA v3 (aq)	$[Na^+]_2$	$[OH^-]_1$
$Eu(NO_3)_3$ (aq)		$[NO_3^-]_2$
NaOH (aq)	$[Na^+]_3$	$[OH^-]_2$
HNO_3 (aq)	$[H^+]$	$[NO_3^-]_3$

Notes:
Subscripts to ions refer to Equation A3.3
The subject species are not included in the Table

$$[H^+]_T = \sum_i [H^+]_i$$

$$[OH^-]_T = \sum_i [OH^-]_i$$

Note that the latter includes the terms $[OH^-]_1$ and $[OH^-]_2$ given in Table A3.1.

The program uses equation A3.3 to calculate the current ionic strength of a sample medium. This value is compared to a user-defined ionic strength and additions of sodium nitrate at a given concentration are suggested to meet this requirement. This process is generally undertaken several times for each sample until the desired values of pH, ionic strength and total volume are realised.

A3.3 Program Versions

The BBC and Apple IIe versions of the program are derived from the same algorithm but with subsequent development to different extents. Besides the calculation of ionic strength, both provide the following useful features:

1 Defaults and options to permit changes in sample concentrations.

2 Warnings of mistaken data entry.

3 Warnings in case the total volume limit of the sample would be exceeded by the suggested addition of electrolyte.

The BBC version listed below contains further refinements:

4 Reference to a brief set of user notes.

5 Production of a hard-copy of the entered data and suggested additions.

A3.3.1 BBC "IONSTG" Program Listing

```
10   CLS
20   REM                          **** IONSTG ****
30   CLS
40   PRINT     "========================================="
50   PRINT          " CALCULATION OF INERT ELECTROLYTE"
60   PRINT        "ADDITIONS REQUIRED FOR IONIC STRENGTH"
70   PRINT      "ADJUSTMENT IN A MULTI-COMPONENT SYSTEM"
80   PRINT     "========================================="
90   PRINT : PRINT : PRINT
100  PRINT           "****  Do you want to read the  ****"
110  PRINT           "****    Release Notes? (Y/N)   ****"
120  INPUT AN$
130  IF AN$ = "Y" THEN GOSUB 1670
140  PRINT : PRINT
150  CLS
160  PRINT : PRINT
170  PRINT           "***** Enter Your Data and Conditions *****"
180  PRINT : PRINT
190  PRINT       "HNO3 Concentration = 0·01198 M, O.K.? (Y/N) "
200  INPUT A$
210  IF A$ = "Y" THEN GOTO 270
220  IF A$ = "N" THEN GOTO 240
230  GOTO 200
240  PRINT "HNO3 Concentration / M = ? "
250  INPUT B
```

```
260  GOTO 280
270  B = 0·01198
280  PRINT                    "Volume of HNO3 / ml = ? "
290  INPUT C
300  D = B * C
310  PRINT : PRINT
320  PRINT          "NaOH Concentration = 0·01094 M, O.K.? (Y/N) "
330  INPUT B$
340  IF B$ = "Y" THEN GOTO 400
350  IF B$ = "N" THEN GOTO 370
360  GOTO 330
370  PRINT                    "NaOH Concentration / M = ? "
380  INPUT F
390  GOTO 410
400  F = 0·01094
410  PRINT                    "Volume of NaOH / ml = ? "
420  INPUT G
430  H = F * G
440  PRINT : PRINT
450  PRINT      "Eu(NO3)3 Concentration = 4·0346*10^-3 M, O.K.? (Y/N)"
460  INPUT C$
470  IF C$ = "Y" THEN GOTO 530
480  IF C$ = "N" THEN GOTO 500
490  GOTO 460
500  PRINT                    "Eu(NO3)3 Concentration / M = ? "
510  INPUT I
520  GOTO 540
530  I = 4·0346E-03
540  PRINT                    "Volume of Eu(NO3)3 / ml = ? "
550  INPUT J
560  K = I * J * 3
570  PRINT : PRINT
580  PRINT "NaOH Concentration in Humic Acid Dispersion = 7·0016*10^-4 M (X),
                    2·53808*10^-3 M (Y), or Other (Z) ?"
590  INPUT D$
```

```
600  IF D$ = "X" THEN GOTO 640
610  IF D$ = "Y" THEN GOTO 660
620  IF D$ = "Z" THEN GOTO 680
630  GOTO 590
640  L = 7·0016E-4
650  GOTO 700
660  L = 2·53808E-3
670  GOTO 700
680  PRINT        "NaOH Concentration in Humic Acid Dispersion/ M = ?"
690  INPUT L
700  PRINT              "Volume of Humic Acid Dispersion / ml = ? "
710  INPUT M
720  N = L * M
730  PRINT : PRINT
740  PRINT                         "Measured pH = ? "
750  INPUT P
760  IF P ≤ 14 THEN GOTO 780
770  GOTO 790
780  IF P ≥ 0 THEN GOTO 820
790  PRINT : PRINT:              "CHECK YOUR pH VALUE ! "
800  PRINT : PRINT
810  GOTO 740
820  Q = 10^-P
830  R = 10^(P-14)
840  PRINT : PRINT
850  PRINT        "Required Ionic Strength, I = 0·005 M, O.K.? (Y/N) "
860  INPUT F$
870  IF F$ = "Y" THEN 900
880  IF F$ = "Y" THEN 920
890  GOTO 860
900  S = 0·005
910  GOTO 940
920  PRINT              "Enter Required Ionic Strength, I /M = ? "
930  INPUT S
940  PRINT : PRINT
950  PRINT              "Total  Volume = 10·00 ml, O.K.? (Y/N)  "
```

```
960  INPUT G$
970  IF G$ = "Y" THEN GOTO 1000
980  IF G$ = "N" THEN GOTO 1020
990  GOTO 960
1000 T = 10·00
1010 GOTO 1040
1020 PRINT                    "Enter Total Volume Required / ml? "
1030 INPUT T
1040 PRINT : PRINT
1050 PRINT          "NaNO3 Concentration = 0·09984 M, O.K.? (Y/N)  "
1060 INPUT H$
1070 IF H$ = "Y" THEN GOTO 1100
1080 IF H$ = "N" THEN GOTO 1120
1090 GOTO 1060
1100 U = 0·09984
1110 GOTO 1140
1120 PRINT                     "NaNO3 Concentration /M = ?  "
1130 INPUT U
1140 REM                       **** MAIN CALCULATION ****
1150 V = ((1/T) * (D+H+K+N)) + (Q+R)
1160 VV = V/2
1170 E = (S-VV) * (T/U)
1180 O = E*1E5
1190 INT (O)
1200 W = O/1E5
1210 X = C+G+J+W
1220 IF T > X THEN GOTO 1300
1230 PRINT
1240 PRINT              "***** TOTAL VOLUME EXCEEDED ! *****"
1250 PRINT
1260 PRINT
1270 PRINT                "***** RE-ENTER YOUR DATA *****"
1280 PRINT : PRINT
1290 GOTO 190
1300 PRINT          "  ==================================  "
```

```
1310  PRINT              " REQUIRED VOLUME OF SODIUM NITRATE "
1320  PRINT                " = " ;W "ml TO GIVE I = ";S; " M "
1330  PRINT          "  ================================  "
1340  PRINT : PRINT
1350  PRINT               " Data Print-Out Required ? (Y/N) "
1360  INPUT PR$
1370  IF PR$ = "Y" THEN GOTO 1470
1380  IF PR$ = "N" THEN GOTO 1400
1390  GOTO 1360
1400  PRINT : PRINT : PRINT
1410  PRINT               "  **** Run  Again ? (Y/N) ****  "
1420  INPUT J$
1430  IF J$ = "Y" THEN GOTO 150
1440  IF J$ = "N" THEN GOTO 1460
1450  GOTO 1420
1460  END
1470  *FX6,0
1480  CLS
1490  VDU 2
1500  PRINT              " **** IONSTG DATA PRINTOUT **** "
1510  PRINT          "       ====================       "
1520  PRINT : PRINT
1530  PRINT        "HNO3 Concentration = ";B; " M, Volume = ";C; " ml"
1540  PRINT        "NaOH Concentration = ";F; " M, Volume = ";G; " ml"
1560  PRINT      "Eu(NO3)3 Concentration = ";I; " M, Volume = ";J; " ml"
1570  PRINT           "NaOH Concentration in Humic Acid Dispersion
                          = ";L;" M, Volume = ";M; " ml"
1580  PRINT                          "pH = ";P
1590  PRINT              "Required Ionic Strength = ";S; " M"
1600  PRINT              "Total Volume (to date) = ";X; " ml"
1610  PRINT        "NaNO3 Concentration = ";U; " M, Volume = ";G; " ml"
1620  PRINT              "Ionic Strength (to date) = ";VV; " M"
1630  PRINT
1640  PRINT         "NaNO3 Volume = ";W; " ml to give I = ";S; " M"
1650  VDU 3
1660  GOTO 1400
```

```
1670  CLS
1680  PRINT                " **** IONSTG RELEASE NOTES **** "
1690  PRINT          "      ====================      "
1700  PRINT : PRINT
1710  PRINT "Author: M.M.Scanlon, Chemical Engineering and Applied Chemistry, Aston
      University, 1989 "
1720  PRINT : PRINT
1730  FOR DEL = 1 TO 5000
1740  NEXT DEL
1750  CLS
1760  PRINT  "IONSTG is a simple program for the calculation of electrolyte additions
             required to give a user-defined ionic strength in a multi-component
             system."
1770  PRINT
1780  PRINT  "The chemical system is composed of a dispersion of a humic acid, a
             trivalent lanthanide metal ion and materials used to adjust the
             composition of the supporting medium to desired values of acidity,
             volume and ionic strength."
1790  PRINT
1800  PRINT                          " <space for more> "
1810  XE = INKEY(50)
1820  IF XE = 32 THEN GOTO 1840
1830  GOTO 1810
1840  CLS
1850  PRINT  "The calculation step uses the formula:
                        I = 0·5 * sum  of  (concentration * ionic  charge 2)
             for each ion in the system, except for the subject species (Eu3+ and
             Humic Acid/Humate). The ions considered are: Na+; NO3−; H+ and OH−.
1860  PRINT
1870  PRINT  "The program offers the option for default or user-defined variables
             for concentrations and volumes of the components. It also provides the
             facility to print input data and the calculated electrolyte addition."
1880  PRINT
1890  PRINT  "The calculated addition should then be made to the system with
             simultaneous observation of the acidity of the medium. The ionic
```

```
                strength should be recalculated after the final addition."
1900  PRINT
1910  PRINT                    " <space to return to program> "
1920  XE = INKEY(50)
1930  IF XE = 32 THEN RETURN
1940  GOTO 1920
```